PRODUCTION OF ALUMINIUM MATRIX COMPOSITES

BY

CHRISTOPHER H. J. DAVIES

A Thesis submitted for the degree of PhD of the University of London.

John Percy Group,
Department of Materials,
Royal School of Mines,
London, SW7 2BP.

October 1990.

TO LOUISE AND RAGS

Abstract

Production of Aluminium Matrix Composites

Composite materials are becoming increasingly attractive to the aerospace and automobile industries because of their potential for high specific strength and modulus. Their application is currently limited by the cost of production, the unreliability of the production processes and the low fracture toughness of such materials.

The objective of this investigation was to find a reliable production route for composites of powder aluminium alloys and particulate reinforcement, and to investigate matrix material factors and extrusion parameters with respect to the structure and properties of the product. Three matrix materials were investigated: commercial purity aluminium; 2014, and an enhanced 7xxx series alloy, CW67. The last two alloys are precipitation hardenable. The initial experimentation involved optimising the mixing of the components and testing a variety of pre-extrusion operations. An investigation of composites in various heat treatment and ageing conditions was also conducted, with a view to determining the microstructural variations and elucidating their effect on the mechanical properties of these materials.

The production route established involved canning, cold compaction, vacuum degassing and hot compaction of the composite prior to extrusion. These operations were found to enhance the properties of the product. The precipitation process in CW67 and 2014 alloy composites is shown, and compared with the unreinforced material. The effect of material parameters (such as matrix type, heat treatment, particle size and volume fraction, and processing) on mechanical properties is demonstrated. The mechanical properties are also compared with predictive equations. The specific proof stress and U.T.S. of CW67 composites were found to be greater than published values for composites of SiC and alloys 6061, 2024 and 8090.

Conclusions are presented which give the possible reasons for the composites' mechanical behaviour, and factors which limit the properties of composite materials.

Acknowledgements

The author would like to express his thanks to Professor Terry Sheppard and Dr. N. Raghunathan for their supervision, guidance and encouragement throughout the duration of this project.

Thanks are also expressed to past and present members of the John Percy Research Group for their help and lively debate. Thanks for technical assistance go to Mr. Alex Neve, Mr. Melvyn Andrews and Mr. Roy Baxter and his colleagues in the workshop for their patience and perseverance with a difficult material. The author greatly appreciates the help of other technical staff in the department for their specialist assistance. Sincere thanks to members of the R.S.M.U. for keeping me sane.

Thanks also go to Fred and Peter for their support, both financial and moral, and to Louise for her love and support throughout this project.

CONTENTS

Results and Discussion

Chapter 6 Composites of Commercial Purity Aluminium

Chapter 7 Composites of 2014

Chapter 8 CW67 and its Composites

List of figures

List of Tables

1. INTRODUCTION

Composite materials have been used by man for centuries: the Bible describes the filling of bricks with straw to improve their strength and rigidity; the practice of the inclusion of twigs in plaster was common around the sixteenth century in Britain. However, it is only relatively recently that the systematic development of composite materials was initiated. Interest in composite systems, and in particular metal matrix composites (m.m.c.s) has waxed and waned since the early 1960's and the advent of boron and carbon fibres. The attractiveness of such systems was, and still is, potentially large increases in strength and stiffness compared with those obtainable by conventional alloying techniques. However, at that time the potential of the materials was not realizable and it is only comparatively recently that a resurgence of interest in composites as engineering materials has been seen. Composite materials are capable of allowing great savings to be made in specific stiffness and specific strength, if the problem of their reliability can be resolved. Allied, and no less important, problems are N.D.T. testing, fabrication, directionality of properties and cost.

Powder metallurgical processes have been in use for somewhat longer. Initially employed in the production of 'Cermets' such as tungsten carbide dies, powder metallurgy has been found useful over a wide range of applications and materials. Advantages of this technique include the production of near net shapes and ease of handling of the green compact. Coupled with this, the use of rapid solidification processing of powder has enabled the use of finer and novel alloy microstructures due to the high cooling rates employed and the resultant greater amounts of alloying elements held in solid solution. Rapidly solidified powder (R.S.P.) is also processed by conventional thermomechanical working routes. Extrusion of powder materials is a simple and effective method of forming.

The combination of reinforcement material with alloy powder to produce a composite is a natural progression. Problems of chemical attack have long been apparent in hot combination of the two components by methods such as casting, infiltration and spray routes. Hence the need for 'designer' fibres , 'AVCO' silicon carbide being a good example of this. Cast composites may also suffer from a high degree of porosity and agglomeration. A powder route negates these problems. Powder metallurgy also points to greater control of product homogeneity than does a melt route.

A wide range of applications has been explored to date. This includes the aerospace and auto industries and also sporting goods. The driving force behind composite development in the aero industry is weight saving leading to greater efficiency. Cost is far more important to automobile manufacturers. Typical

applications currently under investigation in the auto sector are con-rods, piston rings and pistons themselves. Composites for aircraft are more likely to be of a structural nature, with some sources quoting 11% weight saving over an entire aircraft. Fibre and particulate reinforced composites are currently being used in automobile piston crowns and brake liners. M.M.C.s have already been successfully used for sports equipment such as tennis rackets and golf club heads, their desirability emanating from their stiffness. Reinforcement types for these applications range from continuous fibres of carbon and boron, alumina short fibres to particulate silicon carbide.

2. LITERATURE SURVEY

2.1 Development and Applications of Composites

The potential areas of use of composite materials are wide and it is this potential which has driven the current level of interest, and investment, in such materials. The development of composite materials has been governed by development in the component material forms: i.e., as whisker and particulate technology has improved there has been able to be a move away from continuous fibre composites to discontinuously reinforced materials. Developments in production methods have also increased the scope of applications. There are three main areas in which composites are currently being used and it would be useful to examine these prior to an assessment of the literature on the development of the materials themselves. These areas are aerospace, automotive and leisure goods. There are other uses for which composites seem to have advantages over other materials and these will be discussed as well.

The three main types of reinforcement have governed the applications for which they may be employed by their effect on the properties of the resultant material. Feest[1] notes these three types as being characterised thus:

(i) continuous monofilament fibres of diameter 100-200μm, eg. boron or SiC fibres, which have a highly unidirectional load bearing capacity which can be modified in the production by laying the fibres in cross plies; continuous multifilament of diameter 5-20μm, eg. carbon, alumina and SiC,

(ii) short fibres which give some directionality of properties but are more likely to be randomly dispersed;

(iii) particulate reinforcement, such as SiC or alumina, of near-equiaxed or platelet shape and sizes of up to around 10μm which are used primarily for the increased stiffness accompanying reinforcement.

Fuller details of the reinforcement types will be given in section 2.5.

2.1.1 Aerospace Applications

The aerospace industry is continually seeking materials which will allow increased performance whilst giving weight savings. Composites (both metal and polymer matrix) have the potential to achieve this, but alongside the development of these materials is research into aluminium-lithium alloys which offer similar potential[1,2]. However, the cost of Al-Li alloys is substantially lower[1].

Metal matrix composites are currently being tested, or used, for applications in the aero engine, aircraft framework and skins[2,3]. Charles[3] shows predictions that indicate that metal matrix composites will comprise almost 30% of the weight of jet

engines by the year 2010. A similar percentage of the weight will be made up by ceramic matrix composites. Feest quotes higher values, around 40-50%, for the usage of composites. These predictions necessarily also dictate the waning of the use of nickel and titanium alloys. However, it is probable that these alloys will turn up in another guise as composite matrix materials. Charles[3] notes that reinforced titanium aluminides would reduce the weight of a compressor disc from 16kg to 1kg.

High stiffness composites are under consideration for the landing gear of aircraft[1]. These are likely to be fabricated using particulate reinforcement. Other areas which have been identified as potential sites for the introduction of m.m.c.s are the floor beam struts (particulate extrusions), floor beams (fibre and particulate composites) and part of the skin[3]. Weight savings may be substantial: m.m.c. components used in the space shuttle achieved a 44% weight saving over conventional aluminium alloys[3]. Whilst cost is of relatively minor importance in such ventures, the cost of m.m.c.s is substantially higher than that of conventional materials. The joining of composites may be performed by diffusion bonding or, as briefly noted by Stubbington[2], a modified capacitor discharge welding technique, but problems with the *in situ* joining of composites have still to be fully addressed.

Aluminium-lithium alloys can have density reductions of 8 to 10% compared with 7xxx series alloys[2] and modulus improvements of up to 15%. Composites of 7xxx series alloys will obviously have a slightly higher density than the unreinforced material (dependent on the law of mixtures relationship with the reinforcing phase) but may have a similar specific modulus[2]: improvements of between 50-100% in the absolute value are possible, depending on the reinforcement content[2,4]. Another advantage of Al-Li alloys is that the technology for their production is as for conventional alloys.

It is clear that the use of composites and aluminium-lithium alloys in aerospace applications is still in its infancy. Predictions of potential usage are varied but it seems likely that m.m.c.s are destined for use in structural and stiffness governed applications whilst Al-Li alloys may have more bulk applications where their lower density can be best used in reducing weight.

2.1.2 Automotive Applications

Metal matrix composites fulfill many requirements for use in the automotive industry. Their high stiffness make them ideal for high tolerance operations and their thermal fatigue resistance for the selective reinforcement of high temperature

components[5]. Selective reinforcement of piston crowns for diesel engines has reached commercial use[5]. Apart from this, composite materials have made few inroads into the auto industry: Trumper[5] ascribes this to the high cost of the introduction of the new technology required to produce the components. Thus the weight savings accompanying the introduction of composite materials have yet to be realised in terms of reduced fuel consumption. However, it would seem that in such a high volume market, this cost could readily be dispersed.

2.1.3 Leisure Goods

A third major area of application of m.m.c.s is in leisure goods. Such items often make use of developments in the aerospace industry if they are perceived to offer real advantages in terms of performance which can be offset by a higher price. Thus carbon fibre reinforced fishing rods were introduced around 1980 because of their increased stiffness. Metal matrix composites are used in the production of golf club heads and shafts, tennis rackets and bicycle frames[5]. All of these applications rely on the greater specific properties of the materials leading to weight savings. Whilst the price of such objects is initially high, the high volume of trade in leisure goods will necessarily lead to a reduction in costs.

2.1.4 Other Uses

There are many other areas in which the introduction of composite materials would prove beneficial. These include military applications (on which there is naturally very little information) and the use of the thermal and electromagnetic properties of m.m.c.s[1] in the electronics industry. Tank tracks and torpedo hulls are currently being produced from composite materials[1], primarily for the weight saving and stiffness increases enjoyed by such materials. Research is being conducted into m.m.c.s with tailored thermal expansion in order to reduce the failure of semiconductor devices by thermal fatigue[5]. The high stiffness of composites is also being employed in radar technology where a stiff aerial is required for accuracy[5]; the accompanying weight saving is also advantageous. However desirable these applications are it should be noted that they are not currently high volume applications and, perhaps with the exception of the semiconductor devices, probably never will be.

2.1.5 Summary

It is evident from the literature that the potential range of applications of composites is wide. Weight savings and improved properties, such as increased

modulus, are the driving force for the use of composite materials. It is equally apparent that there are a number of problems and obstructions which must be overcome if composites are to realise this potential. The major barrier is the increased cost of production and raw materials. This is unlikely ever to be overcome, but in certain applications, such as aerospace or automotive where these costs can more easily be absorbed, the usage of m.m.c.s is predicted to be high in some specific applications[1,5]. There is also a certain resistance to the introduction of the new, often costly and broadly untried technology required for the production processes. This is evident in the auto industry[5], but the current trend for improved fuel efficiency initiated by the environmental lobby may make wider usage of composite materials more attractive. There are also problems with the easy joining and repair of composites which must be overcome prior to their widespread introduction. It should not be forgotten that other materials offer similar improvements in specific properties, the most notable of these being aluminium-lithium alloys. However, there is current interest in combining composite and Al-Li technology in the production of Al-Li composites[2]: such materials will obviously incorporate the advantages of both technologies.

2.2 Production of Composites

Processing methods involved in the production of composites are varied. It is important that attention is paid to the initial fabrication because this has a major rôle as determinant of the properties of the product. Consideration must obviously be given to the type of reinforcement, alloy type and limitations, required volume fraction and ease of fabrication. The starting point for composite production lies in conventional metallurgical practice- casting and powder routes have been adapted to accommodate the introduction of a ceramic reinforcing medium. This review of processing methods will concentrate on the application to aluminium matrix alloys, but the methods are often applicable to other materials commonly used as matrices, such as steel and titanium. Taya and Arsenault[6] give a good review of the applicability of the following methods to specific composite systems.

2.2.1 Pressure Casting

Pressure casting is here used as a generic term for the process of introducing liquid metal under pressure into a fibre preform.

During squeeze casting (figure 2.1) liquid metal is forced into a closed die containing a heated preform of fibre material which is near the net shape of the final

product. The preform is usually held together by a binding medium, which may consist of an organic and inorganic component[7]. Pressures of between 70-150 MPa aid infiltration[8] and reduce porosity and shrinkage in the cast product, although molten metal can never infiltrate a completely closed pore. The high pressure also aids the wetting of the reinforcement, which is usually poor[9]. The shape and size of the castings are, however, limited by the high pressures involved. Products such as piston crowns are fabricated in this manner. Pressure casting requiring lower pressures of around 15 MPa[8], may be employed for larger structures but is not as efficient in reducing porosity. In both cases infiltration normal to a fibre's transverse direction introduces the problem of compression of the fibres, which will hinder infiltration[10]. This problem is not as evident in random arrays.

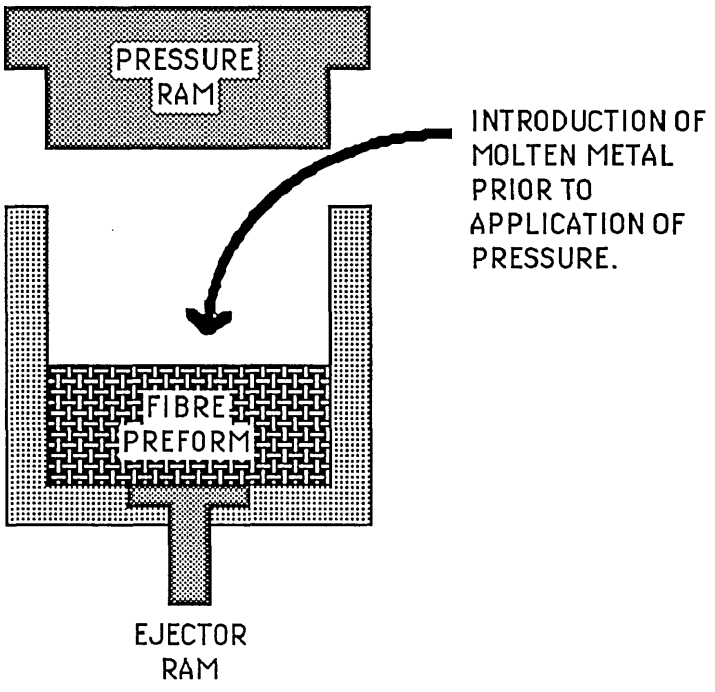

Figure 2.1: Schematic of squeeze casting operation

Investigations of the microstructure of composites produced by infiltration at low pressures showed large amounts of segregation of the fibres and also of alloying elements to the fibre/matrix interface[11]. This clearly will result in a degradation of mechanical properties. Work on squeeze cast 'hybrid' composites[7], containing a combination of fibres and particulates, has shown that the homogeneity is inferior to sprayformed or extruded powder composites. The investigation did show that there was no interface reaction due to the short process time required at the high temperature used (1000°C); however, this neglects any loss of alloying element at such extreme temperatures.

2.2.2 Slurry Casting

The introduction of short fibres or particles into the mushy zone of a solidifying liquid metal has been reported as being an acceptable method of production of composites[8]. Introduction of particles into a fully molten alloy is less popular. Either method is only really suitable for the production of particulate composites. There are a number of apparent drawbacks inherent in casting methods, which have been overcome with varying degrees of success. These include poor particle homogeneity, segregation of alloying elements, poor wetting of the reinforcement and interface reactions. A further factor to consider with slurry casting is that the solidification range of the alloy must be large enough to facilitate the introduction of the reinforcement[12]. This review will concentrate on slurry casting; melt casting will be used as a generic name. Figure 2.2 shows a typical arrangement for the casting of composite materials, the various aspects of which will be discussed below.

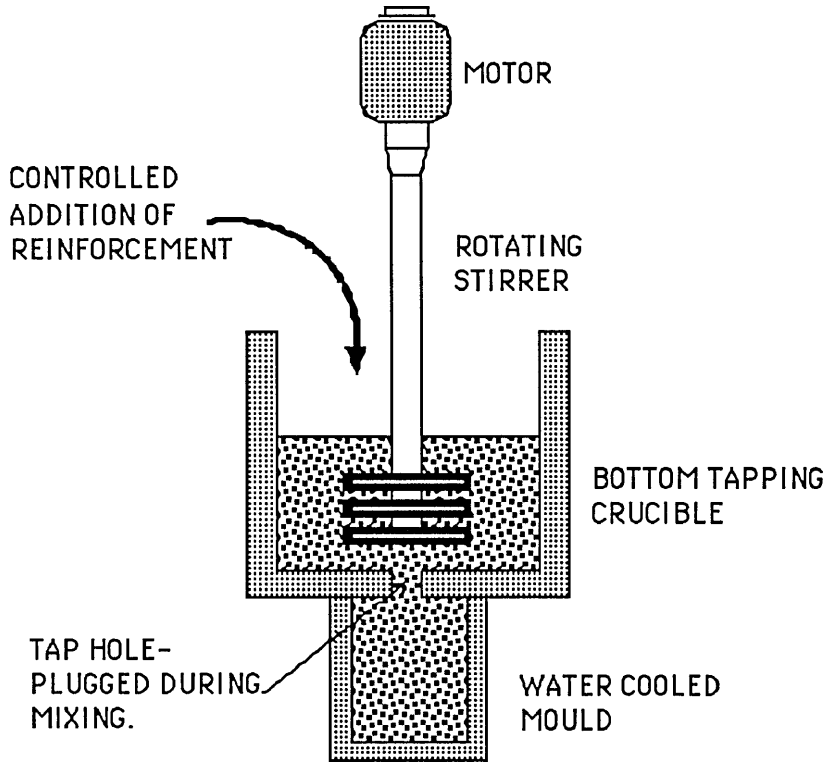

Figure 2.2: Schematic of 'compo-casting' technique

The apparently obvious drawback of segregation of the particles to the inter-dendritic regions does not, according to Baker[13], have any effect on the mechanical properties of the final product. Indeed, Girot et al[9] describe the technique of compocasting, a form of slurry casting, which results in a non-dendritic primary phase and a more uniform microstructure. Excitation of the mixture contributes to its

homogeneity but can do nothing to aid the alignment of fibres. Heating of the reinforcement prior to its addition to the melt goes some way towards counteracting segregation of alloying elements[14].

Wetting of the reinforcement is necessary if the material is to have acceptable properties. Mehrabian et al[15] note that two 'chemical' methods may be employed in dealing with this: the ceramic can be coated with a wetting agent or the wetting agent can be added directly to the matrix alloy melt. The coating of reinforcement also opens up the opportunity to limit interfacial reactions[8,16] (more of which will be described in section 2.5.1). Certain alloying elements (Mg, Si) also promote the wetting of reinforcement by aluminium alloy[17,18], although their use is obviously limited by whether the choice of alloy is free or restricted. Hosking et al[18] observed the formation of $MgAl_2O_4$ and $CuAl_2O_4$ spinels in their preparation of cast 2014/Al_2O_3 composites and imply that good wetting has occurred, but this disregards the potential influence of such reactions on the mechanical properties of the product. Physical agitation of the melt may also promote wetting[15]. The high viscosity of the mixture apparently prevents settling, floating or agglomeration in the initial stages of casting[9]. Never-the-less this technique is limited and Girot et al[9] set the upper limit of reinforcement volume fraction at 0.1.

2.2.3 Rapid Solidification

Techniques for composite production involving rapid solidification as a stage in the process route are best suited to the incorporation of short fibres or particulate reinforcement. All similarly labelled "rapid solidification" methods are not truly R.S. techniques as the silicon carbide is never actually in the molten state, which would require temperatures of over 2000°C (at which the material sublimes anyway). Bearing this in mind, the following production methods are currently in use, or being researched.

2.2.3.1 Sprayforming

Spray co-deposition involves the in-flight atomization of a metal matrix alloy and combination with reinforcement particles, a stream of which is directed at a substantially colder collector plate: this is the 'Osprey' process, a concise review of which is given by Kahl and Leupp[19]. Figure 2.3 shows a schematic diagram of the main aspects of the operation. Alloy material is partly frozen in flight by a stream of nitrogen gas; the final solidification occurs on the collector plate; the solidification process is well demonstrated by Leatham et al[20]. The parameters governing the

solidification sequence are carefully controlled in order to control the microstructure. Ceramic filler particles may be added to the stream of matrix and frozen in position. An Al-5% Si alloy was investigated by Singer and Ozbek[21] and various particles (SiC, Al_2O_3, graphite) of sizes 75-120 μm were successfully incorporated. Some form of secondary processing is required. The resultant plates of composite may be diffusion bonded together and/or formed by forging, rolling or extrusion[12]. Research directed towards this technique suggests two major benefits[21]. Interface reactions and segregation are minimised because of the short time spent at high temperature and as a

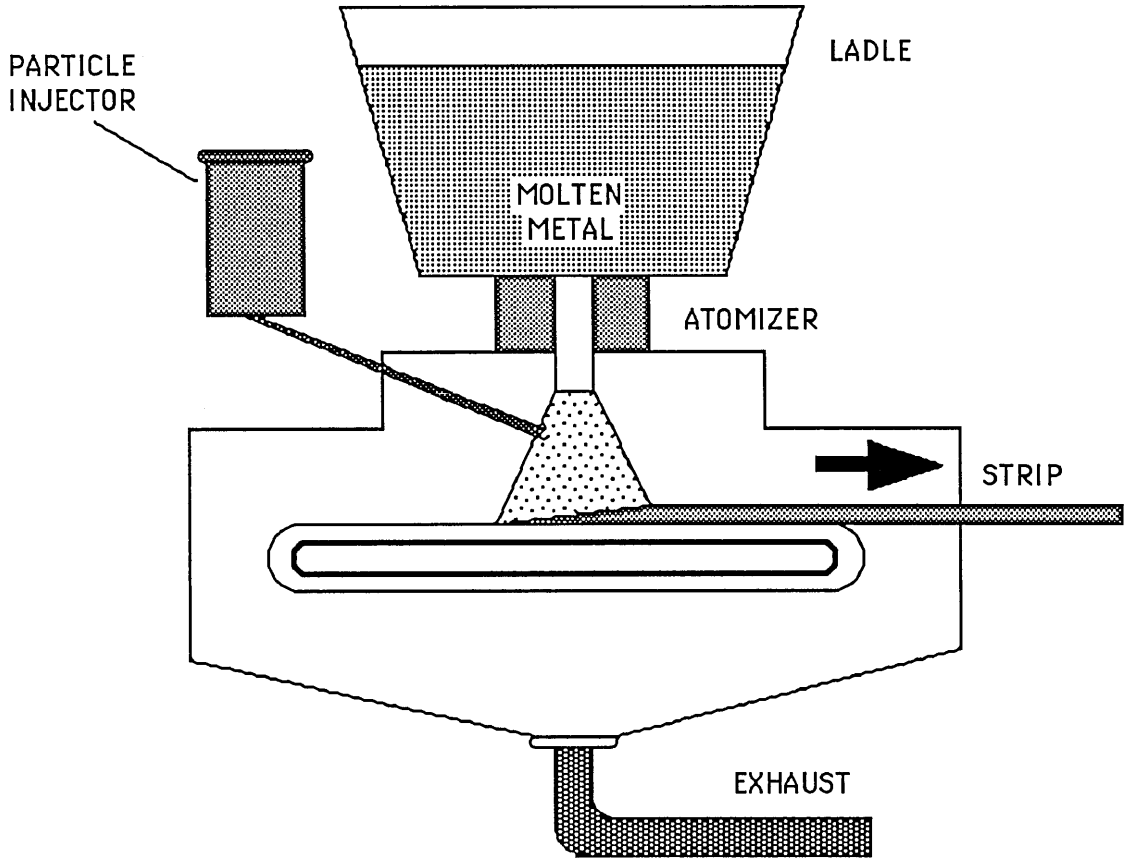

Figure 2.3: Schematic of 'Osprey' co-deposition technique

consequence of the rapid cooling refinement of microstructure also occurs. Apparently good homogeneity was achieved but cracking was associated with the particles on rolling of sheet. Other metal alloys lend themselves to incorporation in composite materials by the Osprey process. These include steels[22] and titanium alloys[23].

2.2.3.2 Melt Spinning

Melt spinning involves the direction of a stream of undercooled material at a rotating wheel made from a good conductor, typically copper. An outline of the process is shown in figure 2.4. This technique may be utilised in two different ways: either the

reinforcement is introduced into the base alloy slurry prior to spinning, or it may be mechanically mixed at a later stage[24]. The spun product is usually in ribbon form as it impinges upon the plate and is immediately ejected as solid. Subsequent to spinning, the ribbons were chopped, cold compacted and extruded. The process apparently gives good homogeneity, although in certain alloys, such as those with a high silicon content, chemical attack of the particles was observed[24]. This technique is very much in its infancy, and thus has had very limited impact on composite production to date.

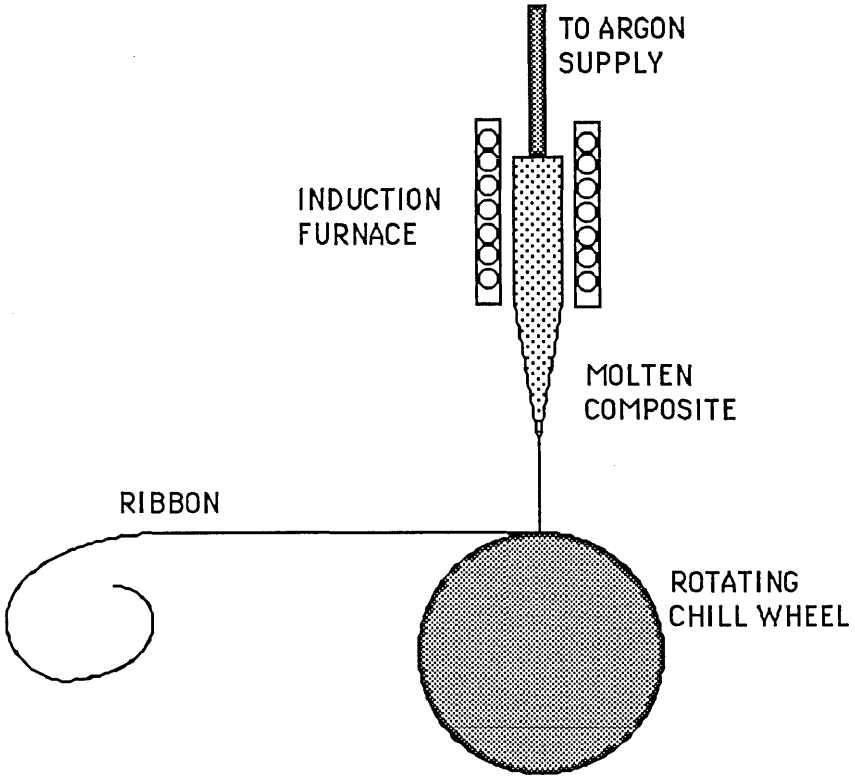

Figure 2.4: Schematic of melt spinning apparatus

2.2.3.3 Powder Routes

The use of powder metallurgy in the production of composites is potentially the simplest of all processing routes; it is, however, also an expensive route. Rapidly solidified alloy powder is mixed with the required volume fraction of reinforcing ceramic, compacted and extruded and then possibly rolled[4]. This route is obviously more suited to the production of composites containing particulate and random short fibre arrays. As with spray forming there is no prolonged contact of matrix and reinforcement at high temperature which may give rise to detrimental interface reactions. The bond at the interface is purely mechanical. A considerable volume of work has been conducted on powder produced composites[25,26,27]. A considerable amount of pre- and post-compaction work is required in order to ensure reliable

material. Many workers are in agreement that some form of hot compaction is required prior to secondary processing in order to limit porosity and improve properties[6,9,28]. Girot et al[9] note that high compaction pressures may result in some degradation of reinforcement. They suggest that hot compaction is advisable in order to circumvent this problem, with the added advantage of improving the interface bond. Mixing of the two components has also been identified as a potential source of problems[29]. However in their comparison of powder and melt processed SiC/Al composites Arsenault and Wu[30] found that they could not produce a cast composite with the same degree of homogeneity and low porosity as a powder processed material.

2.3 Thermomechanical Processing

Much research has been conducted on material which has been thermomechanically worked, but little attention has been paid to the processing itself. Although the production of near net shapes is desirable, rolled and rod products will likely form the major volume of mmc materials. Only limited further processing may be applied to cast, fibre reinforced mmc's whereas extrusion, rolling and forging of discontinuous reinforced composites present a favorable method for production. Note, however, that rolling and extrusion of whiskers can result in a reduction of the aspect ratio by approximately twenty times in some cases[4].

2.3.1 Extrusion of Composites

The extrusion of aluminium alloys is modified by the presence of a reinforcement material[31]. Process parameters such as temperature to achieve breakthrough and flow stress are likely to be altered. Sun and Greenfield[31] have shown that during extrusion as the ratio increases so does the homogeneity of the final product. It is however noticeable that some banding of particles arises[32]. This banding can be eliminated by cross rolling after extrusion. Sun and Greenfield[31] showed that there is a region around a reinforcing particle which is less susceptible to deformation because of the particle's presence. They saw that the flow lines were interrupted by the particle, which in turn will reduce the intensity of any extrusion texture. However, it was observed that increased deformation leads to improved interfacial bonding between matrix and reinforcement. A corollary of this is that in some cases the use of predictive theory, which assumes a perfect bond, will be questionable.

The extrusion of composites may also be modified in another way. In unlubricated extrusion it will be realised that greater die wear will result from the extrusion of composites than would normally be encountered during the extrusion of

ordinary aluminium alloys[33]. Hains et al[33] identified a number of defects at the extrudate surface during extrusion trials. These were surface tearing and cracking and localized melting. Tearing was associated with low speeds, whilst surface cracking occurred at high speeds. Extensive die wear was also encountered. Whilst these observations are of interest, little was proposed in order to counter these defects. Obviously, the optimisation of extrusion speed could eliminate tearing and cracking. The reduction of die wear is more difficult: Hains et al[33] propose the use of cermet or ceramic materials, but the die shape could be modified to reduce friction (e.g. conical dies). Raghunathan et al[34] have identified the need for superior lubrication to that which would be required during extrusion of unreinforced alloys. Extrusion has been most commonly used as a secondary process after spray deposition[13] and powder processing[29,31,34].

2.3.2 Rolling of Composites

The rolling of composite strip is a common step after extrusion or certain melt techniques[21]. Hot rolling of particulate composites after squeeze casting (without intervening extrusion) had less effect on the final properties than extrusion[35]: the U.T.S. values were found to be 520 MPa and 580 MPa for rolled material and extrudate respectively. This was believed to be because the extrusion process resulted in a better alignment of fibres and less fibre breakage. Subsequent to extrusion, rolling is primarily employed to improve the homogeneity. Nieh and Karlak[32] have attempted to roll whisker composites rolling the material subsequent to extrusion and parallel to the extrusion direction. This resulted in some whisker damage. Divecha et al[36] were unable to produce any material when rolling whisker composites in the extrusion direction but gained satisfactory results when cross rolling. The work of Nieh and Karlak[32] showed a decrease in tensile and yield strength after rolling but an increase in fracture strain. The agreement between longitudinal and transverse properties was ascribed to whisker breakage, which may also explain the other variations. Humphreys[37] notes that there will be a lot of redundant deformation due to the presence of the particles and that local strain rates around the particles will be higher. This may account for the lower tensile properties, which would fail at a lower stress if the local strain rate is increased. Clearly this area requires more investigation in order to elucidate the effect of all of the variables.

2.3.3 Forging of Composites

A limited amount of investigation has been directed at forging composites. Miller and Humphreys[38] used forged product in order to conduct their investigations

but do not analyse the forging process itself. Hosking et al[18] used forging in order to further consolidate a cast composite ingot. In this case, the ingot was remelted at a superheat of approximately 50°C. Forging was carried out in a closed die at a pressure of around 200 MPa, the solidification of the product being completed in the die. This is a similar operation to squeeze casting, and resulted in a lower degree of porosity than was observed in the original cast billet. However, the length of time at high temperature resulted in undesirable interface reactions; these will be discussed in section 2.5.1. It was also noted that any agglomeration of the reinforcing medium in the initial cast billet remained in the forged product, even with agitation of the melt just prior to forging. This shows the importance of the initial mixing in determining the homogeneity of the product.

2.4 Types of Reinforcement

In the early 1960s carbon and boron continuous fibres, as well as tungsten wire, were used to reinforce various matrix materials. Since then both reinforcement and method of manufacture have developed considerably. The competition between continuous fibres, whiskers and particles is intense, with each type of reinforcement offering different advantages. The choice of reinforcement type may be dictated by the required properties, available production methods, alloy material or cost. There are three main classes of reinforcement utilised today. These general classes will be reviewed first, followed by a review of specific reinforcement interactions with matrix materials.

2.4.1 Continuous Fibres

There are two distinct classes of continuous fibre[1]. Those used as monofilament are of 100-200 mm in diameter and are usually manufactured by chemical vapour deposition, this process ideally resulting in a uniform, near defect free fibre. Bunched or multifilament products have diameters of between 5-20 mm and may be manufactured by pyrolysis of rice hulls. Continuous fibres have the advantage of being pre-formable thus lending themselves to composite production by melt infiltration. Materials which lend themselves to continuous fibre production are carbon, boron, silicon carbide, alumina; fibres may be made from these elements alone but are often combinations of them. 'Borsic' is a combination of boron and silicon carbide[5]; 'Nicalon' is a nickel coated silicon carbide fibre[6] and 'Avco' SCS-2 is a silicon carbide fibre coated with carbon[8]. These coatings are designed to limit the reaction between fibre and matrix alloy. Composites of all continuous fibre types have unidirectional properties.

Feest[1] notes that the quality of fibres is continually improving, which should benefit the performance of the composite.

2.4.2 Discontinuous Fibres

Short discontinuous fibres or whiskers are able to meet the load bearing requirements of longer continuous fibres and their manufacture is attractively cheaper. Whiskers of β-SiC may be produced from otherwise useless rice hulls. The whiskers are hexagonal in cross section due to the <111> growth direction and are less brittle than α-SiC[36]. Diameters range from 0.2-1 mm. Short alumina fibres such as 'Saffil' and 'Saffimax' (both I.C.I. trade names)[5] are useful for high temperature applications, especially where resistance to thermal fatigue is required due to their low coefficient of thermal expansion. Short fibres may also be combined by melt infiltration if a binder is used to initially bond the structure. It is also possible to include short fibres by casting[9] and powder methods[9,25,36].

2.4.3 Particulate Reinforcement

The use of particulate types of reinforcement has increased in popularity, mainly because of the cheapness of production when compared to fibres. Particulate materials such as SiC and alumina are currently employed predominantly in order to increase the modulus of aluminium alloys[4], although there is scope for much wider use. Particles do not have the same load bearing capacity as whiskers or continuous fibres but present fewer problems at the fabrication stage. Furthermore the properties of particulate reinforced composites are less directional, as might be expected. Also manufactured from rice hulls[36], silicon carbide particles are thus cheap to produce. Alumina is another particulate alternative. Particles especially lend themselves to incorporation into the matrix by powder, spray or casting methods[5,6,12].

2.5 Influence of Reinforcement on Matrix Microstructure

2.5.1 Interfaces in MMCs

The interface between matrix alloy and reinforcement is crucial to the characteristics displayed by the composite. There are two ways in which this interface can influence the composite's behaviour: the coherency of the bond will directly relate to mechanical properties, such as U.T.S., modulus and fracture toughness, by the amount of load transfer and stress concentration; the presence of the reinforcement

may cause microstructural changes which would not normally occur[39] and will also influence the properties. The type of interface is influenced by the process route. Melt routes provide the possibility of interface reactions, contributing to, or detracting from, the bond strength; powder methods provide a purely mechanical bond whereas spray techniques may fall somewhere between the two. In the case of continuous fibres a strong, coherent interface is essential if load is to be borne by the fibres. Likewise, for particles to exert an effect on the stiffness of a material a good bond must exist.

Of prime consideration when considering any melt route is the wettability of the ceramic fibre or particle by the molten aluminium alloy. Most ceramic fibres are adequately wettable by aluminium[4] but the presence of Al_2O_3 reduces wetting[8]. Pressure increases the tendency to wet and overcome capillary effects. Friction due to the viscosity of the melt will increase the pressure required to infiltrate a bundle of fibres[8].

Interface reaction which occurs during the production of composites by melt routes is a problem area. Many interface reactions are considered to be detrimental and it is to this end that designer fibres, such as 'Nicalon' and 'Avco' SCS-2, are produced to resist destructive chemical attack. However it is plain that some kind of bond must exist between reinforcement and matrix to enable load transfer[40]. In the case of the 'Avco' fibre a sacrificial layer of carbon doped with silicon is used. This has no effect on the properties of the composite[8]. In the case of carbon fibres Al_4C_3 was believed to form at temperatures in excess of 500°C[8]. Arsenault and Pande[40] found no evidence of Al_4C_3 in an Al/SiC composite, but reported the presence of a diffused layer of aluminium instead. However, in a recent examination of melt and powder routes by thermal and metallographic techniques, Bienvenu et al[41] did observe Al_4C_3 formation in commercially pure (1050) aluminium reinforced with 'Nicalon'. This was accompanied by a rise in the silicon content of the matrix. Their experiments also revealed that interface reaction only occurred in the powder system (7090 reinforced with 25%, 5μm particulate silicon carbide) when a significant amount of liquid was present, at temperatures above 600°C- above usual processing temperatures for P.M. materials. On this basis they recommended that the P.M. product should not be hot pressed above the alloy solidus of 548°C and that cast material should solidify in less than two minutes.

Examination of other systems, eg. LM10/Saffil by Fox and Flower[42], has shown clearly the existence of a reaction zone with penetration of magnesium into the Saffil. Despite providing a good bond the strength of the matrix may be reduced because of the denuding of the alloy of magnesium, the major contributor to precipitation hardening

during working. Kimura et al[43] note that silicon additions to the matrix alloy lead to reduced interface reactions and that additions of indium, lead and thallium improve wettability by reducing the surface tension. These additions are not always practicable. As was noted in section 2.2.2 reactions at the reinforcement/matrix interface may give rise to spinel structures[18]. These apparently did not detract from the mechanical properties of the composite.

Erturk et al[44] have investigated the dichotomy at the heart of mmc development- the need for low bond strength for good toughness and high bond strength for good tensile properties. Their investigation resulted in the proposal of a 'bimaterial' fibre. Also observed was that improved wettability benefited the transverse properties.

Cooling of composites by quenching will introduce internal stresses in the material due to the large difference in thermal expansion coefficient between aluminium and silicon carbide (or any metal/ceramic system): in the case of Al/SiC, the ratio of the coefficients is about 10:1[45]. These stresses are relieved primarily by dislocation generation, evidence for which is abundant[45,46,47,48]. Thermal strain at the SiC/Al interface introduced after extrusion was seen to increase the dislocation density at the interface which, in turn, is expected to influence the ageing behaviour and mechanical properties[45]. The difference in thermal expansion coefficient may also result in some internal stress remaining after dislocation generation has relieved the majority[37]. The difference in thermal expansion coefficient between aluminium and alumina is not nearly as great, at 4:1[6].

Composite ageing times were observed to have reduced to 1/3 the value for unreinforced material. However, it has been shown that the increased dislocation density does not increase the precipitate concentration or create a precipitate free zone at the matrix/particle interface[46]. Previously it had been shown that the S' precipitates were heterogeneously distributed in the matrix[23] (which was 2124: Al-Cu-Mg) but Christman and Suresh[46] show that this observation was based on an overaged structure.

The investigations of Marcus et al[49] have resulted in the characterisation of interfaces and the manipulation of failure modes in aluminium-graphite, both by electrical means. This, like the work of Erturk et al[44] suggests the possibility of tailoring interfaces.

2.5.2 Ageing Response of Matrix Materials in Composite Systems.

Interest in the way in which reinforcing particles modify the ageing response of matrix materials is a natural progression. There are two important questions that have yet to be answered satisfactorily:

(i) how does the particle affect the ageing- does ageing response vary with particle size, type, volume fraction?

(ii) why does the particle modify the ageing response of the matrix?

The lack of a definitive answer is believed to be due to the large range of investigation and the fact that interest may initially have been limited to what is commercially expedient.

Many authors note the bare fact that the addition of ceramic particles to an age hardenable system results in the reduction of ageing time, often to between a third and a half of the time required for the parent alloy[50], which in this case was 6061. However, there is still some contention over this effect- Stephens et al[51] found the ageing response unaffected in their examination of A356 (an Al- 7Si-0.35Mg casting alloy) reinforced with between 25 and 30% of 30 or 100μm SiC. They ascribed this to the large SiC particle size. This is consistent with the explanation offered by Arsenault and Shi[39] who, amongst others, attribute the rapidity of ageing to the high dislocation density generated by the large difference in thermal expansion coefficients between matrix and filler; the amount of dislocations thus generated is inversely proportional to the particle size[39]. Taya and Arsenault[6] show the calculated dislocation densities for varying particle size. This theory also indicates that the dislocation density is proportional to the volume fraction of particles; this is also demonstrated by Taya and Arsenault[6]. In an attempt to discern the effect of interface reactions on the ageing of composites, Ribes and Suéry[52] compared composites of Al-7% Si-0.3%Mg containing SiC which had been deliberately oxidised with material containing untreated SiC. They found the ageing response of the oxidised-SiC composite curtailed, probably because of magnesium depletion from the alloy to the oxide. The material containing the un-oxidised SiC exhibited a higher rate of ageing than the unreinforced material. They concluded that although the ageing process is accelerated by the presence of the SiC, the nature of the interface will have some effect on this acceleration. This observation may be important when considering the ageing response of cast composites which are likely to have some reaction product at the SiC/matrix interface because of the time spent at high temperature. Furthermore, the results of Stephens et al[51] described above may have been influenced by the same effect (the alloy compositions in both studies are

nearly identical). However, it is difficult to compare the amount of interface reaction in each study.

Although these workers offer a reason for the accelerated ageing the best demonstrations of the effect are given by Petty-Galis and Goolsby[53] and Hunt et al[54] who have respectively examined silicon carbide reinforced 7091 and 8090 by differential scanning calorimetric (D.S.C.) methods. Both sets of research show the modification of the ageing process by the introduction of reinforcement. In each case, the suppression of part of the precipitation reaction is observed. This is attributed to increased dislocation density, but little structural evidence is presented to directly support this.

2.6 Influence of Particulate Reinforcement on Mechanical Properties

The introduction of particles into an alloy is bound to produce a mechanical response which is different to either of the component materials. This section will concentrate on the influence of particulate reinforcement on mechanical properties; this influence will be governed by particle size, volume fraction and type. There is little codified work on the effect of these parameters- this section will attempt to split these parameters as much as is possible or expedient.

2.6.1 Tensile Strength

McDanels[25] and Webster[55], among others[32,36], have found that the yield and tensile strengths increase with increasing reinforcement content, up to a certain point. It was proposed that there is a limit to the amount of strength increase which is governed by the point at which there is no longer enough matrix to redistribute the stress concentration. Thus the material is not able to achieve its potential strength. Taya and Arsenault[6], however, produce evidence to show that the strength of a composite may decrease with increasing volume fraction; this was attributed to chemical attack of the fibre surface.

McDanels and Hoffman[56] appear to be alone in codifying data on the effect of whiskers, particles and nodules of SiC and their influence on strength. The shape of these three reinforcement types is distinctly different: whiskers have a high aspect ratio, whereas nodules and particles have an aspect ratio approaching unity. Nodules have a surface characterised by a large number of projecting asperities; particles are smoother, although both types may have either acicular or near spherical morphology. McDanels and Hoffman[56] observed that whiskers and particles produced similar yield

and tensile strengths whereas nodules reduced these values by about 10%. Divecha et al[36] have reported mechanical properties of 2024 with various proportions of whiskers in the reinforcing material. Work on 20%whiskers/80% particles in a number of volume fractions revealed strength increases lower than expected. This was traced to whisker damage on rolling and may account for the similar tensile and yield strengths observed by McDanels[25]. Bayoumi and Suéry[57] record an increase in proof stress as volume fraction increases for a given particle size. Again, particle size is linked to this effect: as smaller particles have a higher tendency to agglomerate the increases in strength will be lower than anticipated. Miller and Humphreys[38] also show an increase in 0.2% proof stress as volume fraction is increased. It is noticeable from this work that these increases are less pronounced as particle size increases. Miller and Humphreys further record that the volume fraction of particles has a larger effect than is solely due to particle strengthening by load transfer. Increasing volume fraction may also influence the number of thermal mismatch dislocations, the grain size strengthening, residual stresses and the contribution due to work hardening. The equation developed by Arsenault and Shi[39] for dislocation generation due to thermal mismatch also includes a volume fraction term.

The influence of particle size on strength has not been fully investigated by any one worker. As a result of this there are a number of contradictory observations and proposed theories, none of which is satisfactory except in the limited range over which the investigation was carried out.

Particle size is believed to influence the strength of a composite by the introduction of dislocations due to thermal mismatch. Arsenault and Shi[39] give an equation relating this increase to particle dimensions and show some evidence to support this view. However, as only two data points are provided to demonstrate the fit to the theoretical curve, this result must be treated with caution. Miller and Humphreys[38] demonstrate more conclusively the influence of particle size on the strength of commercially pure aluminium (alloy 1050). They showed that the 0.2% proof stress of material of varying volume fraction increased with particle size at high volume fractions, although there was some discrepancy at low fractions. Humphreys suggests in an earlier publication[37] that the smaller particles (a few microns or sub-micron size) may have an appreciable Orowan strengthening term associated with them, but this is countered by the fact that most particles reside at grain boundaries. Bayoumi and Suéry[57] found a slightly different effect of particle size in their investigation of Al-7Si/SiC composites. Their experiments showed an increase in proof stress up to a critical particle size, in the range 7μm to 30μm, after which the strength decreased. This critical size was observed to increase on increasing volume

fraction. The inference drawn is that the proof stress is controlled by the inter-particle spacing, and that agglomeration has a greater effect on strength of small particle composites than it does in composites containing large particles. In comparing aged and solutionised material, it is seen that smaller particles give a greater increase in proof strength. Nardonne and Prewo[58], supported by Jones et al[59], believe that the strength is not proportional to particle size as long as the aspect ratio remains constant. Clearly there is a need to codify this data under a composite strengthening theory which considers all particle sizes.

2.6.2 Modulus

Improvement in modulus is the biggest benefit to be gained from the reinforcement of materials. Values of up to 70% over the unreinforced aluminium alloy have been quoted[4]. A composite's modulus has been shown to increase as the amount of reinforcement is increased although not in a linear manner[25]. The material's stiffness appears to be governed solely by the volume fraction of reinforcement and has no relationship with its morphology or the matrix type[25] (within the broad class of aluminium matrix alloys). Although modulus improvements have been shown to be high, the spread of data is large. Nieh and Chellman[26] report values obtained for aluminium matrix composites by other workers varying over a range of approximately 30 GPa. They thought that these variations may be due to inhomogeneities in the composite structure or differing test methods. It is possible that they may have been due to improved processing, the factor McDanels[25] uses to explain increased ductility. During their work Nieh and Chellman[26] also encountered hysterisis in the load/unload cycling. This they put down to elastic strain associated with some heterogeneity at the fibre/alloy interface.

2.6.3 Fracture toughness

Values for composite fracture toughness are considerably lower than the unreinforced material. Results for 15% SiC in 2024, 6061 and 5456 are quoted as 15, 30 and 17 $MNm^{-3/2}$ respectively[60]. It has been shown by Crowe et al[27] that fracture toughness is dependent on the reciprocal of the projected area of reinforcement in the plane of cracking. From this it is inferred that fracture toughness can be controlled by varying the reinforcement type, size, shape and distribution.

As would be anticipated the K_{IC} is observed to fall as volume fraction is increased[6,36]. As with particle size this occurs because of the influence of volume fraction on inter-particle spacing. Taya and Arsenault[6] say that the stored elastic

energy increases with increasing volume fraction, thus aiding failure. They also note that the overall elastic energy is zero (matrix in tension, particles in compression) and that the particles do not take part in the fracture process. This is a generalisation which has been shown to be incorrect in some cases[61,62] and will be discussed in section 2.6.5. It would seem, however, that the aforementioned stress distribution due to the reinforcing particles should have an influence on the fracture toughness.

The expectation that particle size will have a major influence on the fracture toughness of a composite can be inferred from the concept of the process zone in fracture mechanics. This relates the attaining of a critical stress for failure to microstructural features within a region adjacent to the crack tip. Flom and Arsenault[63] demonstrate the influence of size on the fracture toughness of which there appear to be two regions: up to 20μm the K_{IC} value is approximately constant with particle size; at 250μm the K_{IC} is substantially decreased. This seems to be at odds with the findings of some workers[61], who note that particle cracking is prevalent in two different (one 2xxx and one 7xxx series alloy) composite systems with particles of the same size. The theory governing the prediction of fracture toughness of composites has grown from considerations of two phase alloy fracture. The particle size is intimately linked to the particle volume fraction by virtue of the equation governing the particle spacing, for which there are a number of similar expressions[6,51]. For example, the spacing, s, is related to particle size, d, and volume fraction, Vf, thus:

$$s = 0.77.d.V_f^{-1/2} \quad \text{.....2.1}$$

Arsenault[6] quotes an equation relating particle spacing to K_{IC} as follows:

$$K_{IC}=[\sigma y.\epsilon^*_f.E.f(n)]^{1/2}.s^{1/2} \quad \text{.....2.2}$$

where σy is the yield stress of the composite, ϵ^*_f, the strain to failure, E, the modulus and n, the work hardening exponent. It is plain that this equation predicts that fracture toughness increases with particle size, which is contrary to evidence presented by Flom and Arsenault[63]. They found that toughness was approximately constant up to a particle size of 20μm, after which a test using a particle size of 250μm yielded a lower toughness. The constant value of fracture toughness in the lower region is explained[6] by the fact that elastic stored energy is constant with particle size, being solely dependent on volume fraction; the drop at a particle size of 250μm was attributed to "premature cracking" of the SiC. It is unclear whether the authors mean to imply that the toughness would have remained constant had this cracking not occurred,

however, the very occurrence of these cracks is of note. Contrary to this work, Stephens et al[51] report an increase in fracture toughness with particle size: they investigated both silicon carbide and boron carbide in A356/7 alloy (Al-7Si), and found increases of 2-3 MPa/m$^{-1/2}$ between 30μm and 100μm particles. This is not explained, but is consistent with the equations above. However, it should be noted that the sparsity of the range of data makes any comparison of experiment with theory difficult; likewise any conclusions drawn must be tentative.

2.6.4 Ductility

The low ductility and fracture toughness of composites are the major factors which obstruct the widespread use of such materials in more engineering applications. Elongations of 0.005-0.011% have been reported for 15% discontinuous SiC in 2024 and 6061 alloys in the as extruded and extruded and rolled conditions[60]. Matrix type and volume fraction of reinforcement are evidently important in determining the strain to failure[32]. Bayoumi and Suéry[57] found that ductility decreased considerably as volume fraction was increased. The only way in which ductility may be achieved is through plastic flow in the matrix, due to the very low failure strain of the reinforcement. As reinforcement content increases, the amount of matrix material able to accommodate the strain decreases. Hot rolling after extrusion may increase the ductility[32]. This is probably because the homogeneity is improved and porosity and inclusions are reduced[25]. It is interesting to note that as time progresses the values reported for the failure strain increase. In 1979 Divecha and Fishman[60] reported sub-1% elongations whereas in 1985 McDanels[25] reported elongations of between 6% and 12% for 10-15% SiC in 6061. He links this rise to improved mixing and cleaner, more uniform aluminium powders.

The ductility of m.m.c.s can be connected with the fractography of a failed specimen in much the same way as was considered for fracture toughness. The morphology of the matrix fracture surface changes from dimple, through a transition stage, to cleavage type failure as volume fraction of reinforcement is increased[25,64,65]. Manoharan and Lewandowski[61] note that the dimple size is approximately the same as the particle size in some failed 2xxx series composites and that this implies a low ductility.

Bayoumi and Suéry[57] note that the ductility increases slightly with increasing particle size. Conversely Stephens et al[51] recorded a decrease in ductility as particle size was increased from 30μm to 100μm. Hosking et al[18] report that ductility is

independent of particle size. Clearly there is a need here for some basic investigative work.

2.6.5 Microstructural Characterisation of Failure

At this point it would seem expedient to discuss the ties between microstructure and composite failure. It has already been noted that the failure of composites can be linked with the microstructural features of the material. These include both matrix and reinforcement variables such as heat treatment, sub-grain size and particle size, type, shape and volume fraction. The effect of these features have been examined to varying degrees and the observations are outlined below.

On fracture, composite materials may exhibit ductile and brittle characteristics of fracture depending on a number of parameters. These may include orientation and volume fraction (local and total) of reinforcement, strain rate on fracture and the degree of integrity of the matrix reinforcement bond[60]. Many workers note the presence of dimples at a fracture surface and it has been demonstrated that as reinforcement content increases in alloy 6061 the tensile fracture surface changes from a fine dimple morphology to a brittle like granular morphology with a coarsening of the dimples[25]. This indicates the presence of both fracture modes. Flom and Arsenault[63] found that the fracture is confined to a narrow path with little or no damage to microstructure adjacent to the fracture surface. They postulate that fracture proceeds by the interlinking of micro cracks which develop in front of previous growth.

The relationship between the microstructure of m.m.c.s and the fracture process, whether in tension, bending or impact, has been little researched until fairly recently and is even less understood. Chermant and Coster[66] have presented a review on the establishment of such a relationship but experimental work has lagged behind. King[62] has presented a summary of failure in particulate m.m.c.s but does not fully investigate the relations she draws. She notes that decohesion of the particle/matrix interface is promoted by weak interfaces (such as those which have undergone reactions); particle cracking is due to a high strength matrix and/or coarse particles; and that failure proceeding through the matrix only is promoted by strong interfaces and high modulus particles. The first two of these observations are most likely to apply to powder materials.

Crowe et al[27] established a relationship between fracture toughness and dimple height at the fracture surface of the form:

$$K_{IC} = f(h^{0.5}) \quad \text{.....2.3}$$

This, however, implies a ductile matrix with low reinforcement content: as McDanels notes, dimples do not always occur[25]. Jones et al[59] have taken this work further by relating dimple height to a calculated value for particle spacing using Goods and Brown's[67] work on prediction of cavity nucleation strain in the Fe-Fe_3C system. Full experimental proof of this relationship has yet to be established.

2.6.6 Elevated Temperature Properties

Nair et al[4] state that the temperature dependence of U.T.S. and yield strength of composites follows that of the matrix but still remains higher. Bayoumi and Suéry[57] show that in aluminium silicon casting alloys the composite strength decreases to values close to that of the matrix at elevated temperatures. Raghunathan et al[68] show that the tensile properties of an Al-Fe-Ce composite decrease in a similar manner. In the Al-Fe-Ce system the ductility was increased over the room temperature value. Humphreys[37] demonstrated that the ductility does not increase until about 200°C and that above 500°C it decreases. Bayoumi and Suéry[57] found a similar, though less pronounced, effect between ambient temperature and 300°C. Wu and Sherby[69] showed that composites can exhibit superplastic behaviour, their test specimen failing at 300% elongation during thermal cycles between 100 and 450°C. These examinations show that composites have a questionable advantage over matrix materials at high temperatures, but data on high temperature testing is limited and any conclusions drawn must reflect this.

2.6.7 Creep

Webster[55] in his study of lithium containing alloy composites also gathered data on 6061 and 2024 composites under creep conditions and found their creep resistance to be similar to the matrices. Lilholt and Taya[70] show that composites of 2124 including 15% and 25% SiC_w have improved creep strength compared to the matrix but the stress sensitivity of the creep rate is greater than that of the matrix. This is thought to be due to the interaction between the fibres and the precipitation process. Work conducted to date is limited, but it is clear from these results that an investigation of the mechanisms of composite creep is required in order to fully explain the observations in discrete systems.

2.6.8 Compressive and Shear Strength

Little work has been done on the compressive and shear properties of composites. Divecha et al[36] found improved compressive strengths for 2024 reinforced with 20% and 25% SiC. Shear strength was found to be 30% higher than that of the unreinforced material. Bayoumi and Suéry[57] have shown that the differences between tensile and compressive properties can be analysed in terms of micro and macro residual stresses. Specimens tested after solution treating only showed a compressive yield stress which was slightly lower than the tensile yield stress, and the opposite behaviour to the unreinforced matrix and the aged composites. Bayoumi and Suéry[57] suggest that the internal compressive stresses which build up in the particle are relieved during ageing but contribute to the failure of the solutionised material. In compression, these stresses will act in a manner so as to advance failure, whereas in tension they will resist failure. This implies that the fracture of the particles is the limiting factor in failure, which may be correct in this instance but, as has been noted earlier for composites under tensile loading, it is unclear whether this will always be the case. This is dependent on the relative particle/matrix strength and bonding as described by King[62]. There is a need for more work on the behaviour of composites in compression in order to elucidate the effect of these factors.

2.7 Matrix Materials Utilised in Composite Production

There are three main classes of potential matrix materials for aluminium composite production: various grades of pure aluminium; non heat-treatable alloys, which gain their strength from solid solution strengthening and grain boundary effects; heat treatable alloys which gain strength from the formation of precipitates. Such alloys of aluminium are already well proved in their own right, and thus offer an excellent starting point from which to build and assess composite materials. However, there are few systematic examinations of the effect of adding reinforcing particles to alloys of aluminium and until recently little thought has been given to the rôle of the matrix material, or the tailoring of the matrix material to composite usage. Whilst this thesis does not pretend to have wholly accomplished this, it is an important aspect of the behaviour of composite materials, and as such a review of matrix materials used to date is expedient.

McDanels[25] was among the first to explicitly record the influence of matrix materials on tensile properties. He states that the most important factor influencing the yield and ultimate tensile strengths is the matrix material and its heat treatment condition. Three heat treatable matrices were examined, along with one non heat

treatable matrix. The alloys 2124, 6061 and 7075 were the heat treatable materials, deriving their strength from precipitation in the Al-Cu-Mn, Al-Mg-Si and Al-Zn-Mg-Cu systems respectively; 5083 was the non heat treatable alloy used whose composition is in the Al-Mg group. It was observed that the lower strength matrix materials gained a higher increase in strength than did those with initially high strength. Increases of approximately 30% were achieved for the 6061 composite containing 20% of SiC whiskers whilst its 7075 counterpart gained less than 10% in U.T.S. This is further borne out by the work of Nieh and Chellman[26] who record up to 100% increases in strength for commercial purity aluminium, but much lower increases for initially stronger alloys. The reason for this disparity in strength increases is probably two-fold. The introduction of ceramic particles severely limits the ductility of the material[4,25,26], which in turn may result in the curtailing of the stress/strain curve before plastic flow has been reached: the material fails at the 'ultimate tensile strength' due to the lack of ductility required to maintain plastic flow[25]. Materials such as C.P. aluminium have sufficient residual ductility and thus gain the full benefit from the introduction of reinforcement. It is also obvious that the development of heat treatments specifically designed for composites is necessary[4].

Although the modulus of composite materials is unaffected by matrix heat treatment, it obviously is influenced by the matrix material to a small extent. However, much more influential is the volume fraction of reinforcement[4].

The selection of matrix material has often been based on very loose criteria. A prime influence has been the ease of production of the composite via a pre-determined route. Casting alloys employed include Al-7Si[51,57] and Al-4.6Cu[18], Al-5Si-2Fe[15]. Wrought alloys used include those detailed above. In choosing any alloy for incorporation into a composite system, many authors, it seems, have based their selection on this criterion rather than having first examined the required properties and then sought an alloy and a production process. There are two notable exceptions to this way of thinking. Humphreys, alone[37] and working with Miller[38], has examined commercial purity aluminium composites in order to establish the strengthening mechanisms operating in such materials. A few workers[29,54,71] have chosen the Al-Li alloy 8090 as a candidate matrix material because of its low density, which may lead to high specific properties. This alloy has the advantage of being able to be powder processed, but Al-Li alloys are also notable for low fracture toughness and ductility values.

The information presented in this section suggests that there are a number of properties which are dependent upon the matrix type. The most important of these is

yield stress- the work of McDanels[25] and Nieh and Chellman[26] show that even with the larger increases in strength found for the weaker matrix materials, the highest yield stress is still obtained with the strongest matrix. Ultimate tensile stress behaves in the same way. Ductility of the matrix is also important in determining the ductility of the composite- C.P. composites have a higher ductility[26] than composites of other, age hardenable, alloys[26,25]. For example, a composite of 1100/9% SiC (whiskers) was found to have a failure strain of 16%, a composite of 2124/13% SiC (whiskers), a failure strain of 4.1% in the T6 condition. As was noted above, modulus is dependent upon reinforcement volume fraction alone, within the same group of alloys. Specific properties have also been shown to be able to be controlled by the matrix density.

3. THEORY

3.1 Introduction

This chapter concentrates on the theories which have been developed for composite strengthening but also includes sections on the mixing of powders and precipitation in aluminium alloys. The inclusion of the latter two sections was thought important in terms of the specific details of this research and as such were deemed inappropriate for inclusion in the literature survey.

3.2 Theory of Composite Stress/Strain Behaviour

The reinforcement of an alloy by a continuous fibre is significantly different to the reinforcing effect of a discontinuous fibre or particle but it is expedient to review theories of both in order to gain an appreciation of the problems involved. The theory as applied to particulate composites is similar to, and often derived directly from, short fibre composite theory. This section will first consider continuous fibre composites and then discontinuous composites. The sub-sections will deal with the main mechanical properties.

There are a number of assumptions which should be considered before accepting the validity of the theory as applied to continuous and short fibre composites. The most important is that there is a perfect bond between the fibre and the matrix. If this is allowed then load transfer may take place at its maximum efficiency. In some cases this assumption is obviously invalid- it has already been noted in section 2.5.1 that variables such as processing route and heat treatment can affect the bond. For a perfect bond the interface must also be infinitely thin- this is again invalidated by chemical reactions at the interface. A third assumption is that the matrix material close to the reinforcement must have the same properties as the bulk matrix. This too may be untrue in reality because of interactions between the reinforcement and the matrix[39]. A further assumption is that both components of the system behave as elastic materials and are under equal strain for the purpose of the analysis. This may also be incorrect and is dependent on bond strength (which governs stress and strain transfer to the reinforcement) and orientation of fibres to the applied load. However, the orientation effect is readily corrected for, as is shown below. Furthermore, this assumption is only valid in the elastic region of the stress/strain curve. The final assumption is that the reinforcement is distributed in a regular array. Agglomeration and/or porosity, and the method of production, especially in discontinuously reinforced materials, may lead to the break down of this assumption.

3.2.1 Modulus of Composites

The volume fraction of each component is most important in determining the modulus of a composite. A simple approximation of the longitudinal modulus of continuous fibre composites may be expressed in the law of mixtures:

$$E_c = E_f V_f + E_m(1-V_f) \quad \text{.....3.1}$$

For loading normal to the fibre direction the modulus is given by the 'parallel model':

$$E_c = E_f E_m/(E_f(\ 1-V_f\ ) + E_m V_f) \quad \text{.....3.2}$$

where E_c is the composite modulus;

E_f, E_m are the modulus of the fibre and matrix, respectively;

V_f is the volume fraction of reinforcement.

These formulae are the upper and lower bound solutions for the modulus respectively. Both neglect Poisson contraction.

The introduction of short instead of continuous fibres into an alloy means that effects at the fibre ends must also be considered. In this case both shear and tensile stresses are acting on the fibre.

Cox[72], and Tsai and Halpin (see reference 73) have proposed equations which predict the modulus of a discontinuous reinforced composite. Both of these equations take into consideration the aspect ratio of a fibre and the effect of shear at the fibre ends. Cox simply included a 'length correction factor' in the law of mixtures equation, giving:

$$E_c = \eta E_f V_f + E_m(1-V_f\ ) \quad \text{.....3.3}$$

where η is defined as:

$$\eta = 1-\{(\tanh 0.5Z.l)/0.5Z.l\} \quad \text{.....3.4}$$

and

$$Z = \{2\mu_m/E_f.r^2.\ln(R/r)\}^{0.5} \quad \text{.....3.5}$$

where μ_m is the shear modulus of the matrix

2R is the inter-fibre spacing

r is the fibre diameter, and

l is the fibre length.

The term η can also be arrived at by combining equations 3.1 and 3.3 and assuming that the fibre modulus is much greater than the matrix modulus: this results in the relationship

$$\eta = E_{short} / E_{continuous} \quad \text{.....3.6}$$

It is also possible to include an orientation factor in these equations in order to account for non-aligned fibre distributions. Tsai and Halpin's model[73] is similarly complex, the general equation being:

$$E_c = E_m(1 + C_l n V_f) / (1 - n V_f) \quad \text{.....3.7}$$

The terms C_l and n are defined as

$$C_l = 2s + 40V_f^{10} \quad \text{.....3.8}$$

$$n = (E_f/E_m - 1)/ (E_f/E_m + C_l) \quad \text{.....3.9}$$

where s is the aspect ratio of the fibres.

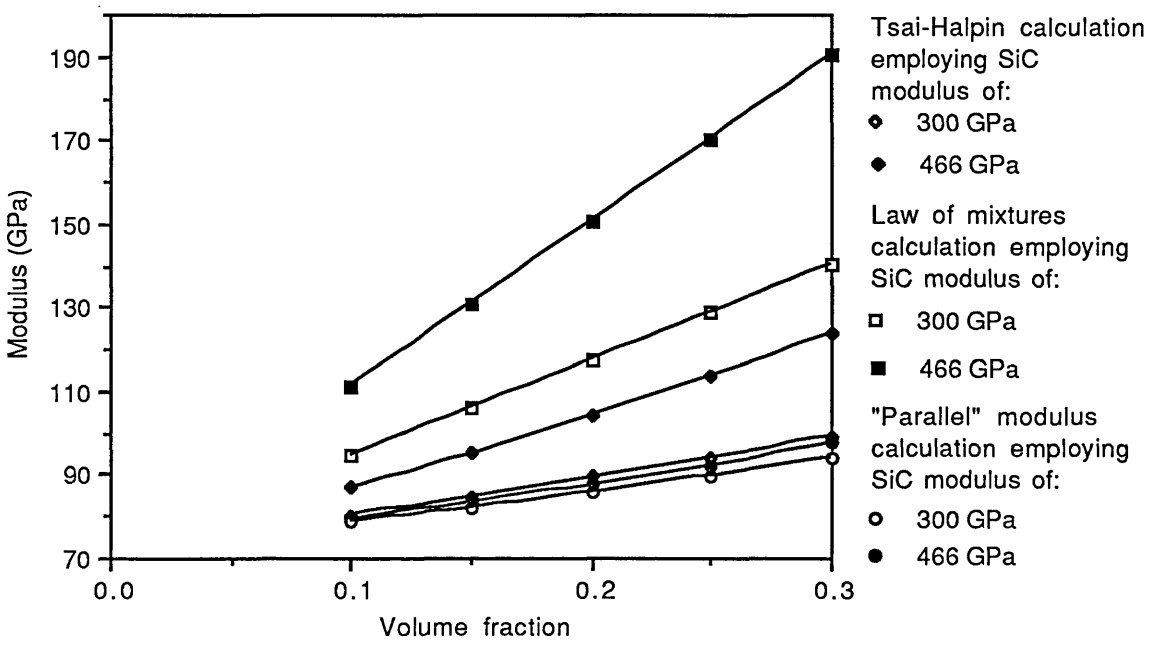

Figure 3.1: Comparison of modulus predictions by various methods.

Figure 3.1 shows a comparison of predictions using equations 3.1, 3.2 and 3.7. It can be seen from this figure that the law of mixtures and the parallel model predictions represent the upper and lower bound theories. Two different SiC modulus values- 300 GPa[74] and 466 GPa[6,26]- have been used in each case in order to show the range of possible predicted values within one model. A single modulus value of 72.9

GPa[75] was used for the matrix modulus. It is important to note that equations 3.1 and 3.6 are iso-strain equations whereas equation 3.2 is based on iso-stress behaviour. Cox's model has been excluded from this comparison because of the reliance on fibre length in the equation, but it has been shown[73] for a number of example materials that as the fibre length increases, the modulus approaches the upper bound law of mixture value. This is to be expected as the fibre end effects become less significant.

The fit of the law of mixtures model to experimental data is quite good for continuous fibres[73], provided that the modulus of the fibres is accurately known. The fit of the parallel model in the transverse direction is also good[73], provided that the fibre/matrix bond is good and the fibres are all aligned. The Tsai-Halpin equation has yet to be fully tested against a wide range of experimental data.

No simple formula for modulus prediction has been developed for particulate composites. At best, estimates may be made from the the previous formulae for discontinuous composites. Here, the aspect ratio would be unity. This still proves unsatisfactory as many of the above equations emphasise the importance of the aspect ratio and minimise the influence of volume fraction. Complex equations have been developed based on the work of Eshelby (see, eg., reference 6).

3.2.2 Tensile Strength

As in the case of modulus, several equations are available for the prediction of the tensile properties of composites based on a knowledge of the properties of the component materials.

The strength of a continuous fibre composite involves a more complex analysis as, for the reinforcement to be beneficial, the volume fraction of fibres must exceed a critical value at which the composite strength reaches the matrix strength (fig.3.2). In the region of the curve between $V_f=0$ and $V_f = V_{min}$, the fibres will be rapidly stressed to failure because there will be an insufficient number to restrict matrix elongation. The initial decrease in strength is therefore due to a decrease in the volume of matrix available to support the applied load. As the volume fraction of fibres is increased there comes a point at which there is sufficient reinforcement to counteract this effect and support load. In this case, the failure strain is equal to the failure strain of the fibres: the matrix also fails at this strain because there is now insufficient matrix to support the load. As the volume fraction of fibres is increased further, the strength of the composite follows the relationship given below as equation 3.10. This analysis assumes that the fibre is more brittle than the matrix which is always the case in practical reinforcement of aluminium.

$$\sigma_c = \sigma_f.V_f + \sigma'_m.(1 - V_f) \quad \text{.....3.10}$$

where σ_f, is the fibre U.T.S.

V_f, the volume fraction of fibres, and

σ'_m, the flow stress of the matrix at a strain equal to the failure strain of the fibre.

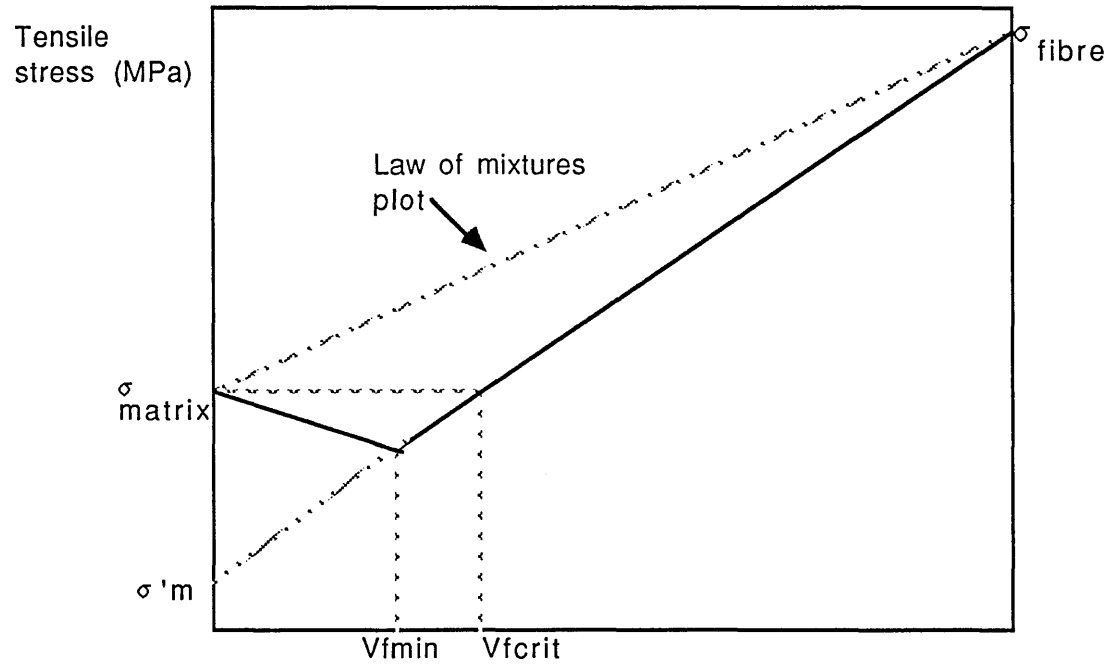

Figure 3.2: Stress against volume fraction for a continuously reinforced composite (after Dieter[76])

For the 'useful' case (as shown in figure 3.2) the composite U.T.S. must exceed the matrix U.T.S. and thus the critical volume fraction which must therefore also be exceeded is given by:

$$V_f crit = (\sigma_m - \sigma'_m)/(\sigma_f - \sigma'_m) \quad \text{.....3.11}$$

where σ_m is the U.T.S. of the matrix.

Figure 3.2 also shows the law of mixtures prediction of tensile strength, which over-estimates the strength of the composite.

The length of short fibres is critical in their strengthening action. As with the analysis for modulus, the theory is based on the 'shear lag' concept with the same assumptions. The average stress on a fibre is less than the maximum stress a fibre can support, for any fibre length greater than the critical length.

$$\sigma'_f = \sigma_f\ (1-l_c/2l) \quad \text{.....3.12}$$

where l is fibre length.
This renders the equation for composite strength,

$$\sigma_c = \sigma_f.V_f(1-\ l_c/2l)\ +\sigma'_m(1\ -\ V_f) \quad \text{....3.13}$$

Considering both tensile and shear loading reveals the expression for l_c, the critical fibre length, as:

$$l_c = r.\sigma_f\ /\tau_i \quad \text{.....3.14}$$

where τ_i is the fibre/matrix shear stress.

Implicit in this expression is the fact that if the fibre is shorter than the critical length for a particular system it can never fail in tension but must pull out of the matrix. The strength of the composite where the fibres are shorter than the critical length is given by:

$$\sigma_c = \sigma_f.V_f.l/2l_c\ +\ (1-V_f).\sigma_m \quad \text{.....3.15}$$

These formulae all assume aligned fibres which is not always the case. Complex analyses for random arrays have been developed[73] but in practice are unwieldy.

When accepted theory of fibre composites is applied to particulate composites, strengths are underestimated. The theory of strengthening by particles has produced two proposed equations, based on different perceptions of the strengthening mechanism by which particulate composites are reinforced. Nardonne and Prewo[58], using a modified shear lag model, arrive at the expression for composite yield strength for platelets of:

$$\sigma_{cy} = \sigma_{my}.\{1\ +\ (L_2\ +\ t).S/4L_2\}.V_p\ +\ (1-V_p).\sigma_{my} \quad \text{....3.16}$$

where σ_{my} is the yield stress of the matrix;
V_p is the platelet volume fraction;
t is the platelet thickness;
L_2 is the depth of the platelet;

and S, the shape factor, is:

$$S = 2L / t \quad \text{.....3.17}$$

where L is the platelet dimension in the tensile direction.
If the thickness is assumed to be much less than the dimension L_2 then the strength can be given by:

$$\sigma_{cy} = \sigma_{my}\{V_p(S+4)/4 + (1 - V_p)\} \quad \text{.....3.18}$$

This can be reduced to:

$$\sigma_{cy} = \sigma_{my} \{V_p.S/4 + (1-V_p)\} \quad \text{.....3.19}$$

if tensile load transfer is ignored.

There have been few attempts to analyse the strengthening due to particles. Arsenault and Shi[39] proposed that strengthening is due to increased dislocation density because of the influence of particles, giving an equation of the form:

$$\sigma_{cy} = \sigma_{my} + \beta\mu b \{(V_f/1-V_f).(B\epsilon/b)\}^{0.5}.(1/t)^{0.5} \quad \text{...3.20}$$

where: β is a constant

b is the burgers vector

B is a geometric constant

ϵ is induced thermal strain, $= \Delta CTE.\Delta T$,

ΔCTE is the difference in thermal expansion coefficient between aluminium and reinforcement,

ΔT is the temperature drop on quenching.

The fit of experimental data to predictions made using this equation are good according to Taya and Arsenault[6], however, the range of data used to validate this is small. The equation is also based on a single strengthening mechanism, which is probably not the case. This, and other more empirical predictive equations based on conventional Hall-Petch and Orowan theories and developed by Miller and Humphries[38], will be tested in chapter 6 which investigates strengthening theory applied to commercial purity aluminium.

3.2.3 Fracture Toughness

The fracture toughness of short and continuous fibre composites can be derived from energetic considerations based on the work required to pull a fibre out of the matrix material. This is of limited use when it comes to assessing the fracture toughness of particulate reinforced composites, and the analysis is included for

consistency with the previous sections but will only be dealt with briefly. The theories assume that the fibres are aligned. For short fibres, two equations relate the work of pull-out to fibre length depending on whether the fibres are shorter or longer than the critical fibre length[6]. These are:

$$W_{po} = \pi.d.\tau_i.l^2/24 \quad \text{for } l \leq l_c \text{.....3.21}$$

$$W_{po} = \pi.d.\tau_i.l_c^3/24.l \quad \text{for } l \geq lc \text{.....3.22}$$

where Wpo is the work required for fibre pull out;

d is fibre diameter;

τ_i is the interface shear strength.

If these equations are converted to work per unit fracture area of composite, and equation 3.14 is used in order to substitute for the shear stress in both conditions (noting that a fibre shorter than l_c will never achieve the fibre tensile strength, only some stress, σ_{max}, defined by the equation 3.14 using 'l' instead of 'l_c') then the work per unit fracture surface area (W_{po}') will be described by the equations:

$$W_{po}' = V_f.\sigma_{max}.l/12 \text{.....3.23}$$

$$W_{po}' = V_f.\sigma_f.l_c^2/12.l \text{.....3.24}$$

The maximum work of pull-out can be seen to occur when the fibre length is equal to the critical length. This analysis is modified for continuous fibres by considering flaws in the fibres: if this spacing is less than a critical flaw spacing, the initial equation is the same as 3.19, whereas if the spacing exceeds the critical spacing, equation 3.20 has the the critical flaw spacing, l_c^*, instead of l_c. This spacing is given by[6]:

$$l_c^* = (\sigma_f-\sigma_f^*).l_c/\sigma_f \text{.....3.25}$$

where σ_f^* is the strength at the flaw. These equations are related to the plane strain fracture toughness by the energy release rate, G_{IC}, in plane strain. The local energy release rate is given by the work of pull-out and any plastic work in the region of the fibres. The total energy release rate is a combination of the local G and a macroscopic G value which combines the fibre and matrix effects individually in a law of mixtures type relationship. The fracture toughness is found from the relationship:

$$K_{IC} = \{E_c.G_{IC}/(1-\nu_c^2)\}^{0.5} \text{.....3.26}$$

where ν_c is Poisson's ratio for the composite. Unfortunately these relationships are of little use in assessing the fracture toughness of composites reinforced with a particulate medium.

The theory behind fracture toughness of particulate composite materials is poorly developed. There are no explicit equations available which provide a deductive theory of fracture toughness. Taya and Arsenault[6] quote a general empirical expression for plane strain fracture toughness:

$$K_{IC} = \{\sigma_y.\epsilon_f^*.E.f(n)\}^{0.5}.s^{0.5} \quad \ldots\ldots\ldots\ldots\ldots 3.27$$

where ϵ_f^* is the maximum strain at the crack tip;

$f(n)$ is some function of the work hardening exponent, and

s is the average particle spacing.

This analysis is similar to equations developed for second phase brittle particles in a ductile matrix (eg. slag inclusions in steel) and assumes crack propagation and growth is by void coalescence. It is by no means certain that this is always the case[25]. Other analyses of fracture toughness based on fractographic examination have been proposed[27,59]: these and equation 3.27 are discussed in section 2.6.3 and 2.6.5 because of their more experimentally derived nature.

3.3 Mixing of Rapidly Solidified Powder and Reinforcement.

The quality of mixing determines the homogeneity of the final product however it is virtually impossible to achieve a fully homogeneous product after mixing[77]. Work must therefore be directed at obtaining the best possible mixing conditions whilst respecting the fact that full homogeneity is unattainable. Campbell and Bauer[77] reported as long ago as 1966 that as mixing time increases after a certain point a cyclic variation between mixing and de-mixing is induced, the minima of each cycle always being greater than the calculated standard deviation for a random mixture. Implicit in this statement is that segregation is the norm. Segregation may occur as hard agglomerates in one of the components of the system, but it is more likely to occur because velocity gradients are set up in the mixer[78]. As the mass is rotated smaller particles are likely to move into voids between large particles. Thus, with time, particles are likely to migrate to a similar path of circulation in the mixer: an individual particle's velocity will be determined by its density and size. After a long time (depending on the mixer speed), smaller particles will thus be found nearer to the centre of the mass. Mixing and de-mixing can occur both radially and axially.

Campbell and Bauer[77] suggest various ways to minimise the segregation and thus promote the homogeneity of the compact. The most obvious solution is to mix particles of a very tight size range. Further to this they discovered that particles of the same size mix together well. However this is often impractical as size distribution is imposed rather than chosen. The different shapes of the component particles was accounted for by the concept of an 'equivalent size' which is defined as the diameter of a sphere having the same volume as the particle under consideration. This 'normalising' of the particle shape facilitated the investigation. It is important to note that particles whose size is similar are merely less likely to agglomerate: their final distribution is still random. The ratio of the volumes of component particles also affects the efficiency of mixing: a ratio which approaches unity is more likely to result in better mixing. Particles of similar density tend to achieve a more homogeneous mix. Donald and Roseman[78] suggest that the best type of mixer does not allow particles to interfere with the motion of others but to remain in motion themselves, i.e. mixing by fluidization. Failing this, their experiments suggest that a cube or 'Y' mixer is the best tumble mixer.

Other workers have found that mixing is improved with pre-heating of the SiC to remove adsorbed species such as ammonia[79]. Also, dispersants which disrupt agglomerates have had some success in increasing the homogeneity of a mix.

The minimising of defective regions is the aim of mixing: the two major defect types which occur in compacted mixtures of two or more powder types are porosity and agglomeration, or segregation. Both of these defect types cause a deviation from the ideal theoretical composite properties.

Porosity reduces the effective load bearing area of any material and also introduces a stress concentration, dependent on pore geometry, which will further serve to reduce the local load bearing capacity. Ghosh et al[80] have attempted to relate the porosity of a particulate composite to its strength. Their work, carried out on a slurry cast Al-4%Mg/Al_2O_3 composite, showed that predictions of a linear variation of strength with porosity were borne out. The simplified equation used to predict the strength is:

$$\sigma_p/\sigma_o = 1 - \alpha P \quad \text{.....3.28}$$

where: σ_p, σ_o are the U.T.S. of the porous material and the pore free material respectively;

P is the total porosity in percent;

and α is a function of the pore geometry and the reduction in area due to the presence of the pore.

Also apparent was that an increase in volume fraction of the alumina inhibited the weakening effect of the pores by limiting the region around them over which weakening occurred.

The dispersion of agglomerates is necessary in most cases to provide uniformity in the product and thus improved properties. It is conjectured that agglomerates are held together by adhesion- static electricity, Van der Waals forces or capillary forces[81]. It should be noted that adhesion will be greater between small particles due to the increased surface area. Agglomerates are known to be associated with porosity and micro cracks[82]. Kendall's work on compacts of titania and alumina has revealed that 'perfect' agglomerates (i.e. those that are defect free) can be strong in their own right[82]. An implication of this is that agglomerate weakening of a composite material may be mainly due to any porosity accompanying agglomerates of reinforcement. However, the inter-relationship between agglomeration and porosity, and the accompanying effects on stress concentration are surely complex and have yet to be investigated explicitly. It is important to note that agglomeration in a powder composite material will also occur in the matrix alloy. Since the matrix is much more ductile however, the greatest effort is directed towards reducing agglomerates in the harder, more brittle ceramic reinforcement.

3.4 Precipitation Hardening

Precipitation hardening is the way in which aluminium alloys of the series' 2xxx, 6xxx and 7xxx attain their working strength. A consideration of the theory behind such hardening methods is important in the context of this thesis for two reasons: (i) a 2xxx series alloy and a 7xxx series alloy are employed as matrix materials in this work, and (ii) there is a body of evidence which suggests that reinforcement particles modify the ageing process (see section 2.5.2). The mechanisms are broadly the same in each case, only the alloying elements, and consequently precipitate type and morphology, differ. Heat treating after solutionising at elevated temperature will result in a series of precipitates, due to alloying elements coming out of solution, depending on the length of time that the material is held at a particular temperature.

Figure 3.3 shows the necessary condition for an alloy to be capable of being precipitation hardened. If the alloy is heated into the α phase field and then quenched, alloying elements will be retained in solid solution. Vacancies will also be quenched in,

which are important for the formation of G.P. zones[83], the preliminary phase in the precipitation sequence of 2xxx series and 7xxx series alloys. Heating at a temperature within the α" + θ" field will result in sequential precipitation until the equilibrium phases are obtained (assuming the time at the temperature is sufficient). The sequential nature of precipitation is more energetically favourable because the formation of precipitates is activation energy controlled. Initially only 'zones' of higher than average concentration of alloying elements form. These are followed by metastable precipitates which are eventually superseded by equilibrium precipitates.

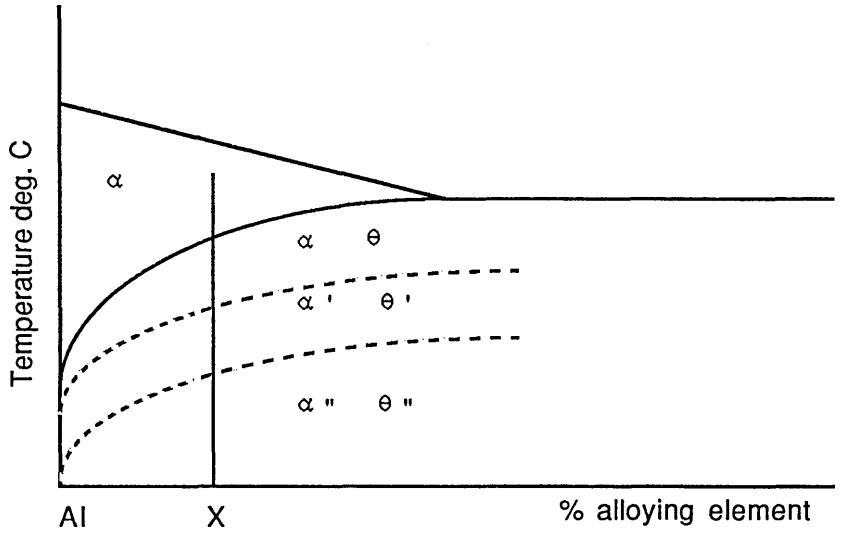

Figure 3.3 Type of phase diagram required for precipitation hardening

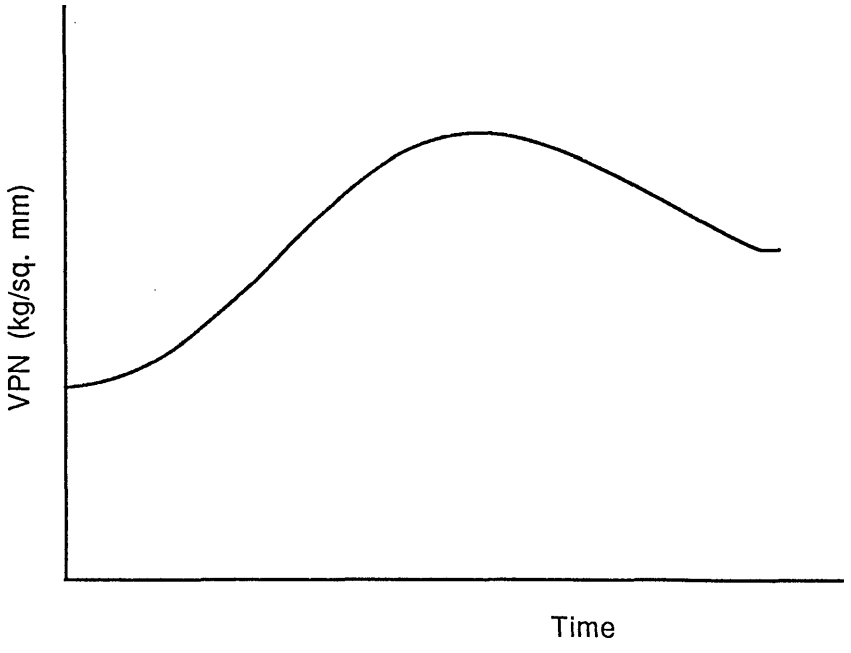

Figure 3.4: Generalised hardness vs time curve for precipitation hardening alloy.

A gradual loss of coherency with the matrix accompanies these changes: optimum strength is achieved by balancing the time and temperature in order to reach the desired point on the graph shown in figure 3.4. The peak in the curve is governed by particle strength: it represents the point at which shearing of the particles by dislocations is superseded by Orowan looping of dislocations around the particles.

3.4.1 Aluminium-Zinc-Magnesium-Copper Alloys

Work in this thesis is predominantly centred on the Al-Zn-Mg-Cu system and thus a review of the precipitation in this system is expedient. Excellent reviews of precipitation in 2014 are presented in a number of texts[83,84] and are the basis for the generalised precipitation sequence above. Work on quaternary alloys of the 7xxx series has been limited, however, there is a large body of information concerning Aluminium-Zinc-Magnesium alloys, to which the quaternary approximates[85]. These alloys are age hardenable by virtue of the presence of zinc and magnesium[84]. Initially, the effect of the alloying elements will be briefly discussed *a priori*; the second part of this section will be devoted to the experimental observations of various workers.

The presence of magnesium and zinc allows for their combination to form Mg_5Al_8, $MgZn_{11}$, Zn, AlZn, $MgZn_2$ or $Mg_3Zn_3Al_2$ as equilibrium phases[85]; Mondolfo[85] gives the limits of composition of all of these phases. The addition of copper allows the possibility of the formation of $CuMgAl_2$ as a distinct new phase. $MgZn_2$, $MgZn_{11}$ and $Mg_3Zn_3Al_2$ are capable of taking up an appreciable amount of copper[85]; the three copper bearing phases which are completely miscible with these are, respectively, CuMgAl, $Cu_6Mg_2Al_5$ and $CuMg_4Al_6$. Additions of copper to this system also give changes in mechanical properties similar to those which would be effected by the addition of an equivalent amount of zinc[85].

The process of heat treating these alloys follows the standard general procedure of solutionising, quenching and artificially ageing at elevated temperature, although there may be some important variations in this route which will be explained later. There are a number of proposed precipitation sequences for the development of properties by ageing at elevated temperature. The most widely accepted, first proposed by Mondolfo et al in 1956[86], is as follows:

supersaturated solid solution-> G.P. zones-> η'-> η

where η is the equilibrium $MgZn_2$ phase. Kelly and Nicholson[83] show this sequence terminating in the T phase ($Mg_3Zn_3Al_2$) whilst Hatch[84] allows a distinct non equilibrium phase, T', after G.P. zone formation. This is, however, a minor point as the T phase does not contribute to the precipitation hardening. Whilst not disputing the operation of this sequence, Ryum[87] questions its unique status and proposes two other decomposition paths in his investigation of Al-5.77 wt.% Zn-1.08 wt% Mg, *viz*:

solid solution-> η

solid solution-> "nuclei"-> η'-> η

The situation is further complicated by Thackery[88], who suggests, on the basis of metallographic examination, that η' does not occur, thus rendering the precipitation sequence:

solid solution-> G.P. zones-> η

A large number of crystallographic orientations between the precipitate and matrix have been observed[85,88,89] and these have undoubtedly added to the confusion. It is generally accepted, by those who acknowledge its existence[83,85,89], that the η' is close packed hexagonal in structure and forms on the {111} planes of the matrix. Ryum explains his proposals in terms of activation energy for precipitation[89]. The reaction resulting directly in the formation of η requires a very high nucleation energy; consequently, this will only occur at grain boundaries and dislocations. The distinction between the other two reactions is said to be controlled by the vacancy concentration and temperature of ageing: a high vacancy concentration results in the un-annotated "nuclei" which only grow at high temperatures; the G.P. zones are a 'low' temperature (up to 180^{o}C) phase whose nucleation and growth is independent of vacancy concentration[87].

A characteristic of the Al-Zn-Mg system is the occurrence of a precipitate free or denuded zone at the grain boundary. Since this will have a bearing on the mechanical properties much work has been directed towards the investigation and elimination of such zones. Kelly and Nicholson[83] note the presence of P.F.Z.s and explain their presence as a result of vacancy depletion with the grain boundary acting as a sink. They concluded that the zone was not, however, denuded of solute. This is confirmed by the investigation of Raghavan[90] who examined the precipitate free zone by micro-probe analysis.

4. EXPERIMENTAL PROCEDURE

4.1 Introduction

This chapter describes the techniques and procedures used during the course of the investigation into aluminium matrix composites. These fall into three categories: (i) the production of the material; (ii) mechanical testing of the product and (iii) physical examination of the product and failed mechanical test specimens. Before expounding on these three categories, it would be useful to examine the methodology of the investigation.

In the examination of any material system a number of aspects must be investigated. These can be broadly defined as *extrinsic* and *intrinsic* factors. In this case extrinsic factors would include processing conditions, alloy type, reinforcement type, volume fraction and size. Intrinsic factors would include structure and reinforcement/matrix interaction. There is an obvious 'grey area' where extrinsic factors influence intrinsic, *viz.* the influence of processing on structure. The work conducted in this investigation has concentrated on the relationship between extrinsic and intrinsic factors: alloy type and reinforcement volume fraction and size have all been examined with respect to their influence on the intrinsic aspects. The process route has also been investigated, and its effect on structure and properties noted, although the actual investigation of the efficacy of various process routes was more a means to an end. Similarly it was felt that mixing was a primary determinant of properties, due to the large influence on homogeneity and porosity noted in chapter 3, but the actual mechanics of the mixing process were not studied.

The experiments within this investigation were, then, employed in order to investigate the relationships between the material parameters, process parameters, structure and properties with varying degrees of emphasis. The chronology of the experiments did not necessarily follow the path laid out below, there were obviously some feedback loops but these will be drawn out in the ensuing 'Results' chapters.

4.2 Material

4.2.1 Rapidly Solidified Aluminium Alloys

The powder alloys employed in this investigation are shown in table 4.1, along with their compositional specifications and source. All powders were inert gas atomized. The compositional analyses were provided by the supplier in each case. An explanation of the series designation code can be found in appendix 2.

Alloy Type	Compositional specification	Source
CW67	8.99%Zn,2.47%Mg,1.47%Cu,0.1%Zr,Fe,Ni & trace; rem. Al	Metalloys
2014	4.4%Cu , 0.5%Mg, 0.8%Si, 0.8%Mn, rem. Al	Imperial College
C.P. Al	99% Al, trace Fe, Si, Cu.	Metalloys

Table 4.1: R.S.P. alloys employed in composite investigation

4.2.2 Particulate Reinforcement Production

The silicon carbide of nominal size 5μm was produced by Sohio Ltd., U.K. and is of a standard polishing grade. The 1μm silicon carbide and 50μm silicon carbide came from AlCoA Ltd. and Goodfellow Metals Ltd., U.K., respectively.

4.2.3 Sizing of Particles

The size distribution of the R.S.P. aluminium alloys was determined by sieving 'thief' samples of 100g for one hour in standard test sieves. These were of mesh size: 125μm, 90μm, 75μm, 63μm, 53μm, 45μm, 38μm, 32μm.

The size distribution of the two finer silicon carbide powders was determined using a Malvern laser particle size analyser. The particles were dispersed in an ethanol medium in a unit cell of small volume and three runs were taken from each quoted size. Particle sizes were determined by the instrument by computing the angle and intensity of the diffracted light, and based on an assumption that the particles are spherical. The particle size distribution of those which were nominally 50μm was determined by sieving using standard test sieves. A sample weight of 50g was employed for this analysis.

4.3 Mixing of Alloy Powder with Reinforcement

4.3.1 Mixing Prior to Extrusion

Mixing prior to extrusion was carried out dry in a 'Turbula' T2C rotating mixer. Two alternating vortices are created by a 3 dimensional movement made possible by two knuckle joints at either end of the container. The mixer is belt driven with speeds between 20 and 90 r.p.m. being available. The maximum load that could be

mixed at any one time was approximately 1kg. Smaller containers, containing between 100-200g, were available and were used in the investigation into the determination of the optimum mixing conditions.The silicon carbide was heated at 300°C for at least 12 hours prior to mixing in order to remove any adsorbed species at the surface[79]. The calculation of the weight of reinforcement required for a particular volume fraction is given by:

$$W_{SiC} = \{W_{total}.V_{SiC}.\rho_{SiC}\}/\{\rho_{Al} + V_{SiC}.(\rho_{SiC}-\rho_{Al})\}.....4.1$$

where: W_{total} is the total weight of composite required;

V_{SiC} is the volume fraction of the silicon carbide;

ρ_{SiC}, ρ_{Al} are the densities of the SiC and the matrix alloy, respectively.

4.3.2 Determination of Ideal Mixing Conditions

Prior to the initial extrusions an investigation was undertaken to establish the best mixing conditions. Simple tumbler ball milling and Turbula mixing, both with and without a silicon carbide dispersant which breaks down the electrostatic surface forces[81], were assessed. Two ball sizes were used; these were 13mm and 25mm diameter. Tumbler ball milling was performed at two speeds, roughly 20 r.p.m. and 40 r.p.m.. Turbula mixing was performed at 20, 42 and 90 r.p.m.. The time of mixing was varied from 15 to 45 minutes. Ten small balls or five large balls were used, the numbers chosen being considered correct for the volume of material to be mixed. The silicon carbide dispersant tried was butanone. In all cases 100g of 10% SiC-C.P. aluminium was mixed. Specimens from the 100g were compacted at a pressure of about 1-2 MPa and then sintered for 1 hour at about 650°C to facilitate polishing and microscopic examination of the compacted structure.

4.4 Thermomechanical Processing

4.4.1 Pre-extrusion Processing

Cold compaction of loose powder was carried out using a Tangye 150T press at pressures between 200 and 400 MPa, depending on the die size (55mm or 72mm). The 72mm die was tapered with an inclination of 1°; dies were lubricated with Stearic acid in acetone to further aid extraction of the compact. Compacted billets were approximately 90mm long. Material canned for degassing was compacted using a hand operated Tangye press to pressures of approximately 55 MPa. Each can was a four piece construction consisting of a base, body, lid and spout, all of 2014 alloy. The 3mm

bore spout was welded into the 3mm thick lid and the base to the body prior to compaction. Cold compaction of canned powder was followed by the welding of the lid to the can. The total length of the can (excluding the spout) was 100mm; the diameter of the can was 70mm outside and 62mm inside. The length of the spout was approximately 300mm.

Vacuum degassing of cans was conducted in a specially constructed furnace with the facility for evacuation through a rubber tube connected to the spout of the can (figure 4.1) and sealed with vacuum grease. The cans were evacuated to a pressure of 10^{-4}-10^{-5} Torr, using 'Edwards' vacuum equipment, before being placed in a vertical tube furnace and heated to 500°C, still under vacuum. Care was required in the initial stages of evacuation to avoid sucking loose powder into the system, which inevitably results in a degradation of the efficiency of the apparatus, even though there was a filter in the system specifically to avoid this. Thermocouples (K type) were connected to the outside of the can and through the spout to the material in order to monitor temperature accurately. The rotary pump was used for the major part of the evacuation operation, with the diffusion pump only being employed for the final ten minutes of the procedure. The pressure during the degassing was monitored using a 'Pirani' gauge and recorded on a four input chart recorder, as were the can temperatures. Once the desired temperature for hot compaction had been achieved the can and contents were held at this temperature so that the lowest pressure possible could be achieved using the diffusion pump.

Heating times were a total of between 45 minutes to a maximum of one hour. The spout was cut using bolt cutters and the hot compaction performed. Hot compaction of selected billets was conducted in the extrusion press with the exit blanked off. This operation was conducted at a container temperature of 500°C and at a pressure of approximately 1000 MPa. The container size for this operation was 75mm. Subsequent to hot compaction, some can material was removed to reduce the billet size to 72mm in order to allow the compact to fit the container easily during the extrusion operation.

4.4.2 The Extrusion Press

The extrusion press used was a vertical ENEFCO 5 MN hydraulic press; extrusion was conducted at ram speeds of between 2-8 mms^{-1}, at temperatures of 270-500°C. The extrudate was water quenched on exit from the die area. The load was measured using a Mayes load cell located directly above the ram; the pressure at the inlet to the main cylinder was also monitored in order to cross check load

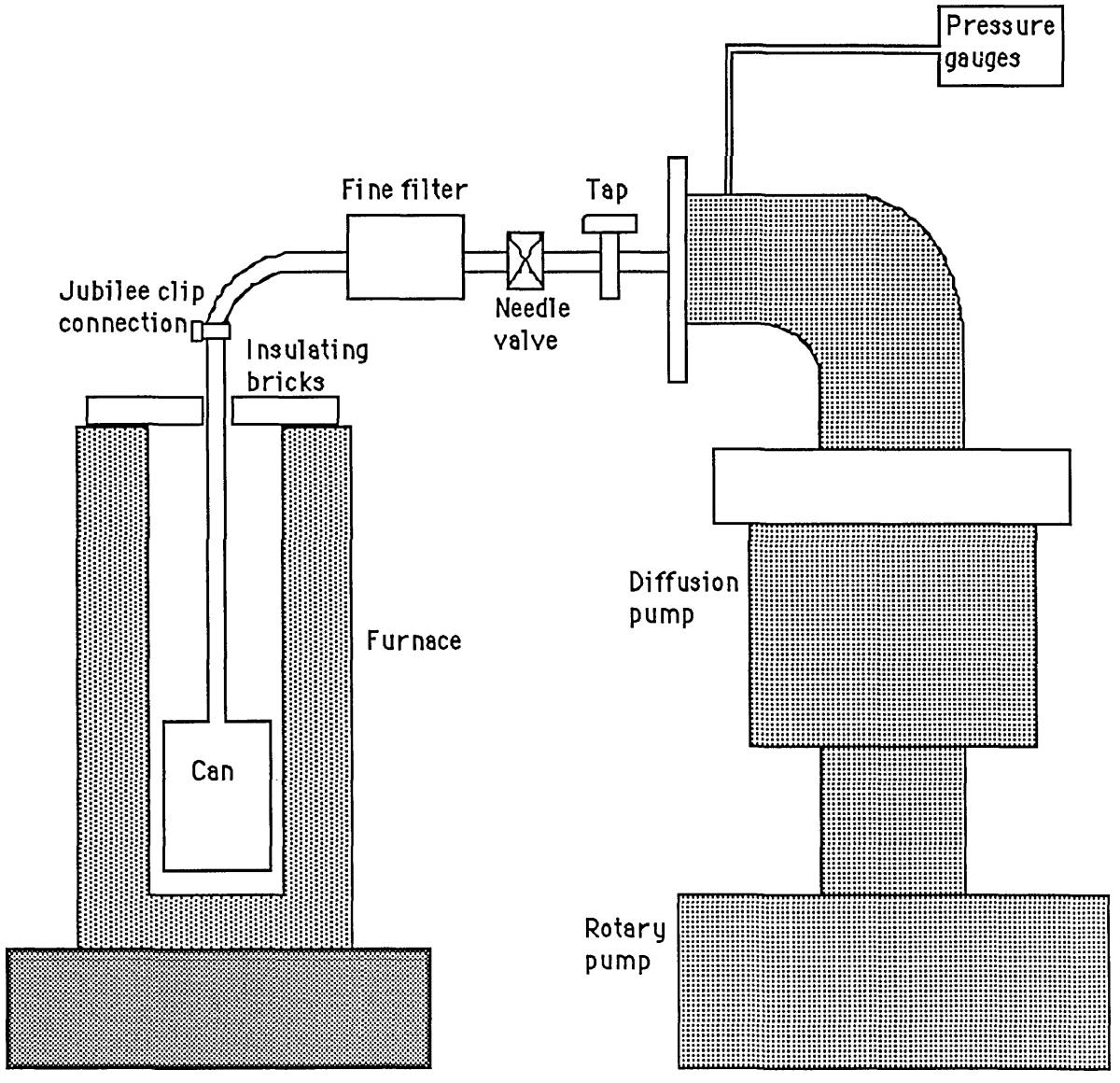

Figure 4.1: Schematic diagram of vacuum degassing apparatus (after Mahmoud[91])

measurements. The ram speed and displacement were also measured using a rectilinear potentiometer situated between the ram and the press bolster. All of these recording devices were activated by a trip switch as the ram descended; the output data was recorded using a 'Datalab' DL2800 multichannel transient recorder and stored on an I.B.M. personal computer. The operation was completed by raising the container, cutting the extrudate and pushing it into the quench tank. The discard was removed using a tight fitting scraper pad which was pushed through the raised container by the main ram.

4.4.3 Tooling

The dies employed in this investigation were all flat faced, made from the standard die steel. Table 4.2 shows the dimensions of each die and the extrusion ratio obtained, depending on the initial billet size.

Die cross section shape	Dimensions (mm)	Container size (mm)	Extrusion ratio
Circular	13.5	75	30
Circular	13.5	57	17
Circular	9.5	75	60
Rectangular	10 x 20	75	22
Rectangular	36 x 7.5	75	16
Square	13.5 x 13.5	75	24
Rectangular	32.5 x 4	75	34

Table 4.2: Die size and ratio used for extrusion

The die land was initially 5mm, but later reduced to 3mm.

4.4.4 Billet Heating

Billets were heated in an air circulating furnace, employing a type K thermocouple embedded in a hole drilled in the billet to monitor the temperature. Typical heating times were around 30-45 minutes. Once in the container temperature was maintained by 14kW heaters in the casing. In this way extrusion could be performed between temperatures of 300-500 ^{o}C. The container temperature was held at normally 30-50^{o}C lower than the initial billet temperature.

4.4.5 Lubrication

All composite extrusions were metal film lubricated. Initially, a heated leader pad of either super pure or commercial purity aluminium was used. Pads tested were either cast or compacted powder of approximately 10mm in thickness with between one and six holes drilled in them to allow the escape of gas. Material which was canned was lubricated by the can material.

Unreinforced alloy extrusion and composite extrusion during the investigation into process conditions was lubricated with colloidal graphite.

4.4.6 Rolling

Rolling of composites and some unreinforced alloy was performed using a single stand 'Farmer-Norton' 100 ton rolling mill, with a roll diameter of 250mm. The billets (from extrudate) were heated in an air circulating furnace or muffle furnace prior to rolling. Subsequent to initial trials the material was also heated between each pass. Only composites of CW67 and C.P. Al were rolled. The starting thickness of the CW67 composites was 4mm, that of the C.P. composites, 5mm. The thickness of the final product was 1.75mm for CW67 composites and 1.9mm for composites with a C.P. Al matrix, after 6 and 7 passes respectively.

4.5 Extrudate Properties

4.5.1 Surface Finish

The surface finish was assessed in a simple qualitative manner. The quality was described in terms of defects. The description ranged from 'good' which indicated a defect free surface, through 'poor', which was used to describe material exhibiting some cracking, to a description of large-scale defects such as surface or edge cracking which extended from a quarter to the total length of the extrudate. The thickness of the lubricating film was also measured at various points along the extrudate.

4.5.2 Density

The density of the extrudate (and billets) was measured by a weight difference technique. Sprayed with a lacquer to prevent the intrusion of water, a short length of the extrudate was weighed in air and then in water. The density was calculated using the formula:

$$\rho = (\rho_{water} \times W_{air})/(W_{air}-W_{water}) \quad \text{.....4.2}$$

where: ρ_i is density of the ith phase
and W_i is the weight of the ith phase.

A comparison was then made with the law of mixtures calculation of the theoretical density. The density of the initial billets was measured in the same manner. All component density data was extracted from the Aluminium Association handbook[75] or the A.S.M. Engineering Composites book[74].

4.6 Heat Treatment Prior to Mechanical Testing

Heat treatment was performed on the machined specimens just prior to testing. All specimens undergoing prolonged heat treatment were wrapped in aluminium foil to prevent surface oxidation. The designation of 'under' and 'over' aged fracture toughness samples was arrived at by adopting heat treatment conditions at which the hardness of the material was found to be 80% of the peak value.

4.6.1 Determination of Optimum Ageing Conditions by Hardness Testing

Vickers indentation hardness tests were conducted on sections of extrudate of composites and unreinforced alloy in order to determine the optimum hardness conditions. A 20kg load was used. The following sections detail the conditions tested for each heat treatable alloy.

4.6.1.1 2014

Composites fabricated using this alloy were tested in the T4 and T6 conditions. The solutionising heat treatment was performed at 500±4°C[75]. Ten minutes was allowed for the specimens to attain the solutionising temperature; this was followed by a one hour soak and water quench. Artificial ageing was conducted at three temperatures- 160°C, 166°C and 180°C- over a range of times and then water quenched. The water temperature was not allowed to rise above approximately 38°C during either quench[75].

4.6.1.2 CW67

Specimens of unreinforced alloy and composites of this alloy were treated as separate materials as far as the determination of optimum hardness was concerned. Each was solutionised at 475°C±5°C for 1.5 hours[85]. Artificial ageing was conducted at temperatures of 120°C, 135°C, 160°C, 180°C and 200°C for a range of times for both composites and unreinforced material. Isochronal ageing tests were also conducted on this alloy at these temperatures for three quarters of an hour.

4.7 Mechanical Testing

4.7.1 Tensile Testing

Hounsfield number 13 specimens were machined from the mid section of the extrudate, as were single shouldered 60mm gauge length modulus specimens. An Instron tensile testing machine was employed, using a 25kN load cell. The crosshead and chart speeds were held constant at 0.2mm/min. and 50mm/min., respectively. Extension of the tensile specimens could not be measured directly during the test because of the small gauge length of the specimens (25mm total). In the case of modulus testing a Schlumberger L.D.T. with a 25mm gauge length extensometer was attached to the specimen. In this way results could be monitored independently of the Instron chart recorder on an x-y plotter. The output of the transducer was calibrated on the x-y plotter using a micrometer to provide the displacement. Load calibration of the x-y plotter was done using a high strength steel to provide sufficient displacement on the load axis.

Tensile specimens from rolled material were stamped out as single shoulder specimens with a width of 7.5mm and total gauge length of 60mm.

4.7.2 Fracture Toughness Testing

Two fracture toughness tests were employed during this investigation. The first was the "Terratek" short rod fracture toughness test, developed by Barker[92]. Test specimens were machined from the central portion of round and square bar extrudate of unreinforced alloy only. The dimensions of the specimens are shown in figure 4.2. The fracture toughness was calculated using the equation:

$$K_V = A.P.B^{-3/2} \quad \text{.....4.3}$$

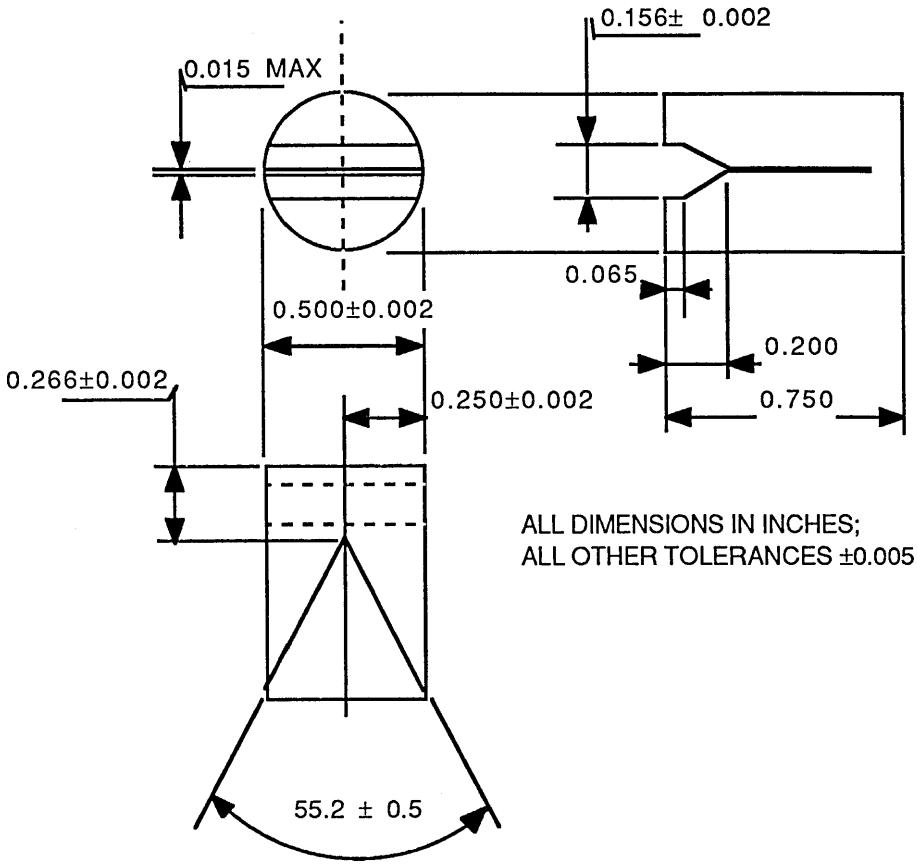

Figure 4.2: "Terratek" short rod fracture toughness test specimen

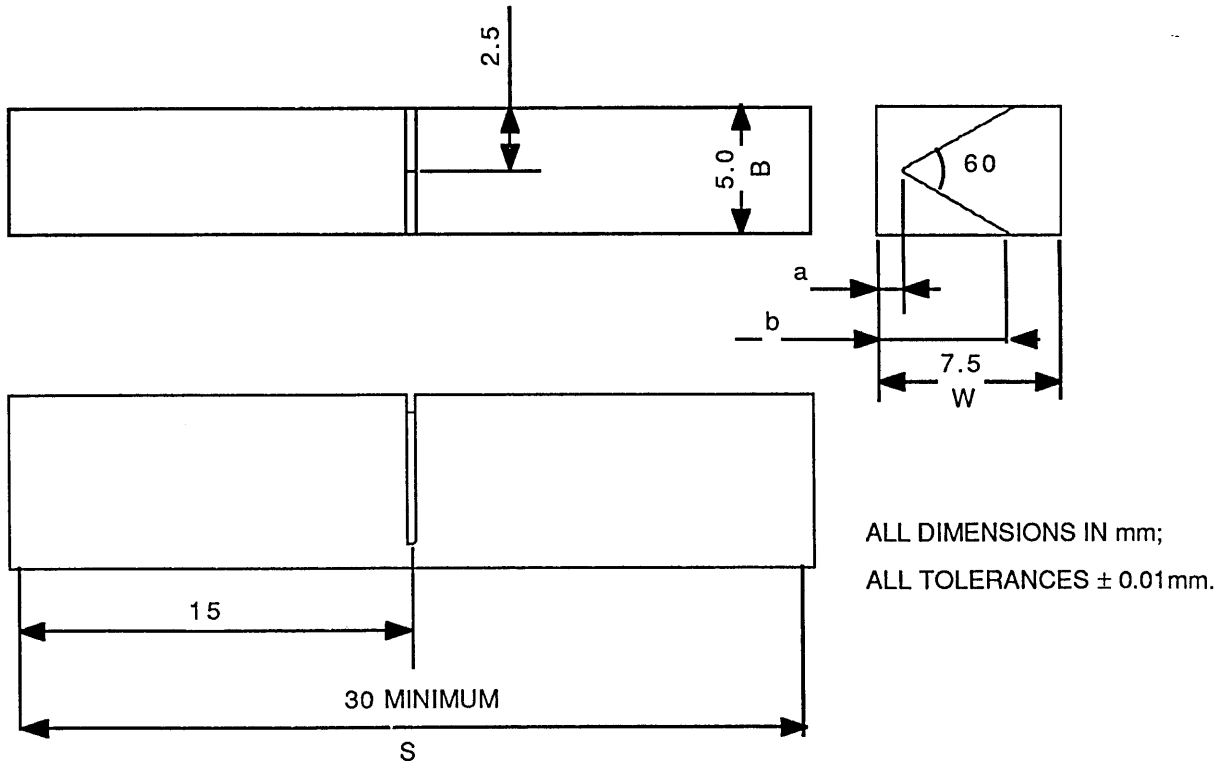

Figure 4.3: Chevron notched three point bend fracture toughness specimen

A is a calibration constant = 22
P is maximum load
B is specimen diameter.

It was not possible to use this test geometry for the testing of composite specimens due to high wear on the tools, which rendered the tolerances unattainable. A similar test, developed by Shang-Xian[93] and employing the same crack geometry, was usable because the notch was machinable by electric discharge machining (E.D.M.). This greatly facilitated specimen preparation. The specimen dimensions used are shown in figure 4.3. The fracture toughness is calculated using the equation:

$$K_{IC} = P.Y_c / (B.\sqrt{W}).....4.4$$

Y_c is a geometric factor, based on the ratios shown in figure 4.3 and is defined as:

$$Y_c = 5.639 + 27.44\alpha_0 + 18.93\alpha_0^2 - 43.42\alpha_0^3 + 338.9\alpha_0^4.....4.5$$

In figure 4.3 the geometrical relationships between the annotated dimensions are as follows: S/W = 4, W/B = 1.5, α_0 = a/W $\geq$ 0.3. The first two relationships determine the specimen size and are derived from the same source which determines the dimensions of the short rod specimens. The last relationship is proposed by Shang-Xian[93] in order to attain good agreement between test data from this experiment geometry and standard test specimens. It can be seen from these geometrical relationships that almost any size test piece can be used as long as the relationships are obeyed.

All tests were conducted at room temperature using an Instron testing machine with a 10kN load cell at a crosshead speed of 0.2 mm/min.

4.8 Analytical Techniques

A number of analytical techniques were employed in order to elucidate the interactions between processing and structure and reinforcement and matrix.

4.8.1 Optical Microscopy

Photomicroscopic study was undertaken using a Nikon inverted stage microscope at magnifications of up to 1000x. Normarski interference contrast was used to achieve a good image. Quantitative measurements were made possible by

comparing measurements made on the photograph with a similarly enlarged photograph of a graticule.

Specimens of extrudate were sectioned both transversely and longitudinally and mounted in 1.25" Bakelite moulds. Pre-grinding was done on silicon carbide paper and polishing down to 1μm was accomplished using near-napless Hyprocel polishing sheets impregnated with diamond grit spray. Specimens of CW67 and 2014 composites, if etched, were etched in Kellers solution (2ml HF, 3ml HCl, 20ml HNO_3, 175ml H_2O) for up to 20s. The sintered compacts were polished and examined in the same manner. The grain size of composites of C.P. Al were examined using Barker's reagent (46ml HBF_3, 7g boric acid, 970 ml H_2O). With the specimen as the anode and using a stainless steel beaker as the cathode, 20V was applied at a current density of approximately 0.2A/cm^2. The structure was examined under polarised light.

4.8.2 Scanning Electron Microscopy

A JEOL T200 or T220A microscope was used to examine the fracture surfaces up to magnifications of 10000x in the upper stage. The accelerating voltage used was 25kV. Fracture surface specimens were attached to an aluminium stub and gold plated for 2 minutes prior to examination in order to avoid charging up of the SiC. Large specimens were clamped directly to the stage after having been gold plated.

4.8.3 Transmission Electron Microscopy

Transverse and longitudinal sections were cut from extrudate and ground to approximately 0.1-0.15 mm with a surface finish of 1200 grit. After this stage, the preparation of unreinforced material and composite specimens differed. Discs 3mm in diameter were cut from the unreinforced material and electropolished using a "Struers Tenupol" electropolishing unit. The solution used was 70% methanol, 30% nitric acid: this was held at approximately -30°C whilst a potential of 15V was maintained between the solution and the specimen.

Composite specimens were subjected to a further polishing operation using 6mm and 1mm diamond grit before being punched to 3mm discs. The thickness of these discs was substantially less than those of the unreinforced material, at between 0.05-0.075mm. The final thinning of these discs was undertaken using a "Gatan" ion beam thinner, using high purity argon gas. This machine consists of a high vacuum chamber with a tilting specimen stage, at which two beams of ionised gas may be directed in order to thin both faces of the specimen. A potential is maintained between specimen

and gas. The voltage of the system was set at 6 kV, with a current of approximately 0.55 mA. The angle of the beam to the stage was initially set at 15° for approximately 9 hours, in order to thin the specimen quickly, before being lowered to 10° in order to produce sufficient thin area for examination. The voltage and current were limited in this case so as to avoid the production of artefacts due to specimen heating, however, for non-heat treated specimens even this did not suffice and a liquid nitrogen cooled stage had to be used. In this case the voltage remained at 6 kV, but the current was increased to 1 mA with no adverse effect. The times and angles remained the same.

CW67 powder specimens were nickel plated prior to polishing and Gatan thinning in the same way as the composite foils. The plating conditions were as follows. A sample of powder was placed on a stainless steel stage in a solution of: 45 ml nickel sulphamate, 4.75g boric acid, and 150ml water with a few drops of H_2O_2 to limit the growth of asperities. A current density of 0.2A/cm^2 was used, and a potential of 20V applied between the nickel cathode and the specimen. The operation took approximately 3 hours.

Examination of the thin foils was performed using a JEOL 2000 FX microscope, at an accelerating voltage of 200 kV, with quantitative EDAX analysis. The high accelerating voltage was necessary in order to allow relatively thick areas of the composite specimens to be examined.

4.8.4 X-ray Diffraction Analysis

X-ray diffraction was performed on CW67 and its composites only, in order to identify phases in both powder and extrudate samples. A 'Philips' x-ray diffractometer was used for this investigation which was carried out with Cu K_α radiation between angles of 10° and 100°. The goniometer used was a PW1050/25 type. Specimens of powder were mounted on a stub whilst extrudate was polished to a 1200 grit finish prior to being examined. The apparatus rotated the specimens during the analysis so as to avoid intense reflections from any preferred orientations, which arise during thermomechanical processing.

4.8.5 Differential Scanning Calorimetry (D.S.C.)

Differential scanning calorimetry was performed on samples of solutionised extrudate using a Stanton Redcroft calorimeter. Specimens of approximately 30 mg in weight were placed in alumina crucibles and heated over the range 30-450°C for CW67 alloy and its composites, and 30-350°C for 2014 and its composites, at a

heating rate of 5°C/minute. A reference sample of super pure aluminium was placed in a second crucible: this was employed in order to negate any random fluctuations in the heating cycle, by subtracting the reference data from the data on the material under investigation. The whole system was sealed in an argon atmosphere during the heating. Data was recorded and stored in an IBM compatible microcomputer.

5. PROCESSING

5.1 Mixing of Composites

The efficacy of the mixing in the production of a homogeneous mixture is obviously significant in determining the homogeneity of the final product. Sizing the silicon carbide is also important in enabling a more accurate assessment of the influence of particle size on mechanical properties of any composite: a wide range of SiC sizes may result in some large variations in properties: this will be explained in the respective chapters.

5.1.1 Silicon Carbide Particle Sizes

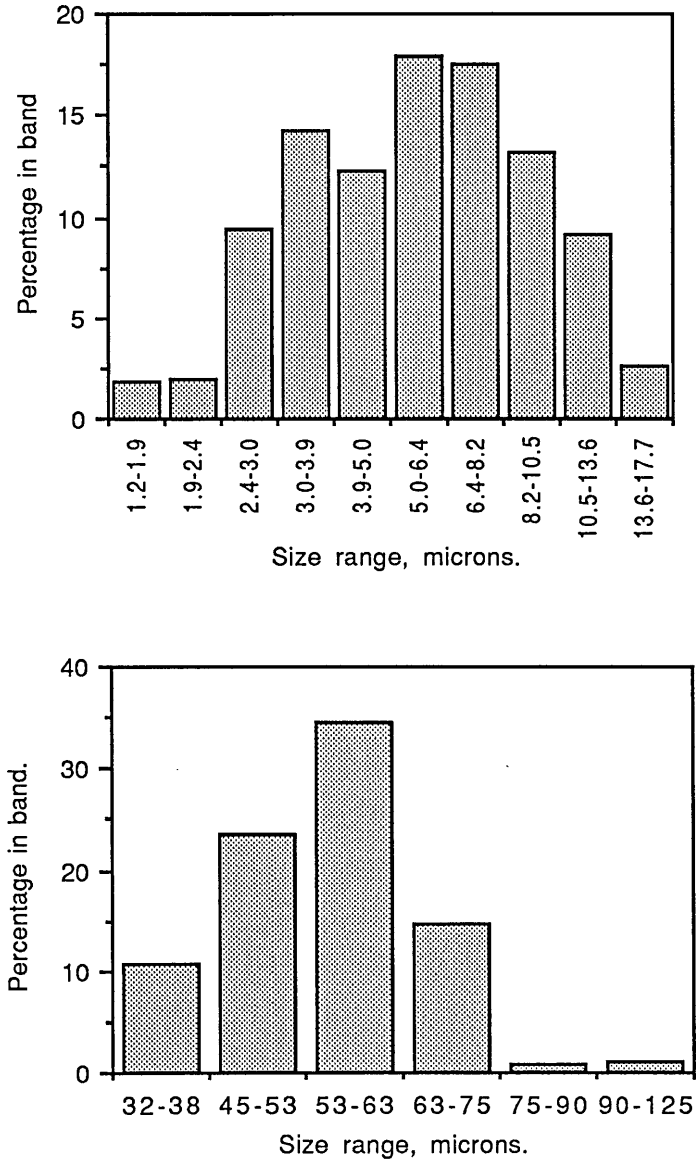

Fig. 5.1: Size range of nominal 5μm and 50μm SiC particles (percentages by weight).

The size of the silicon carbide particles employed in these investigations is shown above in figure 5.1, as measured using a Malvern particle sizer and sieves for the larger sizes. It was not possible to accurately measure the size range of the finest particles because of the inherent error in the analyser at small sizes. The range was designated as being less than 3μm with the majority being close to 1μm, the supplier's specification.

5.1.2 Mixing

Although the flow characteristics of any material will be different, in the case of high speed mixing of similar alloys with the same reinforcement type this effect was considered negligible for the purposes of a determination of mix homogeneity; in both cases commercial purity aluminium was the matrix used. The two types of mixing (ball milling and "Turbula") will be considered individually and then in comparison. Ball milling was conducted using two ball sizes- 13mm and 25mm- and at two speeds- roughly 20rpm and 40rpm. Turbula mixing was able to be conducted at five different speeds, of which only three were used- 20rpm, 42rpm and 90rpm. The resultant mixtures were cold compacted at pressures of less than 10 MPa and then sintered for one hour simply in order to facilitate handling and polishing prior to optical microscopy. The sintering of the compacts was thought to have had a negligible effect on the observed structure due to the short sintering time employed. Thus the agglomeration of the silicon carbide was unaffected by any diffusion or grain growth. It will be realised that these sintered compacts will contain porosity between the aluminium particles which is easily eliminated during extrusion: this was not under investigation. Furthermore the difference in compaction pressures between small and large scale samples was held to be meaningless within the confines of this comparison.

Ball milling at both high and low speed gave samples in which the silicon carbide was highly agglomerated and the structure porous, as can be seen in fig.s 5.2 a and b. Figure 5.2a shows the structure obtained by mixing for 30 minutes at the lower speed (approximately 20 rpm) using the 25mm diameter balls. There are some extremely large pores present and the distribution of the silicon carbide is poor. Mixing at the higher speed (40 rpm) for 30 minutes with 13mm diameter balls resulted in the structure shown in figure 5.2b. The silicon carbide is almost exclusively confined to the voids between the aluminium particles, which will lead to a large amount of agglomeration. At longer times there was a suggestion of over-mixing, but this was not investigated quantitatively. This observation is in accordance with the

(a)ball milled: mixed for 30 minutes, 20rpm, 25mm balls.

(b) ball milled: mixed for 30 minutes, 40rpm, 13mm balls.

(c) Turbula mixer: mixed for 45 minutes, 90 rpm.

(d) Turbula mixer: mixed for 30 , minutes, 42 rpm.

Figure 5.2: Microstructure of material mixed under different conditions, as indicated.

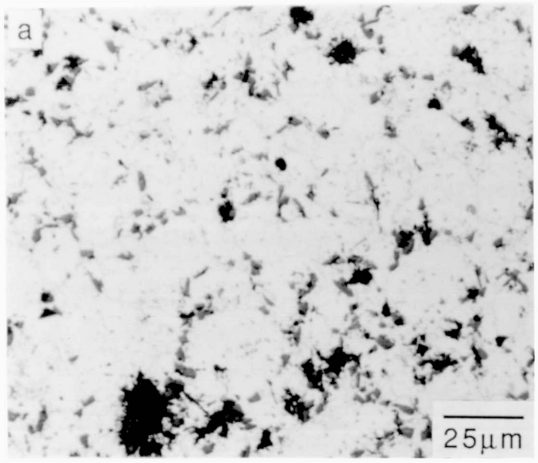
a
25µm

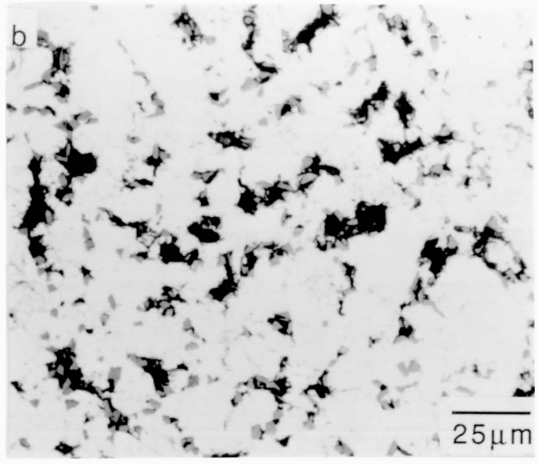
b
25µm

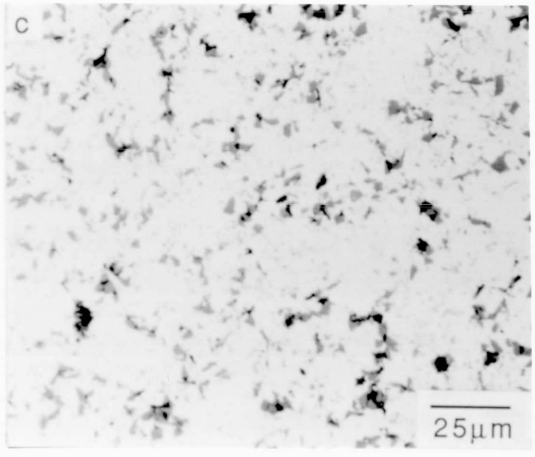
c
25µm

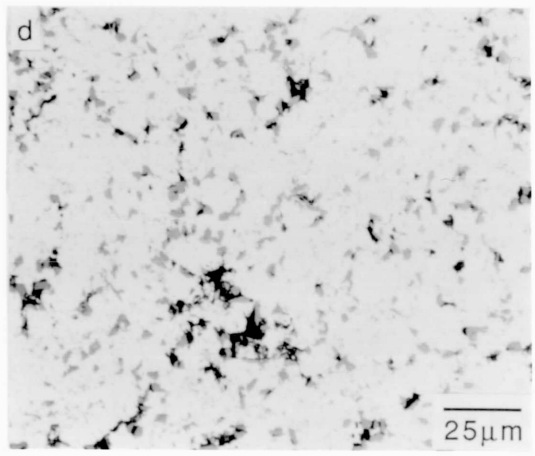
d
25µm

work of Campbell and Bauer[77] who showed that homogeneity increases as mixing time is increased, but may decrease as time progresses beyond a critical time.

Turbula milling generally provided better samples. Mixing at 90 r.p.m. for 45 minutes resulted in a defective structure (fig. 5.2c), but this was not as bad as the 'best' ball milled product. The features to note are the absence of large scale porosity (compared with fig.s 5.2a and b) and the fairly good distribution of the SiC. The slowest speed also resulted in a heterogeneous mix, as was expected. The best approximation to a homogeneous mix was obtained by mixing at at 42 r.p.m. for 30 minutes (fig. 5.2d). The important features to note are the near absence of agglomerates of silicon carbide associated with porosity and the good dispersion of silicon carbide particles amongst the aluminium particles.

Attempts to improve the homogeneity further, using butanone as a silicon carbide dispersant, proved unsuccessful. This was because too many variables were introduced into the experiment: it was impossible to establish the correct amount of dispersant. Variation in the combination of speed and time did not have a major influence on homogeneity as the volume fraction of reinforcement was increased; thus the same speed and time was employed for all volume fractions. The effect of particle size was not investigated quantitatively. It should, however, be noted that calculations of ideal mean particle spacing for 1μm SiC result in an inter-particle spacing which is less than the Al particle size at a value of approximately 3.2μm for 10% SiC by volume. This implies that full homogeneity of a composite containing fine ceramic particles will be impossible to achieve. Campbell and Bauer[77] support this, noting that mixing efficiency increases as the component particle ratio (Al:SiC) approaches unity. However, it is by no means certain that a homogeneous structure will result from these conditions only that a random distribution will be more likely. Turbula mixing provided the best starting structure for subsequent compaction and thermomechanical processing.

5.2 Establishment of Process Route

Although the process route is of ultimate importance to the production of a coherent, non porous, un-agglomerated composite it is, in this work, only a means to an end. Thus, very little systematic analysis of the extrusion or pre-extrusion parameters has been undertaken other than in a rudimentary form.

5.2.1 Compacted Billets

The density of billets which were cold compacted at pressures of approximately 350-400 MPa were measured by the difference method, explained in section 4.5.2. The densities of billets of Al-7Mg and 2014 composites were found to be between 57% and 65% of their theoretical density. This is a very low value when compared to densities for unreinforced powder compacts, which are usually around 80-85%. The decrease in density must be due to the large difference in elasticity and plasticity between the aluminium alloy and the silicon carbide, which increases resistance to compaction.

5.2.2 Initial Extrusion Trials

Initial extrusion trials were conducted with the aim of determining limits to the production of a coherent macrostructure. It was immediately apparent, even before trials commenced, that some kind of lubricant would be required for there to be any hope of achieving this aim. Following the work of McShane[94], commercial purity aluminium heated leader pads were introduced into the extrusion container directly in front of and prior to the billet being extruded. The results of these tests are set out in table 5.1, along with comment on the surface quality.

Alloy & % SiC	Ram speed (mm/s)	Temperature (deg.C)	Ratio	Peak Press. (MPa)	Extrudate surface
Al-7Mg/10%	2	370	30:1	801.3	Blistered
Al-7Mg/10%	5	370	30:1	1125.0	Blistered
Al-7Mg/10%	3	370	22:1	833.0	Blistered
Al-7Mg/20%	5	370	30:1	993.7	Poor
Al-7Mg/20%	5	450	30:1	715.3	Poor
Al-7Mg/20%	3	370	22:1	975.6	Cracked
Al-7Mg/30%	5	370	30:1	977.8	Poor
Al-7Mg/30%	3	370	22:1	934.8	Cracked
2014/10%	3	470	17:1	224.1	Spiral
2014/10%	3	270	17:1	864.7	Spiral

Table 5.1: Variation in extrusion pressures with extrusion parameters and composite compositions.

The first point of note is that the value of the peak pressure appears to be most closely related to the effect of extrusion speed on the integrity of the lubricant film. Extrusion temperature, speed and ratio are seen to act in the expected manner: as temperature increases and speed and ratio decrease, extrusion of the material is facilitated. The choice of a cast or compacted powder C.P. aluminium leader pad did not appear to have a great effect on the peak, but this is probably because they were equally bad where a comparison was possible.

It can be seen from the table that the lower flow stress 2014 alloy has the lower peak pressure; this was to be expected. It should also be noted that the coherency of the lubrication film on the product was best on the 2014 matrix composites. This is probably linked to the speed and lower ratio employed. The pressures required for extrusion of Al-7Mg composites are approximately 2-3 times greater than is required for the extrusion of unreinforced alloy[95] of broadly similar composition at the same ratio.

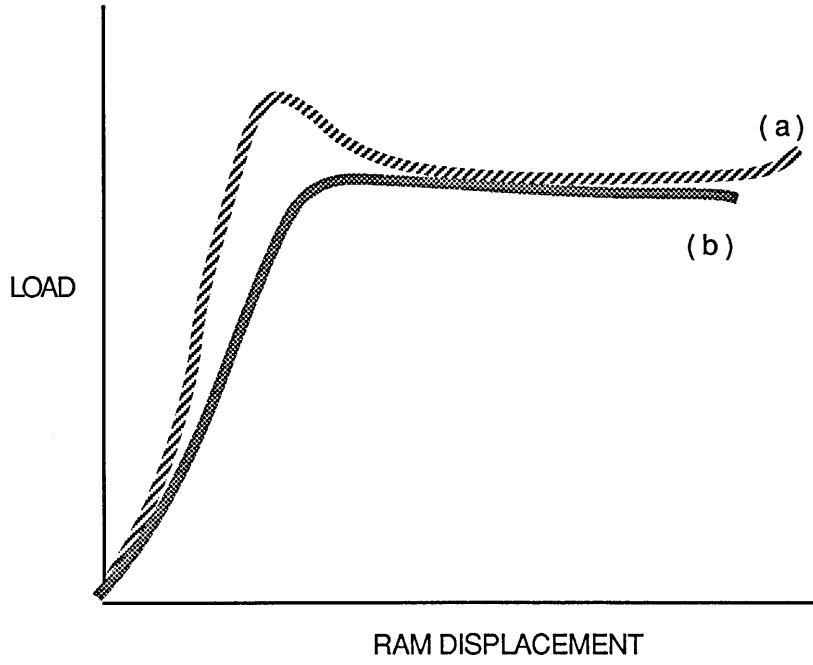

Fig. 5.3: Schematic diagram comparing load/displacement variation during extrusion of (a) unreinforced powder; (b) composite, with coherent lubrication

Where the lubrication is of similar quality it was observed that the higher extrusion temperature resulted in lower peak and steady state pressures. This is in agreement with the theory that the peak is associated with an activation energy to achieve the steady state[96]. At a higher temperature the energy required to achieve

breakthrough will be lower. The designation of surface quality will be explained in section 5.3.

The effect of increasing reinforcement content is somewhat masked by the variable quality of the lubricant coating. The expectation is that peak pressure will increase due to the increased resistance to flow imparted by the particles[31]. This will be demonstrated in section 5.3.

5.2.3 Pre Extrusion Processing

It was evident from the initial trials that the production route was unsatisfactory- reliability of the product and reproducibility of results could not be guaranteed. The trials detailed in the experimental section were instigated in order to compare process routes and as such there is some overlap between this and the previous section. The alloy 2014 was used in this comparison because it gave the most promising results in the initial trials. The volume fraction of 5μm silicon carbide was kept constant at 15% in order to prevent any obfuscation of the results. The results of this comparison are given below, in table 5.2.

PRE-EXTRUSION PROCESSING	T.ext. (deg C)	Ratio	Speed mm/s	Pmax (MPa)	EXTRUDE SHAPE	SURFACE QUALITY
Cold compact	470	30	3	409.7	round	Cracks
Cold compact	470	16	3	375.0	rectangular	Edge cracks
Cold and hot compact	470	30	3	364.4	round	Good
Cold and hot compact	470	16	3	301.0	rectangular	Edge cracks
Can, cold compact & degas	470	30	3	1068.4	round	Good
Can, cold compact & degas	470	16	3	409.7	rectangular	Good
Can, cold compact, degas & hot compact	470	30	3	364.4	round	Good
Can, cold compact, degas & hot compact	470	16	3	294.0	rectangular	Good

Table 5.2: Effect on extrusion of variation in pre-extrusion processing parameters

Hot compaction of the billets, where relevant, was performed at pressures of around 1000 MPa subsequent to degassing of the canned material at 500°C. Degassing of the powder, after cold compaction in the can but before hot compaction, was introduced into the process route in an attempt to reduce porosity and benefit fracture

toughness[97]. The effect of this operation in combination with hot compaction will be demonstrated in section 8.6.2. The distinction between 'degassing' and 'outgassing' should be drawn at this point. Outgassing is simply the evacuation of a sealed unit; degassing involves a chemical dissociation of gases from the material during evacuation at elevated temperature. The trace of pressure during degassing showed three broad troughs at temperatures of 100°C, 300°C and 350°C which clearly indicates that degassing, rather than outgassing, has occurred. This distinction is important in determining the effect of this operation on the properties of the material[97].

Although a "peak" pressure for extrusion is quoted, there was no substantial peak, in the true sense, exhibited during the extrusion under any of the conditions. The general shape of the curve is shown in the schematic diagram fig. 5.3.

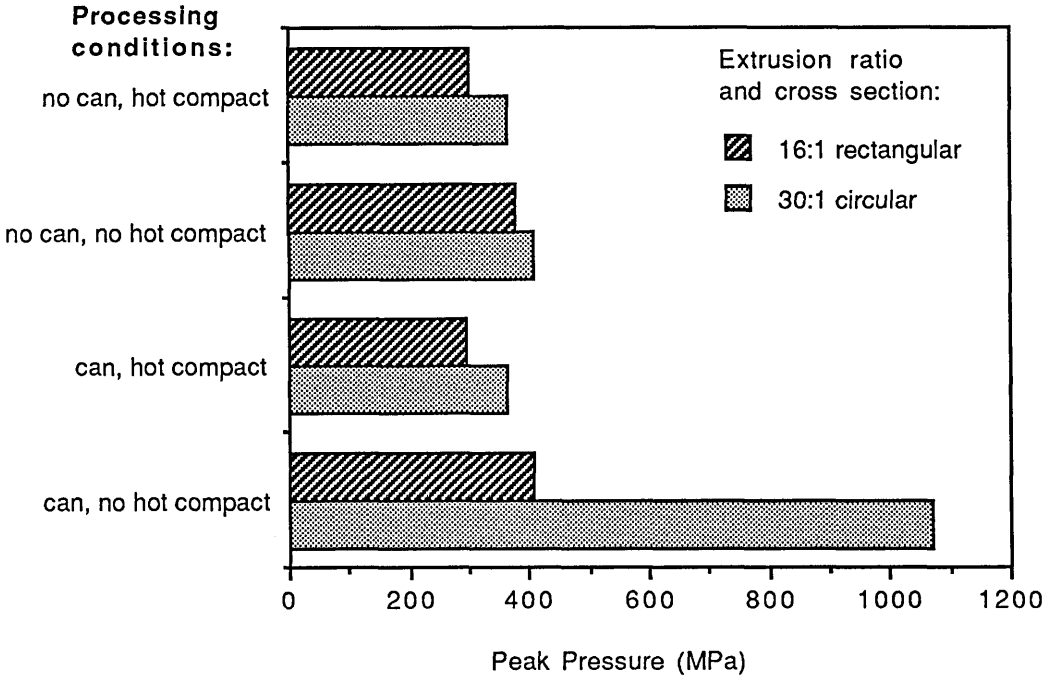

Figure 5.4: Variation in peak extrusion pressure of 2014 composites with processing parameters and extrusion ratio.

There are a number of salient points which emerged from these data. The difference in extrusion pressure between round and rectangular cross section material is probably due to the lower ratio employed during the extrusion of the rectangular bar even though rectangles are generally more difficult to extrude, a premise which is readily demonstrated by the shape factor correction of Subramaniyan[98], based on the concept of a peripheral ratio. The increase in pressure required (under the same conditions) is a function of the ratio of the perimeter of the extrudate shape to that of a round bar of the same extrusion ratio. In this case, the correction factor for the

rectangular extrudate is 1.48, resulting in an "equivalent circular ratio" of 24:1. A comparison of the extrusion of billets which have undergone similar compaction processes reveals that canning results in the need for a higher extrusion pressure, but this is unimportant as other factors will also decide the process route. The low speed of extrusion was necessary to obtain a good surface quality. The chart, figure 5.4, shows the differences in 'peak' pressure required for extrusion. It is unclear why the material extruded in a can without hot compaction required such a high pressure at a ratio of 30:1. It is possible that the void between the top of the powder compact and the can lid (which arises during compaction of the powder and is necessary in order to allow welding) may have contributed to this effect, allied with the low cold compaction pressures used for material in the cans. This effect did not occur in the rectangular extrudate; the reason for this is also unclear.

5.3: Thermomechanical Processing of CW67 and its Composites

5.3.1 Unreinforced Alloy

The unreinforced alloy powder was compacted and extruded using the standard procedure for powder materials[99]. Other billets were extruded after canning, degassing and hot compaction, the procedure which was established as providing the best extrusion conditions for composites. The results are shown in table 5.3.

Processing	Shape	Nominal temp,°C	Speed, mm/s	Ratio, R	Pressure MPa
cold compact	round	425	3	30	457.3
cold compact	round	325	3	30	740.2
cold compact	round	430	3	60	473.1
cold compact	round	325	3	60	830.7
cold compact	round	420	3	30	432.3
cold compact	round	430	8	30	525.3
cold compact	round	430	3	30	493.4
hot compact	square	430	3	24	337.3
hot compact	square	440	3	24	382.5

Table 5.3: Extrusion of unreinforced CW67 alloy

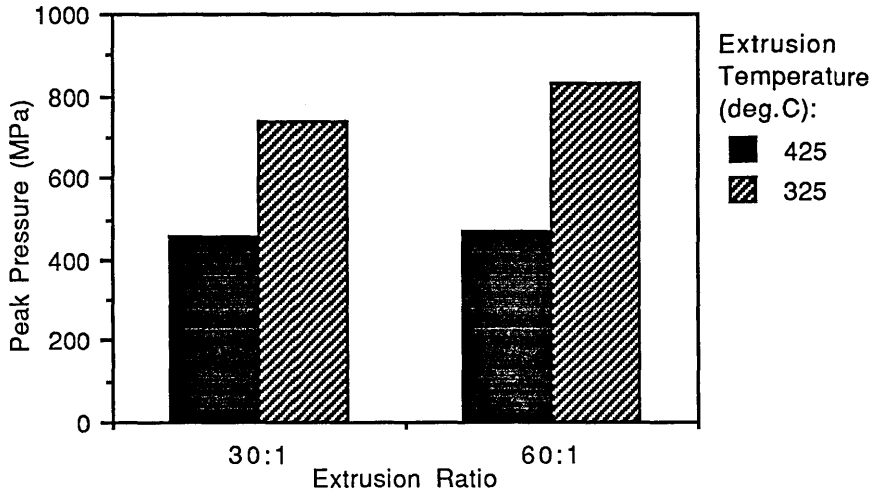

Figure 5.5: Variation in peak extrusion pressure with ratio and temperature for unreinforced CW67.

Table 5.3 simply shows the variation in peak pressure as extrusion ratio and temperature are varied at a constant extrusion speed of $3mms^{-1}$. The trends are as expected: as temperature decreases and ratio increases the extrusion pressure increases (as shown in figure 5.5). The canned material required a lower pressure, probably because of the slightly lower extrusion ratio (although the equivalent ratio is 29:1) and the lubricating effect of the can material. Increasing the extrusion speed is seen to require a greater extrusion pressure.

5.3.2 Composites of CW67

The extrusion load/ram displacement curves for the canned material do not show a large peak; this is probably due to the lubricating influence of the can material and is similar to the schematic curve (b) in figure 5.3. The peak pressures follow the expected trend of an increase proportional to volume fraction as shown in figure 5.6. The fit of the line to the data is reasonable, with a correlation coefficient of 0.92 for the line through the 24:1 data; the limited data available for the higher ratio curve is reflected in the fact that no line was plotted through the points. Obviously, a much larger amount of data is required before any definite predictions are made, but the equation for the plotted line was calculated as:

$$P = 352.8 + 3.34.V_f \quad \text{.....5.1}$$

where P is the peak pressure and V_f is the volume fraction of SiC.

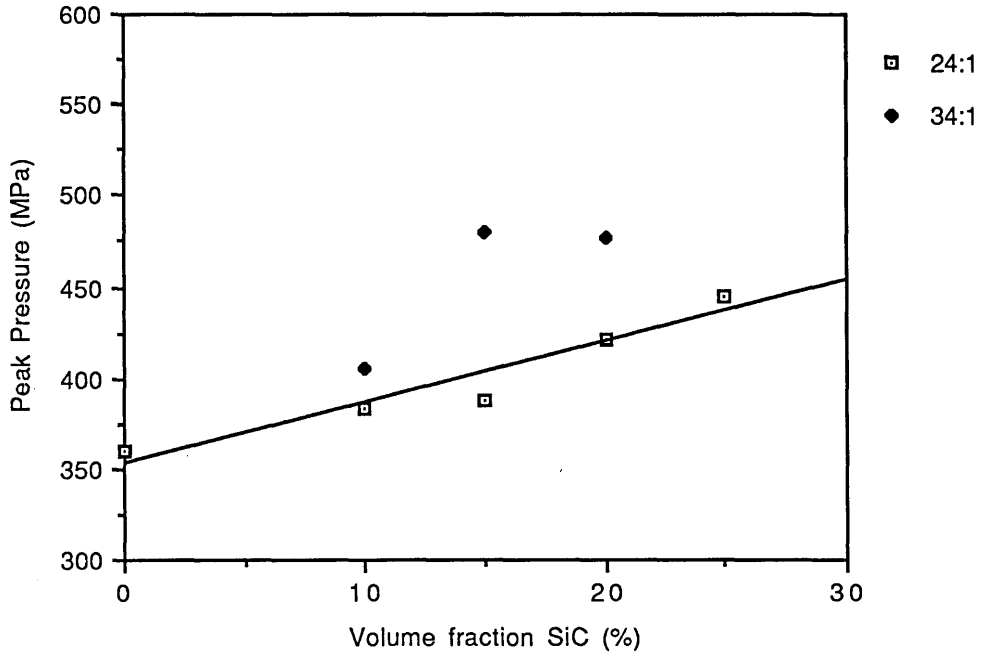

Figure 5.6: Variation in peak pressure with volume fraction of SiC

The results show the expected trend of a rise in extrusion pressure as volume fraction increases. The absolute values of these pressures are in the same range as those required to extrude the unreinforced alloy at approximately 450°C, however, it should be remembered that the composites are all extruded in cans of 2014 which will act as a lubricant during extrusion.

Hot rolling was conducted at an initial billet temperature of 500°C on sections of the extrudate which had been extruded at a ratio of 34:1, resulting in an extrudate thickness of 4mm. This was reduced to 1.75mm by hot rolling, the reduction being spread over 6 passes. This was a total reduction of 56%. A reduction of approximately 13% per pass was employed. Only two billets, containing 10% and 20% SiC, survived the rolling operation. Composite material containing 10% SiC, and other volume fractions, failed by "alligatoring" or cracking along the edges of the plate. "Alligatoring" is caused by the slight misalignment of the rolls[76] and is more easily corrected than edge cracking which was probably due to insufficient heating[76]. This was caused by initial attempts to roll without heating between each roll pass. Subsequent to this set back, billets were heated between each pass which made their rolling easier but will be seen to have affected the properties.

5.4 Thermomechanical Processing of C.P. Aluminium and its Composites

Composites of C.P. aluminium were mainly extruded and rolled. Extrusion was conducted at an initial billet temperature of 500°C. Two extrusion ratios were employed, resulting in two different shapes of extrudate. These were 30:1, resulting in round bar which was tested in the extruded state, and 16:1 for rectangular bar which was subsequently rolled. The extrusion pressures are shown in figure 5.7 below. It is interesting to note that the pressure decreases with increasing SiC particle size. This is thought to be a function of the inter-particle spacing exerting an effect on the flow stress. Further examination of composite extrusion would be required before this hypothesis is substantiated. It is also evident that the ratio and temperature have an effect on the peak extrusion pressure.

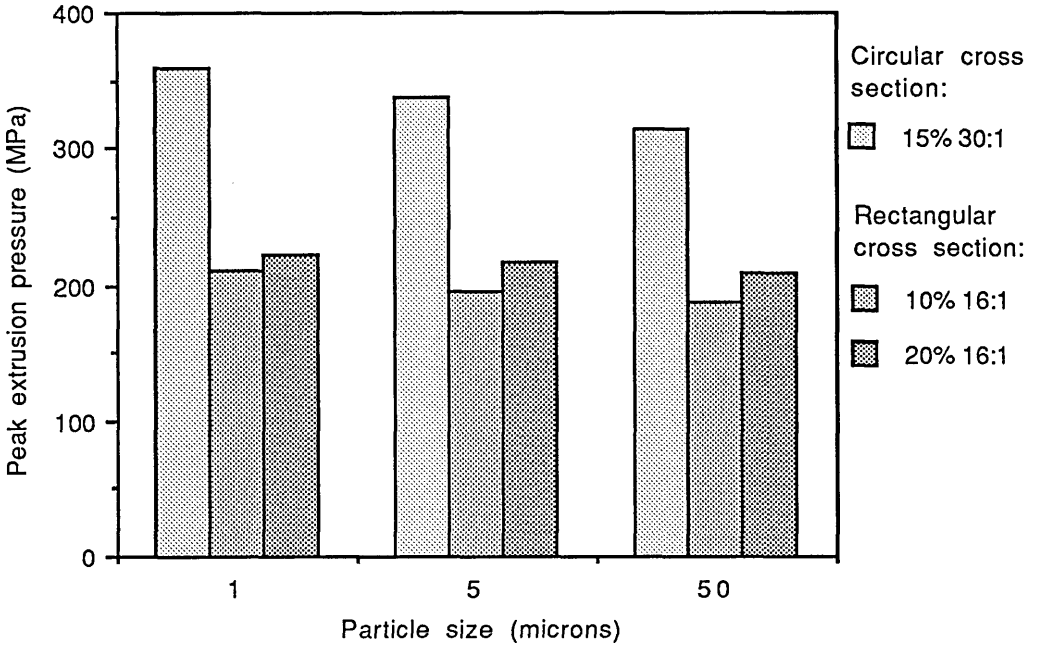

Figure 5.7: Peak pressures required for extrusion of C.P. Al composites

The pressure required to extrude the unreinforced alloy was 310.1 MPa at a ratio of 30:1, and 199.5 MPa at 24:1. A composite containing 15% 50μm SiC was also extruded at the lower ratio: a pressure of 210.1 MPa was required. This is approximately the same pressure as was required for the 20% 50μm composite extruded under the same conditions.

Rolling of the C.P. composite rectangular bar was conducted at 500°C on composite material containing the three particle sizes in volume fractions shown above in table 5.4. A billet containing no silicon carbide was rolled in order to act as a

control. The extrudate was first machined to a thickness of 5mm and then rolled to approximately 1.9mm in 7 passes. This equates to a total reduction of approximately 62% with a reduction per pass of around 12%. Few problems were encountered during rolling. This was because C.P. aluminium has a low flow stress and the material was reheated between each pass.

Particle size (μm)	Volume fraction SiC (%) employed.
1	10, 20
5	10, 20
50	10, 15, 20.

Table 5.4: Volume fraction of SiC in rolled C.P. Al composites.

5.5 Surface Quality

Assessment of the quality of the surface is important in the development of any material. Defects at the surface can render the extrudate useless by encouraging failure or reducing resistance to corrosion. There are a number of problems which may be encountered during the extrusion of unreinforced aluminium alloys, most of which are likely to be exacerbated by the presence of reinforcement particles. The main defects occurring are, in order of severity: die lines, 'pick up', incipient melting, speed and hot shortness cracking. The inclusion of silicon carbide in any aluminium alloy will lead to die scoring and the exacerbation of the above problems[33]: its effect will be discussed in more detail later in this section.

Formation of the surface of the extrudate is at two deformation regions: the shear zone adjacent to the dead metal zones and at the die face adjacent to the throat[100]. Thus the billet surface is subjected to a high degree of work. Die lines form as a result of the influence of the die land region on the extrudate surface. Pick up, leading to surface defects, is due to transient sticking of the extrudate to the die land and removal of material from the die land by the extrudate[100]. Incipient melting is caused by over heating of the extrudate surface, due to the high friction between the container and the billet. Cracking may also result from this increase in temperature, even if the eutectic temperature for the material is not exceeded. This is because as the temperature increases the flow stress of the material (resistance to deformation) decreases dramatically. Thus frictional forces will lead to sticking and tearing of the surface[98,101]. Cracking due to excessive extrusion speed (strain rate) is also common in high strength alloys[102], but more easily eliminated by reducing the speed. Very

little work has been undertaken on the extrusion of composites. Where extrusion parameters have been investigated[33], the parameters leading to defects have been seen to be further restricted.

The quality of the coating on the surface of the extrudate was variable, as the micrographs show. Blistering of the coating was evident in the first extrusions (fig.5.8a). The size of the blisters decreased as the extrusion progressed, as did their frequency; blister size ranged from approximately 10mm at the front end of the extrudate to approximately 1mm or less at the back: this is clearly shown in figure 5.8a. This may correlate to the amount of trapped gas/air in the compact at any particular time during the extrusion. Measurements of density of these billets revealed that they could be as low as 60% of theoretical density, compared with approximately 90% which is routinely achieved for an unreinforced powder compact. This means that there will be a significant amount of air remaining in the billet. If a coherent lubrication film is formed the escaping gas can only form sub-surface blisters, unless there is a poor seal at the back end of the billet where it meets the dummy block. Extrudate without blisters was produced and on investigation some back extrusion was found to have taken place. It is postulated that the gas escaped via this route, as was found by Tan[99].

There are a number of other ways in which the lubrication broke down, some of which are exhibited in figures 5.8b and c. In some instances the material remained intact but the surface has a scaly appearance. Other extrudes were either disjointed (so called 'fir tree cracking') or had surfaces with partial lubricant coverage and scoring, which is probably due to the degradation of the die during a number of extrusions and pick up. In figure 5.8b both of these defects are evident. In the upper extrudate, fir tree cracking has occurred but lubricating material can still be seen to be adhering to the extrudate surface. This is also the case in the lower extrudate which has undergone scoring. These defects are associated with the leader pad sticking, possibly because it was at a lower temperature than either billet or container. The surface quality was unaffected by the use of cast or compacted powder pads.

The surface of the rectangular extrudate (20mm x 10mm, produced from the ratio 22:1) was generally good by comparison (fig.5.8c). Blistering and corner cracking were evident but the overall integrity of the coating was maintained. This may have been due to the lower extrusion ratio and speed.

(a) Al-7% Mg/10% SiC: extruded at 370°C, 30:1; top= front end, bottom= back.

(b) Top= Al-7Mg/20% SiC: extruded at 450°C,30:1; bottom= Al7Mg/30% SiC, extruded at 370°C, 30:1.

(c) Al-7Mg/20% SiC: extruded at 370°C, 22:1; top= front end, bottom= back.

(d) 2014/15% SiC, no can; extruded at 470°C,16:1,top= back,bottom= front.

(e) Unreinforced CW67: top=extruded at 425°C, 30:1, unlubricated; bottom= extruded at 325°C, 30:1, lubricated.

(f) 2014/15% SiC, canned; extruded as fig.5.8d, top= front end showing can spout, bottom= back end.

Figure 5.8: Surface quality of extrudate

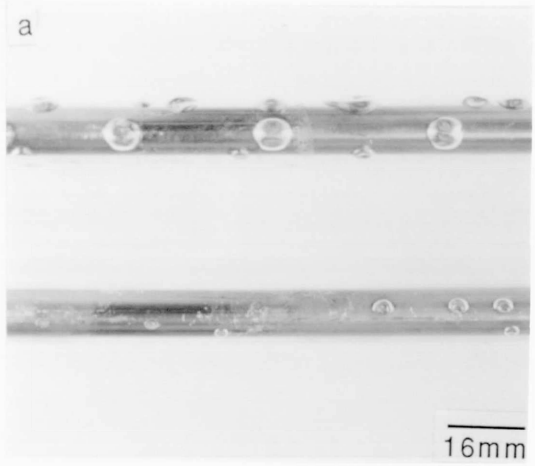
a
16mm

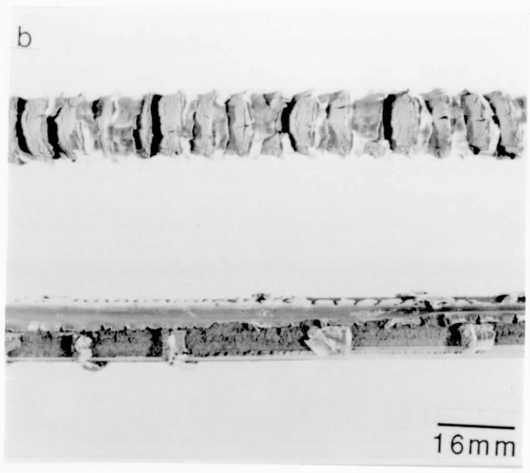
b
16mm

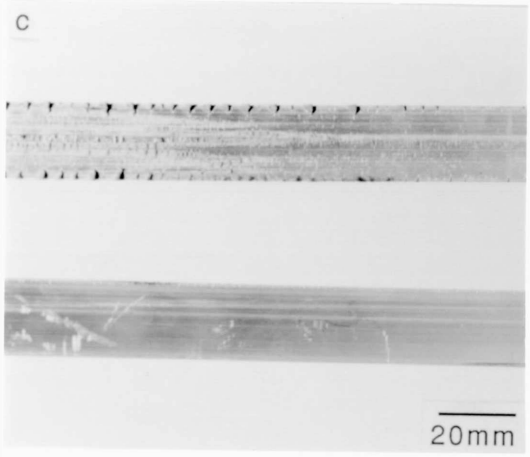
c
20mm

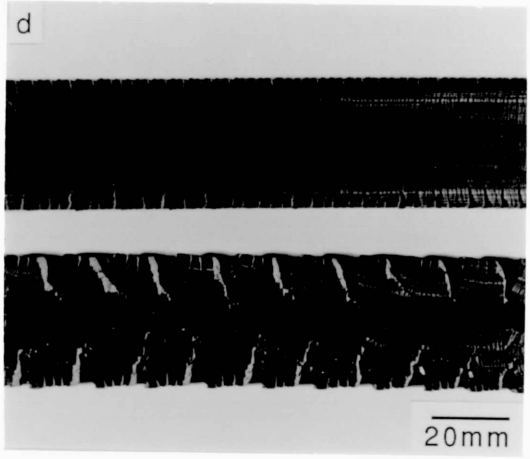
d
20mm

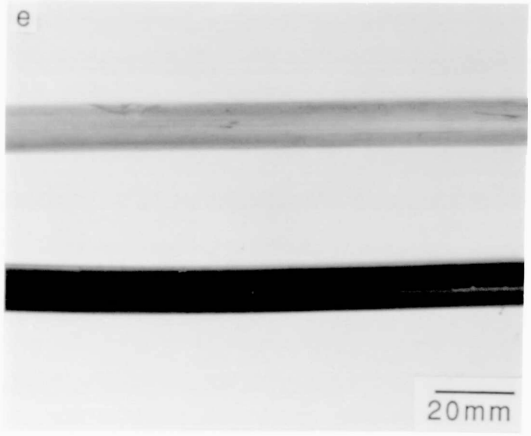
e
20mm

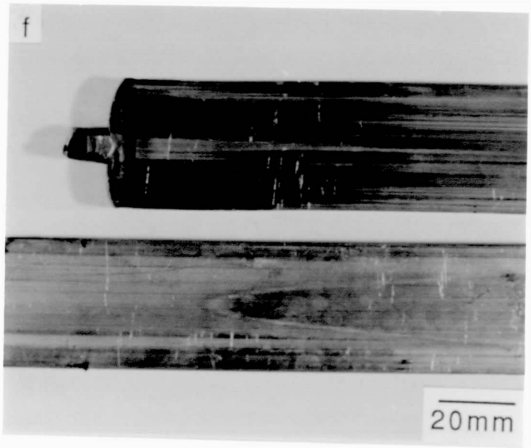
f
20mm

In some cases, although the coating was coherent a wave like or spiral pattern was apparent on the surface. This only occurred in the extrusion of the 2014 composites. This phenomenon may be related to the silicon carbide causing a non uniform stress field at the die entrance, although in some cases the lubricant was seen to be broken along the spiral and it may be that this is another means of gas escape in conjunction with back extrusion as no blisters were evident in these extrusions.

Examination of the transverse section of extrudate showed that the thickness of lubrication varied by up to 400% between front and back. For a flat pad of uniform thickness this was perhaps to be expected. During the establishment of the dead metal zone and for composite material to enter the deformation zone a relatively large amount of lubricant must flow through the die orifice. As a steady state is achieved the lubrication thickness becomes more or less constant until the lubricating material starts to run out towards the back end of the billet: thinner pads usually resulted in poorer lubrication. Clearly there must be a lower limit to the pad thickness, below which full lubrication will not be possible. Leader pad shape would also have an effect on the distribution of the lubricant along the extrudate, however this was not investigated.

Die wear is another important factor in determining the quality of the surface, and also the tolerance of the final product. A quantitative investigation of die wear was considered to be outside the scope of this thesis, however some observations were made. Score lines were observed on the die face after only one or two extrusions, and will probably extend to the die land also. This is clearly due to the presence of silicon carbide which is, of course, a commercial abrasive. It was found that extrusion was facilitated by using a die with a land length of 3mm; initially dies with a land length of of 5mm were employed, which resulted in an unusable product. Hains et al[33] note that the die area which undergoes wear is related to extrusion ratio: at low ratios the face becomes worn, whilst at higher ratios, wear also occurs along the land.

There was a marked difference in surface quality between canned and non-canned product. Extrudate produced from material which was not canned exhibited surface cracking; towards the back end of extrudate which was neither canned nor hot compacted these cracks were nearly completely cross diametral. This may be due to the influence of the particles resulting in a form of hot shortness and stick/slip friction at the die land[33,102]. The surface of the unreinforced CW67 alloy is displayed in figure 5.8e for comparison with the composites. The top extrusion is unlubricated whereas the lower extrudate has a residual coating of colloidal graphite.

Extrudates which had been canned prior to extrusion had a good overall coating of can material, even though some of this had been machined away in the case of the hot compacted billet in order to reduce it to a size to fit the billet container. This was a vast improvement on leader pads which, as noted earlier, were prone to running out before the end of extrusion. It was also found that it was preferable to insert the can into the extrusion container with the cropped spout facing the die, an orientation which resulted in the spout remaining clear of the composite on exit from the die (figure 5.8f). The rectangular extrudate showed similar variations of surface quality to its round counterpart, the only difference being that the cracking (where it occurred) was of a different form, consistent with the change in shape. Extrudate of uncanned material exhibited cracks which started at the corners of the extrude, became edge cracks as the extrusion progressed and finally extended towards the centre. With the introduction of canning the material as a standard procedure, the surface quality of the extrudate was vastly improved in all cases.

5.6 Optical Microscopy

The efficiency of the extrusion process was partly assessed by examining the microstructure in the as extruded condition. Homogeneity of the SiC and porosity was examined in a semi-quantitative manner.

5.6.1 Initial Extrudates

The Al-7Mg/20% composite showed generally low porosity and agglomeration. It was however evident that banding of the silicon carbide had occurred on extrusion (fig. 5.9a), as was also observed by Divecha et al[36]. This banding is believed to originate at the mixing stage where slight differences in size of SiC particles leads to their segregation to specific velocity contours inside the mixer[77]. This is the onset of overmixing, which can be limited but will obviously occur sooner for a wider range of particle sizes; a much tighter control on particle size should go some way to eliminating the banding phenomenon. These inhomogeneities may have an effect on the longitudinal properties of the material. There are also hard agglomerates, which can never be broken down, present in the structures, as can be observed in fig.5.9a. Alloying impurities were also observed in the material. Similar microstructural features were observed in the initial 2014/20% SiC composite.

The size of pore is often large in the high volume fraction composite, as figure 5.9a shows, sometimes being visible to the naked eye. The distribution of the particles appeared improved in the higher volume fraction materials but this may be because of

the denser packing. Many of the particles are linked in lines extending across large parts of the section. There is a possibility that these lines might form a path of low energy for fracture to progress along, thus considerably reducing strength.

5.6.2 Comparison of Processing Routes-2014 Composites

The distribution of the silicon carbide in the transverse plane was observed to be fairly uniform in all cases. Agglomeration was observed, but to no great extent and with little difference between the four extrusion conditions. This is consistent with the theory that it is the mixing which mainly controls the homogeneity of the product[77]. The amount of porosity observed in the structure of each of the four extrusion conditions was, however, significantly different. The extrudate which had been hot compacted (fig. 5.9c) prior to extrusion showed far less porosity than that which had been simply cold compacted (fig. 5.9b). There are two types of porosity which may be encountered in extruded powder mmc.s: independent porosity, which results from poor consolidation, and porosity associated with agglomerates of the silicon carbide. It is the former which is more easily rectifiable and more prevalent in the extrudate which was merely cold compacted. It should be noted that, in theory at least, hot compaction could add to the agglomeration by forcing particles together which would otherwise have remained distinct. Whilst this may be the case it will be shown that the benefits far outweigh this consideration. It is difficult to separate the influence of degassing from hot compaction at this stage because the relative effect of hot compaction is perceived to be much greater. Hard agglomerates are still present in the material, as can be seen at the centre of fig. 5.9b.

The longitudinal section, fig. 5.9d, shows that the banding and agglomeration of the SiC particles is not as evident under these conditions as it is in figure 5.9a. This may be simply because of the lower volume fraction. There are still regions which are devoid of SiC and those which have a higher concentration. Porosity in the longitudinal direction has also been reduced by the hot compaction.

5.6.3 Composites of CW67

The distribution of the silicon carbide was found to be similar to that displayed in figures 5.9c and d for the 2014 composite. The SiC distribution was fairly homogeneous in the transverse section, although banding was still observed in the longitudinal direction. The porosity of the material was low, as anticipated with the process route employed. It was obviously more difficult to assess homogeneity of the composite as the volume fraction of SiC increased, but the values below show that

(a) Al-7Mg/20% SiC; extruded at 450°C, 30:1, longitudinal section.

(b) 2014/15% SiC; extruded at 470°C,30:1, cold compact only, transverse section.

(c) 2014/15% SiC; extruded at 470°C, 30:1, hot compact, transverse section

(d) 2014/15% SiC; extruded at 470°C, 30:1, longitudinal section.

(e) C.P. Al/15% 1μm SiC; extruded at 500°C, 30:1, transverse section

(f) C.P. Al/10% 50μm SiC; extruded at 500°C, 16:1, rolled, annealed at 500°C for 4 hours.

Figure 5.9: Silicon carbide distribution in the various composites

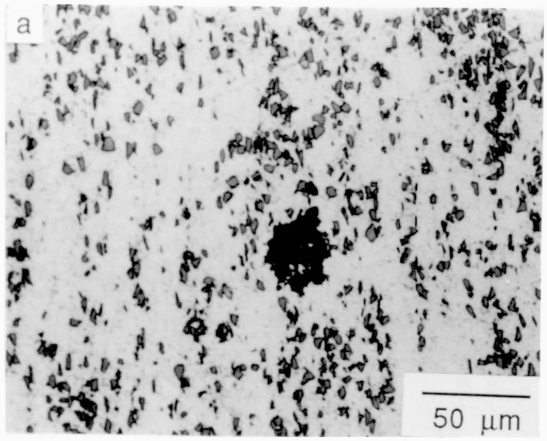
a
50 µm

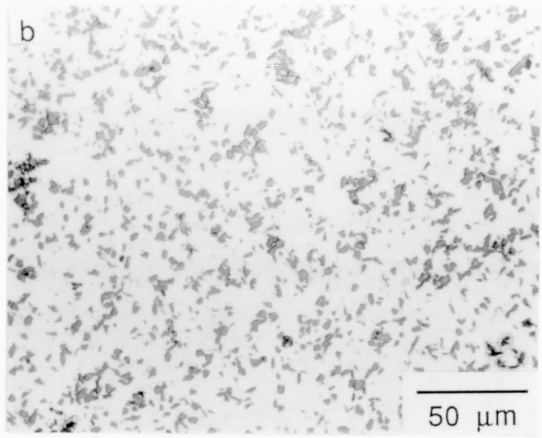
b
50 µm

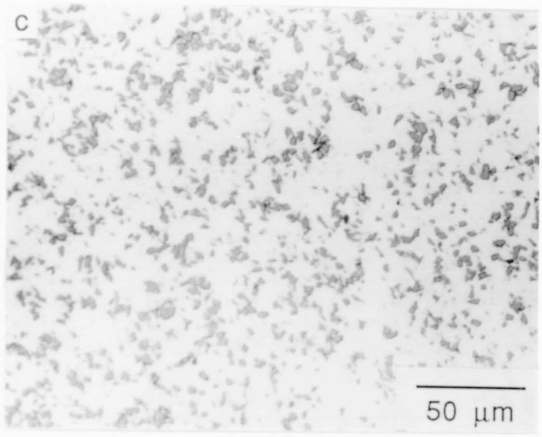
c
50 µm

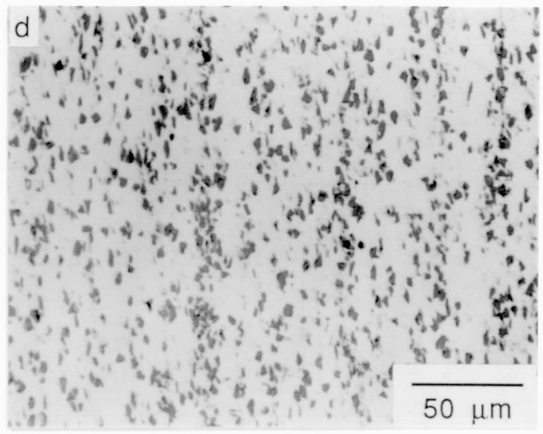
d
50 µm

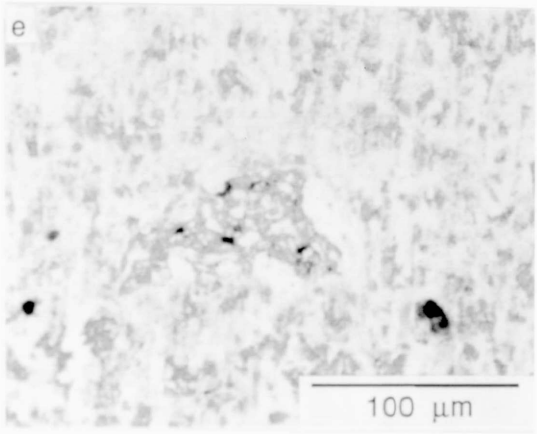
e
100 µm

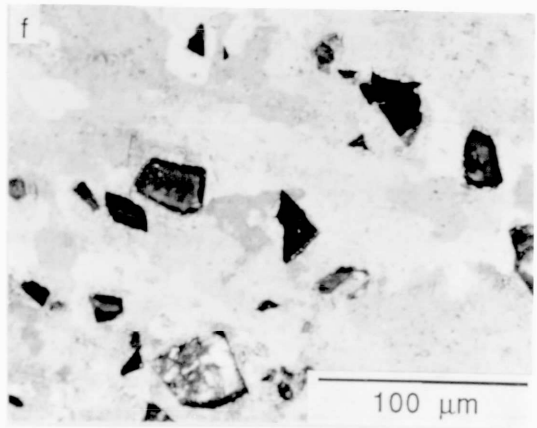
f
100 µm

variations in the transverse direction (measured using the mean linear intercept technique) are not great. There was no significant difference between the front and back of the extrudate.

Nominal volume %	Measured volume %
10	10.3 ± 2.6
15	15.5 ± 2.8
20	19.5 ± 1.8
25	25.8 ± 1.5

Table 5.5: Measured volume % of SiC for CW67 composites

5.6.4 Composites of C.P. Aluminium

Composites of CW67 were processed following the same process route as composites of 2014 and CW67 prior to rolling. The distribution of silicon carbide in the 5 μm composites was the same as was found in these two previous extrudates. The SiC distribution in the extrudate containing 15% of 1μm SiC is shown in figure 5.9e. It is clear from this micrograph that the SiC is heavily agglomerated and that a significant amount of porosity is present. This will inevitably have a detrimental effect on the mechanical properties of these composites.

Figure 5.9f shows the distribution of SiC and recrystallised grains in the 10%, 50μm C.P. Al composite which has been rolled and annealed at 500°C for 4 hours. There is significantly less agglomeration in the larger particle size composite, as was anticipated from the work of Campbell and Bauer[77] (see chapter 3). The grain distribution after annealing is seen to be associated with the SiC particles, with the 50μm particles nucleating one or more recrystallised grain. The recrystallised grain size was found to be 26.2μm ± 10μm across the rolling direction and 64.5μm ± 10μm in the direction of rolling. Grain size measurements of other C.P. composites are given in chapter 6, section 6.4. Discussion of the influence of grain size on strengthening of these composites is also dealt with in section 6.4.

5.7 Conclusions

Composites of all alloys tested in these trials required higher extrusion pressures than the unreinforced alloy. Where a comparison is valid (i.e. the extrusion ratio is the same) the increase in pressure required for composites of CW67 is between 25-50 MPa (7-14%) for between 10-25% SiC extruded at a ratio of 16:1 at

a temperature of approximately 425°C. Composites of C.P. aluminium required decreasing pressure as the size of SiC increased, but the increase over the unreinforced alloy was less than that for the CW67. The decrease in pressure as particle size increased is thought to be related to the inter-particle spacing and ties in with the observed decrease in pressure as volume fraction decreases. Poorly lubricated or unlubricated composites showed a much greater differential in extrusion pressure when compared with unreinforced material.

It is clear from the comparison between processing routes that the process resulting in the "best" product is that of canning, cold compaction, degassing and hot compaction prior to extrusion. This may seem a convoluted, and ultimately expensive, route to take; however, it will be recognised that the process route is a means to an end. An additional bonus of this route is that the presence of can material during extrusion considerably facilitates the production of a coherent surface. Further evidence will be presented in chapter 7 to support this choice. Subsequent to this assessment, all composite material was extruded under these conditions. Unreinforced CW67 alloy was extruded using both 'conventional techniques' and incorporating degassing and hot compaction into the processing route in order to test the effect of this operation on the unreinforced alloy.

6. COMPOSITES OF COMMERCIAL PURITY ALUMINIUM

6.1 Introduction

The incorporation of silicon carbide into commercial purity (C.P.) aluminium has little significance as an industrially desirable system but is ideal for modelling the effect of the reinforcement on properties without the masking influence of precipitates or large numbers of dispersoids. Various theories of strengthening and deformation have been developed using this material, as outlined in previous sections. The work described here aims to test and explain these theories by varying volume fraction and particle size in as extruded and extruded and rolled material. Following this it is hoped that these theories and the results presented herein can be used to help dissect the factors which are influential in strengthening of more complex age hardenable alloys.

6.2 Extrudate Properties

The results of tensile testing of extrudate is shown in figure 6.1. It will be noticed in the figures that there is no value given for 50 μm particles; this is because round tensile samples could not be machined from the extrudate due to the high hardness of the material.

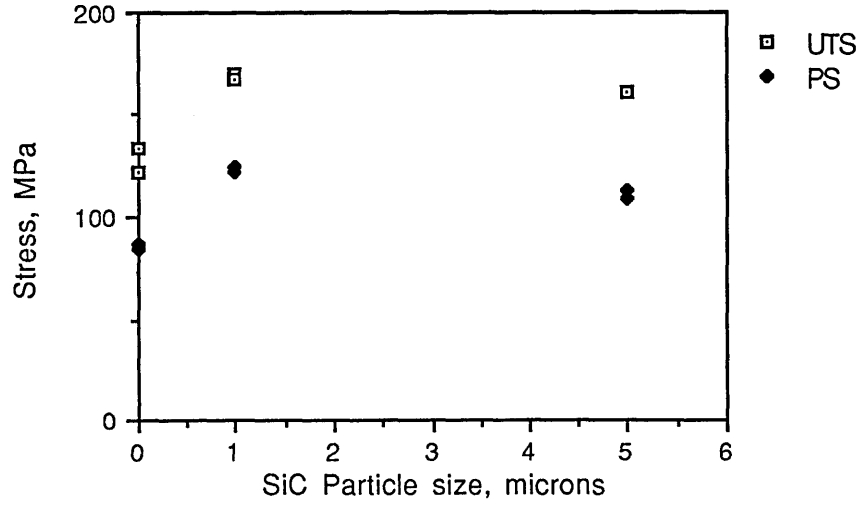

Figure 6.1: Variation of U.T.S. and 0.2% proof stress with particle size for as extruded material.

The variation in tensile strength is as would be expected from conventional considerations of particle strengthening (i.e. Orowan). The very low ductility for the 1μm composite can be traced, in part, to the high amount of agglomeration and porosity. A correlation of this observation is that the strength might have been higher, had the dispersion of silicon carbide been more homogeneous. Because of the absence of data for

the 50μm particle size composite it was at this point that it was decided to roll material in order to facilitate specimen preparation. Thus no further testing was carried out on extrudate.

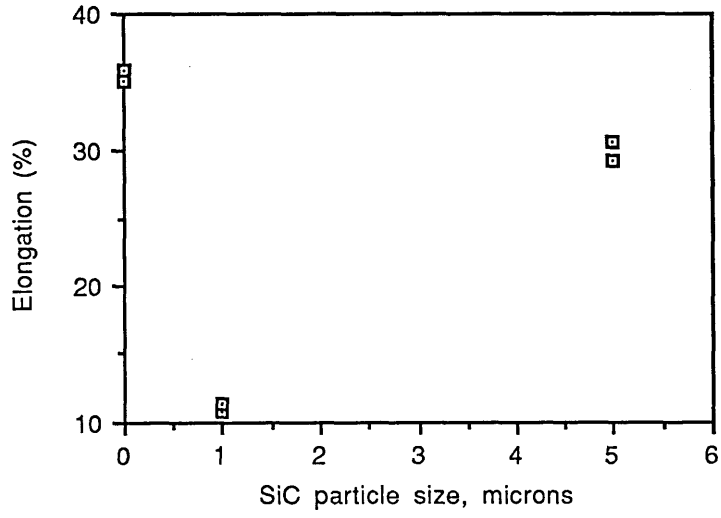

Fig. 6.2: Variation in % ductility with particle size.

The density of the extrudate (with the can removed) was found to be within ±2% of the theoretical density in all cases except that of the 1μm SiC which was substantially lower, at 94%±2% and 93%±2% of the theoretical density for the 10% and 20% volume fractions respectively. Such low values will have a detrimental effect on the mechanical properties of the material. Experimental error prevents any further conclusion from these results.

6.3 Testing of Rolled Material

The rolled material was tested in three conditions: as rolled (and quenched), partially annealed and fully annealed, the heat treatment conditions for these having been given earlier. Results of tensile testing are as follows in figures 6.3 and 6.4.

A number of points are immediately apparent from these curves. In the as-rolled results there seems to be a critical volume fraction, above which the effect of 1μm and 50μm particles is retrograde; indeed, at a volume fraction of 0.2 the 0.2% proof stress of the 50μm particle composite is lower than that of the matrix. The 5μm material shows no peak within the bounds of this experimental work, but the gradient becomes less steep and common sense suggests that the strengthening effect cannot continue indefinitely; this is limited by the ability of the matrix to redistribute stress. As the volume fraction of SiC increases there will obviously be less matrix material available, which will eventually run out of the necessary ductility required to

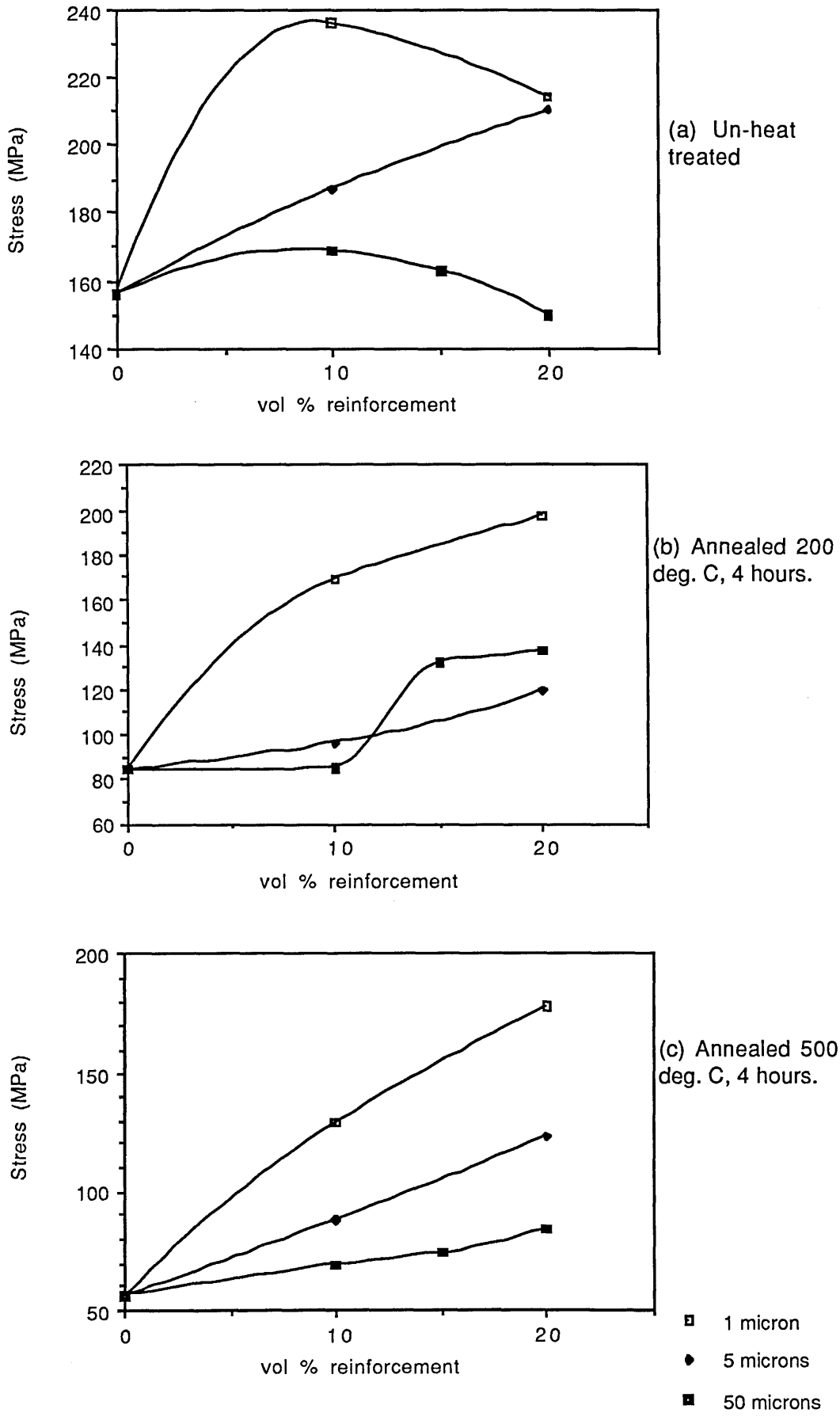

Fig. 6.3: 0.2% proof stress against volume fraction of SiC.

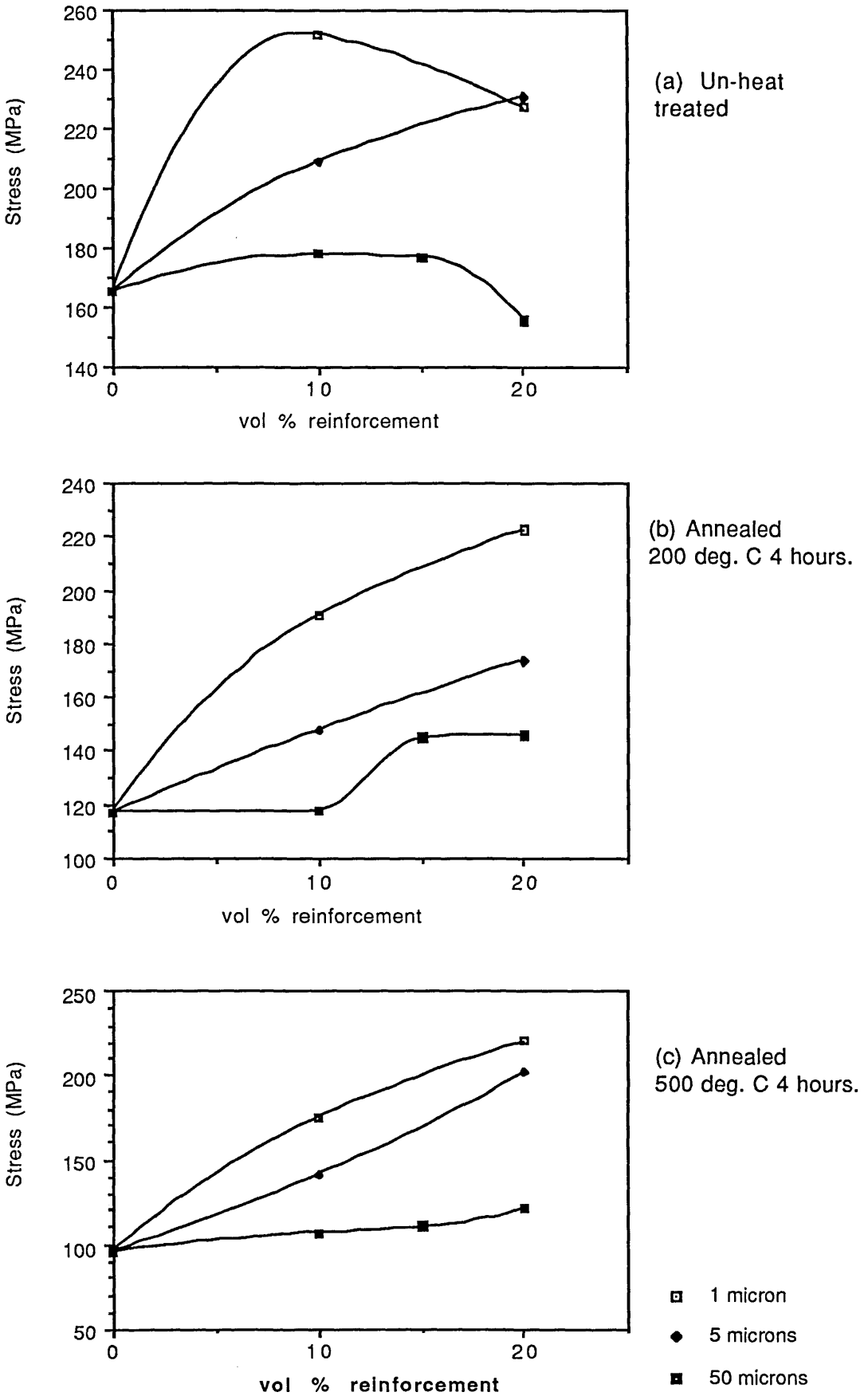

Fig. 6.4: Ultimate tensile stress against volume fraction of SiC.

redistribute the local internal stresses at the silicon carbide particles. In this case the specimen will fail, and is observed to fail, before reaching the plastic region. The highest strength was obtained with 10% of1μm SiC particles: the 0.2% proof stress was measured to be 236 MPa, which is an increase of 51% of the unreinforced material value in the as-rolled condition. Other particle sizes show less increase, within the bounds of this investigation. The 5μm material exhibits a maximum increase of 41% at a volume fraction of 20% with a 0.2% proof stress of 224.4 MPa; the 50μm material has a 0.2% proof stress just 9% over that of the unreinforced material, at 170.8 MPa.

The results for the annealed material show an increasing tendency to shift these peaks to the right (higher volume fraction), which is consistent with the previous explanation. As the degree of annealing increases it will also be noticed that proof strength declines for all particle sizes; this is, of course, consistent with expected trends for the matrix. The greatest proof stress is again exhibited by the 1μm composite, for all volume fractions. The percentage increases in strength are substantially greater in the annealed condition. After partial annealing the 20%, 1μm composite has a 0.2% proof stress which is 143% of the unreinforced material value, whilst after full annealing the increase itself increases to 260%. The increases due to the larger reinforcement particles are not as large, but still increased compared with the as-rolled material. The larger increases in strength as particle size falls may be due to the better retarding of recrystallised grain growth (the Zener pinning effect, which is dependent on the size of the pinning particle), and smaller initial recrystallised grains[38]. The effect of grain size will be discussed in section 6.4. The sub-micron particles may themselves exert a considerable effect on the strengthening (again to be discussed in section 6.4). It should also be remembered that these values are limited by porosity and agglomeration in the 1μm composites, the effect of which is, however, inferred from the graphs to have decreased with annealing, for the same volume fraction of particles. This inference follows from the explanation of the movement of the peak in the strength values, given above.

The ductility of the material increases as the annealing proceeds to completion, again as would be expected. The expected decrease in ductility occurs as volume fraction of reinforcement increases. It is interesting to note that ductility does not vary as size varies monotonically. This is probably due to the large amount of agglomeration in the composite containing 1μm SiC particles.

It is believed that there are two effects which contribute to these results. In the case of the as-rolled material, the heat treatment is less certain than for the annealed

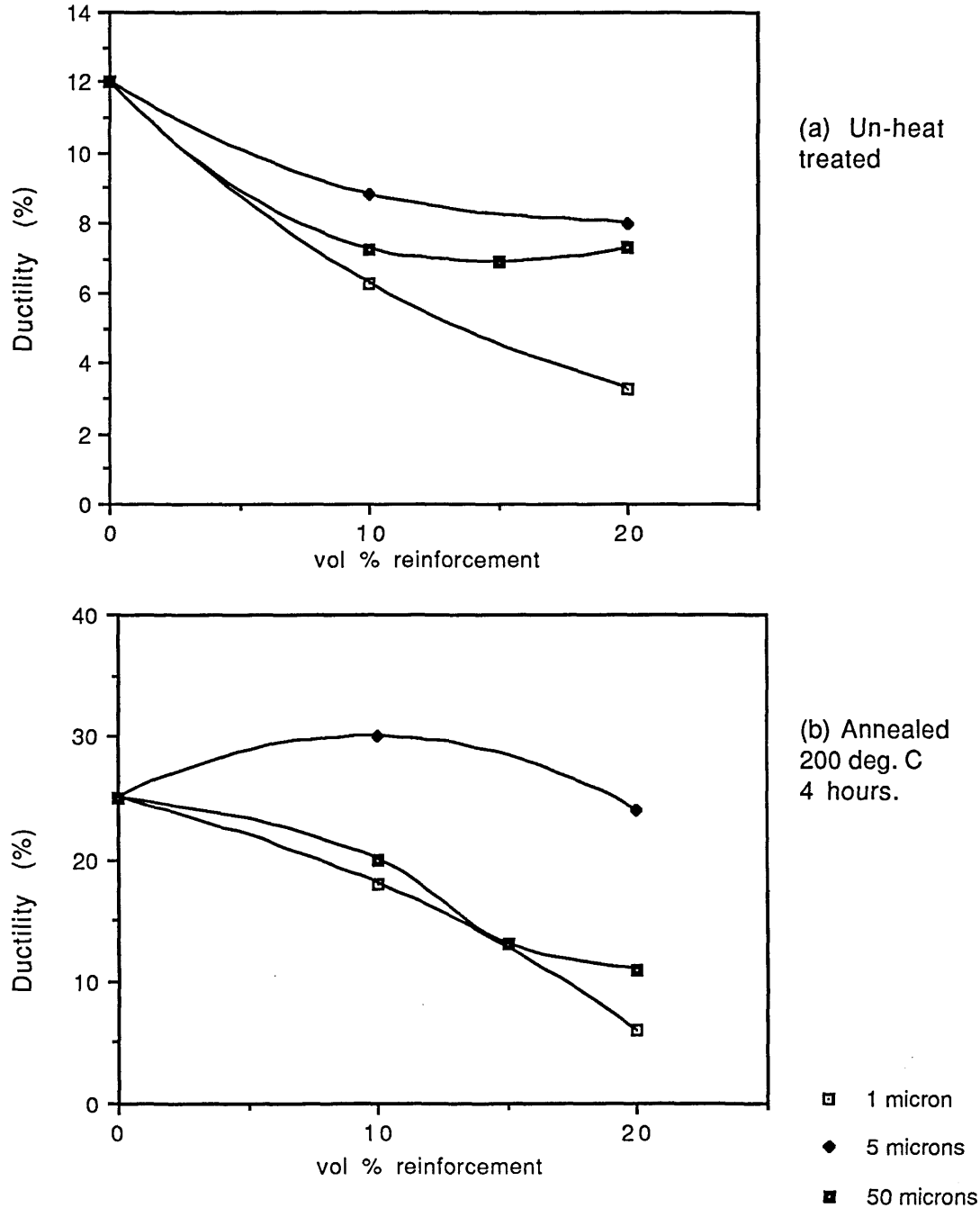

Fig. 6.5: Ductility (%) against volume fraction of SiC.

material. This material will contain the greatest density of dislocations and a high residual internal stress (as exemplified by Humphreys[37]). In the fully annealed material the accompanying changes will make for a more uniform microstructure, and thus more predictable changes in properties. The second effect, which is most noticeable in the as-rolled material, is that as volume fraction increases there will be a greater tendency for the smaller particles to agglomerate; this may explain the "peak" corresponding to a critical volume fraction. In the annealed material, the matrix is able to redistribute the stresses more effectively, thus leading to a waning of the agglomeration effect. Undeniably, there will be a peak to the strengthening effect, but in an 'ideal' composite (one without agglomeration) this will be governed by the amount of matrix, as discussed earlier.

6.3 Strengthening in Commercial Purity Al Composites

There are two approaches which may be taken in order to arrive at a theory of strengthening and deformation of composites. The first is based on load transfer and is characterised by the work of Eshelby and others (see reference 6); the second is a matrix strengthening model, exemplified by the work of Humphreys[38]. This thesis seeks mainly to assess the latter model.

In any material there are a number of sources of strengthening which may arise from the interactions of dislocation with grain boundaries, solute atoms, second phase particles and other dislocations; all of these sources have been thoroughly investigated by many workers. The table below shows the different sources of strengthening which may occur in composite materials. The two components of the system, the matrix and the silicon carbide particles, will each contribute towards the strength but the presence of the ceramic particles will also modify the matrix response and thus lead to changes in the yield strength. This section will first consider the extension of accepted theories for strengthening and then consider the influence of the particles on the matrix.

The Hall Petch equation relationship shows the strengthening due to grain and sub-grain size and it is plain to see that as grain size decreases the material will have a higher yield stress. In the case of aluminium, the constant, K_y, which is associated with propagation of deformation across the grain boundary, can be very low. In material produced from powder, the presence of oxide particles, which are resident at particle and grain boundaries, may have an influence on the value of this constant.

Mechanism	Governing equation	Description	Equation number
Grain & subgrain	$\Delta\sigma = K_y D^{-0.5}$ $D = t\{(1-V)/V\}^{0.33}$	Hall Petch eqn.- grain size strength	6.1 6.1a
Particle hardening	$\Delta\sigma = 2\mu b/l$ $(l=[t^2/V]^{0.5})$	Orowan looping around particles.	6.2 6.2a
Residual dislocations- due to Arsenault & Shi[39].	$\Delta\sigma = \beta\mu b\{(V/1-V)x B\epsilon'/b\}^{0.5}x(1/t)^{0.5}$ $\epsilon' = \Delta CTE.\Delta T$	Relates thermal expansion to dislocation generation	6.3 6.3a
Work hardening- due to Humphreys[37].	$\Delta\sigma = 4.5\mu V\epsilon$	Initial W.H. rate	6.4
	$\Delta\sigma = 5\mu(2Vb/t)^{0.5}\epsilon^{0.5}$	Higher strains	6.5

Table 6.1 Potential strengthening mechanisms operating in composite materials

Definition of Terms:

$\Delta\sigma$ strength differential induced by the specific mechanism

β constant, =1.25 (ref. 103)

μ shear modulus of Al, taken to be 27.5 GPa (ref. 6)

b Burgers vector, 2.86 $x10^{-10}$m

V volume fraction of SiC

B geometric factor, 12 for spherical particles

ϵ' induced thermal strain

t particle size

ΔCTE difference in thermal expansion coefficients; Al=23.6 $x10^{-6}$ $^oC^{-1}$, SiC=2.5 $x10^{-6}$ $^oC^{-1}$ (ref. 6)

Δt temperature difference

l inter-particle spacing

K_y constant, 0.1 $MNm^{-3/2}$

D grain size of Al

ϵ strain

The SiC particles may significantly influence the grain size. Humphreys and Kalu[104] have postulated that particles will stimulate grain nucleation below a particular temperature for a specific strain rate during working, as stress accumulates at the particle/matrix interface, and the Hall-Petch relationship in table

6.1 for grain size is based on this. Comparison of the strain rate during thermomechanical working of material in this investigation with the graphs produced by Humphreys and Kalu[104] suggest that particle stimulated grain nucleation can occur, although their work is only valid up to particle sizes of about 15μm. Examination of the microstructure indeed showed that recrystallisation had occurred and that grains nucleated at the silicon carbide particles (figure 5.9f). Some SiC particles had only one grain associated with them, whilst others nucleated two or more grains. Some grains were observed that were not SiC nucleated in the plane of the metallographic section, but these were in a minority. Grain size measurement was only possible for the larger particles and lower volume fraction: there was a tendency for the etched grains to become obscured as the particle size decreased and volume fraction increased. The grain size distribution of a 15% 50μm SiC composite (as noted in sub-section 5.6.4) was found to vary between average values of 26.2μm across the rolling direction and 64.5μm parallel to the rolling direction. At a volume fraction of 10%, the 50μm composite had a grain size which varied from 30.1μm to 79.5μm, and the grain size of the 5μm composite varied from 19.2μm to 43.4μm, both sets of values being quoted normal then parallel to the rolling direction. The deviation in these measurements was high- approximately ±10μm, which in some cases amounted to 50% of the value. This large deviation occurred as a result of different degrees of grain growth.

The interactions of dislocations with second phase particles depend upon parameters such as particle strength, relative modulii, stacking fault energy. Most of these parameters can safely be ignored in rapidly solidified C.P. aluminium reinforced with silicon carbide; the only important interaction is between dislocations and impenetrable SiC and oxide particles; this is described by Orowan's equation. It will be noted that as particle size decreases the strengthening effect increases dramatically. Furthermore, as particle size increases much above 1μm the Orowan strengthening effect becomes negligible. Work hardening will also occur in these materials by the interaction of dislocations as the dislocation density rises during deformation. Increases in strength due to the presence of SiC particles (i.e. by load transfer) will be governed by the Orowan equation and, as has been noted, will be insignificant for large particles. It is probable that in R.S.P. composites the actual spacing of the SiC particles will deviate from the theoretical spacing as size decreases. This is simply a physical consideration: the theoretical spacing will be smaller than powder particle size (see section 5.1.2). Also in the un-heat-treated state the SiC is likely to be at grain boundaries which will negate the Orowan strengthening effect. The equation for inter-particle spacing is due to Stephens et al[51] and has the same general form as a number of equations for spacing (see Taya and Arsenault[6]).

The presence of silicon carbide, or any other ceramic particle, will produce independent microstructural modifications as well as influencing those described above. Arsenault and Shi[39] have shown that the presence of SiC produces additional dislocations at the particle matrix interface on quenching of the composite in order to relieve stresses due to the large difference in thermal expansion coefficient: 10:1 for Al:SiC. This will necessarily produce increases in the strength of the material. The equation 6.3 given above, in table 6.1, predicts an increase in strength as:

(i) the temperature differential increases

(ii) particle size decreases.

The actual value of the increased dislocation density varies between experiment and theory and between different experiments and theories. Humphreys[37] states that dislocation densities of 10^{13} m^{-2} and 3×10^{12} m^{-2} were found for a composite containing 17% of 3μm SiC quenched to room temperature from 550°C and 200°C respectively. The calculated densities for these conditions were 2×10^{13} m^{-2} and 9×10^{12} m^{-2} . Vogelsang et al[47] observed densities of 2×10^{13} m^{-2} and 4×10^{13} m^{-2} for 20% and 5% whiskers in 6061 furnace cooled from 540°C. Thus, the agreement

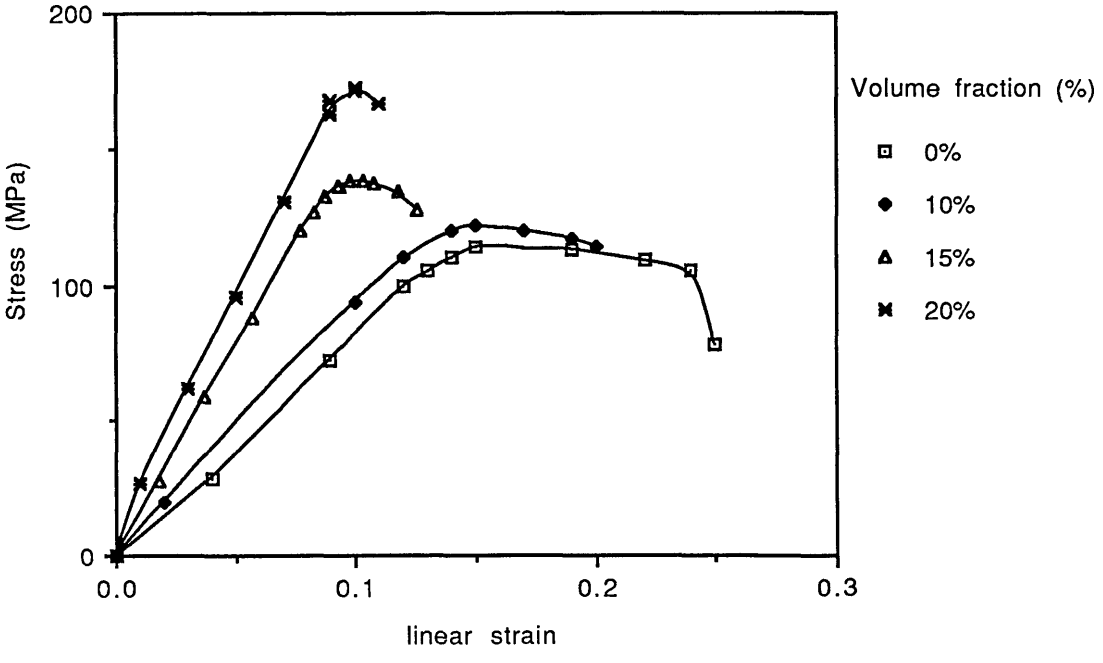

Fig. 6.6 Stress/strain curves for 50μm SiC, partially annealed, various volume fractions as indicated.

between theory and observation is good. The increase in strength due to these additional dislocations alone does not match the observed strength increase. Humphreys[37] also

notes that there will be a residual stress after dislocation generation which is below the critical value for this mechanism to operate.

Work hardening in composite materials is very different from that in the parent alloy. The additional thermally generated dislocations will play a part in determining work hardening rate alongside the usual processes resulting in work hardening. The work hardening of the composites produced in this work is greater than that exhibited by the parent alloy, as can be seen from the graph (fig. 6.6)This is in accordance with the findings of Humphreys[37], who also shows two regimes of work hardening, defined by different dislocation mechanisms operating, the transition between which occurs at a particular value of strain. At strains less than 5×10^{-4} work hardening is apparently due to the presence of unrelaxed loops around the particles. At higher strains other geometrically necessary dislocations are generated, but the work hardening rate is substantially less than at low strains.

.

Upon inspection of equations 6.4 and 6.5 it will be noticed that the initial work hardening rate is independent of particle size, whereas the plastic region work hardening rate does depend on the size of the reinforcement. Both equations are dependent on the volume fraction of SiC present.

As was remarked upon at the start of this section these strengthening factors will be cumulative and thus a yield strength of a composite should be able to be predicted. There are a number of theories that do this, to a greater or lesser degree of success. These theories will be tested against the data from the fully annealed condition as this data is the most consistent.

Arsenault and Shi[39] base their predictions solely on the increase in strength due to thermally generated dislocations. Calculations made using equation 6.3 give a good fit to experimental data, but consistently under estimate the strength, as shown in figure 6.7. The fit to the experimental results improves as volume fraction of silicon carbide decreases, as might be expected. Whilst this fit is undeniably good, it is intuitively apparent that the strength of the composite will not be dependent on one factor alone. The deviation from the curve at high volume fractions may be due to the increasing prominence of work hardening as volume fraction increases (as can be seen in figure 6.6).

Miller and Humphreys[38] use an additive technique where the yield strength is given by:

$$\sigma_{mmc} = \sigma_{Al} + \sigma_{gb} + \sigma_{q} \quad \text{.....6.6}$$

where the term σ_{Al} is 30MPa for coarse grained aluminium and σ_{gb} and σ_q are the grain size and quench (dislocation) strengthening factors respectively. This ignores Orowan strengthening because the contribution is small, and work hardening because the initial strengthening due to work hardening is difficult to calculate. The comparison of this data with experimental results is shown in figure 6.8. The values resulting from this summation are good estimates of the experimentally determined results. Miller and Humphreys[38] note that under estimates may be due to the possible effects of ignoring the work hardening term and errors in the grain strengthening term associated with the constant, K_y. Again, the comparison of the experimental data with the generated curves is shown below for the fully annealed condition. The shift observed in the theoretical curves from over- to underestimate as particle size increases is due to the failure of the assumption that one SiC particle nucleates one grain during annealing; this will be discussed below. Grain growth has also been ignored in this case.

A further theory, based solely on manipulation of data, is proposed. It relies on the observation that the recrystallised grains will be considerably less than one grain per SiC particle in composites containing small particles, and more than one grain per particle for large particle composites. The actual grain size measurements were considered to be too inaccurate for a reliable comparison. It was also noticed that the grain size decreased with increasing volume fraction (the basis of the Zener equation for particle inhibited grain growth) in this work and that of Miller and Humphreys[38]. Thus a 'correction factor' was introduced, based on these observations. The actual form of this term was found by trial and error. This results in a modification of the Hall-Petch term. This new term may then be combined with the terms for thermally generated dislocations and Orowan looping (which will be significant for the 1μm particle). This, effectively, draws from the theories of both Arsenault and Shi[39] and Miller and Humphreys[38]. Thus the governing equation will be:

$$\sigma_{mmc} = \sigma_{Al} + \sigma_o + \gamma\sigma_{gb} + \sigma_q \quad \text{.....6.7}$$

In this equation γ is the correction factor due to grain nucleation and is obtained as follows:

$$\gamma = \ln(S+1)/2.(1-V) \quad \text{.....6.8}$$

The other terms are defined as for equation 6.6, with the exception of σ_o which is the Orowan strengthening term; S, which is the particle size in micro-metres and V, which is the volume fraction of particles. Figure 6.9 shows the application of equation 6.7. It is important to remember that the modifications in this equation are based on an

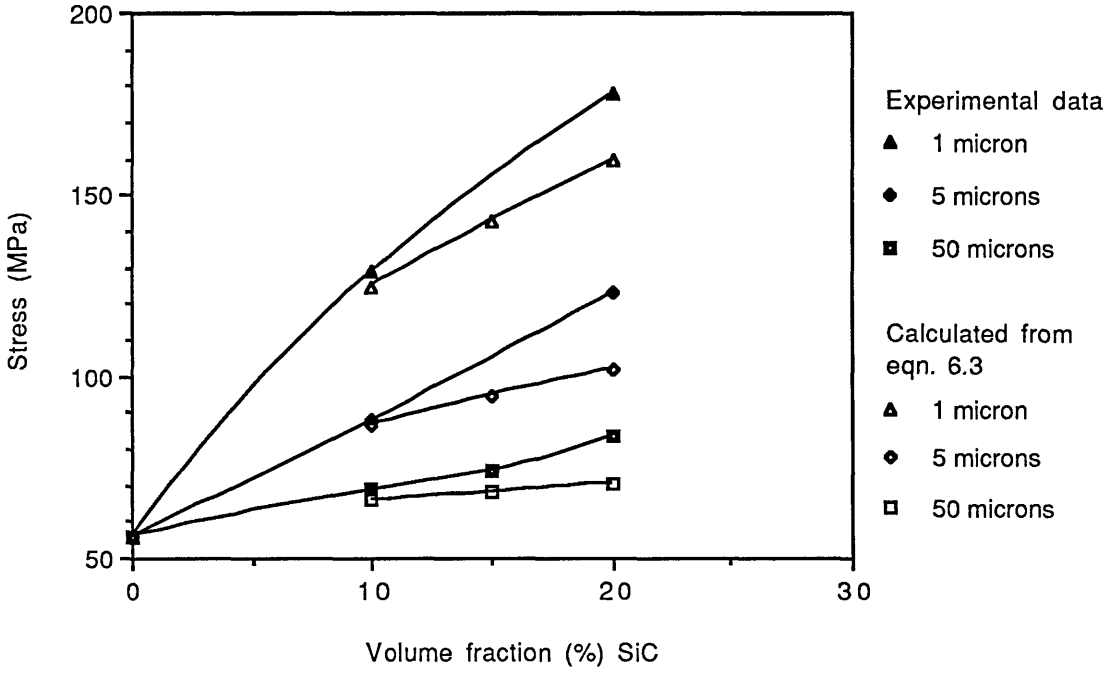

Fig. 6.7: Comparison of 0.2% proof stress experimental data with calculation using equation 6.3

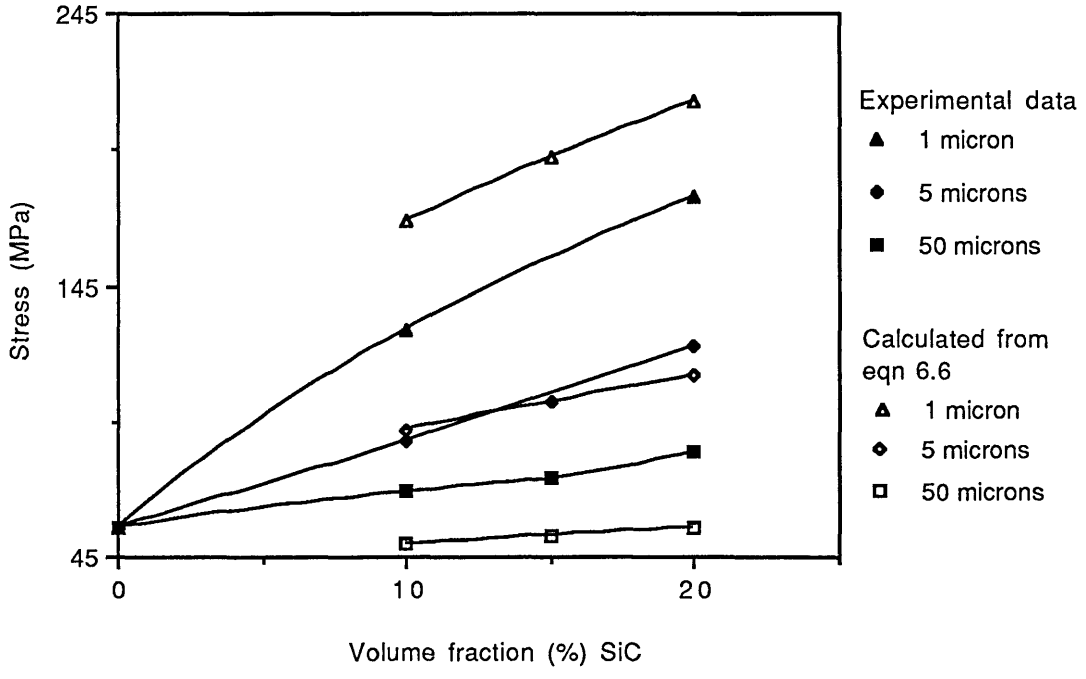

Fig. 6.8: Comparison of 0.2% proof stress experimental data with calculation using equation 6.6

empirical fit only and that whilst the grains are observed to nucleate in the way described above, the accurate measurement of grain size was found impossible for the small particle high volume fraction composites. The increase in g as S increases is based on the grain size observations of Miller and Humphreys[38].

The correction factor, γ, was found to give a reasonable fit to the experimental data, as is seen in figure 6.9. The promising excellence of the fit of the calculated curves to the experimental data must be tempered with some objections. That the fit is better for the smaller particle size and lower volume fraction shows the weighting of the correction factor, as well as the increase in work hardening at higher volume fractions discussed earlier. However, the transformation from fractions of a grain per particle to many grains per particle suggests that there is a point at which one grain nucleating per particle is possible. The theory assumes that the particle size is a fixed single value. This is clearly untrue: as has been shown in section 5.1.1 the range of sizes of the silicon carbide particles is wide. A final consideration is that there has been shown to be an often large discrepancy between 0.2% proof stress and the actual yield stress (as defined by the limit of proportionality) of composite materials[26,37]. This will result in a discrepancy in all of the predictive equations depending on the work hardening rate.

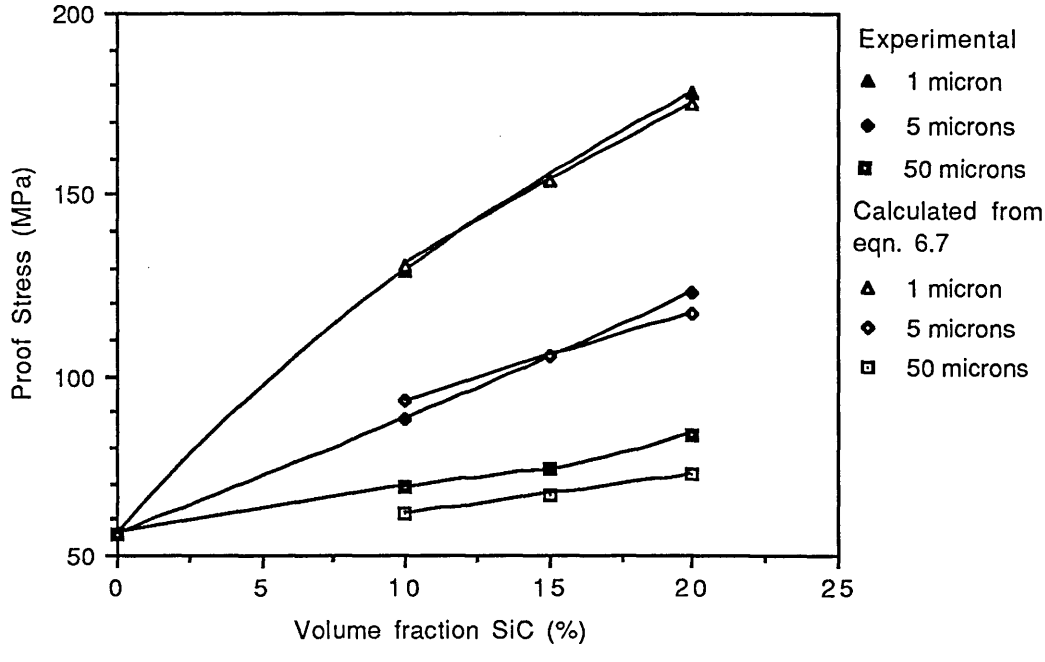

Figure 6.9: Comparison of 0.2% proof stress experimental data with calculation using equation 6.7

6.4 Conclusions

There are a number of tentative conclusions which can be drawn from this work on commercial purity aluminium composites:

(a) The strength of composites increases with particle volume fraction up to a certain point, after which it decreases; this point is governed by the amount of agglomeration (in small particle composites), the volume fraction of SiC and its influence on the amount of matrix remaining and the heat treatment condition of the matrix.

(b) The increase in strength over the unreinforced alloy decreases with particle size and as annealing proceeds. The increase as annealing progresses is much greater for the 1μm particle size composites, with proof stresses in excess of 1.4 times that of the unreinforced alloy in the same condition.

(c) In the fully annealed condition the strength of the mmc increases as SiC particle size decreases.

(d) The ductility of the mmc.s decreases as volume fraction of particles increases and particle size decreases.

(e) Work hardening increases as volume fraction increases.

(f) Recrystallisation was observed to occur in the mmc.s where grain size could be observed. More than one grain was seen to have nucleated at 50μm SiC particles.

(g) Various predictive equations have been applied to the experimental results for fully annealed material. The best fit to the data was found from equation 6.7, employing a correction factor in order to compensate for observed discrepancies between theoretically predicted grain size and actual grain size. These equations increasingly deviate from the experimental data as volume fraction of SiC increases; this is probably due to the increasing importance of work hardening.

7. COMPOSITES OF 2014

7.1 Structural Characterisation of Unreinforced 2014

The alloy 2014 is age hardenable, nominally containing 4.4% copper, 0.8% manganese, 0.8% silicon and 0.6% magnesium with the remaining 94.4%, aluminium[84]. The strength is derived from precipitation of the metastable copper aluminium phase[105,106], as discussed in chapter 3.

No mechanical properties were directly measured for the matrix, as this material was used only to establish processing parameters of composite materials in general. However, D.S.C. and T.E.M. work has been conducted on 2014 powder from the same source and extruded at similar ratios- 20:1 and 50:1. Some mechanical properties were also available for this material[107].

7.1.1 As Received Powder

The analysis of powder size revealed the following results, as shown in table 7.1. Prior to this analysis the material had been sieved to remove all 2014 powder

Particle size range (μm)	Weight % within range.
> 32	63.4
32-38	4
38-45	7.3
45-53	5.7
53-63	4.8
63-75	4.2
75-90	6.7
LOSSES	3.9

Table 7.1: Sizing of 2014 powder

above 125μm in size, as was done prior to the preparation of the composites. Powder from the same source was analysed in detail by Marshall[108]. Particles were found to be spherical with an internal structure which varied from completely partitionless solidification to a cellular structure as particle size increased. Some precipitation of Al_2Cu was observed in some powder particles: this would be eliminated on solution treating. Dendrite arm spacing was measured as varying from 0.49μm for 8μm particles to 2.16 μm for 40μm particles.

7.1.2 Precipitation in the 2014 System

Samples of 2014 were examined by the differential scanning calorimetric (D.S.C.) technique in order to establish a base line for characterising the precipitation process occurring in the composites of this alloy. Subsequent to this, specimens of the alloy were aged at temperatures corresponding to the peaks observed in the D.S.C. curves.

The alloy 2014 is a member of one of the most extensively investigated groups of alloys- those containing copper, manganese, magnesium and silicon. The precipitation process occurring in 2014 is predominantly of the type:

solid solution-> G.P. zones-> θ"-> θ"-> θ ($CuAl_2$)

Ageing over a range of temperatures has shown that the initial G.P. zones undergo full reversion to be replaced by θ" (also historically known as G.P.2 zones)[84]. The coherent θ" is gradually replaced by θ' which exists simultaneously over a range of time and temperatures and is also coherent. θ' may nucleate heterogeneously on dislocations or grain boundaries. θ" and θ' are oriented parallel to the {100} planes of the matrix and both are needle-like in morphology[83]. The final equilibrium phase, $CuAl_2$, is non-coherent. The silicon content may result in the formation of Mg_2Si which is not a major contributor to the hardening, but is significant in other alloy systems[92]. The main influence of silicon is in enhancing the age hardening response. The manganese may tie up some of the copper, thus reducing the amount available for the formation of hardening precipitates[83]. Manganese may aid control of the grain size although in powder alloys this is unlikely because of the small initial grain size.

Temperature range of peak, °C.	Reaction occurring
1) 90-140	G.P. zone formation
150-200	G.P. zone dissolution
2) 220-250	θ" formation
250-270	θ" dissolution
3) 260-290	θ' formation

Table 7.2: Phases formed during D.S.C. of unreinforced 2014 alloy.

The D.S.C. curve for an unreinforced 2014 specimen is shown in figure 7.1. The material was solutionised prior to the heating at a rate of 5°C per minute. From a

knowledge of the precipitation process occurring in these alloys[89,105,106] it can be deduced that the reactions observed probably correspond to the precipitation and dissolution of phases as shown in table 7.2. It should be noted that the G.P. zone formation peak is very broad (peak 1). In contrast to this the peaks due to θ" and θ' formation are clearly defined (peaks 2 and 3 respectively).

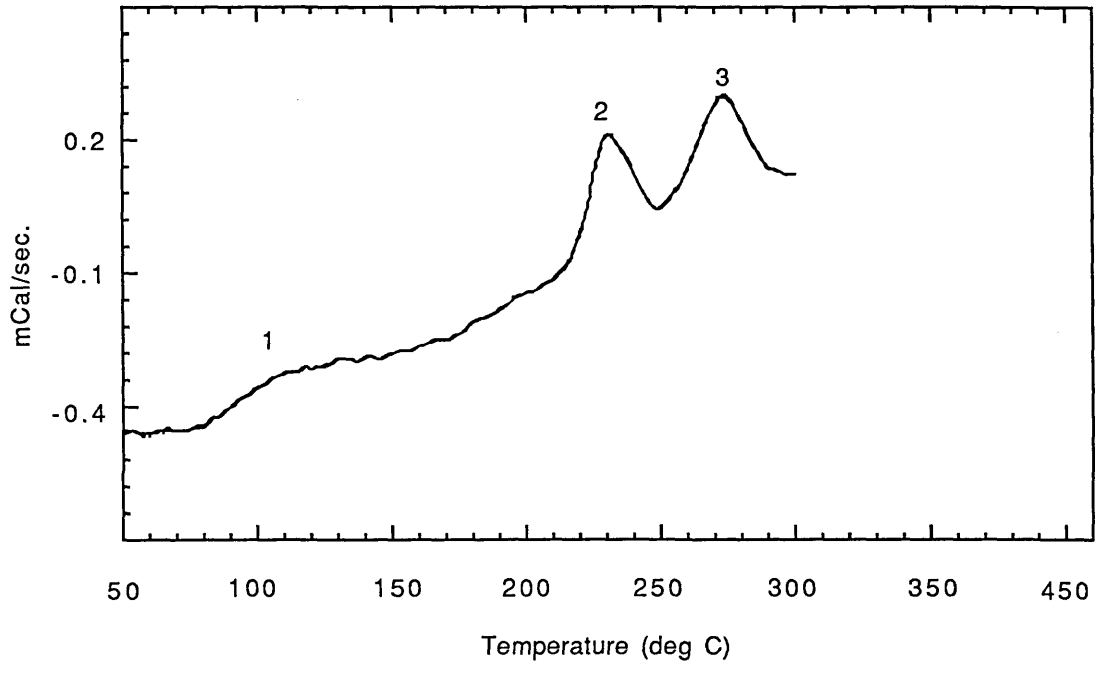

Figure 7.1: Differential scanning calorimetric profile of 2014

A more explicit examination of the precipitation occurring at these temperatures was conducted by T.E.M. examination. Further specimens of the alloy were heat treated to temperatures of 110°C, 235°C and 275°C for three quarters of an hour, and then quenched in order to retain the structure.

At 110°C there was no evidence of any precipitation having occurred in the bright field (figure 7.2a). There was some streaking of the <100> diffraction pattern, which would be expected, and is thought to be due to the formation of G.P. zones[106,83]. Also observed in the matrix are relatively large dispersoids of between 50-200nm in size. These are probably Mg_2Si, $CuAl_2$ or Al_2CuMg and are present in all the structures examined. The sub-grain size of this material is between 1μm and 3μm, which is within expectations for an atomised powder produced material.

The specimen heat treated for three quarters of an hour at 235°C showed some marked differences from the lower temperature specimen. Figure 7.2b shows that there was a uniform distribution of needle-like precipitates throughout the matrix.

(a) Bright field, aged @ 110°C

(b) Bright field, aged @ 235°C

(c) Dark field of the same.

(d) Bright field, aged @ 275°C

(e) Dark field of the same.

Figure 7.2: Microstructure of unreinforced 2014 at D.S.C. peaks, aged for three quarters of an hour at the temperatures indicated

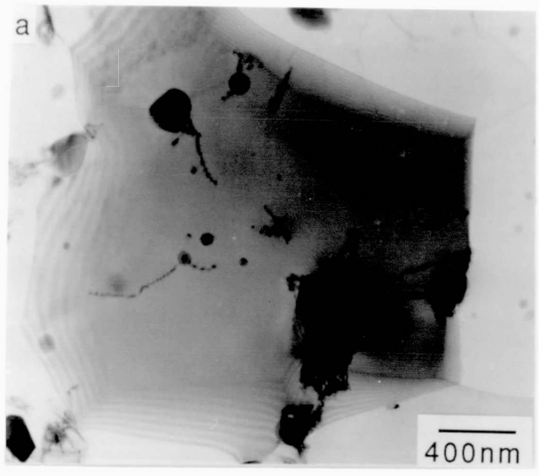
a
400nm

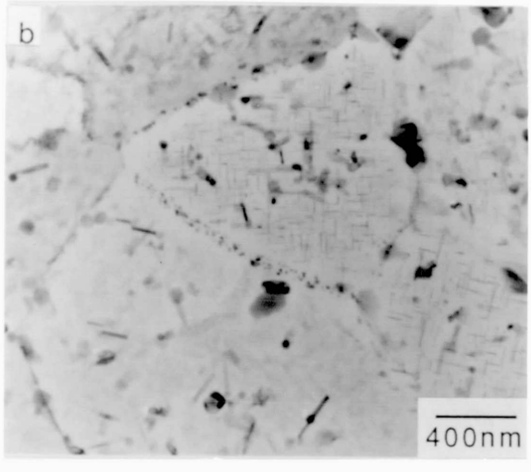
b
400nm

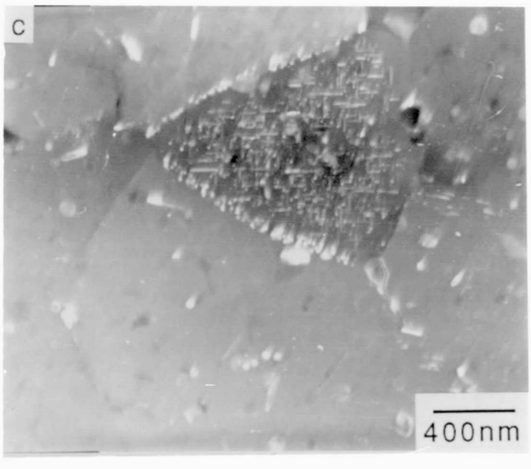
c
400nm

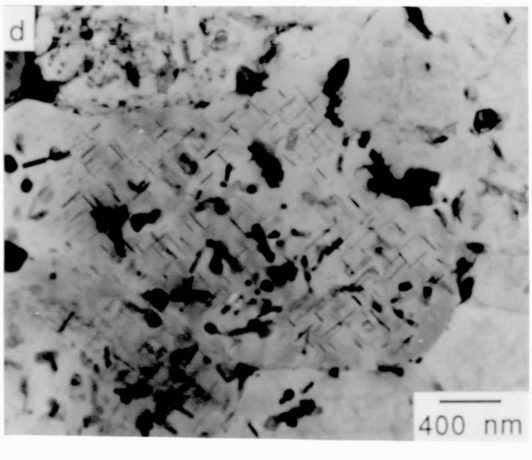
d
400 nm

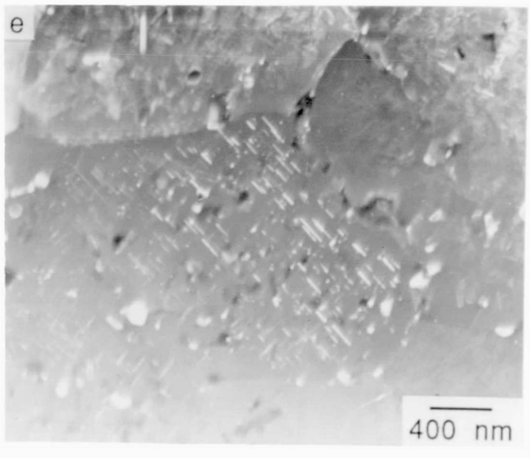
e
400 nm

The diffraction pattern revealed strong streaking of the <100> spots but also the emergence of a separate pattern. The latter pattern is believed to be due to θ' precipitates (by comparison with Bonfield and Datta[106]) having transformed from θ". Dark field imaging of the secondary pattern (figure 7.2c) locates these precipitates at both the grain centre and the grain boundaries. Precipitate size is typically less than 100nm in length and no more than a few nanometres wide. There is some indication of coarsening of the precipitates; larger rod-like θ' can be seen in all of the grains and at the grain boundaries. The structure is therefore a mixture of fine and coarse θ'. No precipitate free zones were observed.

Heat treatment at 275°C (again for three quarters of an hour) resulted in a structure further coarsened, with precipitates of 200nm in length being evident. Dark field imaging (figure 7.2d) shows the structure to be predominantly θ', the image having been obtained from the secondary pattern associated with this coherent phase. The size of precipitates will increase as ageing time progresses[106]. Two distinct regimes of precipitate size were observed: needle like precipitates, approximately 150-200nm in length, with negligible thickness and precipitates with a rod morphology which have an appreciable thickness of between about 15-30nm. Bonfield and Datta[106] suggest that this disparity and increase in size will be due to Ostwald ripening, and thus it would be expected to observe fewer small precipitates at longer times.

7.2 Structural Characterisation of Composites of 2014

It has been shown in chapter 6 that composite materials behave in a significantly different way from their parent alloys. This section sets out the characteristics of composites of 2014 and SiC and compares them with the unreinforced alloy.

7.2.1 As Extruded

The optical micrographs of the extruded 2014 composites are discussed in section 5.6.2. Distribution of silicon carbide was found to be generally good in all cases, with low porosity. The density of the extrudates were found to be 2.81 g/cm^3 and 2.85 g/cm^3 for the non-canned, non-hot compacted material and canned and hot compacted material, respectively. These values represent 98% and 99.9% of the theoretical density of 2.86 g/cm^3. The densities of the canned and extruded and hot compacted and extruded materials were similarly high.

Figure 7.3: Microstructure of as extruded 2014/15% composite.

(a) Bright field, 110°C.

(b) Bright field, 235°C

(c)Bright field, 275°C

Figure 7.5: Microstructure of composite at D.S.C. peaks, aged for 3/4 hour.

Figure 7.6: Microstructure of peak aged 2014/15% SiC.

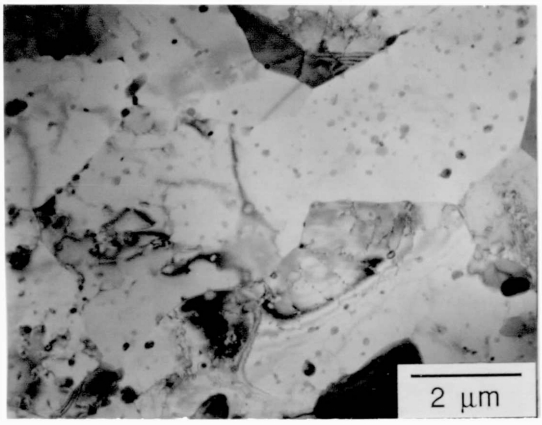
2 µm

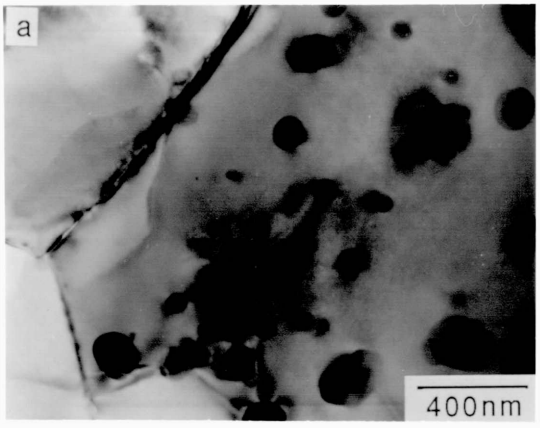
a
400nm

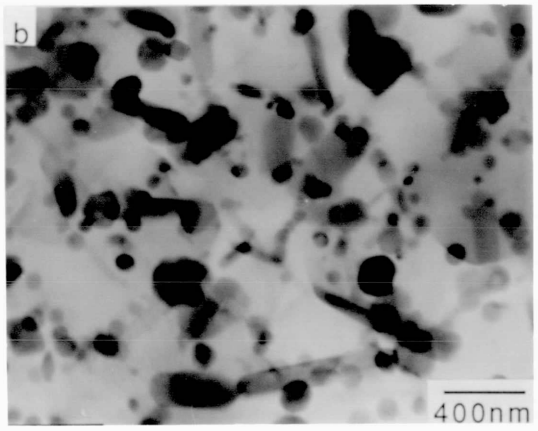
b
400nm

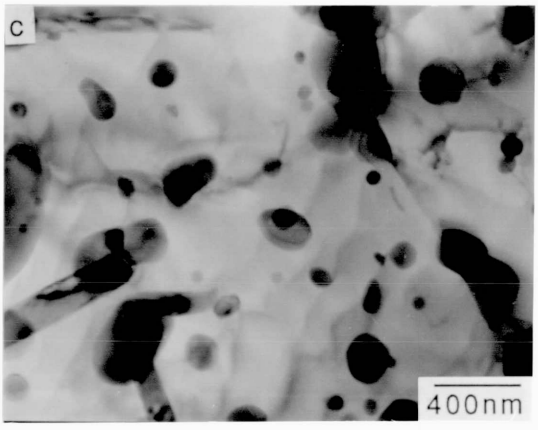
c
400nm

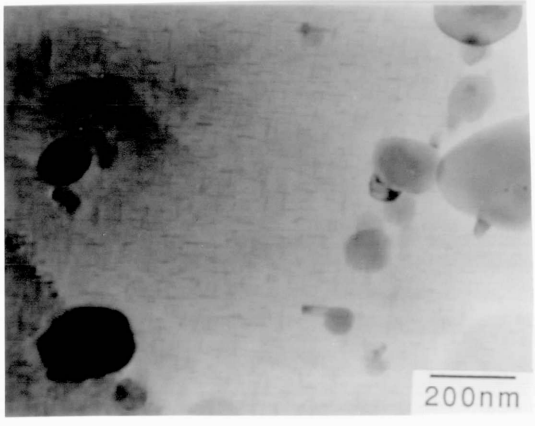
200nm

Transmission electron microscopy of the canned and hot compacted extrudate revealed the presence of dispersoids, probably of Mg_2Si (fig. 7.3), which were found at the subgrain boundaries and within the subgrain centres. As with most powder material bands of oxide were observed in the longitudinal direction. The subgrain size was found to be approximately 1.5-2.5 μm.

7.2.2 Precipitation in Composites of 2014

The precipitation characteristics of the composites of 2014 have been investigated in the same manner as those of the unreinforced alloy. D.S.C., at a heating rate of 5^oCmin^{-1}, was performed on a sample of the composite which had been solutionised. Microscopic (T.E.M.) examination was subsequently performed on material aged for three quarters of an hour at the same peak temperatures as the unreinforced material.

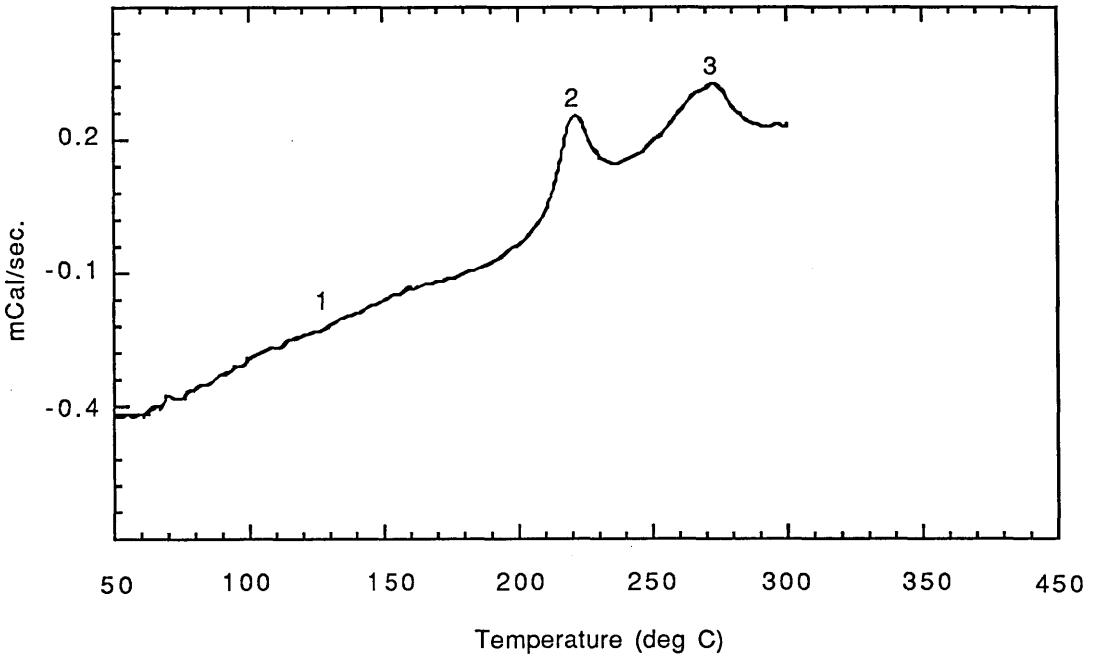

Figure 7.4: Differential Scanning Calorimetric profile of 2014/15% SiC composite

The D.S.C. curve for the composite is shown in figure 7.4. The shape of the curve is slightly different to that of the unreinforced material. The perturbation due to the G.P. zones is not as prominent, and the higher temperature peaks are slightly narrower. The material is seen to follow the same sequence as the unreinforced matrix material with only a slight variation in peak temperatures. the exothermic energy for the θ' precipitation seems to be appreciably less and this may relate to the propensity

for this phase to heterogeneously nucleate on 'preferred sites'. These sites may include dislocations which, as discussed earlier, will be more in evidence in the composite due to the differences in the thermal expansion coefficient of aluminium and silicon carbide.

Figure 7.5a shows the structure produced when the composite is exposed to 110°C for three quarters of an hour. There is no sign of precipitation in the bright field image. The diffraction pattern is comparable to that of the unreinforced material: there is some suggestion of streaking of the <100> spots. Dispersoids such as were observed in the unreinforced alloy are present.

The structures produced by ageing material for three quarters of an hour at 235°C and 275°C (figure 7.5 b and c) are substantially different from those of the unreinforced material aged under the same conditions. The microstructure of the material aged at 235°C is one of coarsened precipitates of a rod like nature approximately 100-150nm wide and 500nm long. The size of these indicates that substantial overageing has occurred. Bonfield and Datta[106] observed that the diameter of the θ' precipitates increased from 88nm to 201nm over a time range of 1 to 160 hours in an unreinforced 2xxx series alloy (designated 'L70'- Al, 4%Cu, 0.8% Si, 0.8% Mg, 0.7% Mn, 0.5% Fe). They also note that the rate of coarsening of the θ' particles is slow. The orientation of the rods parallel to the {100} planes is still evident.

Similarly coarsened precipitates were observed in material aged at 275°C (fig. 7.5c). There was also evidence of nucleation associated with helical dislocations, as described by Kelly and Nicholson[83]. The density of θ' precipitates in this ageing condition, whilst not examined quantitatively, appeared to have decreased. This may be due to the process of Ostwald ripening which is believed to contribute to the high temperature coarsening of these alloys[106], although it is unclear whether such a process could operate within the time scale of this particular experiment. The orientation relationship with the matrix was more difficult to distinguish in this specimen. A distinct separate diffraction pattern was noticed under these conditions.

7.2.3 Age Hardened Composite

Figure 7.6 shows the microstructure of the composite aged at 166°C for 16 hours. The structure does not appear to be substantially overaged when compared to published micrographs of unreinforced 2014 in its T6 condition[84]. Precipitates

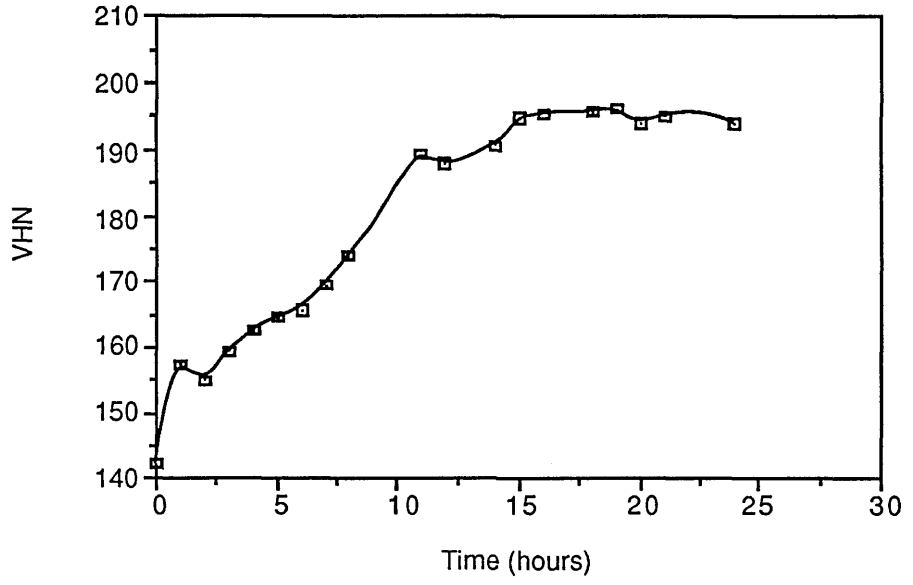

160 deg. C

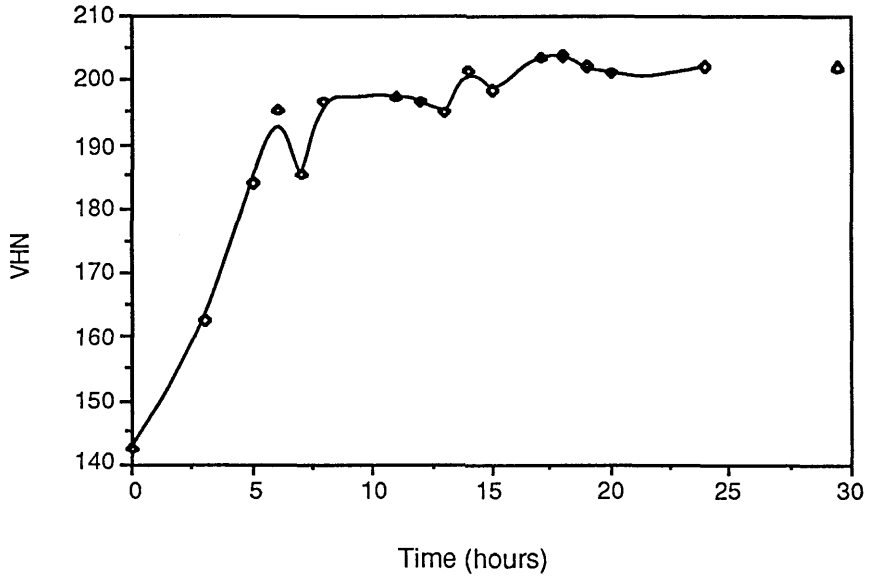

166 deg. C

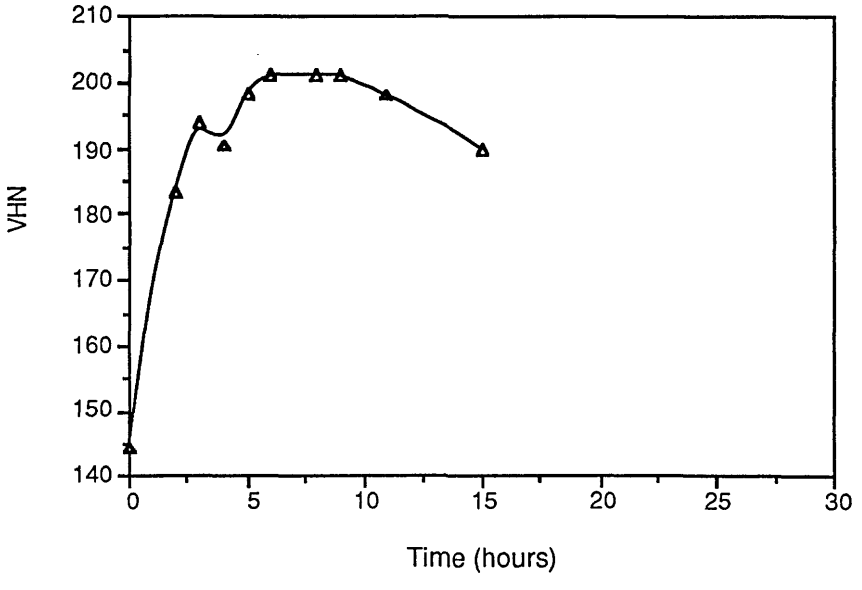

180 deg. C

Figure 7.7: Hardness vs time at various temperatures for 2014/15% SiC composite

within the grain are approximately 30-50nm long, whilst at the grain boundaries they are slightly fattened. Their growth on the {100} planes is evident from the orientation, precipitates being observed in the three principal directions. There was some streaking of the diffraction spots and also a interpenetrating pattern characteristic of the θ' phase. The reason for the lack of overageing is unclear, although it is known that θ' is resistant to coarsening up to long ageing times (100 hours and above) at a temperature of 160°C[106]. Thus overageing is impeded by the slow growth rate of θ' at 166°C and does not seem to be appreciably encouraged by the presence of SiC within the times employed in this investigation. This is in marked contrast to the overageing observed in the CW67 alloy. Overageing of 2014 at higher temperatures proceeds by Ostwald ripening, which is a more rapid process[106]. This would account for the more rapid coarsening observed subsequent to ageing at the higher temperatures investigated in the previous section.

7.3 Characterisation of Composite Ageing by Hardness Testing

Samples of the composite material were solutionised at 500°C for 1 hour and aged at 160°C, 166°C and 180°C for a range of times in order to establish the time and temperature required to achieve peak hardness. The solutionising conditions are the standard conditions for 2014[109]. Curves of hardness against time are shown in figure 7.7. The main point of note is that although the peak hardness is reached after about 16 hours at 166°C this value persists until at least 36 hours; a similar effect was observed in material heat treated at 160°C. This is linked to the observation by Bonfield and Datta[106] that the θ' coarsens only very slowly at around these temperatures. Ageing at the higher temperature produces no such effect, the material losing hardness after about 8 hours. Thus the peak hardening conditions were established as 16 hours at 166°C for 2014 reinforced with 15% SiC by volume; the hardness achieved under these parameters was 205 VHN . This is only two hours less than the standard treatment employed when ageing unreinforced 2014 at 160°C[109]. This apparent contradiction to the general rule that composites undergo accelerated ageing can be accounted for by the slow coarsening rate of the θ' precipitate and the spread of the experimental data. The contrast with the ageing characteristics of composites of CW67 will be shown in section 8.3

7.4 Mechanical Properties of 2014 Composites

The mechanical properties of these composites primarily serve as a guideline to the efficacy of the pre-extrusion processing route. Only later was the material examined with respect to unreinforced 2014. In the first context the four extrusion

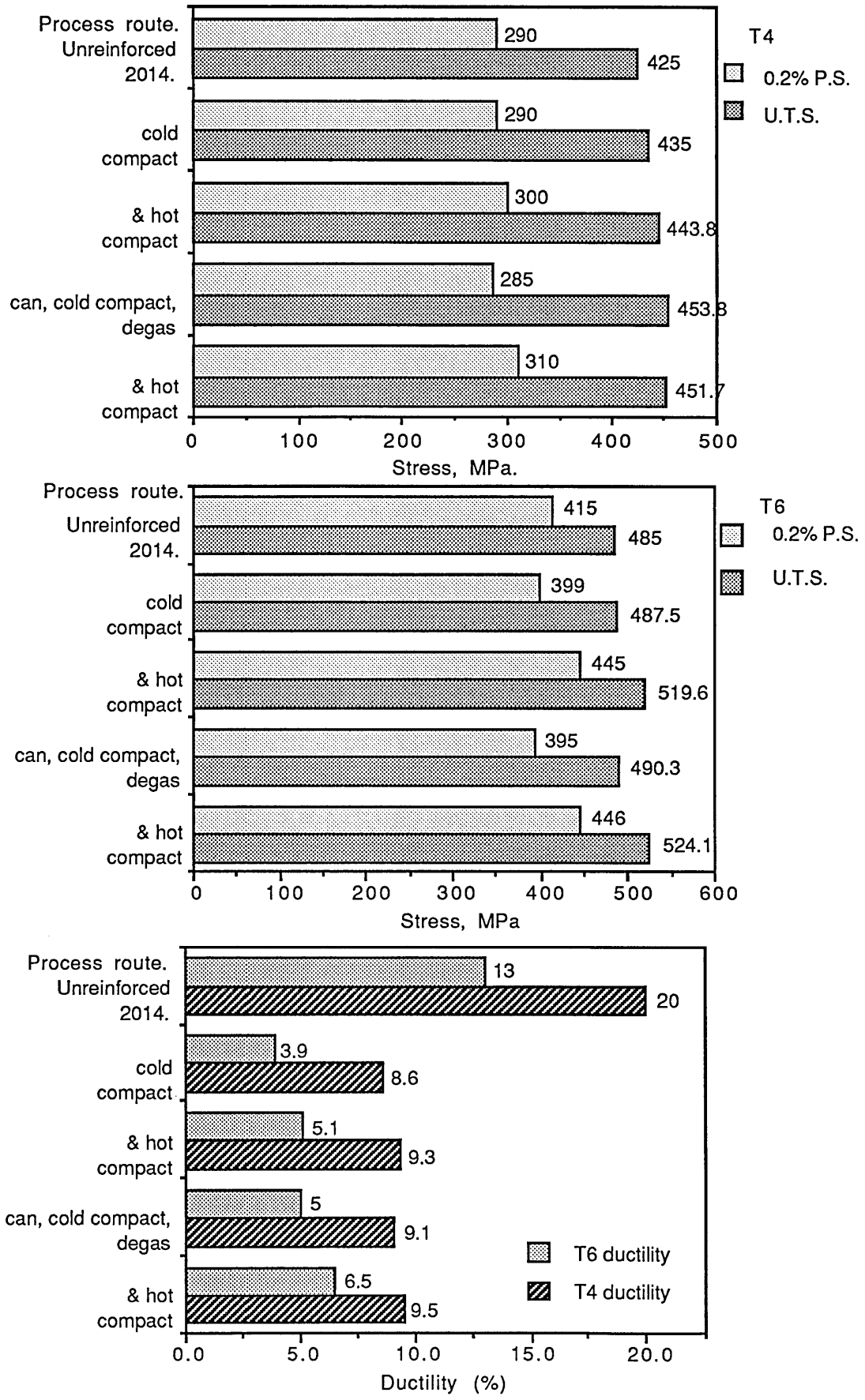

Figure 7.8: Tensile properties of 2014 composites, conditions as shown

groups will be examined *in toto*. For the second comparison only material processed under what were found to be the best conditions will be inspected.

7.4.1 Tensile Properties

The variations in ultimate tensile strength and 0.2% proof stress with processing parameters are shown in figure 7.8. Hot compaction prior to extrusion was found to have a much greater beneficial effect than degassing or simple cold compaction. The T6 0.2% proof stress was determined to be 445 MPa ± 2MPa in material that underwent hot compaction: there was no difference between extrudate which had been merely cold and hot compacted and material which had been canned, cold compacted, degassed and hot compacted. The U.T.S. was similarly consistent at 522 MPa ± 3 MPa. These values are an improvement of 45-50 MPa (approximately 10%) over the material which was cold compacted only. Degassing alone had no discernable effect on the 0.2% proof stress or the U.T.S.. Extrudate which was cold compacted and canned, cold compacted and degassed had T6 0.2% proof stresses which were approximately 15 MPa lower than the unreinforced alloy; hot compacted material showed an improvement of 30 MPa over the T6 0.2% proof stress of the unreinforced alloy. It can be seen from this that hot compaction considerably improves the 0.2% proof stress and U.T.S. in the peak heat treated (T6) condition, both over the unreinforced alloy and the other two consolidation routes.

The as solutionised (T4) values were found to benefit less from hot compaction. The 0.2% proof stress values were 300 MPa and 310 MPa, whilst the unreinforced material is quoted as having a 0.2% proof value of 290 MPa. The 0.2% proof stress of the cold compacted material was 290 MPa and that of the canned, cold compacted and degassed material, 285 MPa. The slightly better relative properties are probably because the matrix is more ductile and thus more able to accommodate stress concentrations[25]. This is despite the fact that non-hot compacted material was found to contain a greater amount of porosity. The effect of degassing on U.T.S. and 0.2% proof stress was thus found to be negligible whilst hot compaction, with or without degassing, was found to improve the tensile properties of the composite significantly.

The changes in properties with processing conditions are reflected in the conventional work hardening exponents. In the T4 condition the work hardening exponent is a uniform 0.20 ± 0.01. However, in the T6 condition the non-degassed material exhibited lower values, as shown below in table 7.3. The variation in the exponent is significant and is probably related to the degassing operation. It is more difficult to correlate these changes to the changes in U.T.S. because of the influence of

the reinforcement and any porosity. The removal of hydrogen by degassing may influence the properties[84,97], but the extent of this influence is not known. Clearly a better understanding of these factors is required before an explanation for the success of degassing can be advanced.

Processing prior to extrusion @ 450°C	Work hardening exponent, n.
Cold compact	0.12 ± 0.02
Cold compact & hot compact	0.10 ± 0.01
Can, cold compact & degas	0.15 ± 0.01
Can, cold compact & degas & hot compact	0.16 ± 0.01

Table 7.3: Work hardening exponent, n, variation with processing parameters for 2014 composites in the T6 condition.

The variation in ductility with processing parameters is also shown in figure 7.8. These differences are more straight forward and are directly related to the introduction of degassing and hot compaction into the process route. Comparing the cold compacted material and the canned, cold compacted and degassed material showed that degassing prior to extrusion resulted in an increase in ductility of 1.1% elongation in the T6 condition; the variance in the results was ± 0.4%. There is a large body of evidence relating the removal of hydrogen to improved ductility[84,97] in aluminium alloys; this is believed to be the reason for the improvement in this case. Hydrogen can cause porosity and blistering in aluminium alloys[84]. Although no analysis for hydrogen content was conducted, the possibility of hydrogen deterioration can be deduced from the degassing curves which indicate the presence of water in the powder material. Thus hydrogen may be liberated at high temperatures. Hot compaction also resulted in improved ductility; values for the T6 ductility of cold and hot compacted material and canned, cold compacted, degassed and hot compacted material were respectively 1.2% and 1.5% elongation higher than the cold compacted counterparts. This increase is due to the reduction of porosity accompanying the process. Hot compaction and degassing added 2.5% elongation to the ductility of the simply cold compacted material in the T6 condition. It will be noticed that the values of ductility in the T4 condition are more closely grouped. This can be seen as the potential maximum ductility that can be achieved in the composites. It will be noted that the ductilities are considerably lower than those quoted for the unreinforced material in the same heat treatment condition[109].

The experimentally obtained values of modulus are presented in table 7.4. Modulus is an intrinsic property of the material and as such is not expected to vary

extensively between heat treatment conditions within a single processing route group[84]. However, there was considerable variation in modulus between processing routes.

Processing prior to extrusion @ 450°C	Modulus, E (GPa)
Cold compact	70.6 ± 0.1
Cld compact & hot compact	80.5 ± 0.3
Can, cold compact & degas	77.7 ± 0.1
Can, cold compact, degas & hot compact	87.8 ± 0.5

Table 7.4: Modulus variations with processing parameters for 2014 composite

Both hot compaction and degassing are observed to enhance the modulus. In the case of hot compaction this is solely due to the increased consolidation produced by this operation. Again, the contribution of degassing is difficult to assess, however the presence of hydrogen is known to cause secondary porosity and "high temperature deterioration"[84] during heating. No experimental work was conducted in order to support this hypothesis.

The modulus is the property which is most likely to benefit from the incorporation of a reinforcing particle, such as silicon carbide, into a material. The degassed and hot compacted extrudate has a modulus which is approximately 15 GPa, 21%, above the modulus of the unreinforced material (approximately 72.4 GPa[109]). This value is, however, well below any law-of-mixtures calculation for modulus. Even the most conservative law-of-mixtures estimates are in the region of 110 GPa for a 15% reinforced composite (this uses the modulus of 72.4 GPa for the alloy and 300 GPa[74] for the SiC). McDanels[25] notes that the modulus tends towards an isostress type behaviour as reinforcement content increases. Indeed, because modulus is so insensitive to alloying variations a comparison with his results for 6061 is possible and yields a similar value (approximately 85 GPa) for the modulus of a 15% particulate reinforced composite. A comparison with modulus values calculated from the Tsai-Halpin equation, presented in section 3.2.1, shows that the modulus of the 2014/15% SiC composite falls within the range of predicted values.

Figure 7.8 also shows the values for U.T.S., 0.2% proof stress and ductility of the unreinforced extruded 2014 alloy obtained from the A.S.M. Metals Handbook[109]. The "best' composite strengths (found in the hot compacted materials) are between only 6-8% higher than those of the unreinforced material, in both the T4 and T6

conditions. Ductility is reduced by over 50% in both cases. This clearly shows the importance of the matrix in determining the U.T.S. and 0.2% proof stress of particulate reinforced composites. The main benefit accompanying particulate reinforcement is the improvement in modulus, as has been demonstrated.

Deductive predictions of the strength of particulate composites are made more difficult because the majority of equations purporting to assess the strength are derived from shear lag considerations, which break down as the aspect ratio tends towards unity. Inductive predictions, reliant as they are on a knowledge of matrix behaviour, tend to become less accurate as the alloy becomes more complex. A calculation of composite yield strength using an equation developed by Nardonne and Prewo[58] (equation 7.1: see section 3.2.2 for further explanation) for rectangular platelets gives a value of 446 MPa for the T6 yield stress of a 15% composite.

$$\sigma_{yc} = \sigma_{ym}\{V(S+4)/4 + 1-V\} \quad \text{.....7.1}$$

σ_{yc} - yield stress of composite
σ_{ym} - yield stress of unreinforced matrix
V - volume fraction of particles
S - shape factor = 2L/t where L is the particle dimension in the tensile direction, t is the thickness, = 2 for particles.

The proximity of this value to the experimental one must be tempered by the fact that the assumptions used to derive this equation do not hold for approximately spherical particles. A calculation using a slightly modified version (equation 7.2) of the equation results in a yield stress of 477 MPa for 2014/15% SiC. This still does not wholly account for approximately spherical particles which is why the value is higher than the experimentally determined 0.2% proof stress.

$$\sigma_{yc} = \sigma_{ym}\{V(S+2)/4 + 1-V) \quad \text{.....7.2}$$

Recalling arguments from Miller and Humphreys[38] and Humphreys[37], which show that the 0.2% proof stress may be a further over-estimate of the yield stress, would suggest that the error in this calculation is greater than just the difference between the experimental and calculated values.

Calculations of proof stress using equations of the type discussed in chapter 6 are of limited use only because a prediction of the strength due to other hardening

sources is difficult, due to additional factors such as precipitate hardening and the influence of solutes and recrystallisation inhibitors.

7.4.2 Fracture Toughness of Canned and Degassed Material

There were two factors which prevented a full comparison of the fracture toughness of composites with unreinforced material and between processing parameters. The first was associated with the machining of the material: it was found that it was impossible to machine short rod geometry specimens from any composite due to prohibitive tool wear. Instead, bar specimens were used, which preclude any direct comparison with short rod specimens because of the different orientation of the notch with respect to the extrusion direction (see section 4.7.2). The difficulty in comparing the fracture toughness resulting from different processing parameters evolved from the fact that the non-canned material did not have an acceptable surface (see section 5.5). Surface defects extended too deeply into the extrudate for specimens to be machined from the remaining material. (Fracture toughness specimens were taken from extrudate of dimensions 36x 7.5 mm whilst tensile specimens were taken from 13.5 mm diameter round extrudate.) Ageing was performed for 3 hours at 166°C to obtain the underaged condition and 24 hours at 180°C for the overaged. Both of these conditions were established by hardness measurement and were the times and temperatures at which the hardness was found to be 80% of the peak hardness at 166°C, determined in section 7.3.

The results of fracture toughness testing are shown in figure 7.9. There was a large spread in the data during testing: this is considered below. The machining of the specimens was found to initially have had as much influence on the properties as any other factor. Machining resulting in the truncation of the test area triangle was encountered in initial trials- this produced an artificially high result of 39.62 MPa$\sqrt{m}$ for the fracture toughness of the non-hot compacted material in the underaged condition because plane strain conditions were not prevalent. This defect was eliminated with experience, but emphasises the sensitivity of the test to machining parameters. The low toughness of one overaged non-hot compacted specimen (8.29 MPa$\sqrt{m}$) was due to a microstructural defect. A large agglomerate was observed along the centre-line of the specimen that produced this result. This emphasises the sensitivity of fracture toughness testing to microstructural variations.

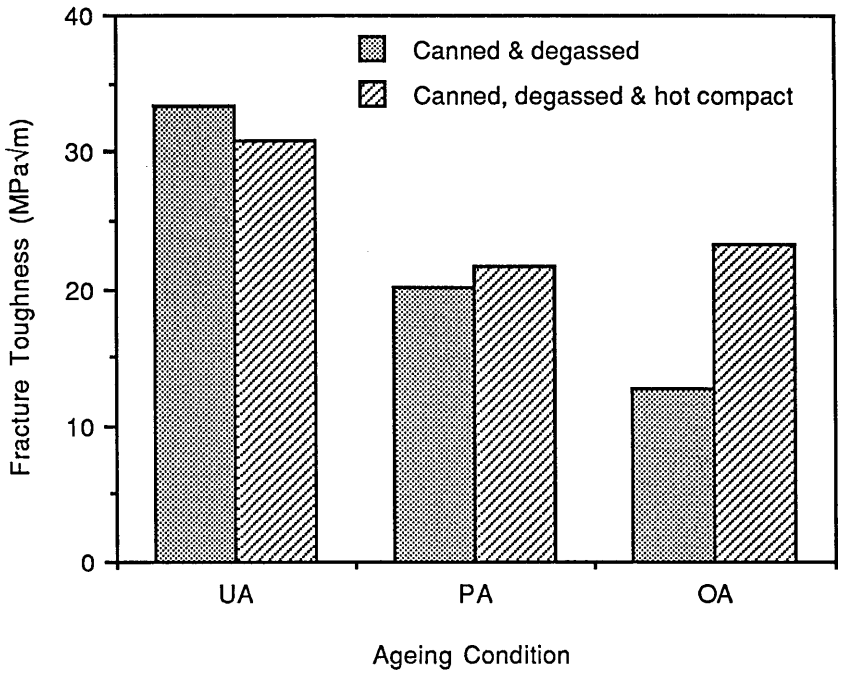

Figure 7.9: Comparison of fracture toughness of composites of 2014

Comparing the fracture toughness of specimens from both processing routes in various ageing conditions showed that whilst the values were similar in the underaged condition, the material which had undergone degassing and hot compaction prior to extrusion maintained a relatively high fracture toughness throughout. Values in the underaged condition were between 29.32 MPa√m and 39.62 MPa√m for the non-hot compacted extrudate (although the higher value is known to be anomalous for the reason stated earlier) and between 26.85 MPa√m and 34.24 MPa√m for the hot compacted material. The difference between the two ranges is insignificant, relative to the large variations in results from individual tests. In the peak heat treated condition the toughness of the degassed and hot compacted material was slightly greater than that of the other group: between 21.66 MPa√m and 21.68 MPa√m, compared with between 19.55 MPa√m and 20.67 MPa√m. In the overaged condition, the disparity became more significant. Specimens of the hot compacted material had fracture toughness values of 20.06 MPa√m and 28.77 MPa√m, whilst testing of the non-hot compacted extrudate yielded fracture toughness values of 8.29 MPa√m to 15.83 MPa√m. The reason for the unusually low value has been presented earlier in this section, however, this does not explain the still large difference. This is thought to be due to the larger amount of porosity known to be present in the material which was not hot compacted prior to extrusion. In the underaged condition, the porosity exerts less influence on the properties as was seen in the comparison of ductility in the T4 heat treatment: thus the fracture toughness of both materials in this heat treatment are similar.

The fracture toughness values in the longitudinal direction (i.e. crack progress is normal to the extrusion direction) are higher than most values for unreinforced 2xxx series alloys. However, it should be recognised that the values quoted here are the result of testing in a different orientation to the composites and that no results for testing in the longitudinal direction were found. Subramaniyan[98] found short rod fracture toughness values of between 24-28 MPa$\sqrt{m}$ for cast 2024; Clode[107] found values of around 12MPa$\sqrt{m}$ for powder 2014 extruded at 450°C and a ratio of 20:1. A comparison of fracture toughness results obtained using the bar test and K_{IC} values is presented in section 8.5.2 for unreinforced CW67 alloy, thus eliminating possible complications due to the presence of the reinforcement.

A direct comparison of these results with those of other workers was not possible, due to different materials and specimen geometries. However, Manoharan and Lewandowski[61] report fracture toughness values of 32-34MPa$\sqrt{m}$ for a 2xxx series alloy (3.5% Cu, 1.5% Mg, 0.21% Mn, 0.4% Zr reinforced with 15% 13μm SiC), with no variation between ageing conditions. Nair et al[4] report values of 13.5-15.5 MPa$\sqrt{m}$ for 2024 reinforced with 15% SiC. The first of these tests was conducted on fatigue pre-cracked specimens, the second using 'V notched' specimens; orientations with respect to the extrusion direction are not reported. Nair et al[4] go on to say that matrix properties are important in the control of fracture toughness, and that lower strength matrix materials yield higher fracture toughness values. This pursues the same line as McDanels[25], and a comparison with the CW67 alloy will exemplify this in sections 8.6.2 and 9.1.

Various authors have tried to predict the fracture toughness of composite material and to relate the fracture toughness to dimple height. A discussion of the usefulness of these methods will be found in section 2.6.3. The only equation which can be applied here is that developed by Jones et al[59] (the others rely on variable volume fraction and the measurement of matrix dimple height by stereo-pair fractography). The equation relates K_{IC} to yield stress and particle spacing thus:

$$K_{IC} = \sqrt{(2E\sigma_y\lambda/3\alpha)} \quad \text{.....7.3}$$

where α is related to the work hardening exponent, n, by the equation:

$$\alpha = 0.65-2.3n \quad \text{.....7.4}$$

and λ is the particle spacing; the other terms are defined as previously in this thesis.

The application of equation 7.3 to these composites is shown in table 7.5. The upper half of the table shows calculated values for the conditions in which the yield (0.2% proof) stress is known. An assumption of a yield stress of 80% of the peak aged value for underaged and overaged materials (consistent with comparative hardness values used in order to determine the ageing conditions) gave fracture toughness values as shown in the lower half of the table. The work hardening exponent of the material in these heat treatment conditions has also been estimated. The variation in values shows some similarities to the accepted trends for the variation of fracture toughness with yield stress in unreinforced aluminium alloys[84]. The fracture toughness is seen to fall as the heat treatment progresses. However, the necessity to estimate the yield stress and work hardening exponent in the under- and overaged conditions renders the results of this prediction somewhat speculative.

Material I.D.	Temper	E, GPa	σ_y, MPa	exponent, n	K_c, MPa$\sqrt{m}$
Can, degas	T4	77.7	285	0.2	31.66
"	T6	77.7	395	0.15	29.42
& hot compact	T4	87.8	310	0.21	37.44
"	T6	87.8	446	0.16	34.56
Can, degas	underage	77.7	316	0.19	31.49
"	overage	77.7	316	0.13	24.53
& hot compact	underage	87.8	357	0.19	35.57
"	overage	87.8	357	0.13	27.71

Table 7.5: Calculated fracture toughness, using equation 7.3

The calculated values do not, however, reflect the experimental findings of Manoharan and Lewandowski[61] who detected little variation in fracture toughness as ageing progressed. It is difficult to determine whether the prediction is incorrect or whether there are too many experimental variables which obscure any underlying trend.

It is interesting to note that the calculated values come close to the absolute experimental values, although they are uniformly higher. No account is made in this equation for the orientation of notch with respect to extrusion or rolling direction, it is assumed that the material is completely homogeneous. This is obviously not the case: banding occurs in the distribution of both oxide and silicon carbide particles, resulting in localised regions of high and low particle spacing. However, this can never be fully

allowed for in theory. The theory of Crowe et al[27] can accommodate this but, as noted earlier, requires stereo-pair microscopy in order to measure dimple size.

7.4.3 Fractography

Fractographs of failed tensile specimens are shown in figure 7.10. Fracture surfaces of tensile specimens had features which were common to all conditions. Figure 7.10a shows a characteristic tensile fracture surface of hot compacted material in the T6 condition. Matrix dimpling is evident, indicating that micro-void coalescence has occurred. The size of dimple was observed to be between approximately 1-7μm, with many below 1μm. Silicon carbide is also present at the fracture surface; decohesion of the particle/matrix interface was observed (as can be seen towards the upper left hand quarter of the micrograph), with little particle cracking. The average size of dimple seemed to be greater in the T4 condition (fig. 7.10b), which relates to a change in the size of particles at which voids are able to nucleate. Inspection of the micrograph shows fewer small dimples, with the size of those present being of the order of 2-7μm. In both heat treatment conditions there was a range of dimple sizes in each condition which made it difficult to determine their origin. This type of fracture surface has been observed by others[63], but not explained. It is believed probable that the fracture surface comprises features due to the matrix (the smaller dimples) and also features which are due to the silicon carbide. The approximate calculations shown in table 7.6 give the stress required in order to nucleate a void around a specific particle type in any matrix. The surface energy values are assumptions, based on the bonding of a particle with the matrix. The modulus value is the experimentally determined value for the material which had received the full pre-extrusion processing. This table indicates that voids may form around the SiC or oxide particles, if the stress conditions are fulfilled. In all cases the yield stress of a material is likely to exceed 229 MPa, and thus nucleation of voids at the SiC particles is favoured.

$$\sigma_N \geq \sqrt{(6E\gamma/d)} \quad \text{.....7.5}$$

Particle description	size,d, μm	surface energy, γ, J/m^2	Modulus,E, GPa	nucln. stress,σ_N, MPa
silicon carbide	5	0.5	87.8	229
peak aged	0.005	1	87.8	10264
over aged	0.05	1	87.8	3245
oxide	0.75	0.5	87.8	596

Table 7.6: Nucleation stress for void formation at a specific particle

(a) Tensile: hot compacted, T6

(b) Tensile: hot compacted, T4

(c) Tensile: cold compacted only, as extruded

(d)Toughness: hot compacted, underaged

(e)Toughness: hot compacted, peak aged

(f)Toughness: hot compacted, overaged

Figure 7.10: Fractographs of tensile and fracture toughness specimens of 2014 composites, testing mode as shown.

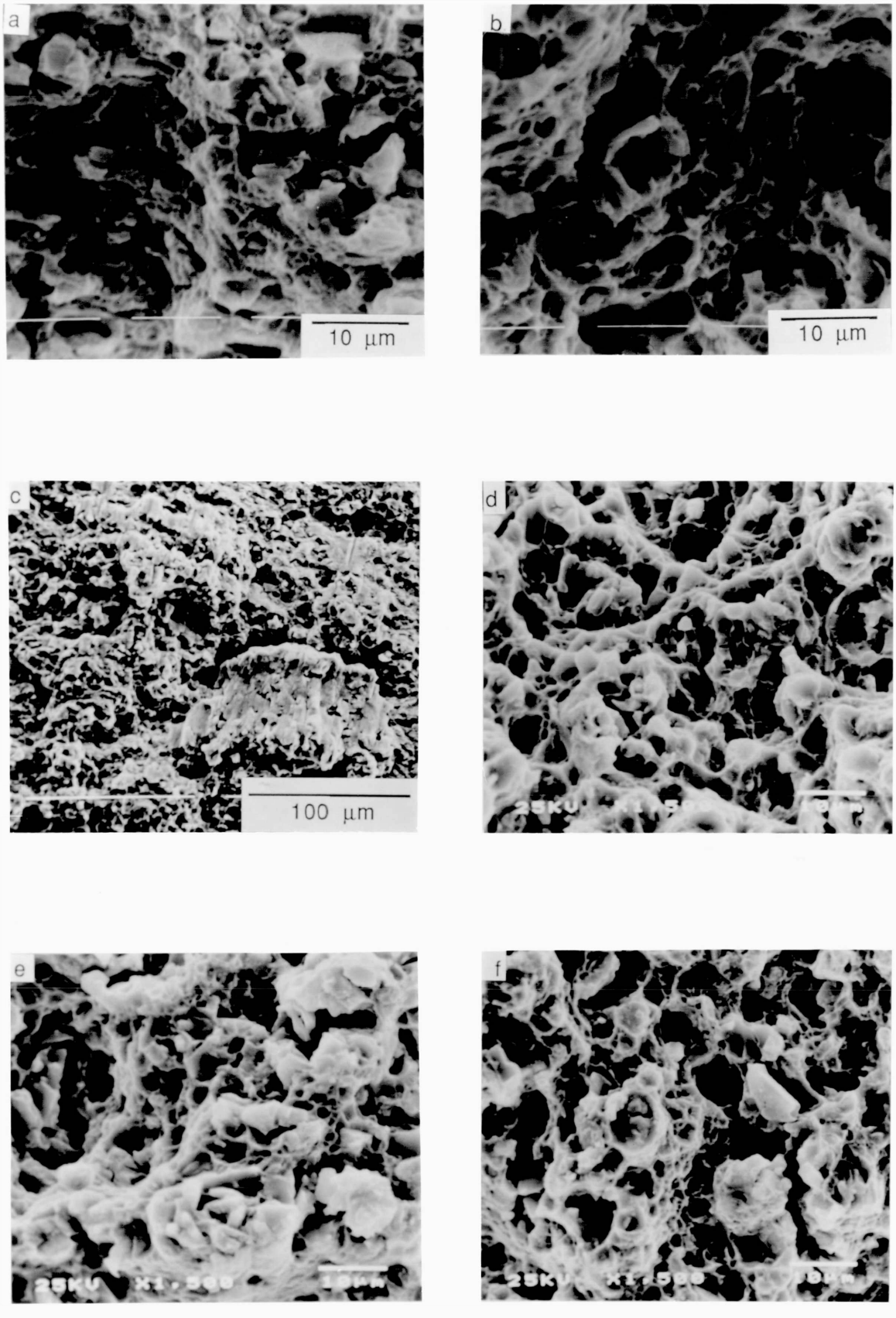
a
10 µm
b
10 µm
c
100 µm
d
e
f

If the yield stress exceeds approximately 600 MPa nucleation of voids will be favoured at the oxide particles. The value of the required nucleation stress will drop sharply as agglomeration of particles leads to a rise in the effective particle size: the oxides occur in bands along the extrusion direction which may effectively lower the nucleation stress. Analysis of the particles leading to void formation is difficult because of the limitations of the microscope at low atomic mass for elements such as oxygen.

Non-hot compacted material may have exhibited slightly greater porosity at the surface, but this is not certain. Figure 7.10c shows a typical region of ductile tearing, which was present at all fracture surfaces. The occurrence of tearing did not seem to be influenced by heat treatment. The prominence of the central feature of this micrograph also indicates some degree of discontinuous crack growth, but this is minimal. This insufficiency of evidence suggests that this is not the dominant mechanism resulting in failure. An additional feature occasionally observed at the fracture surface was delamination at prior aluminium powder particle boundaries. This is a common feature in the failure of powder alloys.

The fracture surface is characterised by mixed modes of failure- evidence suggesting void coalescence and ductile tearing is present. The failure path seems to pass along the SiC particle/matrix interface, where it encounters SiC, suggesting a weak interface. Matrix dimple size is observed to be generally lower in the T6 condition which indicates the increased importance of matrix components at the fracture surface. The implications of these factors will be discussed in greater detail after the examination of fracture surfaces of toughness specimens.

Fractographs of failed toughness specimens are also presented in figure 7.10. The appearance of the fracture surfaces was significantly different from that of the tensile samples. Figure 7.10d shows the fracture surface of an underaged specimen. There are a number of particles in the centre of the micrograph which have clearly failed by cracking; this is distinctively different from observations at the tensile fracture surfaces and is probably due to the more severe stress state. There is also evidence of void coalescence in the matrix, although, as for the tensile specimens there are two distinct regimes of void size. In this condition, it is possible that a large proportion of smaller particles will be able to nucleate voids because the yield stress of the material is relatively high in all the heat treatment conditions. Most of the large voids are associated with the silicon carbide. The fact that these voids have dimensions similar to the majority of SiC particles suggests that very little plastic deformation has occurred around the particles prior to failure. It should be remembered that in all fracture surface examinations, the size of such a void is only related to the area of the

particle which was cut by the fracture path. Thus a 5μm particle may leave a significantly smaller void if only its edge impinges upon the fracture path. Material aged to peak had less cracked SiC at the fracture surface, as figure 7.10e shows. There also seem to be more voids of a smaller size (1-2μm). The overaged material seems to contain voids of a similar size to those in the T6 condition- between approximately 1μm and 10μm, as figure 7.10f evinces. At the centre of this micrograph is a larger than average silicon carbide particle which appears to have fractured near its surface leaving some SiC adhering to the matrix. This is distinctly different from those fractures observed in the material that was underaged. Overall there were fewer cracked particles in the overaged condition. This is at odds with the observations of Manoharan and Lewandowski[61] who observed a uniform tendency to fail by particle cracking in composites of 2xxx series alloy in all ageing conditions. Obviously, this is difficult to confirm quantitatively. King[62] notes that particle cracking is promoted by a high strength matrix and coarse particles but does not quantitatively define these terms. In the overaged material there was significantly less SiC observed at the fracture surface. This is again contrary to the observations of Manoharan and Lewandowski[61] but is consistent with their observations for 7xxx series alloys. They attributed the transition from cracking to decohesion in these alloys to a lower matrix failure strain in the matrix in the over-aged condition when testing in three point bend. Thus the stress required to crack a particle would not be reached. This is obviously difficult to confirm and further work is required in this area.

It should be remembered that the composites being compared are derived from different matrix materials, but perhaps more significant is the difference between the heat treatments applied to the different materials. Manoharan and Lewandowski[61], subsequent to solutionising at 495°C for 1 hour, aged their 2xxx series composite for 3 hours at 190°C (underaged), 8 hours at 190°C (peak), 24 hours at 190°C (overaged). The ageing conditions used in this study were as follows:

(a) underageing- 3 hours at 166°C;

(b) peak ageing- 16 hours at 166°C;

(c) overageing- 24 hours at 180°C (in order to achieve the same hardness value as the underaged material).

The fracture surface morphology is indicative of failure at finer particles in the matrix: the obvious candidates in a powder material are the inherent oxide particles.

7.5 Conclusions to Chapter

The work presented in this chapter has revealed a number of important aspects about the production and testing of mmc.s. There are two areas which can be discussed: the processing parameters and their effect on mechanical properties (and consequently the establishment of the 'best' process route) and the absolute values of the mechanical properties in relation to the unreinforced material and predicted values.

The canning, degassing and hot compaction had a prominent influence on the properties of the extrudate in all heat treatment conditions. The combination of these two operations gave the best overall properties but each operation exerted an influence on individual properties to a different degree. Hot compaction resulted in an improvement in tensile strengths and modulus. The values for hot compacted extrudate were approximately 10% higher than those for extrudate which had not been hot compacted. The degassing operation had a modest influence on ductility: the degassed material exhibited ductilities which were approximately 20% greater than the non-degassed counterparts. Material consolidated by cold compaction alone had ductilities in the T6 condition of 5% ± 0.4% for the degassed extrudate compared with 3.9% ± 0.1 % for the non- degassed material. The material which had hot compaction included in its consolidation showed a similar trend: degassed material had a ductility of 6.5%± 0.6%, whereas non-degassed extrudate had a ductility of 5.1% ± 0.3%. The work hardening exponent was higher in degassed material than non-degassed. Hot compaction preceded by degassing was seen to give the greatest improvement in properties over the simple cold compaction route.

In comparison with unreinforced material the hot compacted material was found to have better properties: in some cases, non-hot compacted material exhibited worse tensile strengths than the unreinforced material. The increases in strength were, however, modest. Improvement in U.T.S. and 0.2% proof stress was confined to 6-8% at best. The greatest gains were found on the modulus of the composite, reaching 20% above the modulus of the unreinforced alloy. Ductility was found to have decreased by over 50% in both heat treatment conditions, but surprisingly fracture toughness was found to be high. This is due to the orientation of the specimen with respect to the extrusion direction. The effect of the difference in orientation will be examined in section 8.5.2, where specimens of unreinforced CW67 are compared in both short rod and bar testing geometry with the K_{IC} results obtained for the same alloy by Hildeman et al[110].

The prediction of yield stress using equations 7.1 and 7.2 was found to be in reasonable agreement with the experimentally determined values. The validity of these predictions is, however, questionable because the equations are based on the shear lag model and were originally derived for whisker or platelet type reinforcement. The calculation of yield stress using methods developed in chapter 6 was not a viable alternative because of the influence of other sources of strengthening apart from those included in these analyses. Fracture toughness was able to be more successfully calculated from theoretical considerations. This was because the theory was more easily adaptable to the reinforcement morphology.

8. CW67 AND ITS COMPOSITES

8.1 Structural Characterisation of CW67

Very little published work is available for the CW67 alloy, but comparisons with similar Al-Zn-Mg-Cu and Al-Zn-Mg alloys should yield useful results. This microstructural investigation will be divided into three parts:

(i) examination of the as received powder and as extruded microstructures;

(ii) examination of the material in a number of heat treated conditions corresponding to those used during mechanical testing;

(iii) examination of the material in heat treatment conditions corresponding to peaks on the D.S.C. curve.

8.1.1 As Received Powder

The analysis of powder size revealed that 80.9% (by weight) of the particles were below 32μm, with 10.2% between 32-38μm and 6.7% between 38-45μm, the remaining 3.2% being above 45μm or due to experimental losses (0.9%).

The CW67 powder was examined by optical and electron microscopy techniques. Figure 8.1a shows the rounded shape of the as received CW67 powder and the range of sizes present. The rounded shape is characteristic of gas atomised powders.Examination of the electron micrograph, figures 8.1b shows the dendrite structure. Powder particles had a dendrite spacing of between approximately 0.5 and 3 μm. This is close to the values given by Hildeman et al[110], of between 1 and 5 μm. No large dispersoids were visible in the as received powder specimens. Other specimens showed the phases of growth common to rapidly solidified powder particles. Solidification usually commences at the edge of a liquid metal droplet and progresses across the droplet to completion. The structure changes from supersaturated to cellular as distance from the initiation of solidification increases. This transformation is due to rejection of solute ahead of the solidification front as undercooling and interface velocity diminish leading to instability in the interface[111].

Examination of the powder by x-ray diffraction shows the expected peaks from aluminium at the 2θ values shown below in table 8.1. There is quite a high amount of error in the calculation of these values due to the setting of the machine and the width of peaks (as described in the experimental techniques section)- it was approximately ± 0.005Å. This error was present in all the x-ray diffraction work. The full x-ray diffraction pattern is included in appendix 1.

(a)S.E.M. micrograph

(b)Dendrite spacing

Figure 8.1: Structure of powder CW67

(a) Transverse section: extruded at 425°C, 30:1

(b)Transverse section: extruded at 425°C, 60:1

(c)Longitudinal section: extruded at 425°C, 24:1

Figure 8.2: Microstructure of as extruded, unreinforced CW67

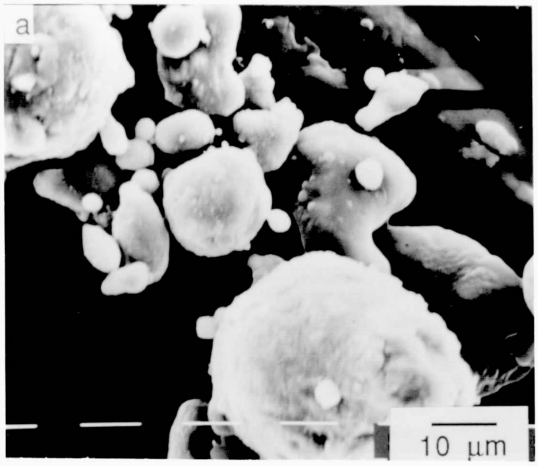
a
10 µm

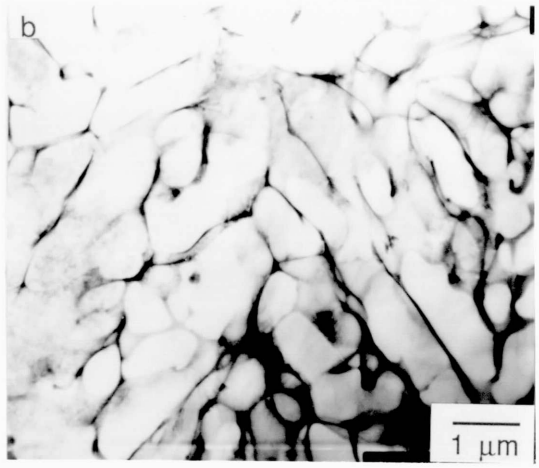
b
1 µm

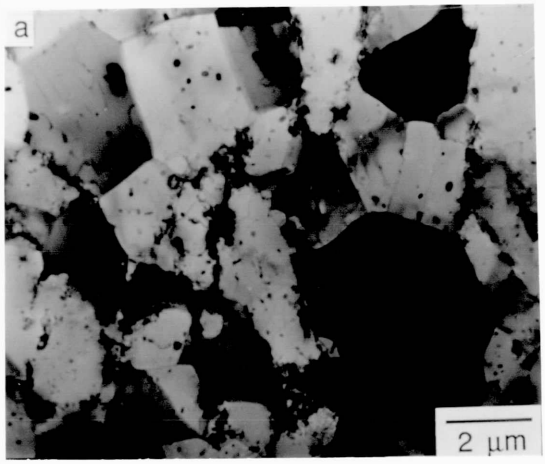
a
2 µm

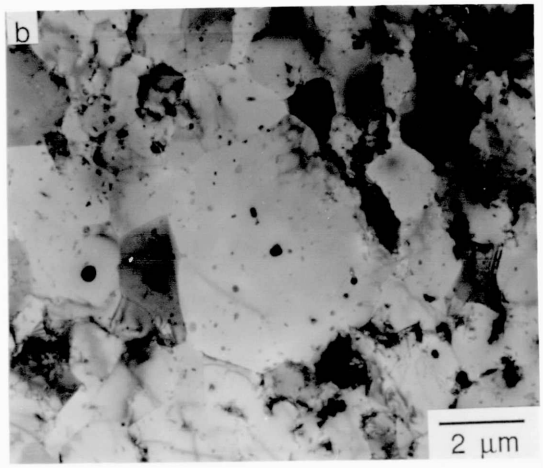
b
2 µm

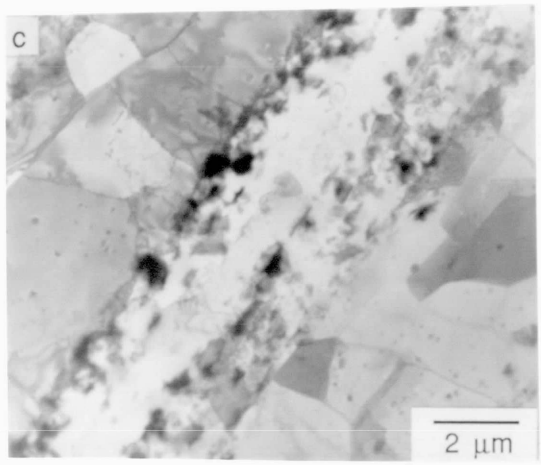
c
2 µm

2θ	d (Å)	h	k	l	a (Å)
38.4	2.3421	1	1	1	4.056
44.65	2.0277	2	0	0	4.054
65	1.4336	2	2	0	4.054
78.1	1.2226	3	1	1	4.055
98.9	1.0137	4	0	0	4.055
112.2	0.9280	3	3	1	4.045
116.4	0.9063	4	2	0	4.053

Table 8.1 Lattice parameter of CW67, calculated from x-ray diffraction

The value for the lattice parameter for powder CW67 averages to be 4.054Å ± 0.005Å which is greater than the 4.049Å given by Mondolfo[85] and calculated from an x-ray examination of powder C.P. aluminium. A rough calculation, which assumes each element is fully in solution, yields a lattice parameter of 4.056Å for a ternary alloy with the same amount of zinc and magnesium as CW67. This is based on information given by Mondolfo[85]: zinc shrinks the lattice parameter virtually linearly from 4.049Å at 0% Zn to 4.018Å at 57% Zn, whilst magnesium expands it, again linearly, to 4.129Å at 17% Mg. Also observed in the powder diffraction pattern are peaks which are probably due to Zn-Mg-Al, although this is uncertain. These occurred at values of the inter-planar spacing (d) of 2.447Å, 2.427Å, but have not been indexed. A peak probably due to Al-Zn was observed at 1.220Å, and was again unable to be indexed. These phases probably resulted from the high cooling rate prevalent during rapid solidification and are non-equilibrium. No peaks were identified as being due to any zirconium containing phases.

8.1.2 As Extruded Material

The sub-grain size of the extruded material varied as shown in table 8.2 below. The values were calculated using the mean linear intercept method[112]. However, the number of readings taken was low, which dictates that the quoting of a range of sizes is preferable.

Figure 8.2a shows the sub-grain size of material extruded at 425°C and a ratio of 30:1. Also present are dispersoid particles which are discussed below. As extrusion temperature was reduced, sub-grain size decreased. There was some evidence to suggest that a small number of recrystallised grains had nucleated at the edge of the material extruded at 430°C with a ratio of 60:1. The grain at the centre of figure 8.2b exhibits a high degree of mismatch with its neighbours, and is rounded in shape. Recrystallisation is a temperature and strain activated process and it is possible that

some recrystallised nuclei could have formed at the periphery of the extrudate section, which undergoes greater deformation on extrusion. A large amount of oxide,

Extrusion conditions, Te (°C) and R.	Average sub-grain size, μm	Figure number
Te=425, R=30	2.5-3.5	8.2a
Te=425, R=60	3 - 4	8.2b
Te=325, R=30	2 - 3	-
Te=325, R=60	1.5-2.5	-
Te=425, R=24	3 - 4	8.2c

Table 8.2: Transverse sub-grain size of as extruded CW67 processed under various parameters

common in all powders, was observed to be distributed in bands in the extrusion direction. This occurrence was isolated. The longitudinal section, figure 8.2c, shows that this oxide has broken up and extended in the extrusion direction. A further point of note is the presence of material between the oxide bands (the central strip in figure 8.2c): this indicates the break down of surface oxide and the extrusion of material between powder particles. During the investigation into this alloy no Al_3Zr particles were imaged or able to be detected by x-ray techniques; the only Zr present was in small amounts in combination with aluminium, zinc and magnesium. The absence of Al_3Zr was also noted by Hildeman et al[110]; and may partly explain the occurrence of some recrystallised grains at the edges of this extrudate.

The as extruded material contained some relatively large near-spherical dispersoids, varying in size between 50-150nm (see figure 8.2 a-c). These were analysed by x-ray dispersive techniques as containing aluminium, copper (the possibility of the copper arising from the specimen holder was not discounted), nickel and iron. During the course of this investigation particles could occasionally be imaged as two overlapping particles, one of which may have nucleated on the other. These were separated into either iron or nickel bearing. Further quantitative compositional investigation was not possible due to the limitations of the accuracy of the detection system at the particle sizes under investigation.

The density of the extrudate was determined by the difference method (section 4.5.2) to be 2.83 g/cm^3.

8.1.3 As Solutionised Material

Specimens in this heat treatment condition only exhibited substructural differences to the as extruded specimens. There was no significant alteration of the sub-grain size, however the dislocation density appeared to have decreased consistent with recovery of the substructure having taken place during solutionising.

X-ray diffraction analysis of the as-solutionised material differed in one marked way from the powder pattern- an extremely strong peak was observed at a value of the inter-planar spacing of d= 2.574Å ($2\theta \approx 34.7^{o}$); this can be seen in appendix 1. Although no positive identification was made, it was thought to be due to the iron nickel phase $Al_9(Fe,Ni)_2$ identified by Hildeman et al[110] as being present in CW67 in the extruded condition but not in the as received powder. This is supported by the appearance and identification of large numbers of iron and nickel bearing particles subsequent to extrusion. The peaks which were believed to be due to Zn-Mg-Al and Al-Zn in the as received powder do not occur in the solutionised sample. This supports the belief that they were non-equilibrium phases which form during the rapid solidification. A number of intense peaks were found at inter-planar spacings of 2.140Å, 1.181Å, 1.177Å; two less intense peaks were observed at d= 1.292Å and 1.119Å. This series corresponds to values for a number of Al_3Zr planes: the first two would be {008}, {201}, the rest are unindexed but known to be present. It is unclear whether these do correspond to Al_3Zr as there is a lack of microscopic evidence and many intense peaks are missing from the series, although the two most intense would be obscured by the {111} and {200} aluminium peaks.

8.1.4 Precipitation in the CW67 System

This section seeks to determine the precipitation reactions of the CW67 alloy in order to be able to compare them with other 7xxx series alloys and the composite material.

Differential Scanning Calorimetry (D.S.C.) was performed on solutionised CW67, the treatment being the same as that employed prior to artificial ageing. Interpretation of the data relies on the knowledge that a positive displacement is an exothermic reaction, characteristic of the formation of precipitates; an endothermic reaction signifies the dissolution of a phase. The generally accepted precipitation sequence for Al-Zn-Mg and Al-Zn-Mg-Cu alloys follows the scheme:

Supersaturated solid solution -> G.P. zones -> η' -> η (equilibrium $MgZn_2$)

There is some debate as to whether one or two G.P. zone reactions occur. Petty-Galis and Goolsby[53] identify the formation of two types of G.P. zones, based on their nucleation consisting of either clustering solute atoms (G.P.I) or vacancies (G.P.II). Other workers[85] discount this idea, which seems to rely at least partially on the definition of the stage at which G.P. zones become η' precipitates.

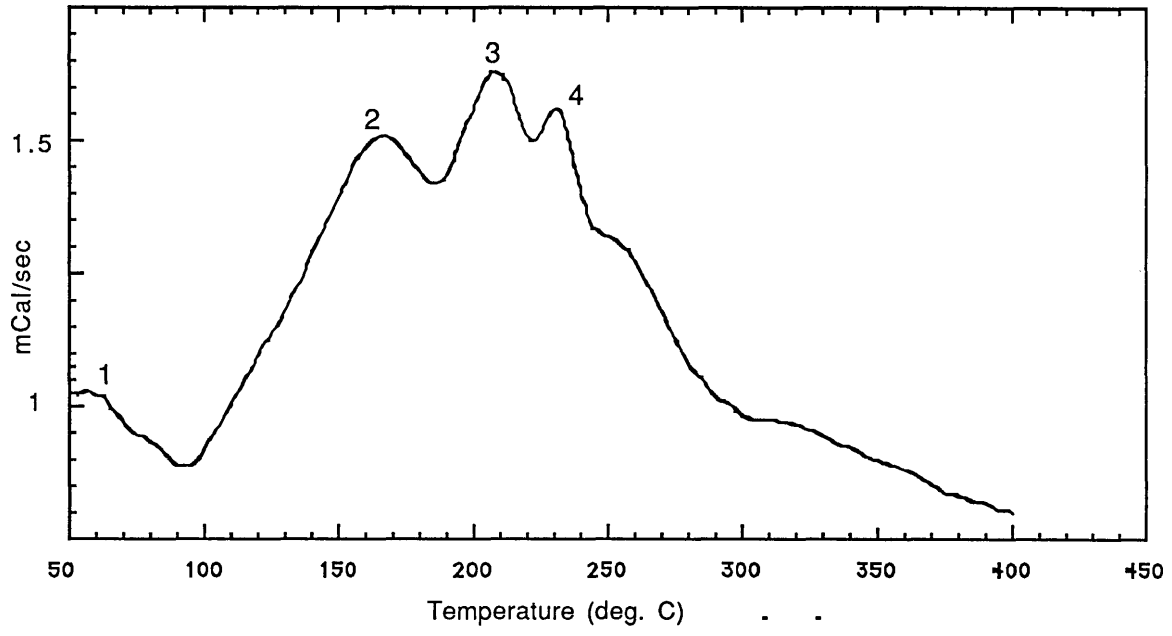

Figure 8.3 Differential scanning calorimetric profile of CW67

The peaks were able to be compared with work on similar alloys by other authors[53,113]. It should be noted that whilst this work has concentrated on the peaks produced during the D.S.C. examination, the positively inclined foot of a peak indicates the *onset* of a precipitation reaction. It should also be noted that the peaks will overlap. This is important in interpreting the combination of precipitates present under any discrete ageing condition.

Figure 8.3 shows the D.S.C. curve for the as-solutionised alloy heated at a rate of 5°C per minute. Table 8.3 shows the temperatures given by three groups[53,113-115] for the reactions occurring in 7xxx series alloys. An initial comparison of the shape of the curves, and the relative intensities of the peaks, showed slight deviations in temperature to achieve peak. These peak temperatures are between 50-60°C lower than those given by Petty-Galis and Goolsby[53] for the same reaction. This disparity may be explained by compositional differences (Petty-Galis and Goolsby[53] used 7091 which contains 6.5% Zn, 2.5% Mg, 1.5% Cu and 0.4% Co) and also by the difference

in heating rate- 20°Cmin^{-1} compared with 5°Cmin^{-1}- which will tend to shift the reactions to higher temperature as heating rate is increased. The temperatures are only slightly lower than those given by Radomsky et al[113], even though the composition used by this group is different (4.5% Zn and 2-3% Mg) and their heating rate much greater (80°Cmin^{-1}). This difference may be due to the wide range of temperatures quoted by these workers and that the material is tested in the aged condition rather than as solutionised. The third comparative work[114,115] also quotes a wide range of temperatures for the salient reactions, for 7xxx series alloys containing from 6.1-7.2% Zn, 2.2-2.4% Mg and 1.4-2.6% Cu with some trace elements including either Cr or Zr as grain refiners. As with the work of Radomsky et al[113], the reactions are identified with the material at a particular heat treatment condition, and thus a comparison of the shapes of the curves is meaningless. The heating rate used in this series of experiments was moderate, at 10°Cmin^{-1}. The quoted range of temperatures is in good agreement with Petty-Galis and Goolsby[53] and Radomsky et al[113]. Bearing in mind the differences in composition and heating rate, the reactions occurring in CW67 can be identified.

Reactions occurring	Temperature range of peak reaction given by specific authors (°C)			Temperature (°C)
	Petty-Galis & Goolsby[53]	Radomsky et al[113]	Delasi & Adler[114]	CW67
G.P. I formation	60-140	20-70	-	40-50
G.P. II formation	120-160	-	-	-
G.P. I reversion	160-220	130-200	113-217	90-100
η' formation	220-270	130-200	113-217	150-165
η' dissolution	220-270	-	164-245	170-180
η formation	220-320	230-270	217-271	200-220
η dissolution	320-445	300-420	271-448	220-230
T formation	-	270-300	-	230-240
T dissolution	-	300-420	-	250-400

Table 8.3: Temperatures of peak reactions observed in 7xxx series alloys

The first exothermic reaction (peak 1), at 50-60°C in figure 8.3, is identified as corresponding to the formation of G.P. zones. This is followed by G.P.Z. dissolution which occurs at between 90-100°C. There was no clear indication of a peak related to G.P. II zone formation, as identified by Petty-Galis and Goolsby[53]. The second major peak is observed at between 140-200°C, and is due to η' formation; dissolution of this

metastable phase commences soon after this peak. The peak due to η formation is found at temperatures between 190-245°C. In some cases a further precipitation reaction was observed at between 240-260°C; this was thought to be due to the T phase (see Radomsky et al[113]), although the Zn:Mg ratio of 3.6:1 for CW67 is slightly higher than is quoted for its formation as an equilibrium phase[85]. The final endothermic reaction is the dissolution of all precipitates.

X-ray diffraction analysis was performed on specimens heated at the same rate as was employed during the D.S.C. analysis ($5°Cmin^{-1}$) to temperatures of 160°C, 180°C and 200°C in order to further elucidate the precipitation process. There are two areas of interest in these plots: the shifting of the primary aluminium peaks and the growth of low angle peaks. The lattice parameter values for the Al peaks shift from 4.041Å at 160°C and 180°C to 4.016Å at 200°C. The shift may be related to the growth of the low angle peaks described below, but the significance of this shift is unclear; Mondolfo et al[86] note a drop in lattice parameter as time increases at constant temperature and relate it to the appearance of precipitates. However, the observed shift was not as large as the 0.025Å ± 0.005Å observed in this work. The measurements were taken from the higher order peaks, because those for {111} and {200} were considered too broad to be reliable; however the error was still high, at around ± 0.005Å. The extreme width of these aluminium peaks also precluded the detection of any of the three main $MgZn_2$ (η) peaks- due to the planes {112}, {201} and {004}- or any of the less intense peaks occurring at values of 2θ up to 48°. The fact that these peaks are so wide would seem to indicate that there are other peaks which are contributing to the broadening, particularly in comparison with the as solutionised pattern.

Figure 8.4 shows a schematic diagram of the growth of low angle peaks during the heating of the alloy up to the three temperatures shown. These peaks are thought to be due to the formation and growth of metastable (η') precipitates on the {111} plane of the aluminium. The growth of these peaks probably corresponds to the {100} plane of the metastable precipitate. The values for lattice spacing, d, are close to that for the stable η {100} value of 4.51Å, and are tending towards it as the sequence progresses. The values for inter-planar spacing ('d values') are 4.18Å, 4.24Å and 4.40Å (the breadth of these peaks limits the accuracy of calculation) for heating to 160°C, 180°C and 200°C respectively. The specimen heated to 200°C has a second low angle peak, as can be see in figure 8.4. This has a 'd value' of 4.24Å, which is close to the d= 4.27Å for {002} planes of $MgZn_2$. Coupled with these changes is the increasing intensity of a peak at d= 1.30Å, which is found to correspond to the $MgZn_2$ peak for the {220} planes.

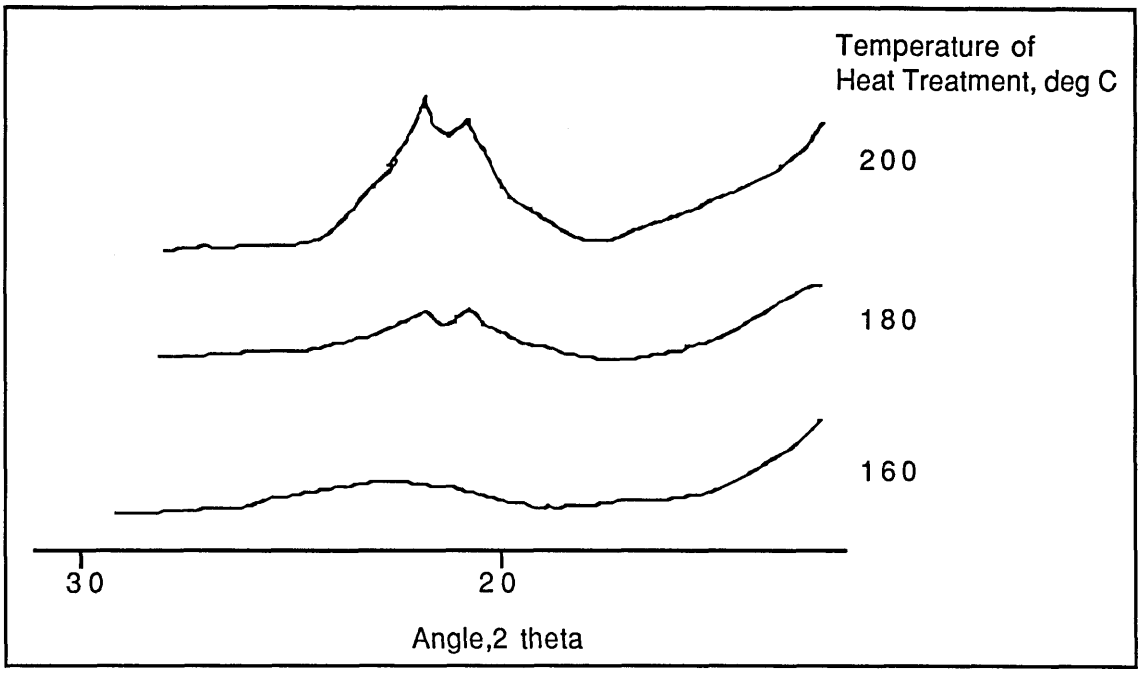

Fig.8.4 Schematic of Low Angle Range of X-Ray Diffraction Patterns of CW67 Heat Treated at 5 degrees/minute to the temperatures shown

The x-ray investigation has shown the sequential nature of the precipitation process and that $MgZn_2$ (η phase) develops from a metastable precipitate. It has also been shown that the η phase comes to dominate the structure as ageing time and temperature are simultaneously increased. T.E.M. examination was conducted on material solutionised and aged for three quarters of an hour at the temperatures at which the D.S.C. peaks were estimated to be a maximum: 50°C, 160°C, 210°C and 240°C. This was done in order to further isolate the precipitation reactions occurring in CW67. The results of T.E.M. examination of these specimens are shown in figure 8.5.

Material aged at 50°C (fig. 8.5a) showed no signs of any precipitation in either the bright or dark field. The diffraction pattern (fig. 8.5b), which is of the <001> zone type, shows slight streaking of the {111) spots, but this is unclear. In some cases the electron diffraction pattern showed one or two extra spots, but these were found to have been caused by large dispersoids within the grains.

The specimen aged at 160°C had a precipitate structure that was already showing signs of coarsening, with a precipitate size of around 5-10nm, as figure 8.5c demonstrates. A precipitate free zone is also clearly visible, bordered by slightly larger precipitates (approximately 50nm by 20nm) of η phase. The <111> zone axis diffraction pattern (fig. 8.5d) shows an intense ring of spots around the transmitted beam, which has been shown to be due to the presence of the equilibrium phase, η^{88}.

(a)Bright field, aged at 50°C

(b) S.A.D.P. of same, <001> type zone axis

(c) Bright field ,aged at 160°C

(d) S.A.D.P. of same, <111> type zone axis

(e) Bright field, aged at 210°C

(f) S.A.D.P. of same, <110> type zone axis

(g) Bright field, aged at 240°C

(h) S.A.D.P. of same, <100> type zone axis

Figure 8.5: CW67/0%SiC after ageing to D.S.C. peak temperatures for 3/4 hr.

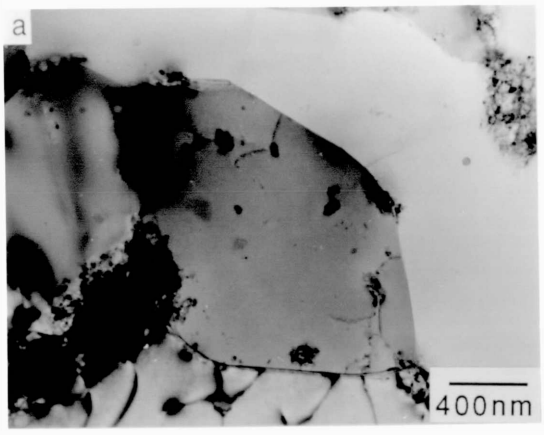
a
400nm

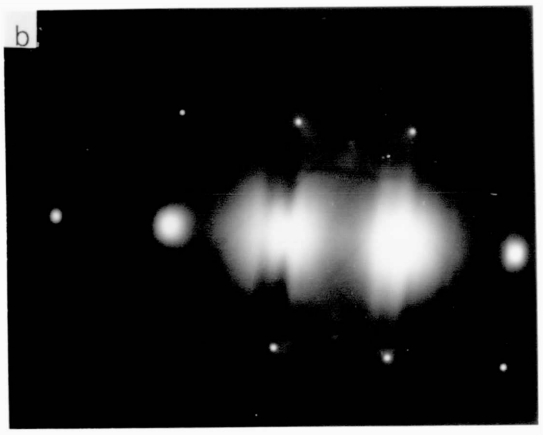
b

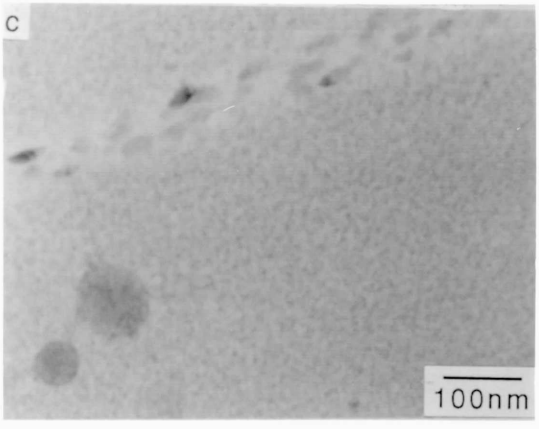
c
100nm

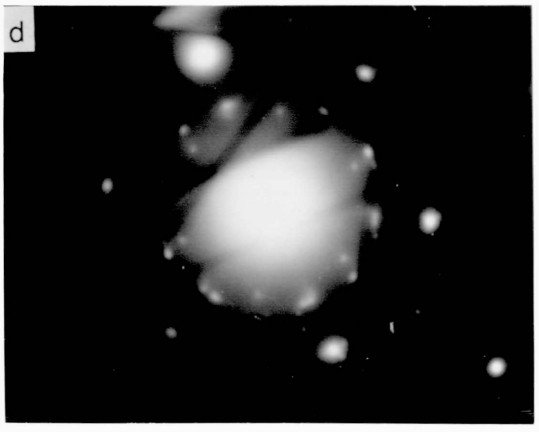
d

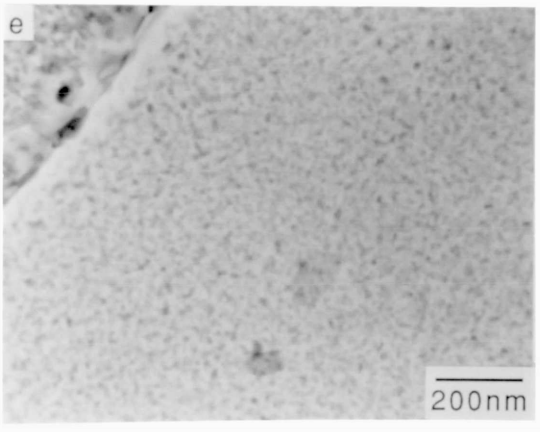
e
200nm

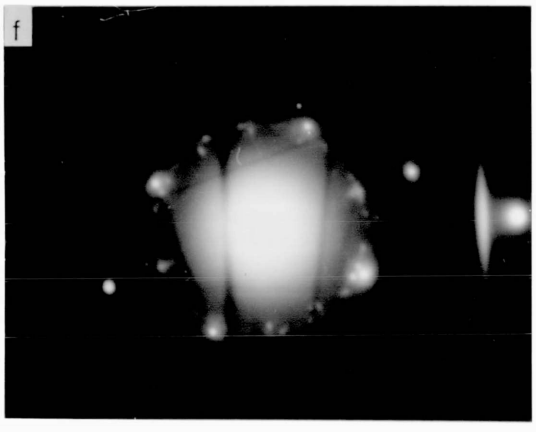
f

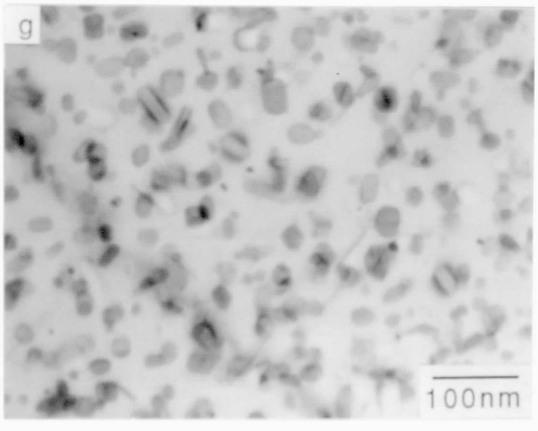
g
100nm

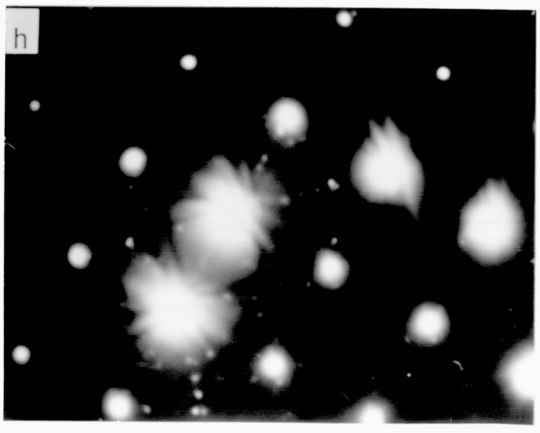
h

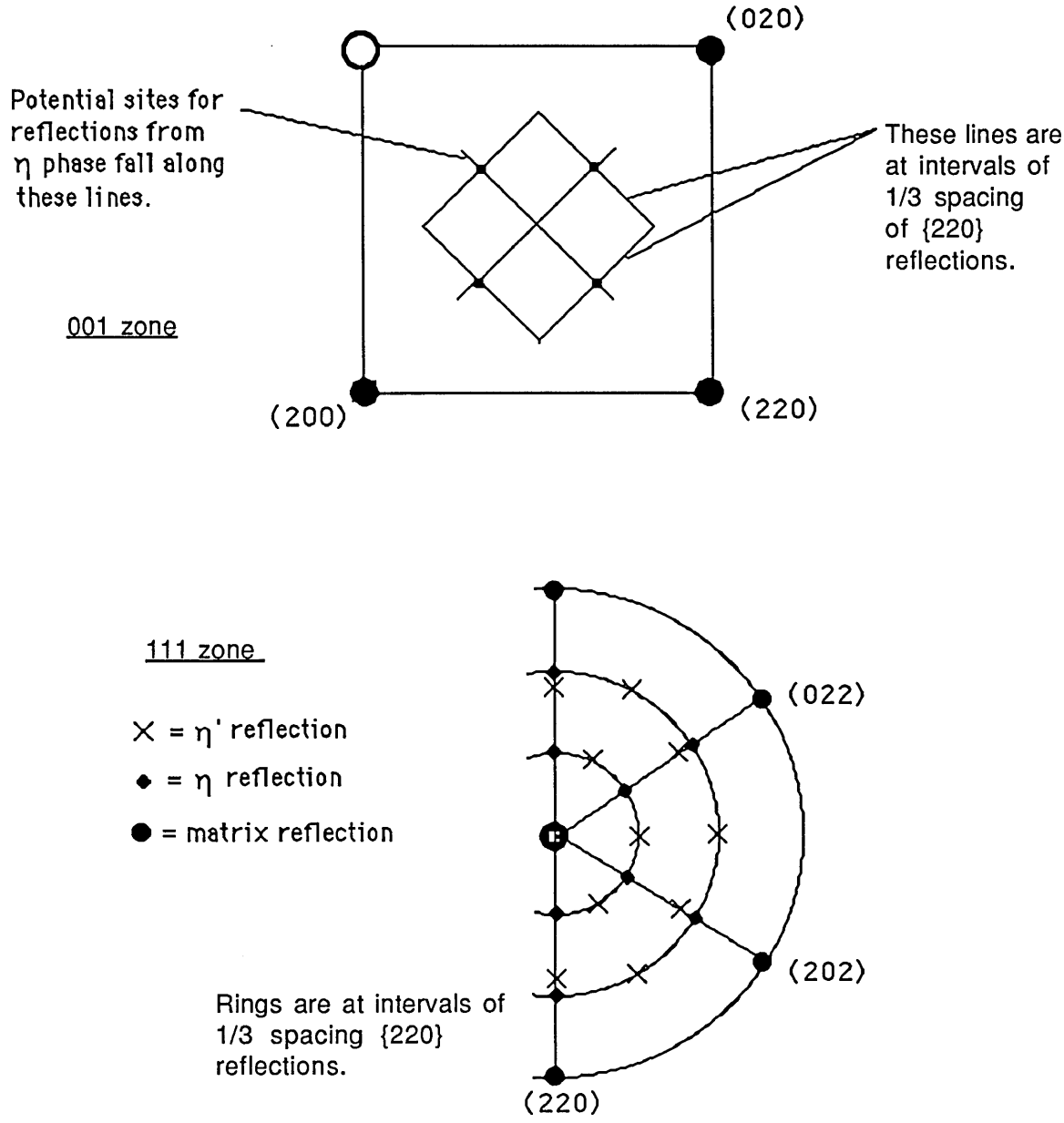

Figure 8.6: Potential sites for η and η' precipitate reflections in diffraction patterns of 7xxx series alloys (after Thackery[88]).

Some spots in this ring also corresponded to the η' phase. Figure 8.6 shows the potential sites for the appearance of diffraction spots corresponding to both the equilibrium and metastable phases. Spots may not necessarily appear at all of these sites. The spots which occur outside the ring of matrix reflections are due to what Thackery[88] calls 'X phase', but admits may be η'. Under these ageing conditions, the precipitates are predominantly the equilibrium η phase.

Ageing at 210°C for three quarters of an hour resulted in a coarsened precipitate structure, as shown in figure 8.5e. A precipitate free zone, approximately 150nm wide, may be seen in the bright field image. The precipitate size is of the order of 10-20nm, and predominantly comprised of η phase laths or rods as the diffraction pattern evinces. Although the zone axis in this case is of the <110> type (fig. 8.5f), the ring of spots is still at a distance which is a multiple of $^1/_3$ R_{Al220}. Comparison with the work of Radomsky et al[113] also lends weight to this identification.

Figure 8.5g illustrates the microstructural change that occurred at the ageing temperature of 240°C. Precipitates were observed to be predominantly circular or rounded oblong in cross section, with some polyhedra. Precipitate size was found to be between 30-50nm long by 20nm wide. Strain contrast from some precipitates is noticeable in the bright field. This is probably coarse η phase, but may contain a proportion of T phase. The reason for this ambiguity is twofold. The D.S.C. trace shows a high temperature peak, which is thought to be due to T phase[113], and there are a number of diffraction spots in figure 8.5h which could not be identified by comparison with any other work[88,116]. Mondolfo[85] states that alloys with a Zn:Mg ratio of between 2:1 and 3:1 may precipitate $MgZn_2$ at below 200°C and $Mg_3Zn_3Al_2$ (T phase) above this: the alloy CW67 has a Zn:Mg ratio close to this grey area, at 3.6:1. Ryum[89] shows T phase as a rod-like precipitate, similar to those observed here, but it is known that η also assumes a rod or lath like morphology[85,88,116]. It is therefore likely that the structure is a combination of η and T phases.

8.1.5 CW67 Artificially Aged to Peak Hardness

The structures displayed by all extrusion conditions were, to all intents, the same: this section will concentrate on the material extruded at 450°C, at a ratio of 30:1. The material was aged at 120°C for 13.5 hours, which were found to be the optimum ageing conditions to produce peak hardness in this alloy (see section 8.3).

The microstructural features of the peak aged material are broadly the same as those described in the previous section: the microstructure is characterised by a fine

dispersion of precipitates, with a precipitate free zone at the sub-grain boundaries. Precipitate free zones in Al-Zn-Mg alloys are generally held to be of the vacancy depleted, rather than solute depleted, type. The mechanism of formation of P.F.Z.s by vacancy depletion is shown in figure 8.7. A critical vacancy concentration is required before G.P. zones can nucleate; this is only achieved at a specific distance from the grain boundary which is dependent upon factors such as solutionising temperature, quench rate and ageing temperature. The distinction between vacancy and solute depleted P.F.Z. formation is demonstrated by Raghavan[90] by micro analysis of the P.F.Z. region. In the vacancy depleted case precipitates at the sub-grain boundary and at the P.F.Z. boundary are often observed to be coarser than those at the grain/sub-grain centre. This is due to solute diffusion from the P.F.Z. in order to reach an equilibrium concentration throughout the grain; this will occur only as ageing progresses (at times in excess of 1 hour at 200°C[90]). The precipitate free zones observed in the CW67 powder alloy are considerably narrower than those generally found in cast materials. Kirman[117] measured P.F.Z. widths of 300nm ± 50nm in cast 7075 sheet in the T6 condition. This difference is directly related to the processing, and will lead to less deterioration of the properties of the powder material.

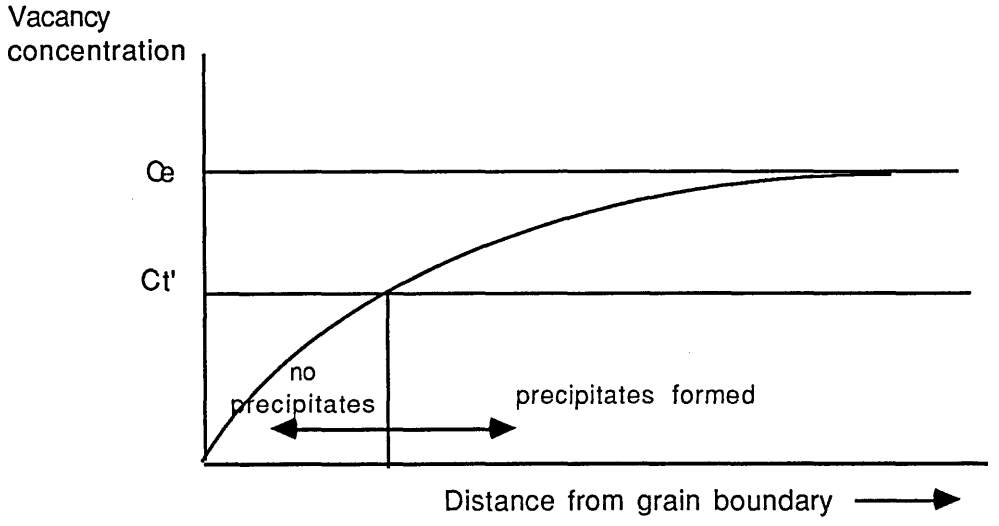

Figure 8.7: Variation in vacancy concentration leading to the formation of a P.F.Z. Ce = equilibrium concentration; Ct' = critical concentration required for G.P. zone formation (after Embury and Nicholson[116])

The problem of P.F.Z.s has been addressed by many workers[90,116,118,119] and has resulted in a number of two step ageing routes being proposed, in order to reduce the width of P.F.Z.. All rely on ageing at a high temperature, followed by a period at a lower temperature. Ageing at the higher temperature will induce a particular P.F.Z.

width, characteristic of a particular vacancy concentration. Subsequent ageing at a lower temperature will result in the filling in of the previously formed P.F.Z. with fine precipitates to a width consistent with ageing at this temperature as if the first stage of ageing had not been performed[116]. Embury and Nicholson[116] conclude that whilst the vacancy concentration profile is dependent upon quench temperature, and rate, it is stable during ageing. This was thought to be because the profile was predominantly determined above 200°C; ageing below this temperature would thus have little effect on the concentration. Two step ageing routes are as numerous as they are varied and attempts at establishing a two step route for the alloy CW67 were soon abandoned as this was not the main aim of the work.

The first feature of note in figure 8.8a is the occurrence of a precipitate free zone (P.F.Z.) at the sub-grain boundaries. This was less than 50nm in width. Enlarged precipitates, approximately 75nm long by 30nm wide, of $MgZn_2$ were observed to have nucleated at the sub-grain boundary. Further precipitates, believed to be $MgZn_2$, were observed to have formed at the P.F.Z. boundary; these were between 10-30nm in size. Similar precipitates were also found to have nucleated on the iron and nickel rich particles, but were unable to be analysed due to the proximity of the much larger dispersoids. Both of these features are deleterious to mechanical properties, P.F.Z.s particularly limiting stress corrosion resistance.

In the main body of the grains a homogeneously distributed fine precipitate was observed (fig. 8.8a). Precipitates were able to be imaged at around 10nm: many were smaller than this but were not able to be imaged because of their size. Comparison of diffraction patterns with those of other workers[88,113,116] indicated that this was a combination of η' and η, the transition and equilibrium $MgZn_2$ phases respectively. The pattern shown in figure 8.8b is of the <001> type zone axis. Two rings, at a distance of $^1/_3$ and $^2/_3$ R_{Al220} can be seen. Diffraction spots which occur at points in the spaces between the axes of the {220} matrix reflections are due to both η and η'. Spots along these axes which occur at exactly intervals of $^1/_3$ R_{Al220} are from the η phase and those which are slightly offset originate from the metastable η' phase. There are also diffraction spots which are probably due to the larger dipersoids observed in the bright field. The shape of the η phase was found to be generally lath or rod like; the η' phase was difficult to image alone satisfactorily.

X-ray diffraction patterns of the heat treated matrix showed the presence of a metastable phase at $2\theta = 20.95°$; it was thus not possible to index this peak which was thought to be due to the η' phase. Peaks were also present which were calculated as being due to the {112} and {004} planes of $MgZn_2$, the stable η phase. The lattice

(a)Bright field (b) S.A.D.P., <001> type zone axis

Figure 8.8: Microstructure of CW67 heat treated to peak hardness.

(a) Aged 1 hour at 120°C (b) Aged 24 hours at 120°C

Figure 8.9: Microstructure of non-standard ageing treatments

Figure 8.10: Microstructure of as extruded CW67/20% SiC composite

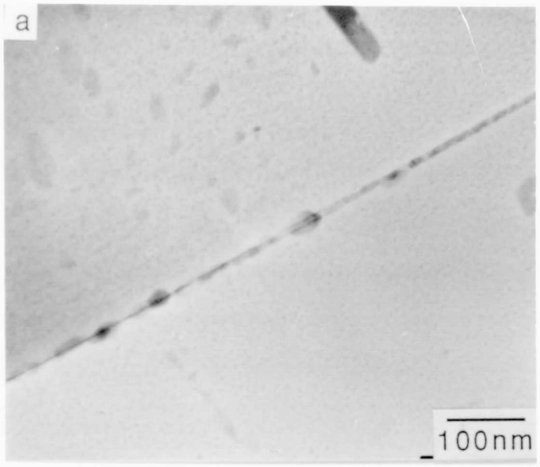
a
100nm

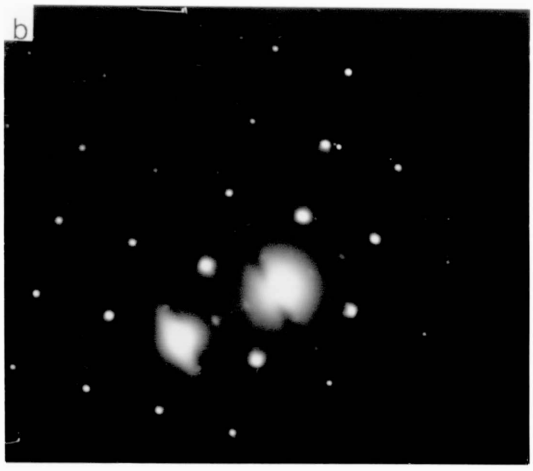
b

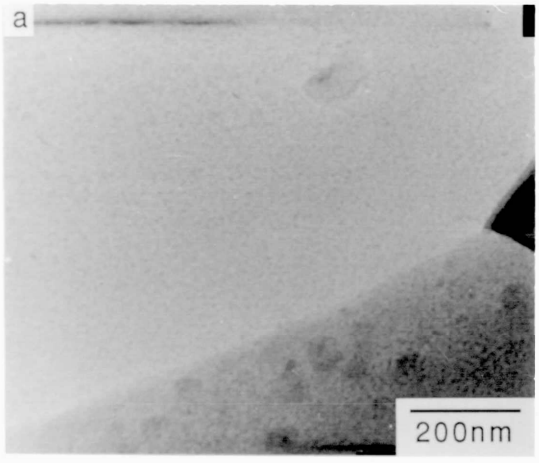
a
200nm

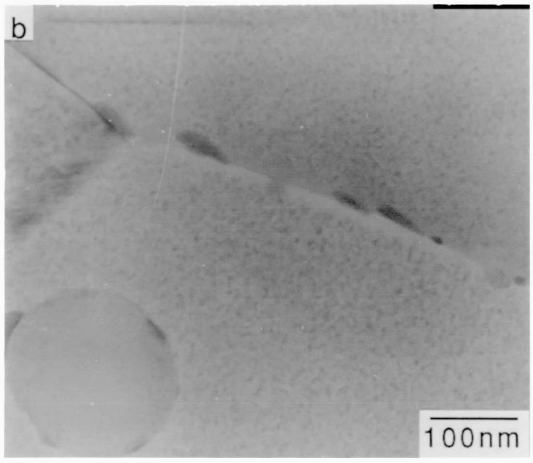
b
100nm

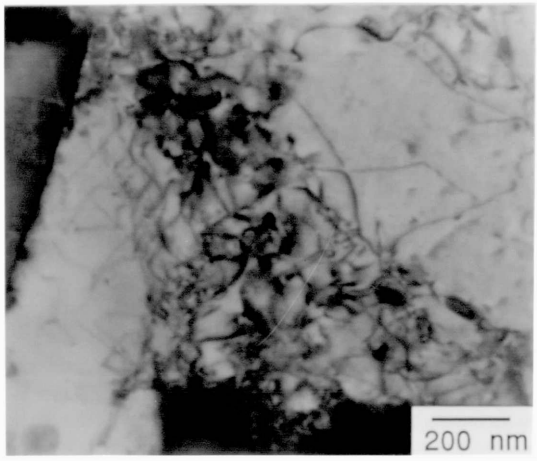
200 nm

parameter of the aluminium was calculated as being closer to its standard value: the narrower higher order reflections, from {220}, {311} and {222} planes, gave values for this parameter of 4.043Å, 4.049Å and 4.049Å respectively. This change must have occurred as a result of elements coming out of solution. Obviously either all of the zinc and magnesium could have come out of solution, but this seems unlikely.

A comparison of the effects of each on the lattice parameter, as given by Mondolfo[85] and in section 8.1.1, shows that this value would also be reached if the Zn:Mg ratio were at least 8.65:1. This is at odds with the fact that zinc diffuses faster than magnesium in aluminium and that some authors[85,120] report that G.P. zones form by the build up of zinc, followed by the diffusion of magnesium to these clusters at a slower rate. However, the incorporation of the copper into $MgZn_2$, leading to the nomenclature $Mg(Zn,Cu)_2$[110],may exert an effect, as will the strain due to coherent or semi-coherent precipitates.

8.1.6 Non Standard Ageing Treatments

A very fine dispersion of precipitates was observed in underaged material (figure 8.9a). In a few cases there was no discernable precipitate free zone. Embury and Nicholson[116] note this feature too and associate this variation of P.F.Z. size with low disregistry boundaries only, at values of 0-5° (i.e. sub-grain boundaries). In work conducted for this thesis and in the work of Embury and Nicholson[116] the appearance of a P.F.Z. was observed in other regions of the specimen, with outsized $MgZn_2$ particles at its boundary. These are the same as was found in other aged specimens (e.g. those mentioned in section 8.1.5).

The precipitate size remained low even after substantial ageing: figure 8.9b shows precipitates in material aged at 120°C for 24 hours which are approximately 10nm in size. There was a strengthening of the diffraction pattern ring corresponding to the η precipitates, which would suggest that the main change is from η' to η with little scope for coarsening of the structure. This was observed in both the material aged for 24 hrs at 120°C and material aged for 13.5 hours at 120°C and 1.5 hours at 160°C. The widths of the respective precipitate free zones were not significantly different. This is in accordance with the findings of others[90,119] who, as has been noted earlier, observed the dependence of P.F.Z. width on ageing temperature alone which is in turn characteristic of a vacancy depleted P.F.Z.. Furthermore, they note that the final width will be governed by the lowest ageing temperature. In this work, as the treatment at 160°C was applied second, the width of P.F.Z. and precipitate morphology will not be affected. Had the higher temperature treatment been applied

first, the structure would be characterised by a 'double P.F.Z.' consisting of an in-filling of the P.F.Z. established at 160°C with finer precipitates, as shown by Embury and Nicholson[116]. Also observed in this micrograph is the nucleation of precipitates of what are assumed to be $MgZn_2$ on a large dispersoid particle (analysis was impossible because of their proximity to the dispersoid).

8.2 Structural Characterisation of Composites of CW67

Large differences are to be expected in the structures of composite material when compared with their parent matrix[6]. The extent of these differences, and their effect on properties have not yet been quantified for more than a few alloy systems. For this reason the prediction of the structure and properties of composites of heat treatable alloys is not possible beyond a qualitative description. The structural changes due to the incorporation of silicon carbide in CW67 are presented herein with a view to explaining any changes in mechanical properties.

8.2.1 As extruded composite material

Composites of CW67 were extruded with four volume fractions of SiC- 0.1, 0.15, 0.2 and 0.25- at a single extrusion temperature of 450°C. All of the material was canned and degassed and extruded at a ratio of either 24:1 or 34:1.

Examination of the extruded structure by transmission electron microscopy revealed that there was little difference between the composites and unreinforced material with respect to dispersoid distribution. Particles containing aluminium, iron, nickel and possibly copper were identified and are of the same morphology as those found in the unreinforced material. The dislocation density was much greater in the quenched composite materials. This can be seen in figure 8.10, and is due to the large difference in thermal expansion coefficient between aluminium and silicon carbide. This phenomenon has been observed by many other authors[32,39,47]. The dislocations appear to be more numerous closer to the SiC particles and are extremely tangled in these regions. Humphreys[37] notes that the dislocations will tend not to be grouped around the SiC particles in C.P. aluminium but may be in Al alloys, in which the friction stress to move the dislocations is considerably higher. The subgrain size of the extruded composites was found to be slightly lower than the unreinforced material extrude at the same temperature, although a full comparison could not be instigated because of the temperature and ratio limits for successful composite extrusion. The size of subgrain could not be measured using the same method as was employed for the unreinforced material due to the presence of the silicon carbide: grain diameters were

measured individually, which will lead to some discrepancy in the comparison with the unreinforced material and a less accurate result. Sub-grains in the composite were found to be in the range 1.5-2μm for all volume fractions. It is possible that subgrain formation is independent of volume fraction of reinforcing particles although their size may be expected to fall as the inter-particle spacing decreases. It is probable that the technique of measurement has as much influence as any other factor, thus obscuring any small variations in subgrain size.

Material	Measured Density (g/cm^3)	Calculated Density (g/cm^3)
CW67	2.83	-
CW67 10% SiC	2.88	2.86
CW67 15% SiC	2.89	2.88
CW67 20% SiC	3.02	2.90
CW67 25% SiC	2.92	2.92

Table 8.4: Experimentally determined density of CW67 composites

The densities of the composites were determined for extrudate material from which the surrounding can had been scalped. The densities are presented in table 8.4, along with the law of mixtures density based on a silicon carbide density of 3.18 g/cm^3.

It can be seen from this table that the error in the comparison is quite high. This was either due to losses during the weighing operation or in the assumption of the value for the density of the SiC. These results do not establish the degree of porosity in the extrudate; they only show that the material is close to its full density.

8.2.2 As solutionised Composites

Little work was conducted on the composites in their solutionised state. The quench from the solutionising temperature resulted in a dislocation structure similar to that observed in the as extruded material. The observed dislocation density will have evolved for the same reasons as were proposed to explain the high density in the extruded material, i.e. because of the difference in thermal expansion coefficient affecting the quench.

8.2.3 Precipitation in CW67 Composites

The precipitation process in composite materials is believed by many authors[39,46,47] to be substantially different from that in the parent unreinforced alloy, but the reasons for, and evidence of, this difference are less forthcoming. This section seeks to examine the precipitation reactions occurring in composites of CW67 by a combination of D.S.C. analysis, x-ray diffraction and T.E.M. examination. All of these techniques have been employed in examining the unreinforced alloy, which should facilitate the interpretation of the data presented here.

The D.S.C. curves of two composites, 10% and 20%, are shown in figure 8.11. The material was analysed under the same conditions as the unreinforced alloy- solutionised and then heated at a rate of $5^{o}Cmin^{-1}$. It will be noticed that the shape of the two curves is quite different in the mid range of the test. The initial G.P. zone formation is observed at the same temperature range as the unreinforced material (peak 1). In the range at which the G.P. zones dissolve the curve for the 20% composite is slightly shallower than the other two specimens. The D.S.C. path of the 20% composite becomes further divorced from those of the unreinforced alloy and the 10% composite when a peak is observed at 120°C, followed by dissolution at about 150°C. The next peak in the 10% composite is observed at 170°C and falls into the range Radomsky et al[113] give for the formation of η'; by inference the peak in the 20% material which was observed at 120°C is also due to η' formation. This is consistent with theory, expounded by Petty-Galis and Goolsby[53], which dictates that the peak temperatures fall as SiC concentration increases, due to the greater internal energy of the system. Not only does the η' peak get shifted but it is also suppressed as the volume fraction increases. The suppression of this peak is believed to be enabled because the increased strain energy, due to the greater number of residual dislocations (i.e. after solutionising), leads to the easier surmounting of the activation energy barrier for η' formation. The corollary of this is a microstructure of mainly coarse particles of the η ($MgZn_2$) type in the case of the 20% composite if the material is aged under similar conditions to its parent alloy.

Subsequently, η' dissolution is followed by the precipitation of the equilibrium phase, η, which corresponds to the peak at approximately 210°C (peak 3). The 20% composite appears to rejoin the path of the two other compositions at this point; this may be due to the better annihilation of dislocations at such an elevated temperature. There is a further peak (4), common to all the samples, at between 230-240°C which, to remain consistent with the previous observations, is believed to be the peak

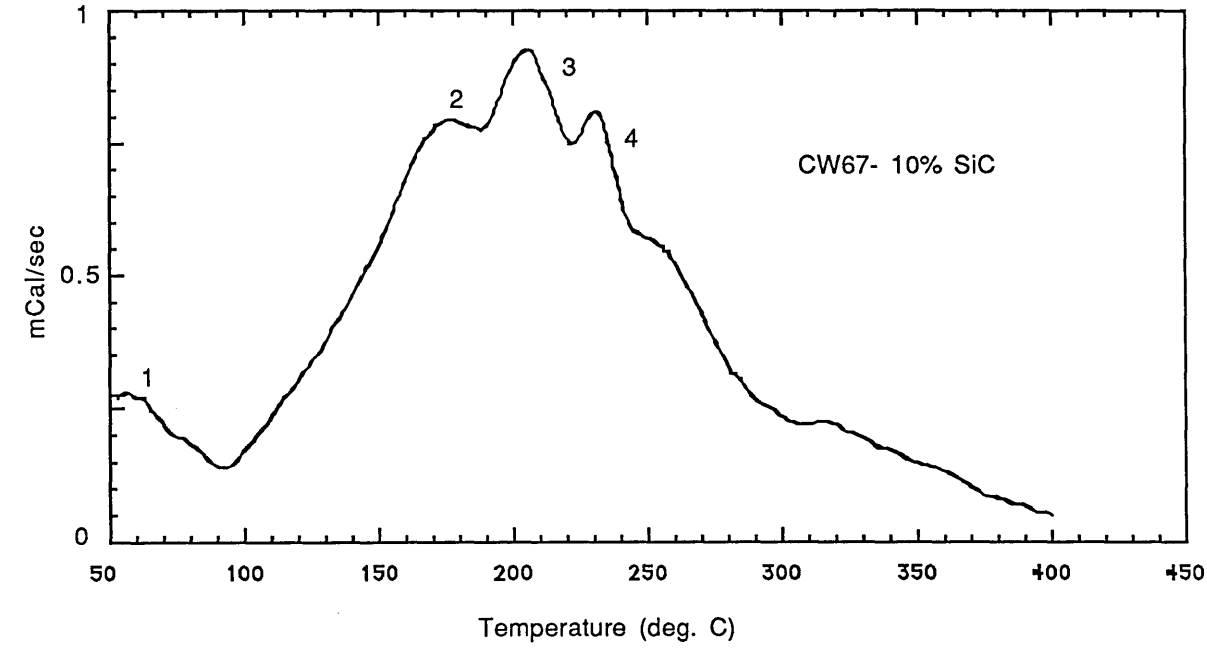

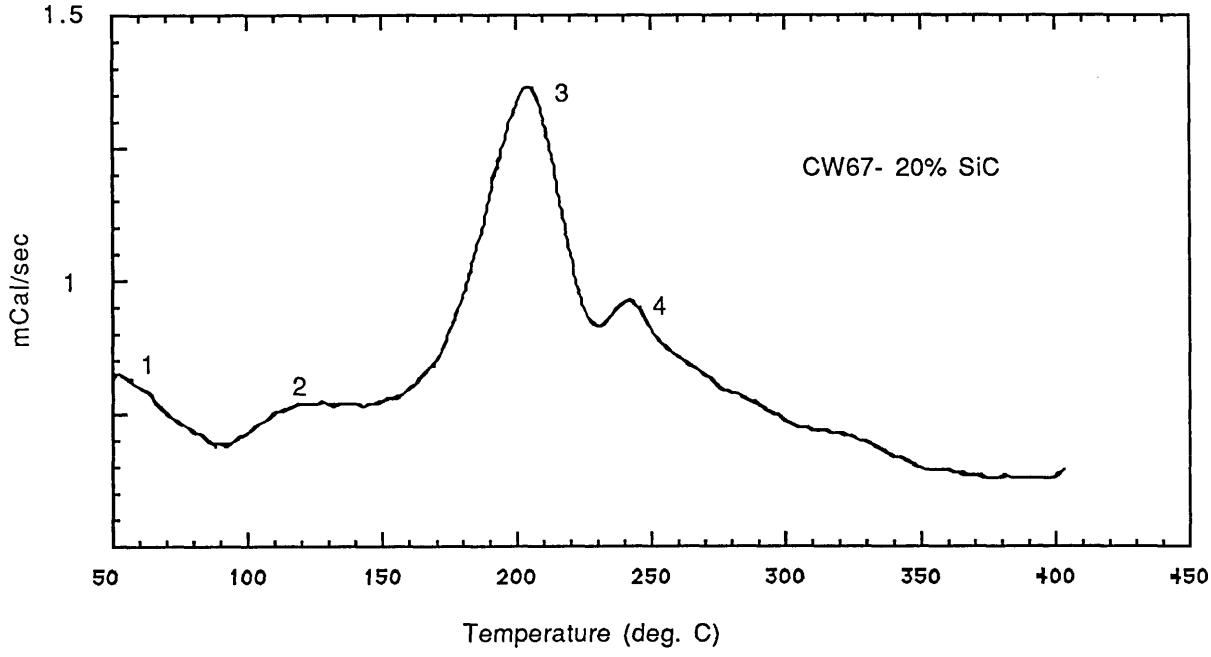

Figure 8.11: D.S.C. profiles of composites of CW67.

due to T phase ($Mg_3Zn_3Al_2$) formation. This is slightly suppressed in the 20% SiC composite.

D.S.C. analysis has revealed that the composites of CW67 behave differently to the unreinforced alloy when subjected to heating after solutionising. The difference is exacerbated as the reinforcement content increases. The total energy required, as calculated from the area under the curves, is seen to fall as the volume fraction of SiC increases. X-ray diffraction analysis of composite material was performed on material heat treated at a number of temperatures, given below, for three quarters of an hour. In order to analyse the x-ray diffraction patterns of the composites with any hope of success, it was necessary to establish the pattern for the silicon carbide. This having been accomplished, these peaks were discounted from the analysis which concentrated on the changes (if any) in the precipitation processes of the composite materials when compared with the unreinforced alloy and amongst themselves.

Composites containing 15% silicon carbide were examined by x-ray diffraction after having been solution treated and isochronally aged (for three quarters of an hour) at temperatures of 120°C, 135°C, 160°C, 180°C and 200°C. Composites containing 20% SiC were examined subsequent to isochronal ageing, for the same time, at 50°C, 160°C, 210°C and 240°C; these temperatures correspond to those employed in investigating the unreinforced material subsequent to D.S.C. analysis. Finally, CW67 containing 25% SiC was examined after isochronal ageing at 160°C and 200°C.

The first point of note was the appearance of peaks corresponding to the $MgZn_2$ {201} and {112} planes (the most intense) at 120°C in the 15% SiC composite. Comparison of these peaks with those present in the unreinforced material was, however, not possible, due to the extreme broadening of the two main aluminium peaks in the unreinforced alloy in this range obscuring any $MgZn_2$ peaks. The low angle peaks due to the metastable phase do not appear until 160°C, as in the unreinforced material. The interpretation of this data is unclear because of the lack of information available for comparison with the unreinforced material. This peak undergoes the same changes as those observed in the unreinforced material as temperature is increased. In the 20% and 25% composite, however, the growth of this series of peaks was much more advanced at 160°C, the shape of the curve equating to the observed curve for the unreinforced material which had been heat treated at 180°C. This may be an indication of the acceleration of ageing. The peak believed to be due to the phase $Al_9(Fe,Ni)_2$ is present in all of the diffraction patterns, as would be expected.

An interesting observation is that all of the aluminium peaks displayed by the composite materials were substantially narrower than those of the unreinforced alloy. Although the apparatus was set up primarily to analyse for the presence of various phases, the lattice parameter for aluminium was calculated for the composites. It should be noted that the error in the calculation of these values is of the order of ± 0.005Å because of the width of peak, and other factors mentioned in the experimental section. The values obtained are generally lower than the observed and theoretically calculated value for the un-treated powder (section 8.1.1) of 4.056Å. There was little significant variation in lattice parameter observed with increasing temperature. The values for lattice parameter calculated for the composites heat treated at 160°C are 4.042 Å, 4.045Å and 4.033Å for the 15%, 20% and 25% composites respectively.

Specimens of the 10% and 20% composites were aged under the same conditions as unreinforced material at the temperatures corresponding to the peak temperatures of the unreinforced material for consistency of method. The results are presented below in table 8.5, including the unreinforced material for comparison. The determination of the type of precipitate present was made by comparison with other work on similar alloys and the observed structures and diffraction patterns. Progression across the table diagonally from top left to bottom right shows an increasing propensity for overageing.

AGEING TEMP. (°C)	CW67-0% SiC	CW67-10% SIC	CW67-20% SiC
50	No visible precipitates	No visible precipitates	fine precipitates-η' ≤5nm. PFZ 30-50nm
160	fine precipitates, η' and η ≤10nm. PFZ ≈ 50nm	similar to 0% material PFZ ≈ 75-100nm.	coarse precipitates, 20 -40nm. PFZ ≈ 75-100nm.
210	larger precipitates, mainly η ,10-15nm. PFZ 75-100nm.	lath-like η ≈ 25-60nm long. PFZ ≈ 150nm.	lath-like η ≈ 50-75nm long. PFZ ≈ 150nm.
240	40-50nm precipitates PFZ ≈ 75-100nm	lath & polyhedral η (and T) 100-200nm. PFZ indeterminate	lath and polyhedral η (and T) 100-250nm. PFZ indeterminate

Table 8.5: Comparison of predominant precipitate morphology under heat treatment conditions corresponding to D.S.C. peaks.

(a) 20% SiC, 50°C

(b) 10% SiC, 160°C

(c) 20% SiC, 160°C

(d) 10% SiC, 210°C

(e) 10% SiC, 210°C

(f) 10% SiC, 240°C

(g) 20% SiC, 240°C

Figure 8.12: CW67 composites aged to D.S.C. peak temperatures, for 3/4 hr.(volume fraction and temperature as shown)

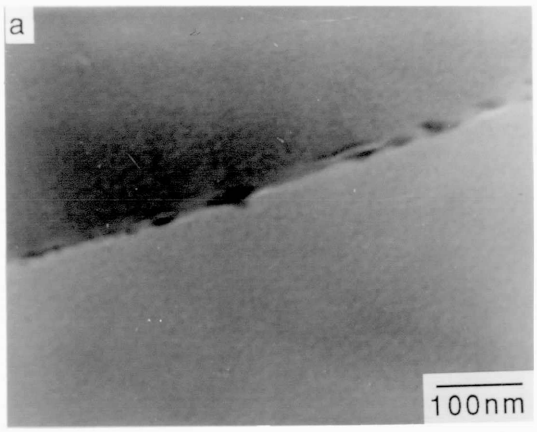
a
100nm

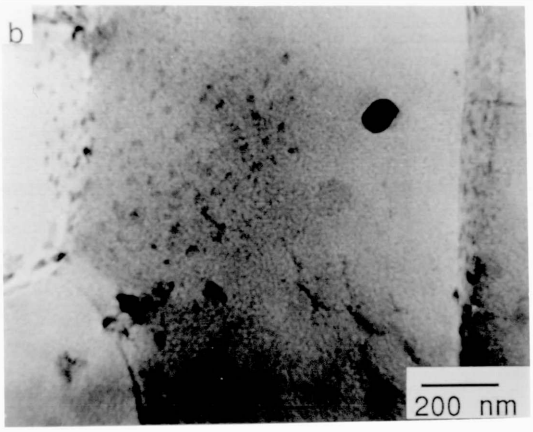
b
200 nm

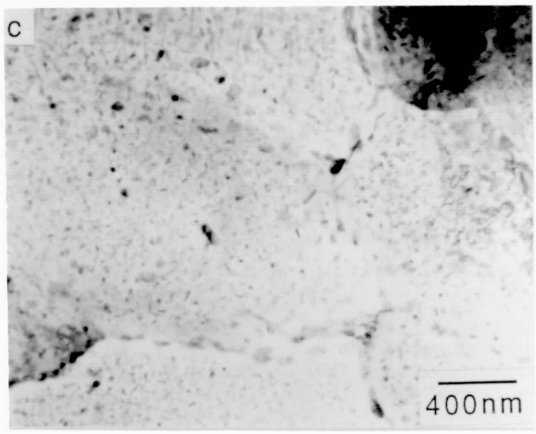
c
400nm

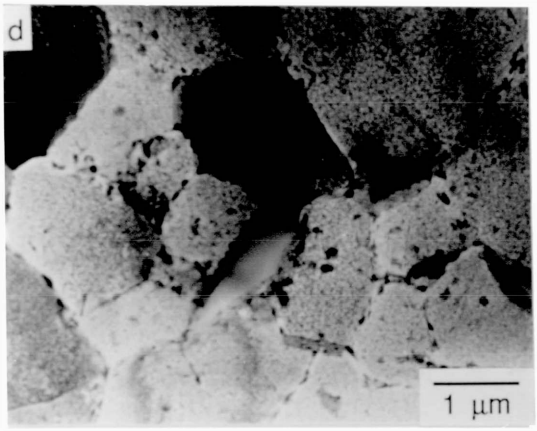
d
1 µm

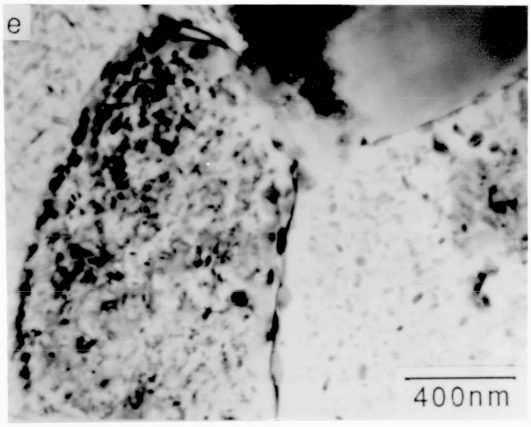
e
400nm

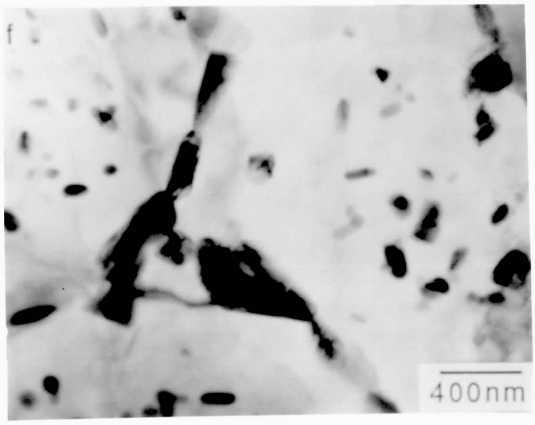
f
400nm

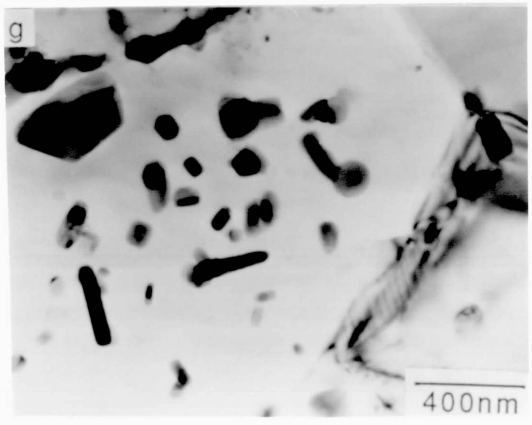
g
400nm

Ageing at 50°C resulted in little change in the 10% SiC composite whereas the 20% SiC material had developed a fine precipitate structure (figure 8.12 a). This is believed to be η': the proximity of the ageing temperature to the start of the D.S.C. peak for η' would suggest that η' commences precipitation at a lower temperature. The diffraction pattern showed a few spots in the η' positions in the <111> type zone shown in figure 8.6. The lower fraction reinforcement composite followed the same path as the unreinforced material.

The difference between the microstructure of the materials is most noticeable as the temperature of heat treatment increases. At 160°C, the precipitates observed in the 10% composite (figure 8.12b) are only slightly larger than those observed in the unreinforced material: approximately 10nm in diameter. At this stage, as figure 8.12c shows, the 20% SiC composites have developed a structure of rod like precipitates of about 20nm in diameter and 50-75nm long, which are probably nearly all η. The diffraction pattern confirmed this: there was a marked increase in spots at the η sites in the <111> type zone axis pattern, with few η' spots. Thus the ageing process is observed to accelerate with increasing volume fraction of SiC. This is in agreement with the observation of an increase in dislocation density due to punching from the particles[39] as volume fraction increases. The size of precipitate free zone was found to be the same, within the limits of measurement, for both volume fractions (see table 8.5). This is a further indication that the P.F.Z. formation in CW67 is due to vacancy depletion: if solute depletion were the cause, the size of P.F.Z. might be expected to increase with volume fraction as precipitation proceeds at the greater rate. The P.F.Z. size was, however, slightly larger than that found for the unreinforced material: an explanation for this is proposed in the next section, 8.2.4. The distribution and size of coarse dispersoids was the same as was found in the unreinforced material- approximately 50-200nm in size. Larger precipitates of the equilibrium phase were observed at the grain boundaries, as were seen in the unreinforced material; these were between 50-150nm in size.

As temperature is increased further both composite structures coarsen, as can be seen in figure 8.12 d and e, and f and g. There is a large increase in particle size between 210°C and 240°C which was also observed in the unreinforced material. Subsequent to ageing for three quarters of an hour at 210°C the precipitate morphology was more clearly defined as a mixture of rod and coarse lath features. Some circular plate precipitates were also observed. These different morphologies are common in 7xxx series alloys[85,88]. The size of the P.F.Z. was found to be approximately 150nm for both volume fraction composites. It is not clear whether the precipitates produced at 240°C are very coarse η phase or the T phase. It is probable

that the structure is a mixture of these two phases: the argument for this uncertainty is the same as was adduced for the unreinforced material in section 8.1.4. The size of the precipitates, as noted in table 8.5, was found to be between 100-200nm for the 10% composite and 100-250nm for the 20% material; the measured difference between the two composites was minimal because of the size and scarcity of the precipitates. Similarly, it was not possible to determine the size of precipitate free zone because of the large size of precipitate and consequent sparse distribution. The morphology of the precipitates varied in both cases from rod like to polyhedra and near circular platelets. These types have been observed by Ryum[89].

Figure 8.13 shows the effect of isochronal ageing on the hardness of composites; a curve for unreinforced material has been included for comparison. The important points to note are: (i) the greater decrease in hardness after the material has passed the peak as volume fraction of SiC increases and,

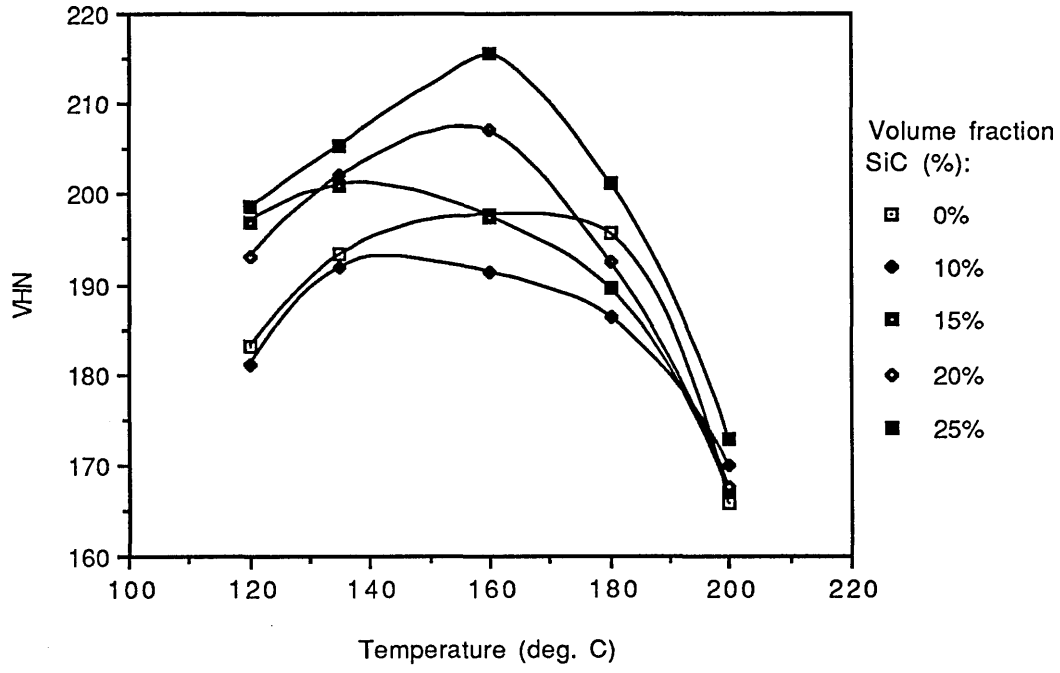

Figure 8.13: Isochronal hardness vs temperature for a range of volume fractions.

(ii) the position of the peak which is roughly centred around 160°C. The relative rates of hardness decrease indicate the acceleration of ageing kinetics as volume fraction is increased; the absolute values of hardness are meaningless within the context of this analysis. The position of the peak corresponds to the precipitation of η', observed in the D.S.C. experiment but it is unclear whether this is significant for any underlying reason.

8.2.4 Composites Aged at 120°C for 13.5 and 6 Hours.

Composite materials were aged at these treatments in order to compare structures (and, later, mechanical properties) in aged conditions with those of the unreinforced alloy. Figure 8.14 shows the different bright field images of 10% and 20% SiC aged under both of these conditions. In both cases precipitate free zones are observed to be wider than observed in the unreinforced material: approximately 100nm. This may be due to the influence of the silicon carbide on the vacancy concentration. The lower thermal conductivity of the SiC means that it will cool down slower and must influence the cooling rate of the composite as a whole. As the quench rate decreases the 'quenched in' vacancy concentration will drop, thus increasing P.F.Z. size. The influence of quench rate on P.F.Z. size is shown by Embury and Nicholson[116]. No difference between the two volume fractions was distinguishable. It might also be expected that the increase in dislocation density would lead to preferential precipitation, but this was not observed. Ageing time had no discernable influence on P.F.Z. width, as would be expected from a P.F.Z. formed by vacancy depletion.

The material aged for just 6 hours exhibited a structure which was comparable with the peak aged unreinforced alloy, with precipitates of approximately 10nm in size. Comparisons of the structures produced by ageing at this time (figures 8.14 a and c) showed that there was no detectable difference between the size of the precipitate particles in the two volume fraction composites. This structure was the closest to that of the peak aged unreinforced material, although the precipitate size is slightly greater in the composites.

After 13.5 hours the size of the precipitates within the grains is comparable with material aged at 160°C for three quarters of an hour, i.e. overaged. Precipitate size was approximately 10-20nm for the 10% SiC composite and 50nm for the 20% material (shown in figures 8.14 b and d respectively). Figure 8.14d also shows that a proportion of the precipitates have a lath or rod like morphology, a feature which was encountered in the high temperature D.S.C. specimens (eg. figure 8.12e). The four micrographs of figure 8.14 show further evidence for the accelerated ageing of composites with respect to unreinforced material.

(a) 10% SiC, aged 6 hours @ 120°C

(b) 10% SiC, aged 13.5 hrs @ 120°C

(c) 20% SiC, aged 6 hours @ 120°C

(d) 20% SiC, aged 13.5 hrs @ 120°C

Figure 8.14: Microstructure of aged composites, volume fraction, time and temperature as indicated.

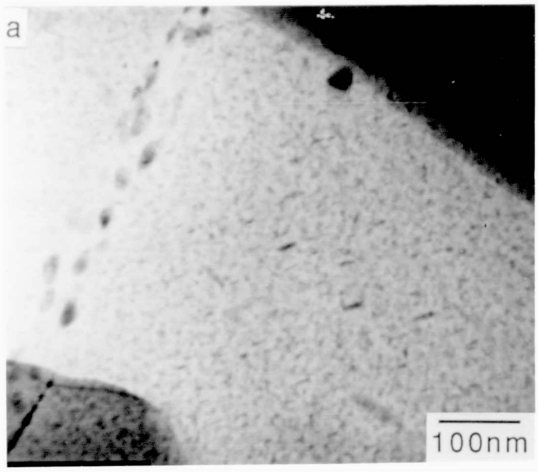
a
100nm

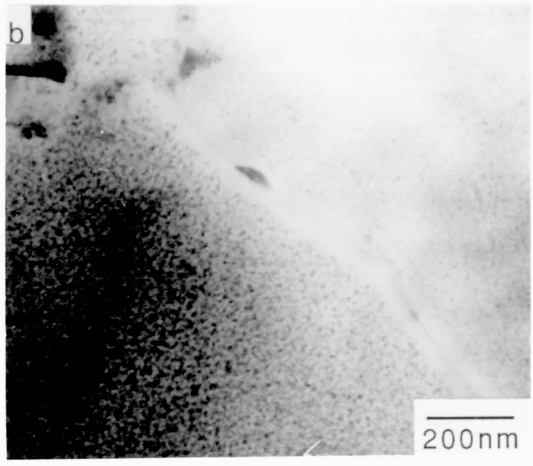
b
200nm

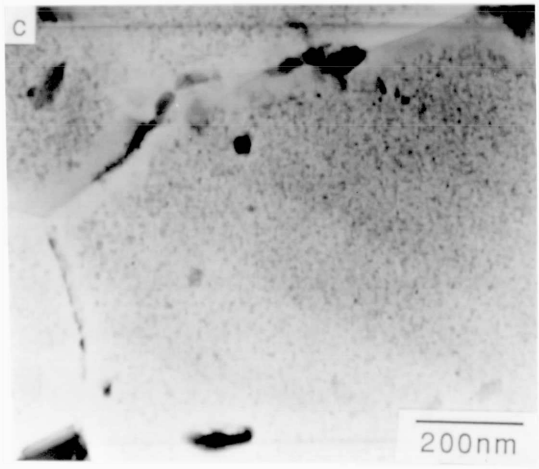
c
200nm

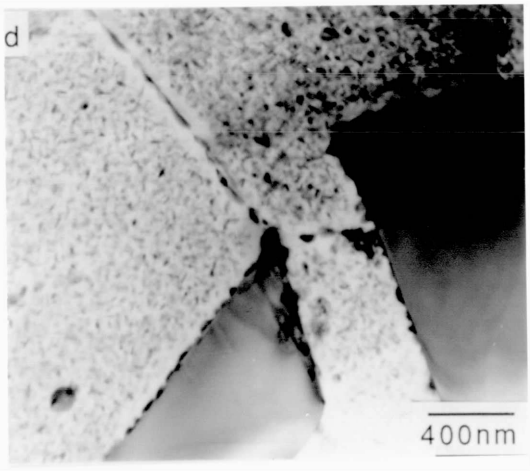
d
400nm

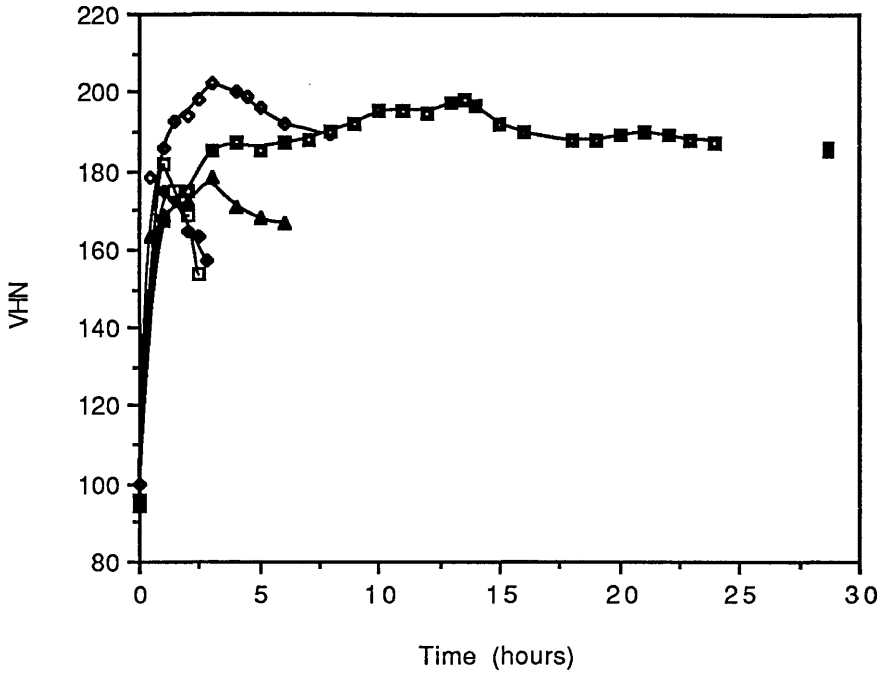

Full plot

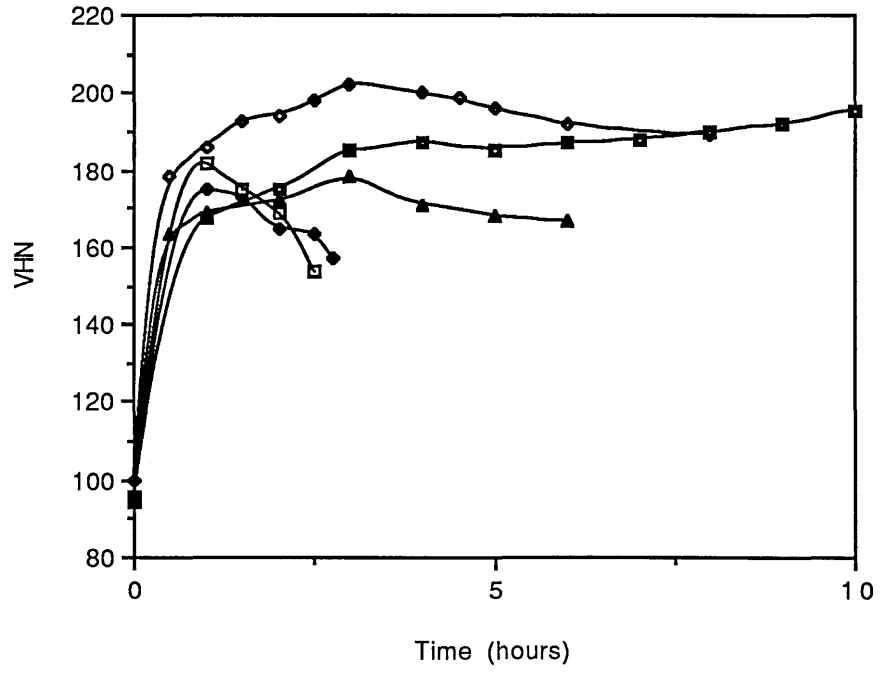

Expanded low time region.

Test temperature (deg. C)

- ◆ 200
- ▫ 180
- ▲ 135
- ◇ 120
- ■ 135

Figure 8.15: Isothermal plots of hardness vs time for unreinforced CW67

8.3 Determination of Optimum Ageing Conditions by Hardness Measurement

The determination of optimum ageing conditions by measurement of hardness over a range of times and temperature was conducted under isothermal conditions. Ageing was conducted at 120°C, 135°C, 160°C, 180°C and 200°C at times ranging from half an hour to 30 hours for isothermal ageing. Unreinforced material and composites were investigated in this way.

8.3.1 Unreinforced Material

The isothermal ageing curves for the unreinforced alloy are presented in figure 8.15. Although there should be no major difference in ageing characteristics due to extrusion temperature or ratio if the solutionising operation has been carried out to completion, tests were also conducted for the lower temperature extrudate: the results of this test are shown in figure 8.16.

The curves in figure 8.15 show an increase in hardness to a peak as time is increased. After the peak is achieved there is a drop in hardness, the rate of which increased as temperature increased. At 120°C the hardness remained within 5% of the peak value after 29 hours ageing, approximately 10 hours after the peak was reached. Ageing at higher temperatures resulted in a much faster decay in hardness: the hardness dropped by about 15% of the peak value, 5 hours after achieving its peak at 135°C and by a similar amount after only 2-3 hours at 180°C. Time to achieve peak hardness also decreased as temperature increased. The peak was reached after less than one hour at 200°C, whereas at 120°C the peak was not reached until 13.5 hours. This is consistent with expectations.

Whilst ageing at 135°C resulted in the highest hardness value of 202 VHN, after 3-4 hours, ageing at 120°C gave the most stable peak and thus was considered to be the optimum ageing temperature for the unreinforced material. Peak hardness was established as 198-199 VHN after 13.5 hours at this temperature.

The isothermal plots in which the effect of extrusion temperature on ageing characteristics was investigated are shown overleaf (figure 8.16). The investigation was conducted at 120°C, the temperature which had previously been decided as yielding the optimium ageing conditions. Although the two curves split in the central portion of the graph, it is possible that this is due to experimental error. In all other respects

the two plots are the same. Thus the influence of extrusion temperature was found to be minimal.

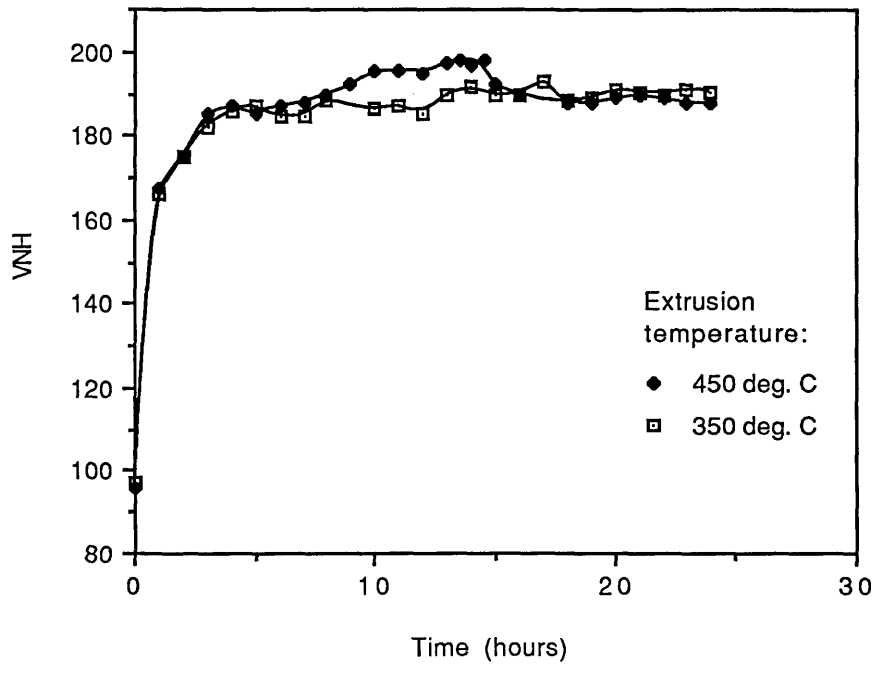

Figure 8.16: Isothermal ageing at120°C for different extrusion temperatures.

8.3.2 Composite Materials

Isothermal ageing curves for composite materials are shown in figures 8.17-8.20. Specimens of the composite containing 10% SiC were aged at 120°C, 160°C, 180°C and 200°C; 25% SiC composites were tested at 120°C, 180°C and 200°C and material containing 15% SiC was aged at 120°C. The graphs are grouped by temperature rather than volume fraction of SiC in order to compare the behaviour of the different compositions.

In both the ageing curves of the composites and those of their parent alloy the initial portion of the curve shows a steep rise in hardness from the as solutionised value to within 15% of the peak in as short a time as half an hour at the higher temperatures. However in the case of the composites the peak was achieved in a shorter time in all cases, although the decay after reaching the peak at the higher temperatures seems to be less pronounced than in the unreinforced material. This was probably due to the presence of the silicon carbide affecting the sensitivity of the test, as is explained below.

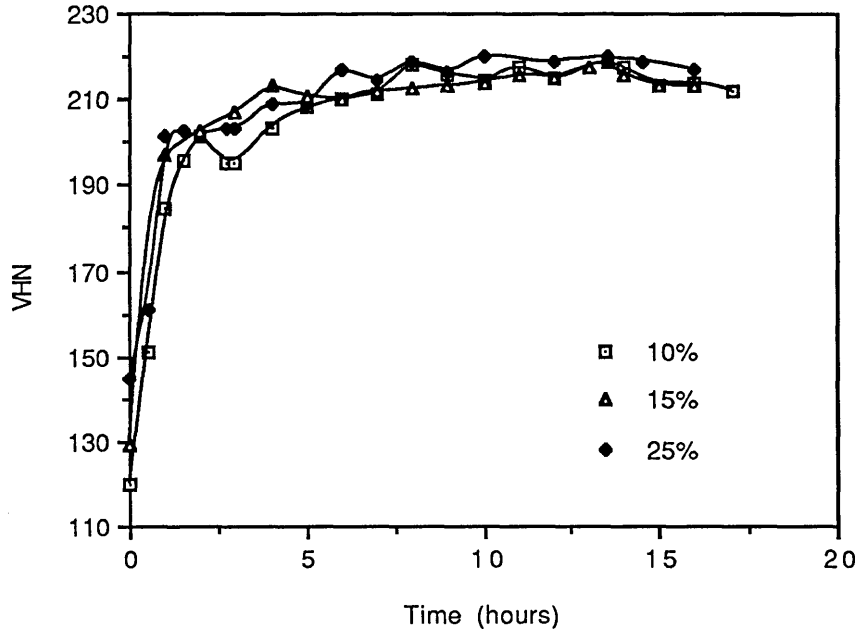

Figure 8.17: Hardness vs ageing time for composites of CW67 at 120°C

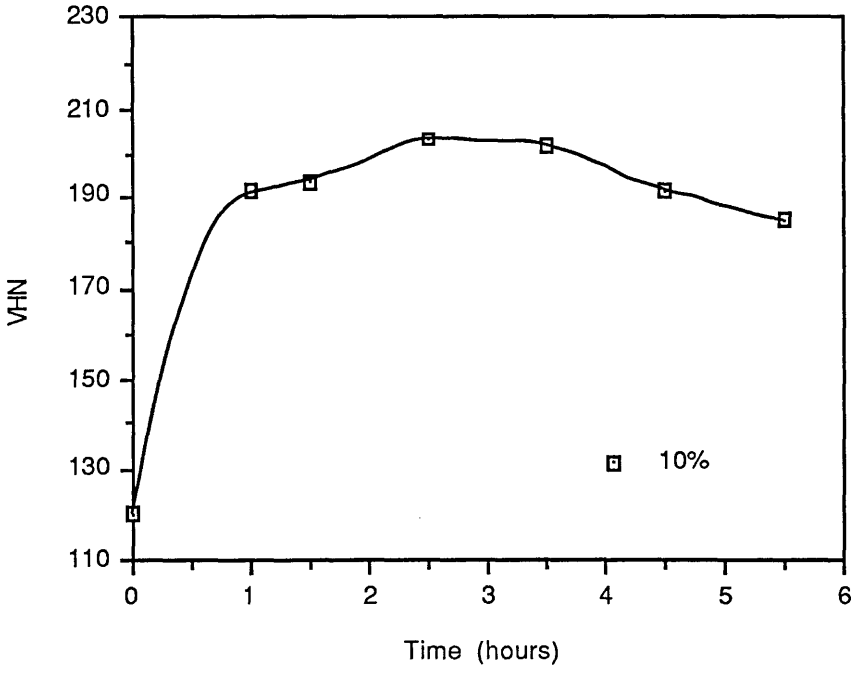

Figure 8.18: Hardness vs ageing time for CW67/10% SiC at 160°C

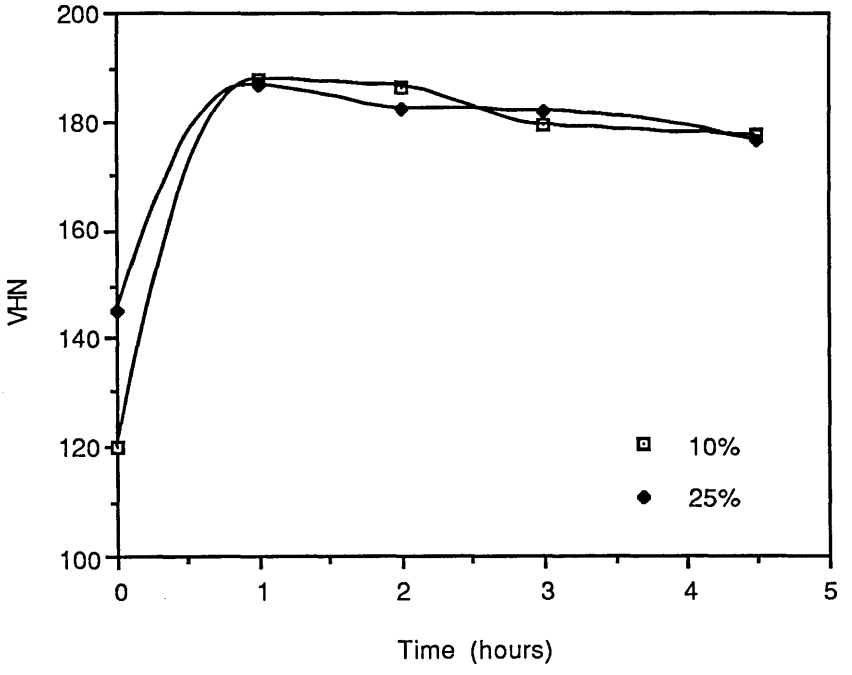

Figure 8.19: Hardness vs ageing time for composites of CW67 at 180°C

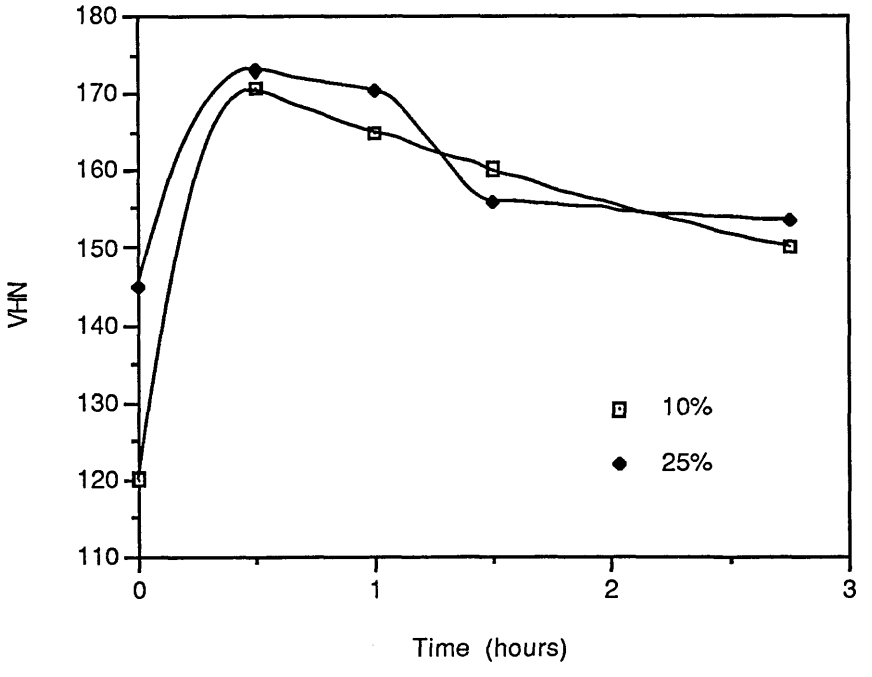

Figure 8.20: Hardness vs ageing time for composites of CW67 at 200°C

Time to reach peak hardness was found to be independent of reinforcement volume fraction, although the absolute values of hardness reflected the respective reinforcement contents of the composites. The time to achieve peak hardness was difficult to identify at low temperature. This was because of the clouding influence of the SiC particles, making the test less sensitive to small matrix microstructural changes. Thus, although 120°C was chosen as the ageing temperature the optimum time was indeterminate. Times of 13.5 hours and 6 hours were chosen, the former being selected so that a comparison could be made with matrix material at its optimum time, the latter, because of a combination of T.E.M. observations and the hardness measurement.

The ageing of composites of CW67 was seen to be accelerated when compared with the unreinforced alloy. A combination of D.S.C., microscopy and hardness testing has shown this. The acceleration of ageing is much more evident in CW67 composites than in composites of 2014. This is probably due to the propensity of η phase to coarsen in the composite system within the time range of these experiments (compare figures 8.14 a and b and 8.14 c and d), whereas it is known that θ' in 2014 takes a very long time to coarsen[106], although the coarsening with time was not investigated for the composites.

It was evident from this work that the choice of ageing conditions should not rest on a single test, such as hardness testing, in which the response of the material is rendered insensitive by the reinforcing particle.

8.4 Summary of Results of Characterisation of CW67 and its Composites

The CW67 powder in the as received state was found to have a dendrite spacing of between 0.5-3μm. The aluminium lattice parameter was found to be approximately 4.054Å, close to the theoretical value of 4.056Å calculated for this alloy. There were a number of phases which could not be positively identified by x-ray diffraction, but were close to peaks for Al-Mg-Zn and Al-Zn phase peaks. Solution heat treating led to the formation of a phase which is thought to be of the type $Al_9(Fe,Ni)_2$, observed by Hildeman et al[110] and thought to correspond to dispersoids observed under T.E.M. (as shown in figure 8.2). This phase was also observed in the composite material at all volume fractions. No conclusive proof of the presence of Al_3Zr was found, either in x-ray diffraction or x-ray spectroscopy of thin foils, although some diffraction peaks were found which fit part of the series for Al_3Zr (section 8.1.2). This coherent phase is important as it would inhibit grain growth and was expected to be present due to the alloy composition. Some difference was observed in as extruded sub-grain size of

composites when compared to the unreinforced material and between volume fractions. The sub-grain size of the unreinforced material was in the range 3-4μm for extrusion conditions of 425°C and a ratio of 24:1, whilst the subgrain size of composites under the same extrusion conditions was found to be in the range 1.5-2μm. Composite material had a higher dislocation density in the as extruded and heat treated states than unreinforced material; dislocations were clustered around the silicon carbide particles. Oxide particles were found to occur in bands in the extrusion direction in the base alloy and the composites. Some banding of the silicon carbide was also evident.

The composites of CW67 were found to respond to heat treatment in a manner which varied between volume fraction of reinforcement; this was, in turn, distinctly different to the response of the unreinforced alloy. All material was found to follow the generally held precipitation sequence, *viz*:

$$\text{S.S.S.S.} \rightarrow \text{G.P. zones} \rightarrow \eta' \rightarrow \eta\ (MgZn_2)$$

This was confirmed by D.S.C. analysis. The temperatures at which the precipitation occurred in the unreinforced material were found to be as follows:
(i) G.P. zones- 50-60°C
(ii) η'- 140-200°C
(iii) η- 190-245°C

A fourth peak was observed at 240-260°C; this was thought to be due to the T phase ($Mg_3Zn_3Al_2$), as this alloy has a Zn:Mg ratio which is on the borderline for its favoured nucleation. There is evidence to suggest that T phase is the stable precipitate in such alloys aged above 200°C, and that η is the equilibrium phase if ageing is conducted below 200°C[85].

Whilst the composites were found to follow the same sequence, the temperatures at which the changes occurred were different. The contrast between composite and unreinforced alloy was greater at a higher volume fraction of reinforcement. The precipitation reactions of the 20% SiC composite were found to take place at the following temperatures:
(i) G.P. zones- 50-60°C
(ii) η'- 120-150°C
(iii) η- 190-220°C

The major difference is the peak corresponding to the formation of the metastable precipitate, but the peaks are also smaller which implies that less energy has been

required in order to effect the change. The fourth peak, thought to be due to T phase, was observed at a similar temperature to the unreinforced material.

Transmission electron microscopic examination of material heat treated to the conditions corresponding to the peaks of the unreinforced material showed that precipitate size (and thus "degree of ageing") varied greatly between samples of unreinforced alloy and composites. At 160°C the precipitates were of the order of 5-10nm in size in the 0% and 10% material, and were predominantly η'. The 20% composite contained precipitates of significantly different morphology (rod-like) which were 20nm by 50nm in size and probably nearly all η. At the higher temperatures of 210°C and 240°C the unreinforced alloy maintained a fairly low precipitate size: 15nm, rising to 40nm at the higher temperature The composites contained precipitates which were in excess of 100nm in size at the higher temperature. These different precipitate sizes are shown in figures 8.5 and 8.12.

Peak ageing conditions were established (by hardness testing) as 13.5 hours at 120°C for the unreinforced alloy and approximately 6 hours at the same temperature for the composites. Both ageing treatments were preceded by a solutionising treatment of 1.5 hours at 475°C. Composites were also aged for 13.5 hours at 120°C in order to compare the precipitate structure with the unreinforced alloy.The determination of peak ageing conditions by hardness testing was found to be fairly insensitive for composite materials; this is thought to be due to the silicon carbide masking matrix structural changes. Ageing conditions unique to a specific volume fraction were not determined, although the D.S.C. and T.E.M. suggests that this may be desirable. This was simply a matter of the chronology of the experiments. The temperature at which unreinforced alloy was extruded was found to have no effect on the ageing characteristics of the alloy at 120°C.

There were a number of features in the aged material that varied from composite to composite and between composite and base alloy. Examination of the unreinforced material aged for 13.5 hours revealed precipitate sizes which were less than 10nm (accurate sizing below 10nm was difficult); these were found to be a combination of η' and η. Similarly aged composites contained precipitates which were much larger: 10-20nm in the 10% SiC composite and approximately 50nm in the 20% SiC composite. These were found to be predominantly η phase. The width of the characteristic precipitate free zone also differed: approximately 50nm in the unreinforced material and 100nm and above in the composites. This was thought to be due to the influence of silicon carbide on the local quench rate in the material, although the extent of this influence was not able to be determined. Both of these P.F.Z.s are,

however, smaller than are usually encountered in cast 7xxx series alloys. Composites aged for 6 hours exhibited precipitate sizes closer to 10nm for both volume fractions. The ageing time did not affect the precipitate free zone width; this is an indication of a precipitate free zone which forms due to vacancy depletion.

Having established the structural and ageing characteristics of the alloy and its composites the results of mechanical testing may be interpreted.

8.5 Mechanical Properties of Unreinforced CW67

Examination of the properties will be split into two sections: tensile properties and fracture toughness. Fractographs obtained from specimens will be discussed and compared last.

8.5.1 Tensile Properties

The tensile properties were measured in the as extruded condition, T4 and T6 conditions. The T6 (peak heat treatment) condition was established by hardness testing as being 13.5 hours at 120°C, a temperature employed by a number of workers[109,110] with this type of alloy, but a much shorter time than the generally held 24 hours for 7xxx series alloys. These properties are shown in figures 8.21-8.23.

There are a number of prominent points emergent from these data. The material with the highest U.T.S. was found in the as extruded condition. Those with the highest values were extruded at the lower temperature. This can only have been due to solid solution and substructural strengthening developed during working, as the extrudate was quenched directly on exit form the die. The 0.2% proof stress of as extruded material was, however, lower than that of the alloy in the T6 condition. This can be related to the difference in work hardening exponent between the heat treated and F temper states (figure 8.22). The highest U.T.S. and 0.2% proof stress observed in the heat treated state (T6) were obtained for the extrudate processed at 350°C, values for which were 649 ± 10 MPa and 572 ± 5 MPa respectively. The difference in strength between alloy extruded at different temperatures implies that there was some retained substructural strengthening. This trend was also observed in the 0.2% proof stress of the material in the T4 condition. There was little difference between the strength of extrudate produced at the two different extrusion ratios. This may be expected of a peak heat treated material because, if solutionising is performed correctly all of the solute

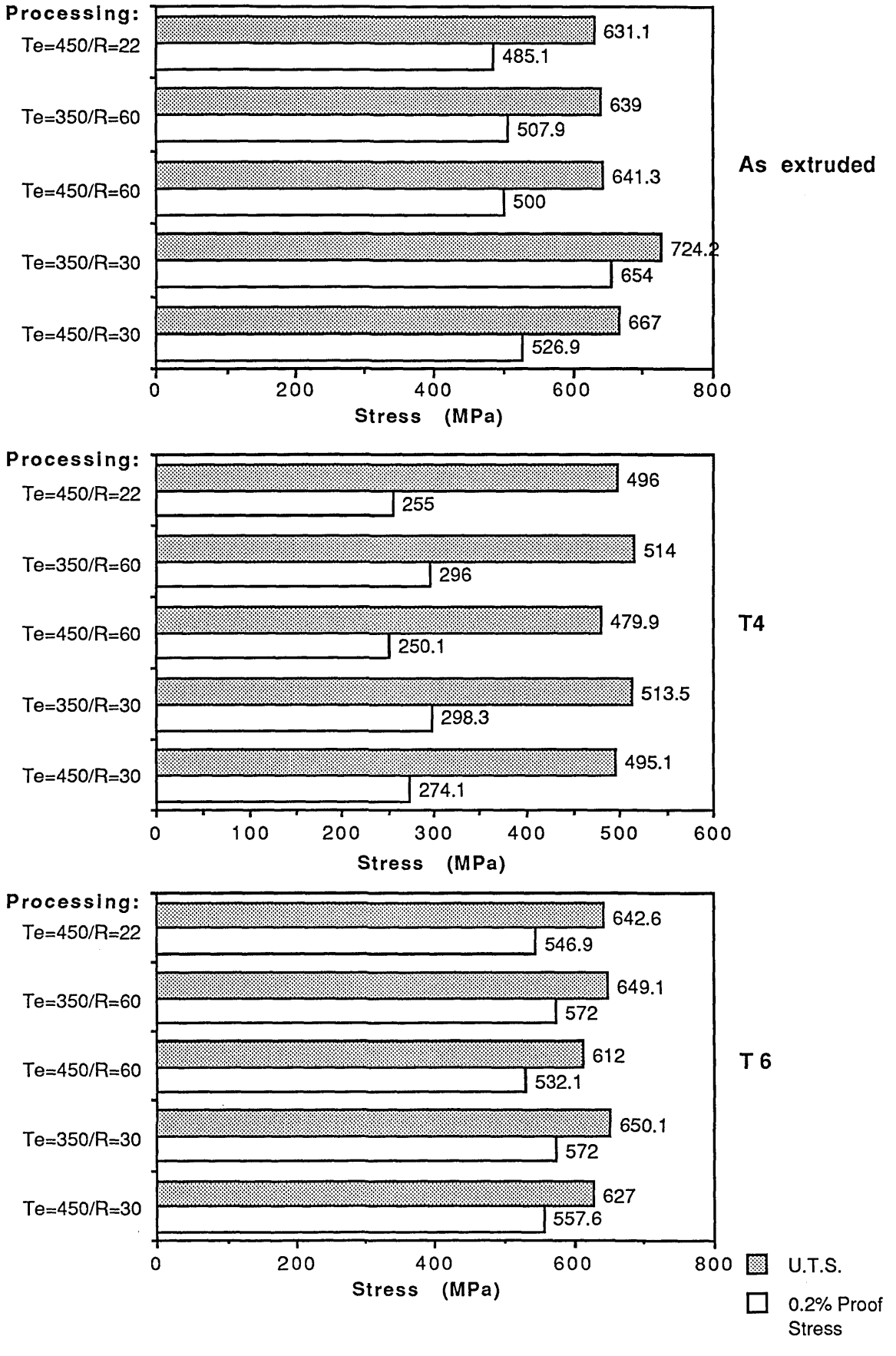

Figure 8.21: Variation in tensile properties with extrusion and heat treatment parameters

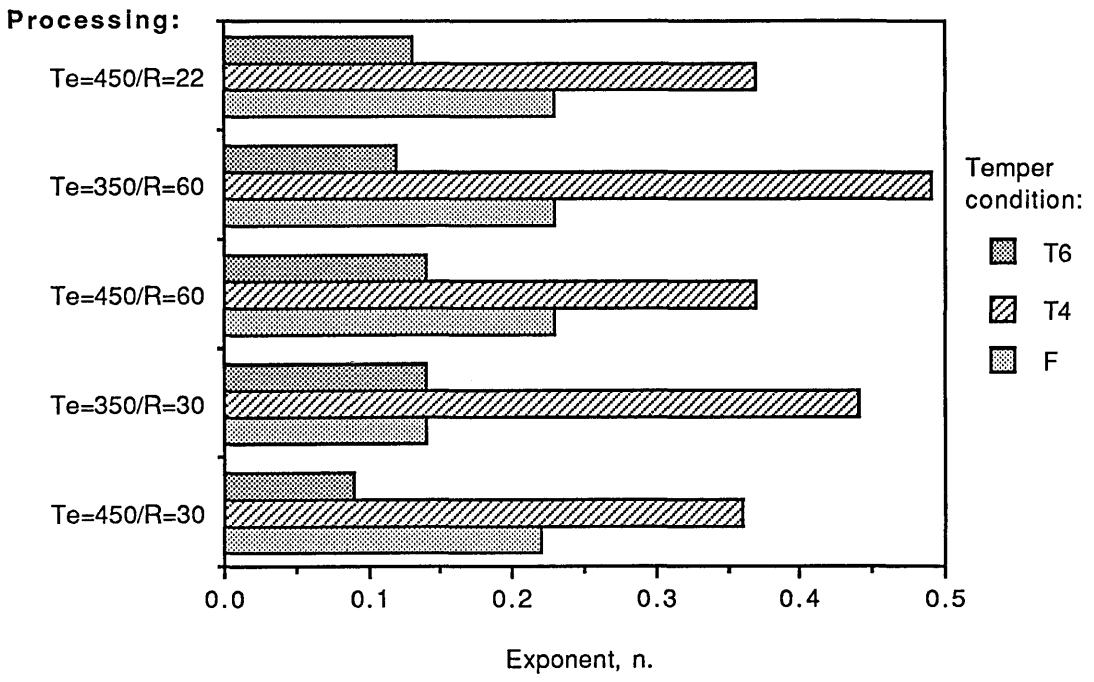

Figure 8.22: Variation in work hardening exponent, n, with extrusion conditions and heat treatment

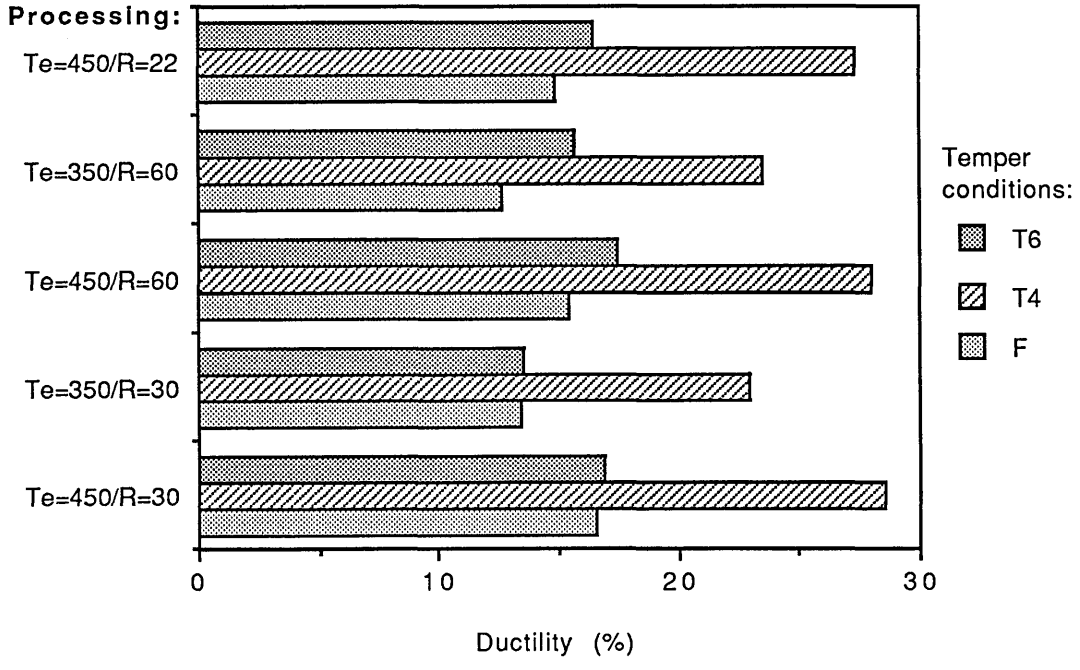

Figure 8.23: Variation in % elongation with extrusion conditions and heat treatment.

will go into solution and be retained upon quenching to be given up on ageing at an elevated temperature. The 0.2% proof stress increased from 250-300 MPa in the T4 condition to between 570-590 MPa in the T6 condition.

The ductilities shown in figure 8.23, as measured by extension of the specimen, seem rather high when compared with those quoted by other workers for CW67[110] and 7xxx series alloys in general[84]. This can only be attributed to inaccuracy in the experimental method: an extensometer with a small enough gauge length was not available. Values were determined to be approximately 1-2% of extension higher than those found by Hildeman et al[110] in the T6 condition- between 14 and 17% (depending on the extrusion conditions) compared with 12%. The variation in work hardening exponent with heat treatment condition is consistent with expectations. There is no systematic variation in this exponent in the 'F' and 'T6' tempers, but in the 'T4' condition the material extruded at 350°C has a higher work hardening exponent and in this condition the evidence suggests that the higher ratio results in a higher exponent. These values reflect the greater amount of work put into the extrudate with higher exponent resulting in lower sub-grain size. The substructure and precipitates in 'F' and 'T6' tempers, respectively, will reduce any work hardenability compared with the T4 condition.

Modulus measurements were made in the T6 condition only, on material extruded at the same ratio but at the two different temperatures. The modulus of the alloy was determined to be 73.15 GPa $\pm$ 0.5 GPa. There were no significant variations in the result between the two temperatures.

8.5.2 Fracture Toughness

The fracture toughness results obtained by the two methods employed in this thesis will first be considered separately and then in parallel. The purpose of this is two-fold. A comparison of the short rod and chevron bar methods applied to unreinforced material would seem expedient in order to assess the amount of any difference due to orientation. Secondly, the measurement of fracture toughness of the unreinforced material using the chevron bar method gives a base line against which the composites can be compared. Hildeman et al[110] have also reported fracture toughness of canned and degassed R.S.P. CW67 in the three salient orientations, which should aid the comparison. In all cases, 'non-standard' ageing conditions were chosen as being 80% of peak hardness. Thus the underaged conditions were 1 hour at 120°C, whilst overageing was reached by ageing to T6 (13.5 hours at 120°C) followed by treatment at 160°C for 1.5 hours.

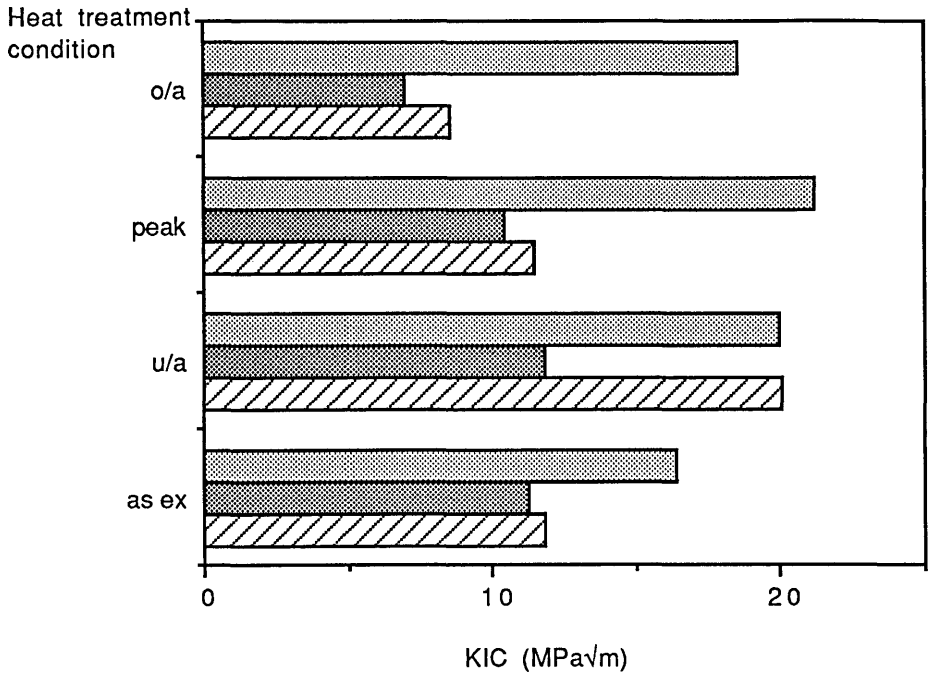

(a)

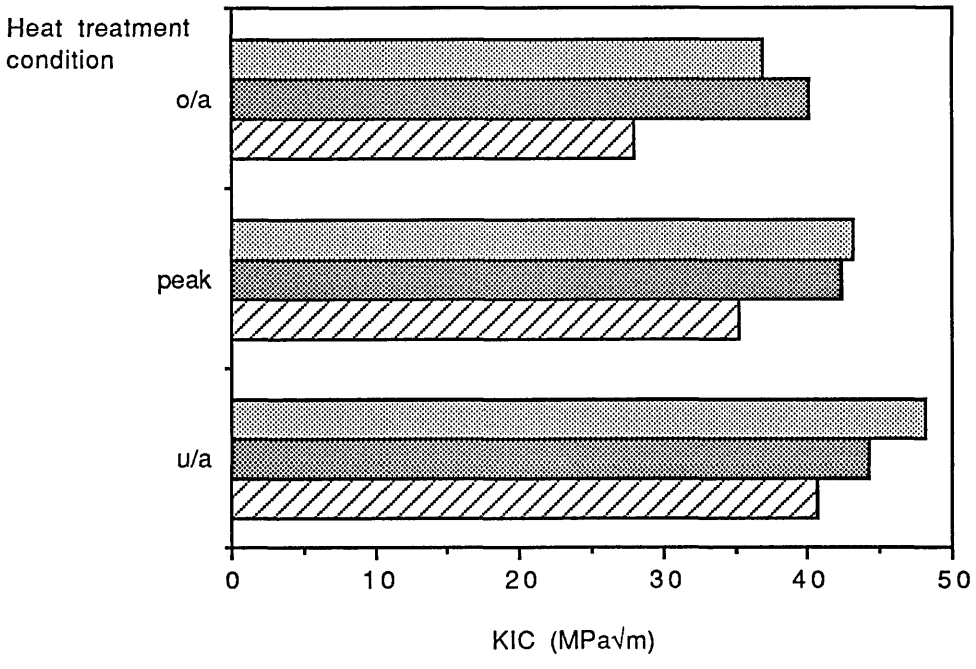

(b)

Extrusion condition.

Degassed, Te=450, R=22

Te= 350, R=30

Te=450, R=30

Figure 8.24: Fracture toughness measurements using (a) short rod and (b) chevron bar methods.

The short rod fracture toughness values (figure 8.24a) are uniformly low, as is common in powder alloys. This is exacerbated by the crack propagation direction which is parallel to the extrusion direction. The trend in the non-canned material shows a decrease in fracture toughness as ageing proceeds. This is consistent with work on 7050 alloy (5.28% Zn, 2.71% Mg, 1.62% Cu, 0.21% Fe, 0.08% Si, 0.19% Cr, 0.032% Ti, 0.04% Mn) at an ageing temperature of 120°C[117]. However, it should be noted that other results obtained by the same author[117] at higher ageing temperatures (150°C and 177°C) show an initial fall in toughness, followed by a slight increase in toughness as ageing time progressed. The difference between toughness values at the same yield stress (and hardness value) for different ageing conditions is ascribed to the coarsening of matrix and grain boundary precipitates at the longer times[117]. The canned, degassed and hot compacted CW67 maintained a high value of short rod fracture toughness in all ageing conditions, which in the peak and overaged conditions is almost double that of specimens from the other two extrusion conditions at 20-21 MPa$\sqrt{m}$. The contrast with the trend observed for the non canned material shows that there is a clear advantage in degassing and hot compacting powder CW67 prior to extrusion.

The chevron bar specimens exhibit fracture toughness values higher than short rod results for all materials in all extrusion conditions. The difference between the values obtained using this testing geometry and the more usual short rod geometry may be ascribed to the difference in orientation of the crack with respect to the extrusion direction. Short rod geometry means that the crack will travel along the weakest direction of the extrudate. Conversely, chevron bar specimens have the notch cut so that the crack will travel across the extrusion direction. There is one anomalous result in the chevron bar testing group: the material extruded at 350°C with a ratio of 30:1 had an unusually high toughness; this was found to be due to a large amount of gas in the specimen which was contained in pores elongated in the extrusion direction, thus providing an effective barrier in the path of crack growth (see schematic figure 8.25). The actual fracture surface is shown in figure 8.26f and described in sub-section 8.5.3. This gas is believed to have become entrapped during the extrusion process at the lower temperature and ratio, expanding on heating to the solutionising temperature. The load/ displacement curve was also modified when testing these specimens: immediately after crack initiation the curve became serrated and remained at a high value for a longer time than other specimens whose load dropped off smoothly after crack initiation. The manifestation of this phenomenon was not observed in the tensile or short rod fracture toughness and it is possible that it may be related to the position along the extrudate from which the specimens were taken (as described in chapter 4) and the orientation of the notch. Toughness specimens were taken from front and back of the central portion of the extrudate and it seems likely that these

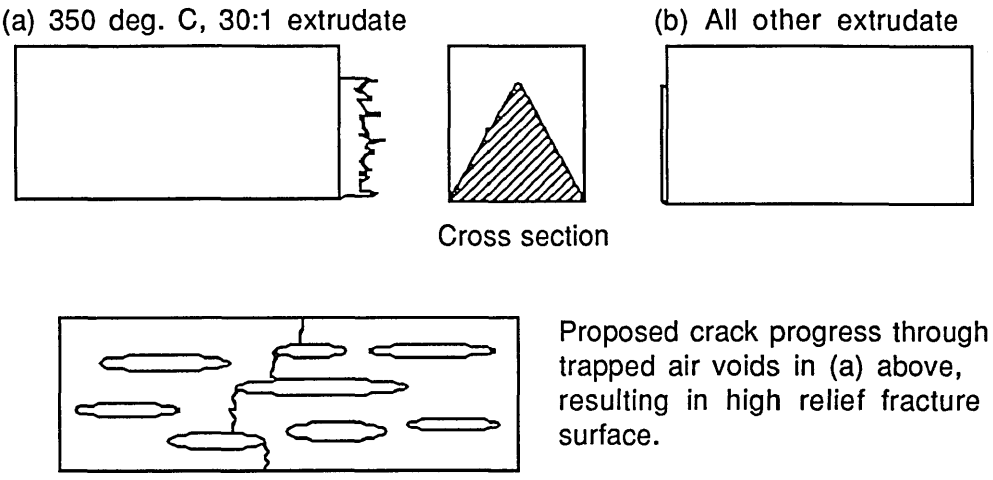

Figure 8.25: Schematic diagram of failure in low temperature, low ratio extrudate.

particular chevron bar specimens were cut from the front end, where more entrapped gas is likely to reside[99]. The phenomenon would also be more evident in this situation because of the geometry of the specimen. Gas entrapment was not a problem in the higher temperature or ratio extrudate simply because the conditions employed would allow more gas to escape. Again, this indicates that degassing would result in more predictable material properties. Gas entrapment has been more fully discussed in chapters 5 and 7.

The values found here are in good agreement with work by Hildeman et al[110] who found values of 26 MPa$\sqrt{m}$ in the short transverse direction and 47 MPa$\sqrt{m}$ in the longitudinal direction for material extruded and heat treated to the T7 temper (slightly overaged for damage tolerance). These directions correspond respectively to the short rod and chevron bar testing geometries. Results from this experimentation were approximately 21 MPa$\sqrt{m}$ for the short rod test and 44 MPa$\sqrt{m}$ for the chevron bar test in the T6 condition.

There are a number of points relating to the chevron bar test which bring into question its validity and should therefore be addressed. This test is not a 'recognised' test, as the short rod test is. The theory for the test is, however, derived from the same source[92,93] (see section 4.7.2). The machining of the notch is by electrical discharge machining (E.D.M. or 'spark erosion'); this will inevitably heat up the surface layer of the notch root and may lead to microstructural changes. This treatment was observed to affect the progress of failure, but not the peak load, in the original work on the development of the chevron notched bar test performed by Shang-Xian[93]: the observation and explanation are described below.

Shang-Xian[93] describes the phenomenon, 'pop-in', in work on bearing steels. This was characterised by a noise on cracking and an initial linear portion on the load/displacement curve due to a higher load being required to initiate a crack in the tougher surface layer. This effect was thought to have no effect on the maximum load because, after the surface layer has been breached, the crack will continue to grow stably until the maximum load is achieved. It is not known how this assumption would extend to aluminium alloys, however, the microstructural changes on machining can be postulated. The layer at the immediate surface could have melted and resolidified, destroying the extrudate sub-structure. If the specimen is in the aged condition, the heating may cause either precipitate growth or, possibly, dissolution depending on the heat treatment condition and alloy type. It was therefore decided, because of the potential for microstructural variations, to heat treat the specimens after machining. Care was taken to ensure that there was limited exposure to the atmosphere at high temperature by wrapping the specimens tightly in aluminium foil.

8.5.3: Fractography of Unreinforced CW67.

Fractographs of tensile specimens in the T4 and T6 heat treatment conditions are shown in figures 8.26a and 8.26b, respectively. Failure was primarily by void coalescence, although other features were noticeable. Figure 8.26a shows some decohesion, in the top left quadrant, which was possibly due to failure along a prior powder particle boundary. Regions of flatter fracture, which is probably due to tearing , may also be seen in this micrograph. Examination of other fracture surfaces revealed regions which appeared almost 'laminated'. This is thought to be due to the presence of discontinuous crack growth prior to failure but was not a common feature. The main difference between failure surfaces of material treated under different conditions was the size of dimple: in the T4 condition the dimple size was uniformly larger than in either the F or T6 condition: 2-5μm (fig. 8.26a) compared with 1μm and less (fig.s 8.26b). The nature of the dimples was similar in each instance, regardless of the size: in plan the dimples resembled a flower with features radiating from a central depression whilst the side elevation was cuspate. These features, characteristic of a ductile alloy, can be seen in figures 8.26a and b. The void will have nucleated at the particle which was in residence at the top of the cusp- the centre of the flower. This was probably an oxide particle. It would be expected that a material which contained precipitate free zones in the T6 condition would exhibit intergranular fracture in this condition due to the lower strength of the P.F.Z. region. This was not discernable in this investigation. The bright particles at the centre of the dimples in figure 8.26b are charged particles of detritus.

(a) Tensile: extruded at 425°C,30:1 T4 condition

(b) Tensile; extruded at 425°C, 30:1,T6 condition.

(c) Short rod fracture toughness specimen: extruded at 425°C, 30:1, T6 condition.

(d) Bar toughness specimen: extruded at 425°C, 30:1, underaged

(e) Bar toughness specimen: extruded at 425°C, 30:1, T6 condition.

(f) Bar toughness specimen: extruded at 325°C,30:1, as extruded.

Figure 8.26: Fractographs of unreinforced CW67 tensile and toughness specimens, tesing mode and ageing as shown

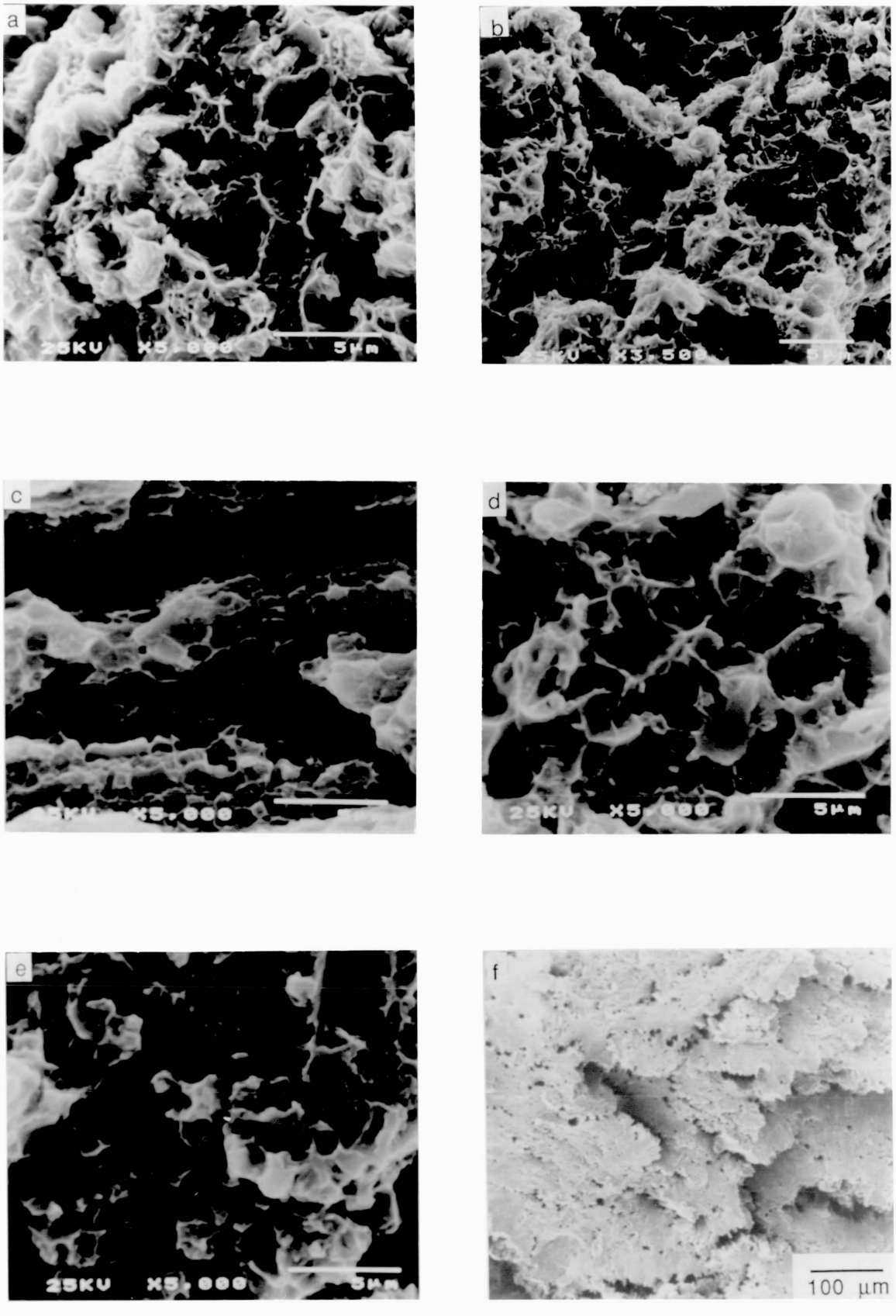
a
25KU X5,000 5μm
b
c
d
25KU X5,000 5μm
e
25KU X5,000 5μm
f
100 μm

The fracture surfaces of short rod and chevron bar specimens are also compared in figure 8.26. The photomicrographs clearly show the difference in crack morphology, the short rod specimen (figure 8.26c) having failed parallel to the elongated microstructure whereas chevron bar specimen failure is less easily related to sub-grain structure (figure 8.26d and e). Both structures are underpinned by matrix dimpling, indicative of failure by void coalescence. Figures 8.26c and e are fractographs of material in the T6 condition and as such have a low size of matrix dimple, of the order of 1-2μm and less. The appearance of this underlying dimple structure differed very little from that of the tensile specimens. The short rod specimen has some indication of discontinuous crack growth prior to failure; this was not observed in the bar specimens. The chevron bar specimen in the underaged condition exhibited a slightly larger dimple size, at between 2-4μm. The difference between the underaged and peak aged dimple sizes may be accounted for by the fact that the nucleation stress for void formation at oxide particles would be attainable in underaged material aged to within 80% of the hardness of the peak aged material. The stress value required for nucleation at oxide particles calculated from equation 7.3 is 540.9 MPa- 80% of the highest T6 0.2% proof stress is approximately 460 MPa. This calculation is only used as a guide as it does not account for stress concentration but the general trend is shown.

Figure 8.26f shows the fracture surface of extrudate processed at 350°C and a ratio of 30:1. The features protruding from the surface extended up to a distance of 3mm; this is shown schematically in figure 8.25. These large protrusions are thought to have occurred during the solutionising or ageing stage of the heat treatment, when trapped gas has expanded. As was noted earlier, it is believed that the combination of low temperature and low extrusion ratio allowed air to become entrapped during extrusion. The generally porous look of the fracture surface is thought to be due to smaller pores of entrapped gas.

8.6 Mechanical Properties of Composite Material

Composites of CW67 were tested under similar conditions to the unreinforced alloy. Only one extrusion temperature was employed in the production process but two ratios were used: 24:1 producing square bar of side length 13.5mm, and 34:1 producing rectangular bar 32.5 x 4mm for rolling trials. Extruded material will be considered first, initially as a discrete group and then in comparison with the unreinforced alloy. As in previous chapters, an assessment of various models of composite strengthening will be made.

8.6.1 Tensile Properties

Tensile properties of extruded CW67 composites were measured in the F, T4 and T6 tempers. Rolled material was assessed in F temper, T4 temper and various degrees of heat treatment. The tensile testing of rolled material was undertaken merely as a comparative exercise; no structural work was conducted on this material.

8.6.1.1 Extruded Composites of CW67

The tensile properties of extruded composites are shown in figures 8.27 to 8.30. Figure 8.27 shows that in the as extruded state the 0.2% proof stress increases from the unreinforced value of 485.1 MPa to a maximum, within the bounds of the volume fractions investigated here, of 570.8 MPa. The increase is not linear; the low strength of the 20% composite is believed to be anomalous, although no physical explanation could be found to account for this. The U.T.S. shows an initial drop in strength and then follows the same trend as the proof stress. There is not as much variation in the value of the U.T.S. as there is in the 0.2% proof stress. This may be due to the restriction of ductility of the composites, as noted by McDanels[25], which will be examined later in this section.

The material exhibits similar trends in the T4 condition (figure 8.28) as were observed in the as extruded state, although the variations are less pronounced. Strength drops slightly as volume fraction increases and then rises to a value, at a volume fraction of 25%, of 563.3 MPa and 646.1 MPa for 0.2% proof stress and U.T.S. respectively. As volume fraction increases above 25% it is probable that the strength values will increase to a maximum, and then fall away as agglomeration and associated porosity increase (as was seen in chapter 6). A further influential factor will be the increase in stress concentration leading to limited ductility, as is described below for material in the two aged conditions.

The variation in tensile strengths of material tested in the two heat treated conditions is shown in figures 8.29 and 8.30. The two graphs follow very different trends. An explanation of the trend observed in the material aged for 6 hours will be followed by an examination of the observed trend in the material aged for 13.5 hours in terms of the initial proposal. Subsequent to heat treatment for 6 hours at 120°C the composite material was found to have 0.2% proof stress and U.T.S. greater than the unreinforced material. The proof stress of the composites was between 90-60 MPa greater than the unreinforced value of 546.9 MPa for alloy extruded at the same ratio

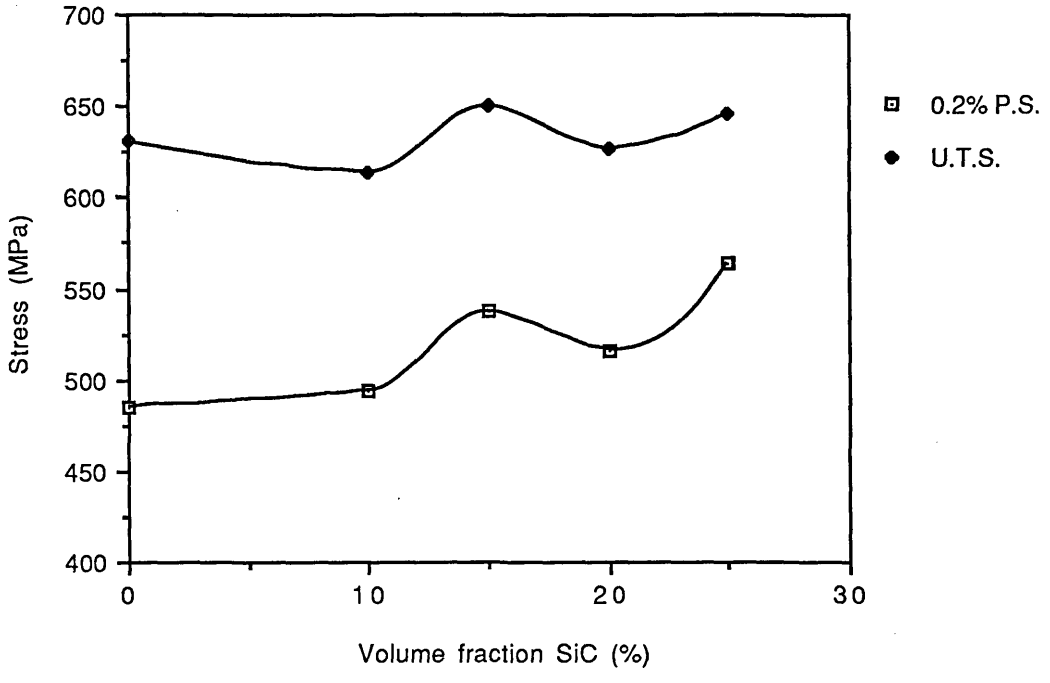

Figure 8.27: Variation of 0.2% proof stress and U.T.S. of composites in the as-extruded state.

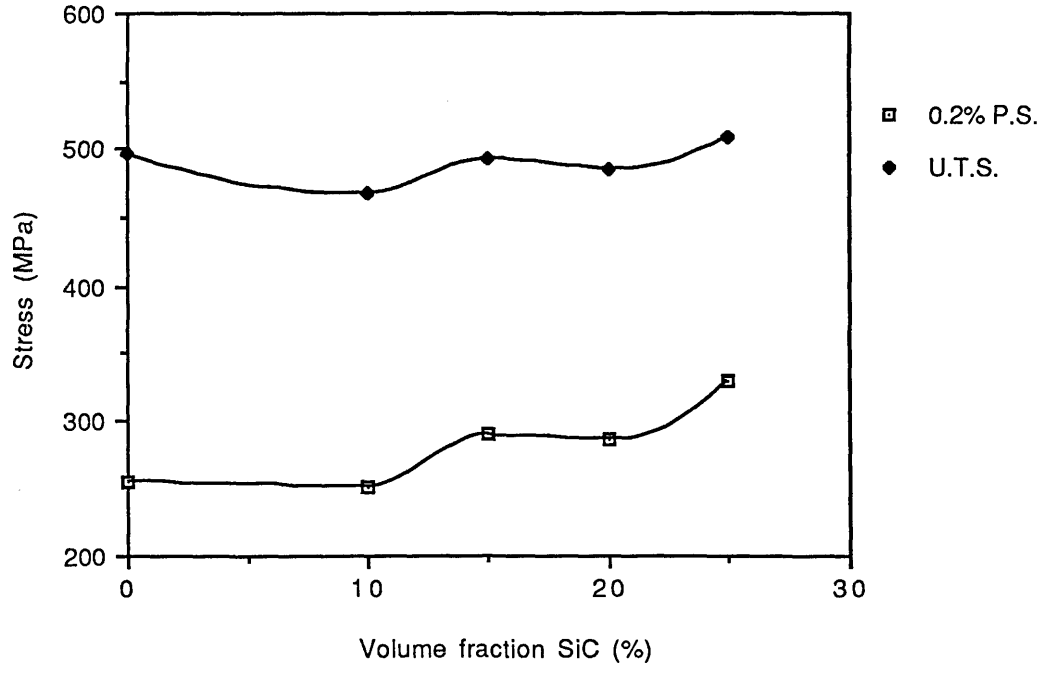

Figure 8.28: Variation of 0.2% proof stress and U.T.S. of composites in the T4 condition

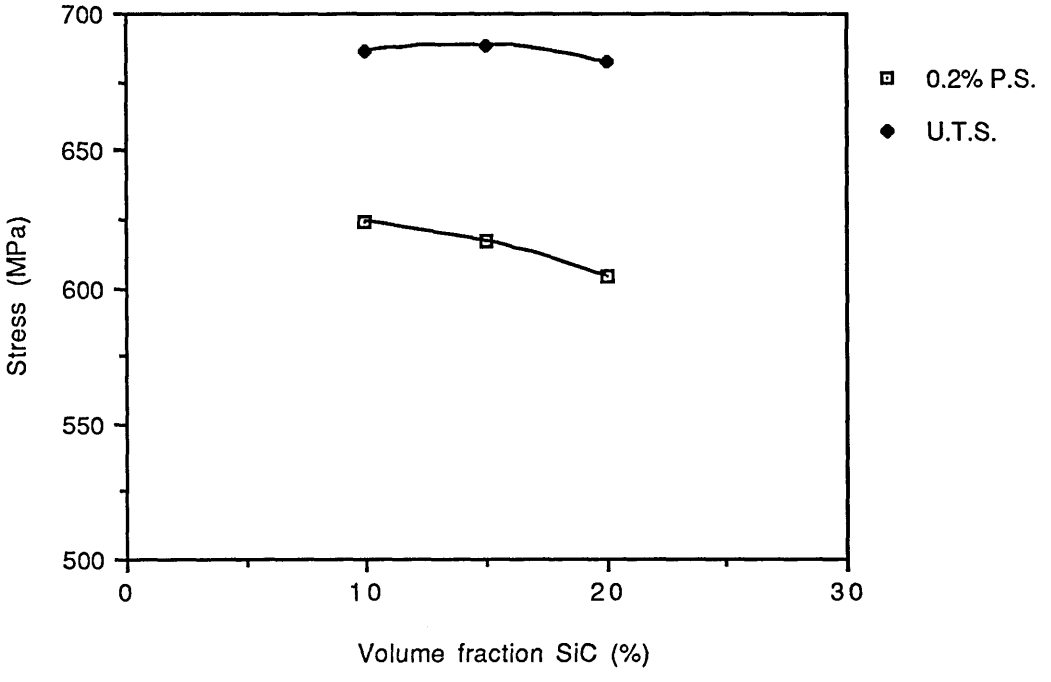

Figure 8.29: Variation of 0.2% proof stress and U.T.S. of composites aged for 6 hours at 120°C

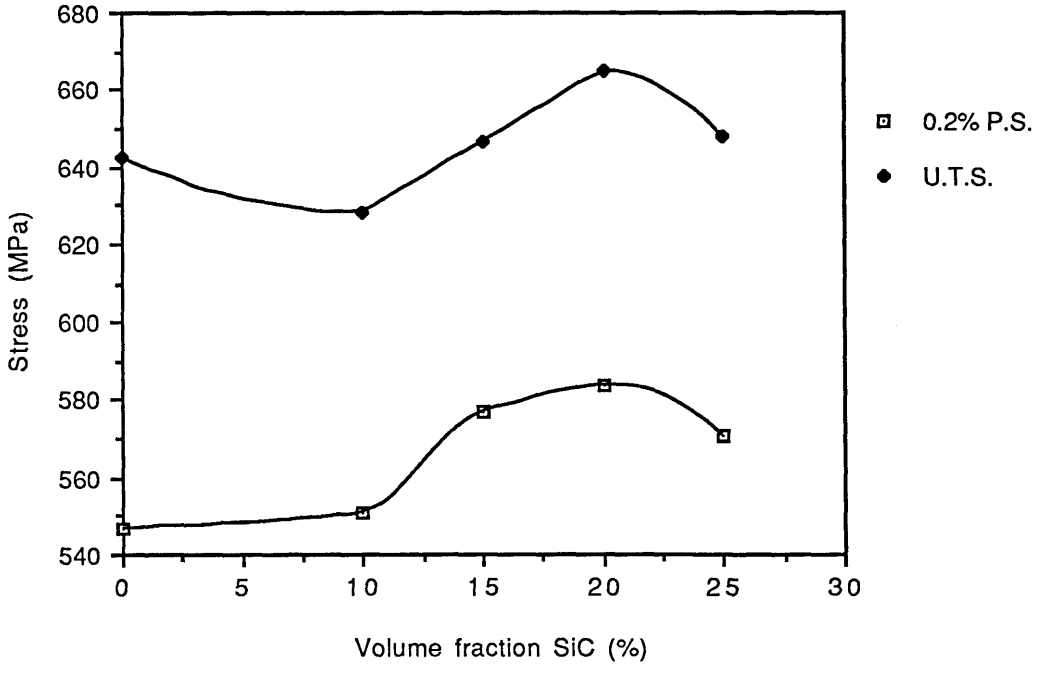

Figure 8.30: Variation of 0.2% proof stress and U.T.S. of composites aged for 13.5 hours at 120°C

and temperature as the composites. This represents an improvement of a maximum of 16%.

Both the proof stress and U.T.S. of the composites decreased with increasing volume fraction in the T6 condition (aged for 6 hours at 120°C). A decrease in the U.T.S. can be explained by the failure of the material occurring progressively sooner with the result that the material cannot reach its potential maximum strength: this is a strain limited situation, briefly mentioned earlier in this thesis as being likely in the aged condition (section 7.4.1). However, the proof stress should continue to rise as volume fraction increases. The fact that it does not may be because of the influence of the volume fraction of SiC on ageing characteristics. This may be the result of a cumulative effect in the factors which lead to yielding (as defined by the point at which void nucleation occurs). The factors affecting void nucleation are matrix strength, matrix/particle bond strength and work hardening behaviour of the composite (as evinced by equation 7.3). Humphreys[37] gives an explanation of the processes affecting failure. During deformation, additional dislocations will build up at the particle boundary in order to relieve local stress concentrations. This relaxation will become progressively more difficult as volume fraction increases because dislocation movement will be inhibited. This effect will be further exacerbated in the T6 condition due to the presence of precipitates. This is the main cause of the loss of ductility in composites, which in turn is the reason that composites do not achieve their potential U.T.S.[25,37]. Hunt et al[122] note that higher work hardening results in greater local stresses around the particle, and that void nucleation, not growth, is the critical factor in composite failure. These phenomena will work in tandem, and as volume fraction increases the yield strength may decrease because the local stresses at the particle boundary are high enough to initiate the failure process. The work hardening exponent (a measure of work hardening capacity) is observed to increase as the volume fraction increases in all but the T4 condition, where it was fairly constant- this is shown in figure 8.31. The increase may be thought of as being due to a complex interaction of the following:

(i) initial dislocation density (which increases with volume fraction[6]);

(ii) the ease of stress relaxation (which decreases as volume fraction increases[37]);

(iii) the effect of any precipitates on dislocation motion (which may vary depending on the type of precipitates present for different volume fraction materials aged for the same time), and

(iv) the effect of any substructure.

The first two factors will be more or less constant over the range of experimentation, being sensitive to quench temperature and volume fraction alone. As volume fraction increases, the initial dislocation density and the density due to relaxation will increase.

The slight decrease in exponent in the T4 condition shows the underlying trend as stress relaxation at the particles competes with dislocation motion. The presence of precipitates will act so as to inhibit the motion of dislocations. In the highly overaged condition this will probably occur by bowing, requiring a higher stress and thus increasing the exponent. There will probably be a range of different precipitate sizes corresponding to the different volume fractions aged at the same time, leading to a range of values for the work hardening exponent which increase as volume fraction increases (figure 8.31). The drop at 25% may be due to insufficient data, because of the associated decrease in ductility leading to the truncation of the stress strain curve. The 'as-extruded' work hardening exponent increase is probably due to a decrease in subgrain size as volume fraction increases; although this was not able to be accurately measured, other authors present evidence to support this assumption[25]. This effect is eliminated in the solutionised and aged specimens.

The composites which were aged for 13.5 hours at 120°C exhibited a slightly different trend when tensile tested. The 0.2% proof stress and U.T.S. increased to a maximum at around 20% SiC after which a decrease in values was found: figure 8.30 shows this. It is believed that this trend is the same trend as was observed in the peak aged material. However, in this case, the volume fraction at which the 0.2% proof stress and U.T.S. reach a maximum has been displaced to a higher value because the overaged precipitates are not as effective a barrier to dislocation motion as those found in the peak aged system. This also implies that if testing had been conducted on a number of low volume fraction composites (less than 10%) aged for 6 hours at 120°C, a rising slope would be observed. The absolute values of proof stress and U.T.S. are lower in the overaged condition. The difference is greatest for the 10% composite: the 0.2% proof stress was found to be 624 MPa after ageing for 6 hours compared with 550.8 MPa after ageing for 13.5 hours. The difference decreases as volume fraction increases because of the opposite slopes of the curves in figures 8. 29 and 8.30.

The different degrees of work hardening in a 10% SiC composite are shown in figure 8.32. This figure shows the different amounts of work hardening under different heat treatment conditions. The figure also shows how the yield stress varies- the material with the highest work hardening exponent has the lowest yield stress. The effect of work hardening in the other volume fraction material is similar to that shown in this example.

The ductility of composites of CW67 decreases as volume fraction increases, as may be anticipated, but at a particular volume fraction for a specific ageing condition there is a sharp deviation, after which the ductility is the same. This is shown in

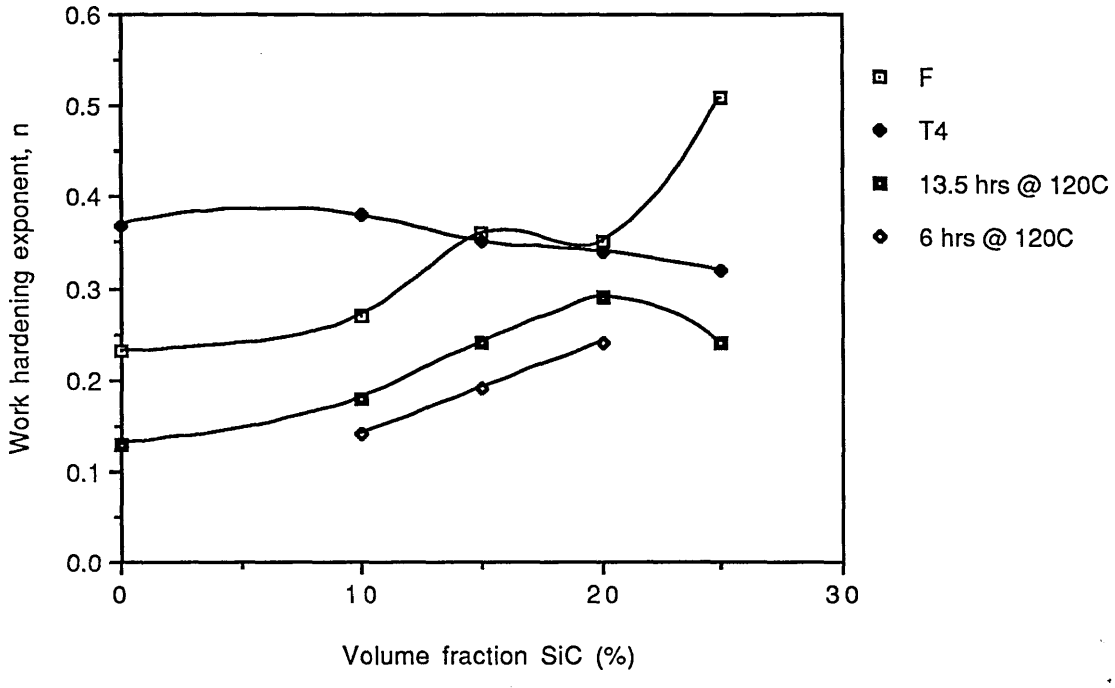

Figure 8.31: Variation in work hardening coefficient with volume fraction for a number of heat treatment conditions.

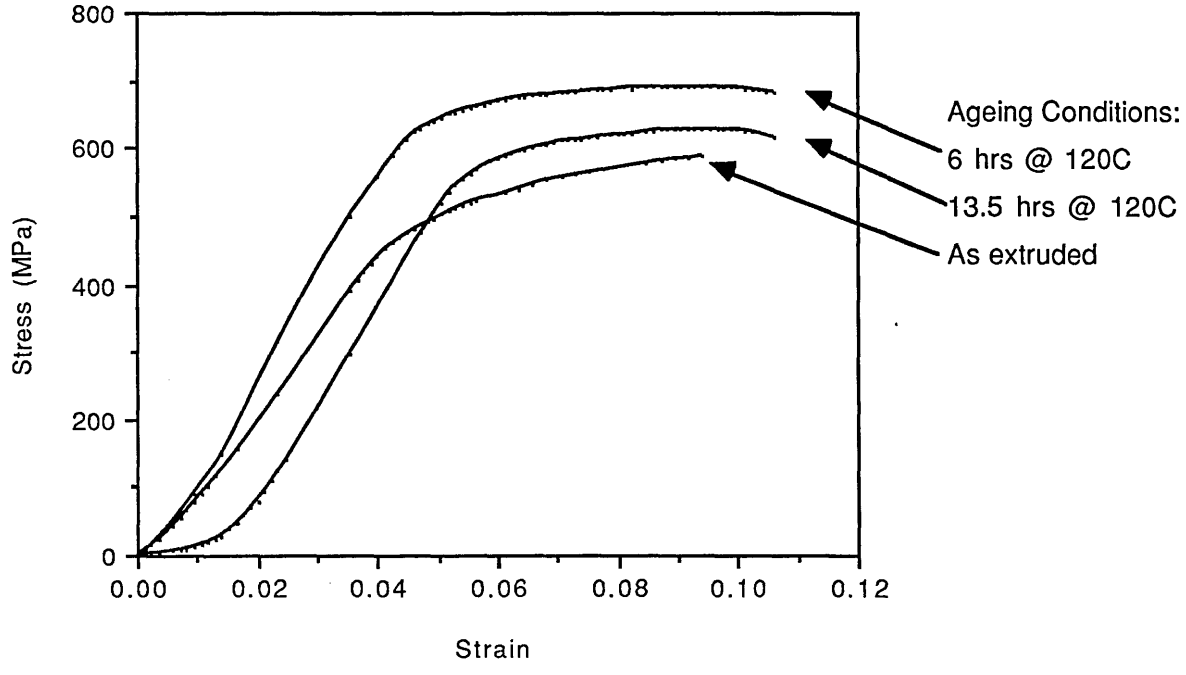

Figure 8.32: Variation in stress /strain curves for CW67/10% SiC in various ageing conditions.

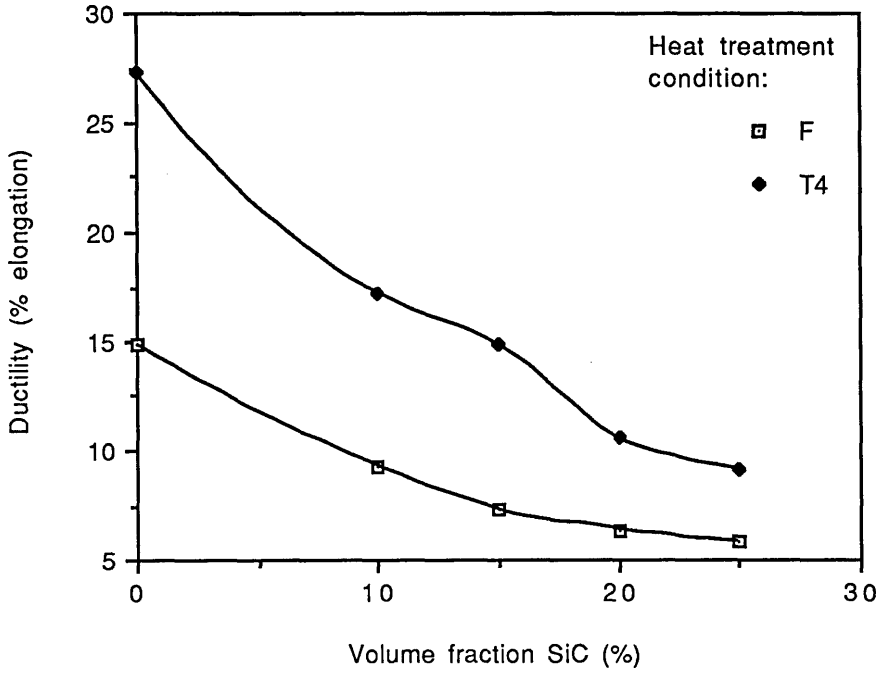

Figure 8.33: Ductility of composites of CW67 in the F and T4 conditions

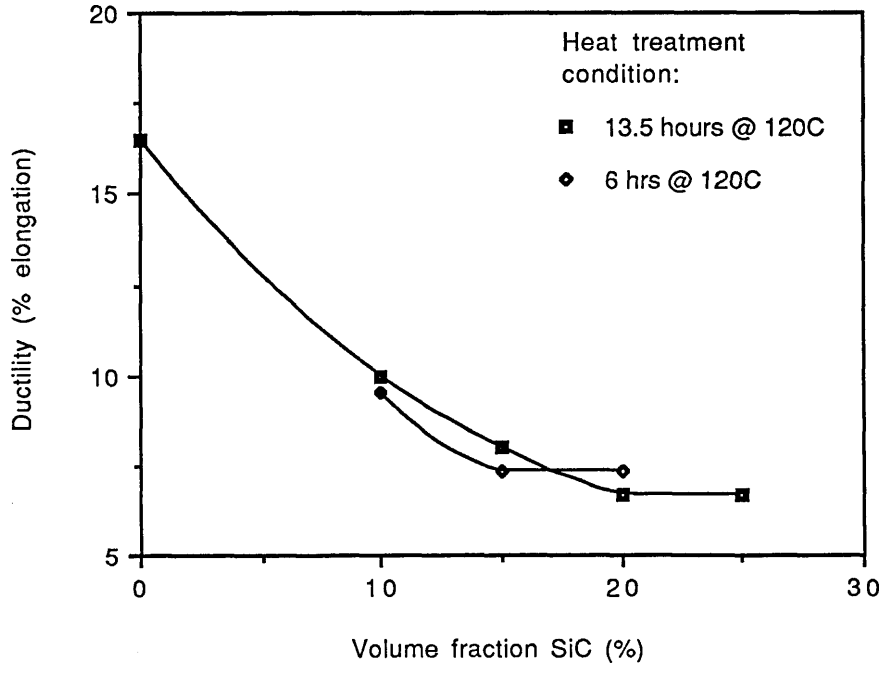

Figure 8.34: Ductility of composites of CW67 in the aged conditions

figures 8.33 and 8.34. The low range of volume fractions tested means that it is unclear whether this effect is due to experimental variation or is an actual phenomenological observation. It is possible that the sharp deviation is due to a change in the mechanism controlling failure. Martin[123] shows that for volume fractions of particles up to 0.159 (see equation 8.1) the fracture strain is equal to the void growth strain, but above this volume fraction the growth strain is zero; therefore the fracture strain is controlled by the nucleation strain, which is constant. The equation for growth strain, e_g, is as follows:

$$2r(1 + e_g) = r\{\sqrt{(2\pi/3V_f)} - \sqrt{8/3}\}.....8.1$$

where r is the particle radius and all other terms are as previously defined. This is compatible with the previous physical explanation offered. The ductility will be limited by the ability of the material to redistribute stress, as described previously, and it seems probable that at a certain volume fraction the size of the matrix ligament joining SiC particles will be too small to support any further extension of the material, resulting in failure. This limiting ligament size (and the nucleation strain) will necessarily be further influenced by the presence and morphology of any precipitates in the matrix. Thus the material aged for 6 hours will have a different ductility to the material aged at 13.5 hours at the same temperature, and will also have a different nucleation strain for void formation. The un-aged material will not have reached a limiting volume fraction within the scope of these tests. The gradient of the curves showing decrease in ductility with volume fraction in the F and T4 conditions has not reduced as dramatically as for the aged specimens. Both curves show indications of becoming shallower and can be interpreted as being at different stages of progress towards reaching their limit. The T4 curve will obviously reach a higher volume fraction before ductility is restricted. A comparison of properties with theoretical predictions, similar to that made in section 7.4.1 yielded the following results:

$$\sigma_{yc} = \sigma_{ym}\{V(S+2)/2 + 1-V\}.....8.2$$

Volume fraction SiC	Predicted σ_{yc} (MPa)	Actual $\sigma_{0.002}$ (MPa)
0	-	546.9
0.1	601.6	624.1
0.15	628.9	619.4
0.2	656.0	607.1
0.25	683.6	-

Table 8.6: Predicted T6 yield stress of CW67 composites (equation 8.2)

The values predicted using equation 8.2 start off as underestimates, rising to a substantial overestimate of the yield strength of the composites in their peak aged state. This can be explained within the context of the previously discussed mechanism of composite failure. The values found here can be thought of as tending towards the potential strength of the material whilst the effect of dislocation interactions is ignored. A comparison of the experimental and calculated values shows the competition between the relaxation of stress at the particle boundary and dislocation motion: at high volume fractions the relaxation of stress at the particle is severely inhibited thus promoting failure at a lower than predicted stress; at low volume fractions the additional dislocations are able to contribute to the strength of the material.

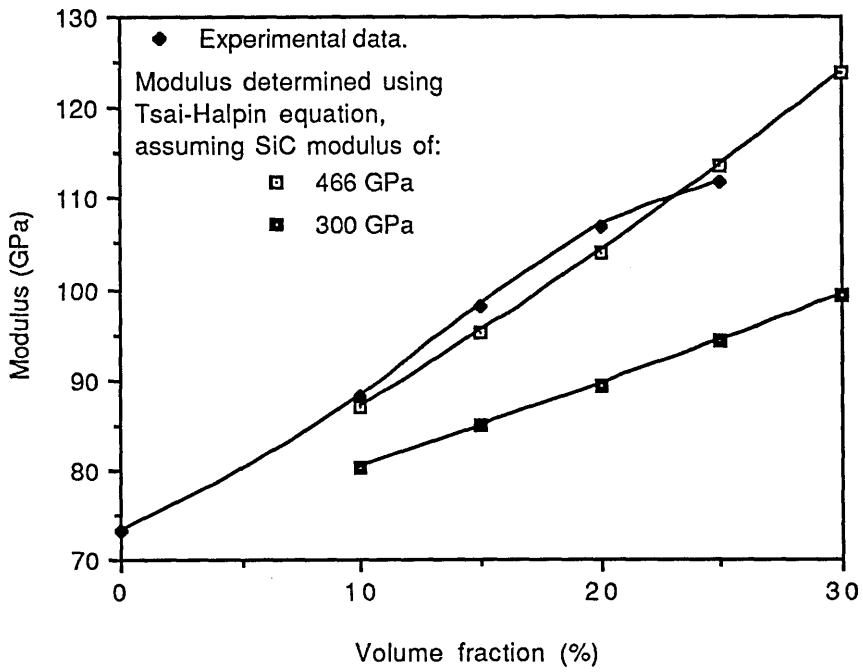

Figure 8.35: Variation in modulus of composites of CW67 with volume fraction, compared with predicted values.

The modulus of the CW67 composites showed a monotonic variation with volume fraction as shown in figure 8.35. As with the values found by McDanels[25], they do not conform to the law of mixtures calculation (cf. fig. 3.1). However, the values do lie very close to those predicted by the Tsai-Halpin equation but it should be noted that this can be achieved by manipulation of the modulus data for silicon carbide. The two SiC modulus values are the maximum and minimum values found quoted in various literature[6,26,74], as the modulus of the SiC used in this work was unknown. The trend followed is, more significantly, different: the increase in modulus of the CW67 composites tends to fall away as volume fraction increases whereas the Tsai-Halpin equation predicts a slight acceleration in modulus increase. This is probably due to the

difference between SiC types accounted for by the equation (platelets or short fibres) and that employed in this experimental work.

In comparison with particulate composites of 6061/20% Al_2O_3, 2124/20% SiC and 8090/20% SiC (investigated by Peel et al[71]), and 6061/20% SiC (investigated by McDanels and Hoffman[56]) the CW67 composites produced in this investigation exhibit superior specific 0.2% proof stress and U.T.S. values and 'mid-range' specific modulus values. The comparison is shown in table 8.7 for composites containing 20% reinforcement only, in their peak heat treated condition. It should be noted that the CW67 10% and 15% composites have higher specific proof stress and U.T.S. values.

Composite	Specific 0.2% P.S. (MN.m/kg)	Specific U.T.S. (MN.m/kg)	Specific modulus (GN.m/kg)
CW67/20% SiC	209.0	233.8	36.9
6061/20% Al_2O_3	145	175	33
2124/20% SiC	155	220	36
8090/20% SiC	190	225	38
6061/20% SiC	127.1	152.8	38.6
Target[71]	220	290	45

Table 8.7: Comparison of specific properties of CW67 with various other particulate composites

CW67 composites containing 10% and 15% SiC have specific 0.2% proof stress values of 218.2 MNm/kg and 215.1 MNm/kg respectively, and specific U.T.S. values of 238.5 MNm/kg and 237.8 MNm/kg. The specific modulus values for these composites are respectively 30.8 GNm/kg and 34.1 MNm/kg. The table 8.7 also shows the large influence of the matrix properties on those of the composite. Although the aluminium-lithium alloy, 8090, has a lower density than 7xxx series alloys the 8090 composite's specific 0.2% proof stress is significantly lower than the CW67 composite. Furthermore the values for the CW67 composite are considerably greater than those for the 6061/20% SiC composite, a material which contains possibly the most commonly used matrix.

It should be noted that the specific property values for neither the CW67 composites nor composites of 8090 reach the 'target' properties set by Peel et al[71]. The specific proof stress is attainable, and may be achieved with a 7xxx series alloy or by using a lower density matrix alloy, but it should be remembered that the absolute

values of the properties are also important. However, the failure mechanisms operating, as described earlier in this section, may make it impossible to achieve the combination of target specific proof stress and U.T.S. because of the reduction in strain to failure. Increases in specific modulus can only be achieved by the addition of larger amounts of reinforcement or by further reduction of the matrix alloy density.

8.6.1.2 Rolled CW67 Composites

Sections of sheet were aged for a number of different times prior to tensile testing. In the as rolled condition the 0.2% proof stress was found to be 377 MPa and 393.2 MPa, the U.T.S., 492.2 MPa and 469.1 MPa, for the 15% and 20% SiC composites respectively. The results of testing of heat treated material are shown in figure 8.36 and 8.37.

The main point of note is that the 0.2% proof stress and U.T.S. are lower than encountered in the extruded material. The highest proof stress was found in the 20% SiC composite after ageing for 8 hours, and after 6 hours in the 15% composite. The values were, respectively, 492 MPa and 477 MPa. The accompanying U.T.S. values were 604 MPa and 598 MPa, although the highest U.T.S. was found after 6 hours, for the 20% composite. The reduction in tensile properties after rolling is common in aluminium alloys[84,124] and may be due to static recrystallisation occurring between passes[76], but in this case the lower strengths cannot be wholly accounted for in this way. It is thought that the properties are limited in the same way as those of the extruded materials: the additional deformation due to rolling results in a further increase in dislocation density and the restriction of stress relaxation at the particle boundary. This is evinced by the fact that the specimens all failed before reaching a maximum in the load/displacement curve and at low elongations (see figure 8.37). Ductilities were found to be 7.25% in the T4 condition, for the 20% composite, and, at the peak ageing condition, just 2.9% for the 15% composite.

Figure 8.38 shows the stress/strain curve of the rolled material in the T4 condition.

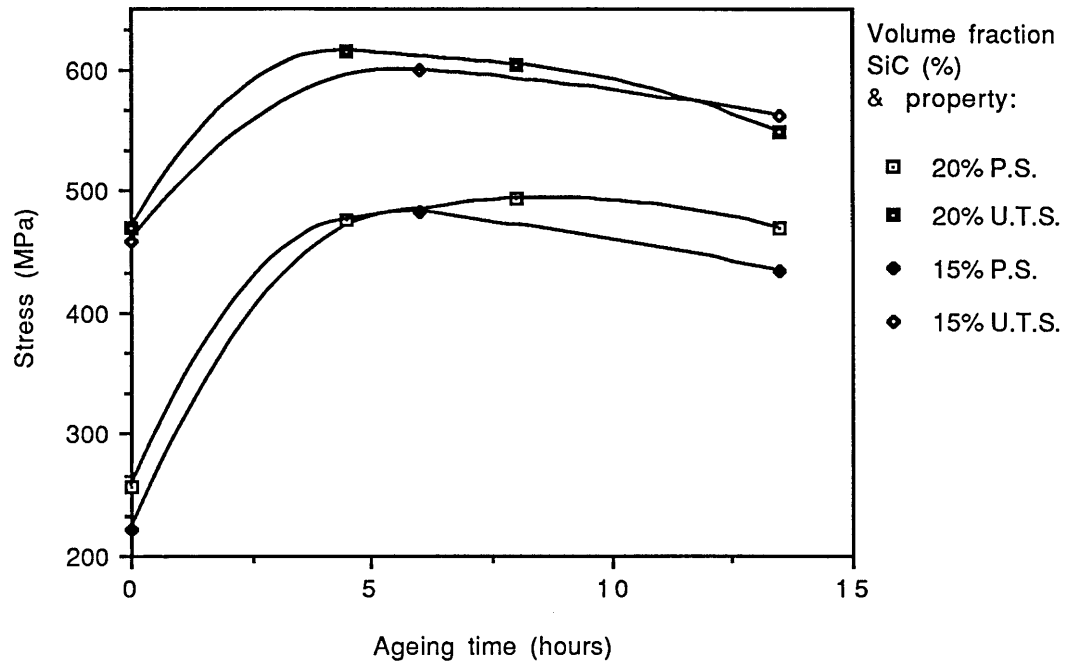

Figure 8.36: Variation of 0.2% proof stress and U.T.S. with ageing time for rolled CW67 composites

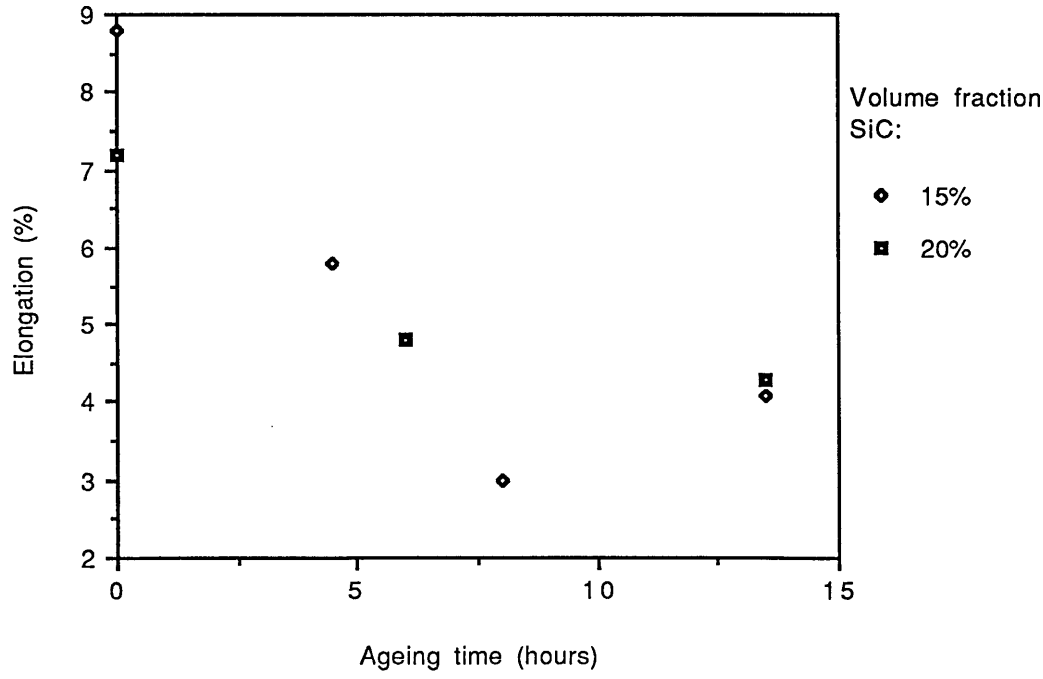

Figure 8.37: Variation of ductility (%) with ageing for rolled CW67 composites

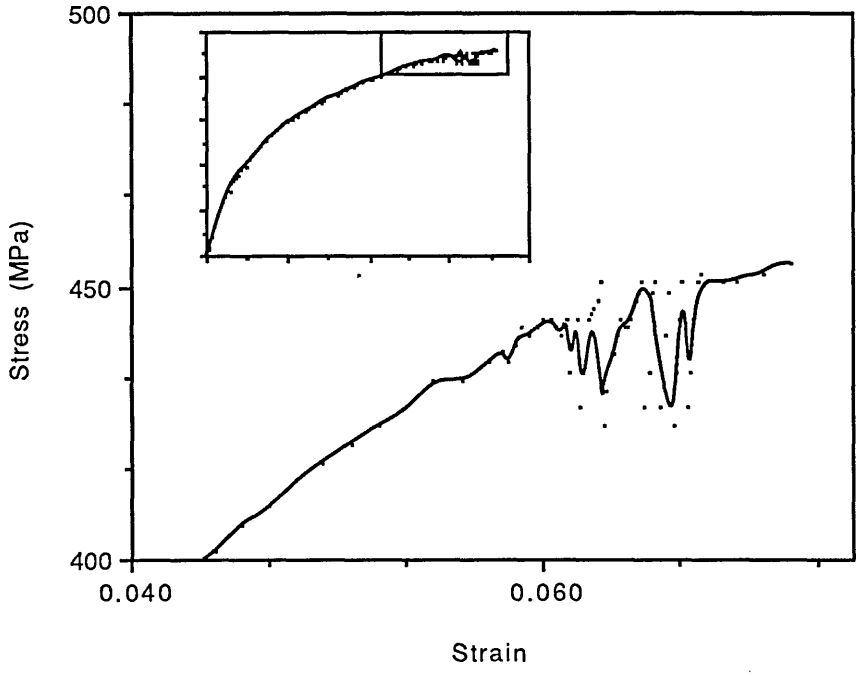

Figure 8.38: Stress/strain curve of rolled CW67/15% SiC composite

8.6.2 Fracture Toughness

The fracture toughness of these composites was measured using the chevron bar technique, the potential limitations of which have been discussed earlier (section 7.4.2). The technique is useful in comparing the fracture toughness of the composites, where no other method of machining specimens was available. The values will also be compared with those obtained from bar specimens of the matrix material in the same heat treatment conditions.

The variation of fracture toughness with volume fraction is shown in figure 8.39. The trend with ageing time is similar to many unreinforced alloys[84]. These results cannot be compared directly to the unreinforced material in all ageing conditions because the "overaged" time in the composite series is equivalent to the peak time for the unreinforced alloy. Furthermore, in this instance the "overaged" time was not established by hardness measurement: it was considered more desirable to have a direct comparison with the peak aged unreinforced material. This is why the trend in toughness variation with ageing condition differs to the unreinforced material.

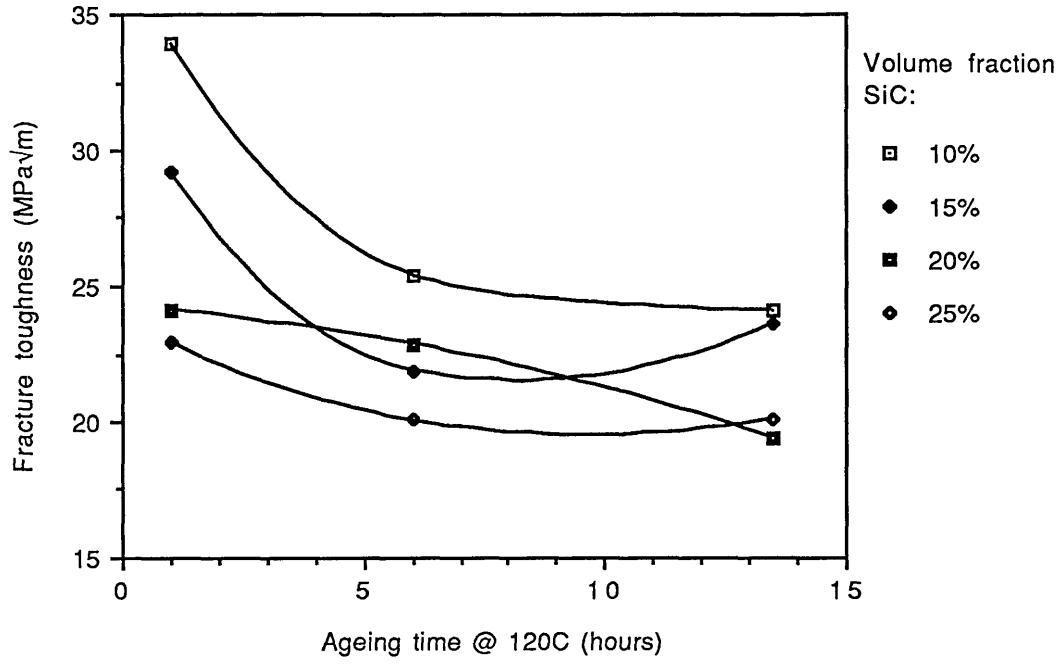

Figure 8.39: Variation in fracture toughness with ageing time.

The absolute values of the fracture toughness are higher than those consistently quoted for composite materials, values for which are between 10-20MPa$\sqrt{m}$[4,27,63]. It is probable that part of this increase is due to the degassing and hot compaction operation, which was so efficacious in improving the fracture toughness of unreinforced CW67. A description of the processing of the material used in these references is either vague or not included and thus a comparison of values with those presented in this thesis may not be valid. The testing direction will also have affected the value, as was seen in the case of the unreinforced alloy. The variation of toughness with volume fraction in each ageing condition is displayed in figures 8.40 and 8.41. The decrease in toughness with increasing volume fraction of silicon carbide is consistent with expectation. The slightly anomalous value for the 20% composite in figure 8.42 is considered to be due to the wide range of experimental data in this group, but may be related to the lower 0.2% proof stress, shown in figure 8.21; however, no structural differences were found in this material. The fracture toughness curves, which were obtained by interpolating between the points, are similar to a logarithmic decay; however, in the peak heat treated condition the data for the composites also fits a straight line within its experimental error. Thus all that can definitely be stated is that the variation in the fracture toughness of the composites in the peak treated condition is less than that in either the under- or overaged condition.

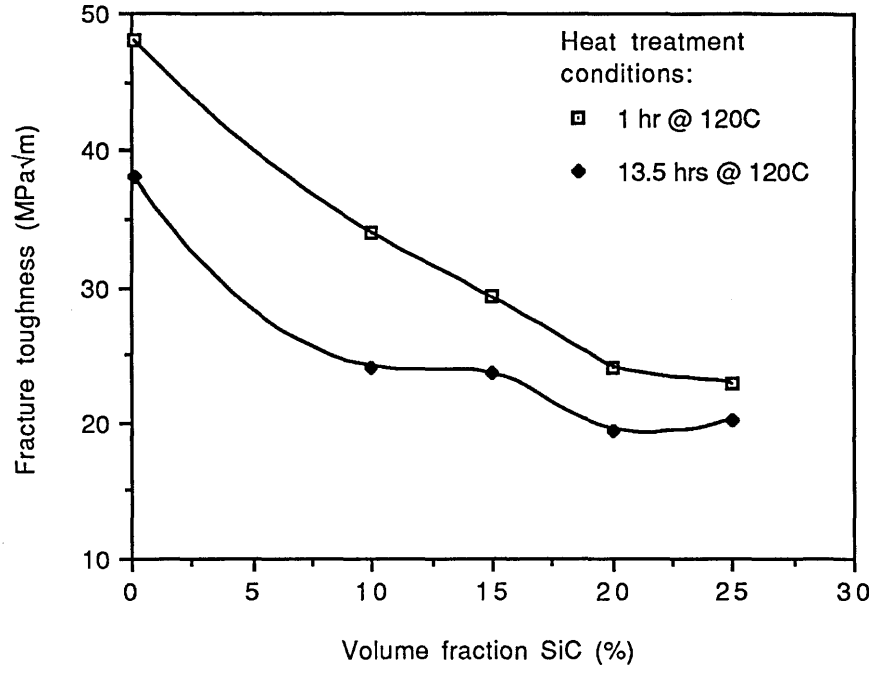

Figure 8.40: Variation of fracture toughness with volume fraction in under- and overaged conditions.

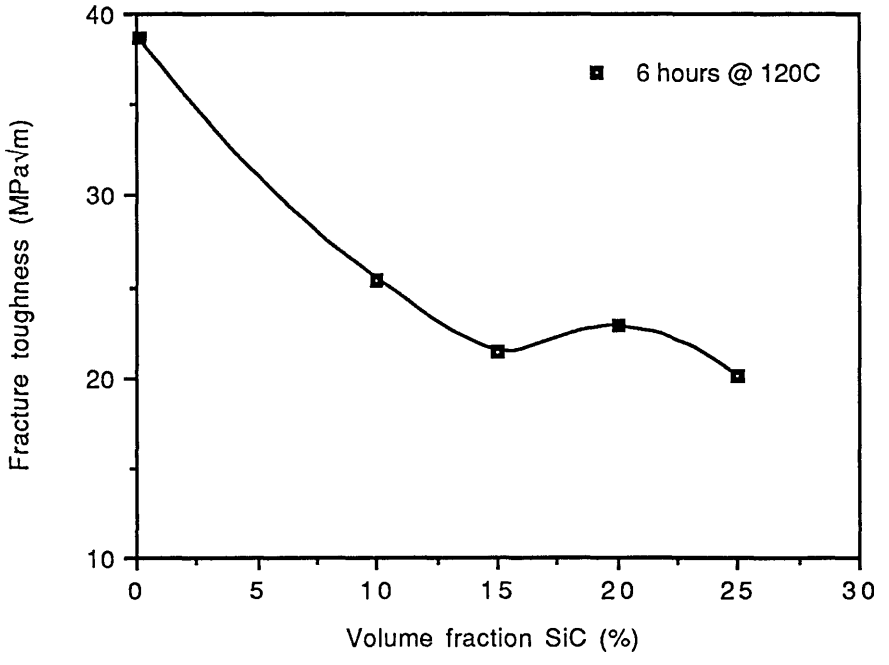

Figure 8.41: Variation of fracture toughness with volume fraction in peak aged condition.

This is consistent with previous explanations for failure of composites in which it is accepted that failure is dependent on the void nucleation[122]. In the peak aged condition the restriction of dislocation movement away from the SiC particles due to precipitates and other dislocations will lead to a build up of stress at the particle boundary. The tailing off of the reduction in toughness as volume fraction of SiC increases is similar to the variation in ductility shown in section 8.6.1, figure 8.34. It is probable that the same explanation can be applied to fracture toughness- that of a limiting matrix ligament size between the SiC particles below which stress cannot be redistributed through the matrix. It can also be seen from figures 8.40 and 8.41 that the volume fraction at which the gradient of the curve becomes substantially shallower is lower for the peak aged material. This shows the influence of the fine precipitate structure on the dislocation movement away from the SiC particles.

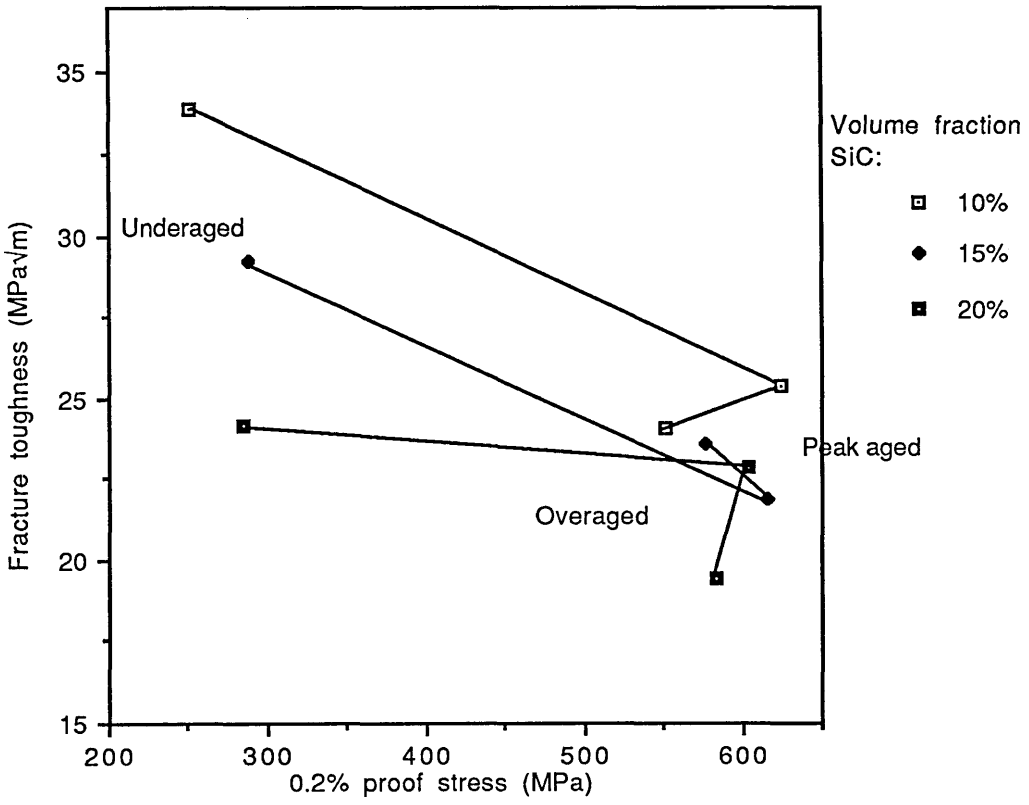

Figure 8.42: Fracture toughness vs 0.2% proof stress for various volume fractions of SiC.

The variation of fracture toughness with 0.2% proof stress is shown in figure 8.42. The 0.2% proof stress of the solutionised material has been used for the underaged condition, as a guideline only: it is recognised that this will not be the actual value in this condition. The trend is similar to that observed by Manoharan and Lewandowski[61] for composites of a 7xxx series alloy, although the actual values are different because of the difference in alloy composition, composite composition and

testing direction. This trend is attributed to differences in the micromechanisms of failure, which are described below.

The different matrix precipitate particles present at different ageing times will exert an effect on the failure because of their relative strengths (requiring either shearing or bowing around) and also because of the effect they have on the stress relaxation around the SiC particles (as has been discussed earlier in this and other sections). The direction of the curve is reflected in the change in ductility of the materials in two of the three volume fractions investigated. Figure 8.34 shows that the ductility of the 10% and 15% composites is higher in the 13.5 hr heat treatment condition whilst the 20% composite exhibits the opposite trend. The 10% composite is the only one out of step with figure 8.34. There is no reproducible physical explanation for this although it would seem more likely that fracture toughness would decrease with ageing time[117]. It is possible that slight differences in the specimens may cause minor variations in the results. In all of these cases it should be noted that the fracture toughness in the longitudinal direction remains high in the peak aged condition.

The fracture toughness of the composites compares well to the values for the unreinforced alloy, as is shown in figures 8.40 and 8.41. The effect of the testing direction must play a major rôle in 'elevating' the composite fracture toughness values, but in the peak aged condition they are, never-the-less, approximately 50% of the value for the unreinforced alloy. This large drop in fracture toughness is one of the constraints on the use of composite materials; it appears that the best that can be done is limit the detrimental effect of the particles by careful processing.

A comparison of the experimentally obtained values with fracture toughness calculated in the same manner as in section 7.4.2 breaks down when the work hardening exponent exceeds 0.28 (table 8.8) because the term for α in equation 8.3 below becomes negative. The equation used to calculate the values in table 8.8 is as follows:

$$K_{IC} = \sqrt{(2E\sigma_y\lambda/3\alpha)} \quad \text{.....8.3}$$

where: the term λ is the inter-particle spacing;
and α is related to the work hardening exponent, n, by the equation:

$$\alpha = 0.65-2.3n \quad \text{.....8.4}$$

As volume fraction increases the predicted values become nonsensical because of the increase in modulus and yield stress with little variation in work hardening exponent: a 20% composite aged for 13.5 hours at 120°C is predicted as having a fracture toughness of 299 MPa√m. Calculated values for lower volume fractions are also higher than the experimentally determined fracture toughness. The terms in the above equations are defined in section 7.4.2. Martin[123] quotes an equation which relates the volume fraction of inclusion to fracture toughness of ductile materials containing brittle inclusions. The extension of this treatment to particulate composites is simple and figures 8.43-44 below show the results of applying equation 8.5 to composites of CW67. There are a number of assumptions used in this treatment which do not hold in practice: a unique particle size has been chosen to represent the inclusions, but it is plain that the SiC varies in size and that, in some heat treatment conditions, the influence of oxide particles may be heightened. The equation is as follows:

$$K_c^2/E = \sigma_y \delta_c \text{.....} 8.5$$

where δ_c is the crack opening displacement which in this case is equivalent to the particle spacing[6,123]; the other terms being as prior definitions.

Composite vol.%	Heat treatment	E, GPa	σ_y, MPa	W.H. exponent	K_c, MPa√m	Experimental K_c, MPa√m
10%	u/a	88.10	251.0	0.38	-	33.92
	peak	88.10	624.0	0.12	35.55	25.41
	o/a	88.10	550.8	0.18	42.05	24.08
15%	u/a	98.2	288.8	0.35	-	29.22
	peak	98.2	616	0.185	48.14	21.89
	o/a	98.2	576.8	0.24	70.50	23.6
20%	u/a	106.9	285	0.34	-	24.13
	peak	106.9	604.5	0.225	64.76	22.86
	o/a	106.9	584	0.28	299.14	19.42

Table 8.8: Calculated fracture toughness of CW67 composites, using equation 8.3

The application of this equation requires the calculation of particle spacing, which, as has been shown in section 6.3.4, may be calculated using a number of different equations. Thus, an examination of this term is necessary before using the whole equation in order to attempt to predict K_{IC} values. Martin[123] uses a relationship of the form:

$$\delta_c \approx S_p = C.d_p/_3\sqrt{V} \quad \text{.....8.6}$$

where S_p is the particle spacing, C is a constant, dp is the particle size and V, the volume fraction. Stephens et al[36] quote a relationship for particle spacing which depends instead upon the reciprocal of the square root of the volume fraction (sub-section 6.3.4 and overleaf); figure 8.43 shows the effect of both roots on the square of the fracture toughness.

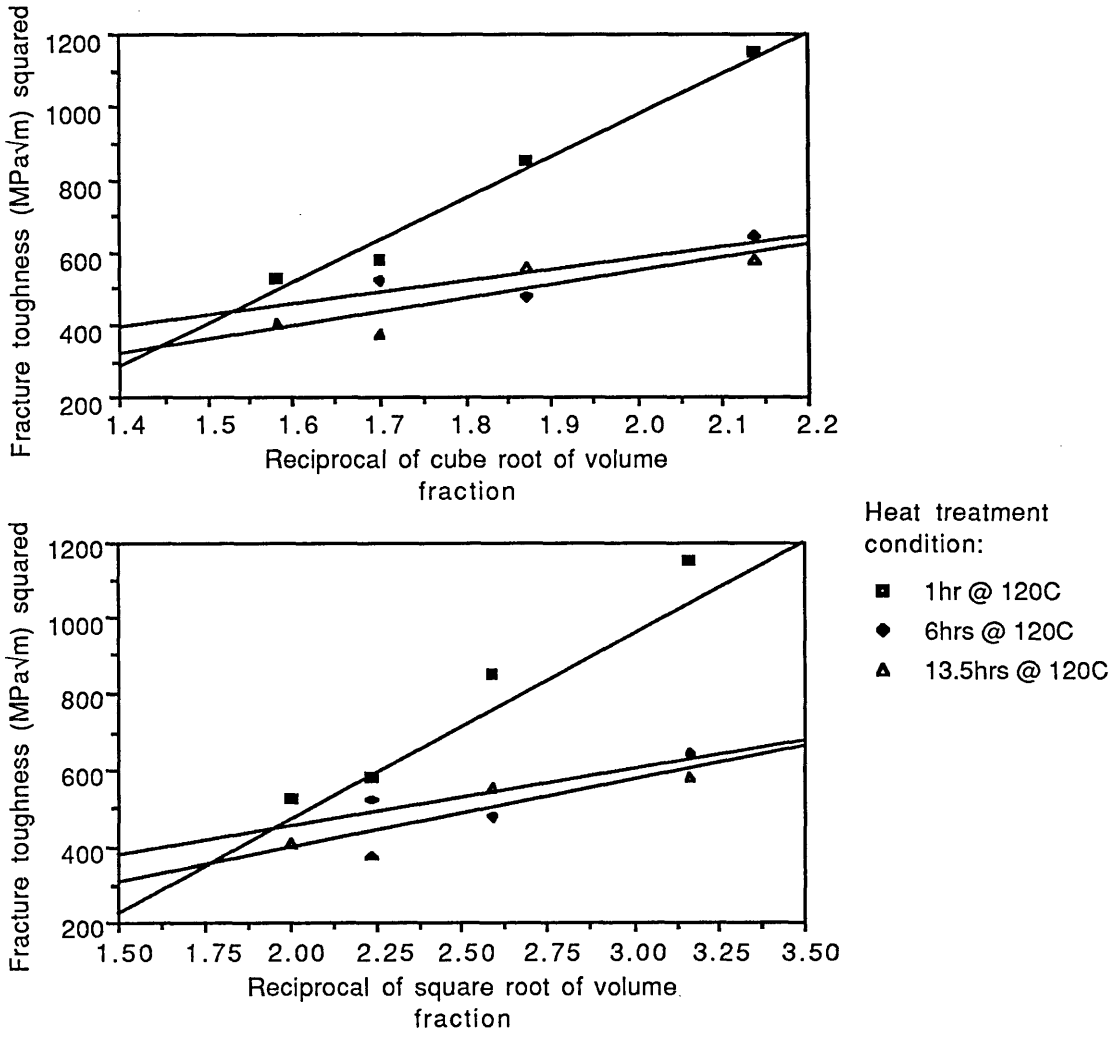

Figure 8.43: Square of fracture toughness vs reciprocal of roots of volume fraction.

The two relationships for volume fraction yield similar results, the correlation between data and the straight line is only marginally better for the square root calculation. This shows that the calculation is relatively insensitive to the method of calculation of the particle spacing. In the underaged condition the 'square root data' conforms to a straight line fit, the correlation being 0.983. However, in the other two conditions the correlations are not good, at 0.635 and 0.771 respectively for the

material aged for 6 hours and 13.5 hours. The correlation coefficients may be directly related to microstructural observations at the fracture surface. It was noted previously (sub-section 7.4.3) that voids may only form at features at which the local stress exceeds the nucleation stress for a specific particle. If we temporarily ignore the build up of stress due to the inhibition of stress relaxation, it can be estimated that the stress to nucleate voids at the majority of oxide particles will be unattainable in the underaged state, but may be achieved for some larger oxides and as ageing raises the yield stress of the material.

Table 8.9 shows the stress needed to nucleate a void at oxide and SiC particles in various composites of CW67; equation 7.3 has been used for the calculations, with the same assumptions as were applied in sub-section 7.4.3. It should also be noted that the comparison of these stresses to yield stress neglects any stress concentration effect which may raise the local stress at an oxide or SiC particle, thus allowing void formation. From this table it can be deduced that the conformity of the plot to a straight line in the underaged condition will be better because the effect of oxides is minimal, whereas their influence has not been accounted for in the other two plots.

Volume fraction (%)	Particle size (μm)	Modulus (GPa)	Surface Energy (J/m^2)	Nucleation stress (MPa)
10	5	88.1	0.5	230.0
10	0.75	88.1	0.5	593.6
15	5	98.2	0.5	242.7
15	0.75	98.2	0.5	626.7
20	5	106.9	0.5	253.3
20	0.75	106.9	0.5	653.9
25	5	111.9	0.5	259.1
25	0.75	111.9	0.5	669.0

Table 8.9: Calculated nucleation stress for void formation in composites of CW67

Plots of calculated fracture toughness may be compared with experimentally determined results (figure 8.45). The calculation of particle spacing used the equation due to Stephens et al[51], quoted below and in section 6.3.4.

$$S_p = \{d_p^2/V\}^{0.5} \quad \text{.....8.7}$$

The calculated fracture toughness values are uniformly higher than the experimental values, but this may be due to the influence of agglomeration and banding of the silicon carbide particles accompanied by the effect of a range of particle sizes in the real material. The values thus calculated are considerably more realistic than those yielded by equation 8.3, although the dependence on work hardening is considered to be valid. It must be remembered that equation 8.3 was developed for discontinuous fibre composites. Equation 8.5 only accounts for yield stress variations and thus would predict that the peak heat treated specimen will have a higher fracture toughness than an underaged specimen for the same volume fraction. This is clearly contrary to experimental evidence. Thus, whilst both of these equations show trends in fracture toughness within a specific heat treatment condition both equations fail to incorporate

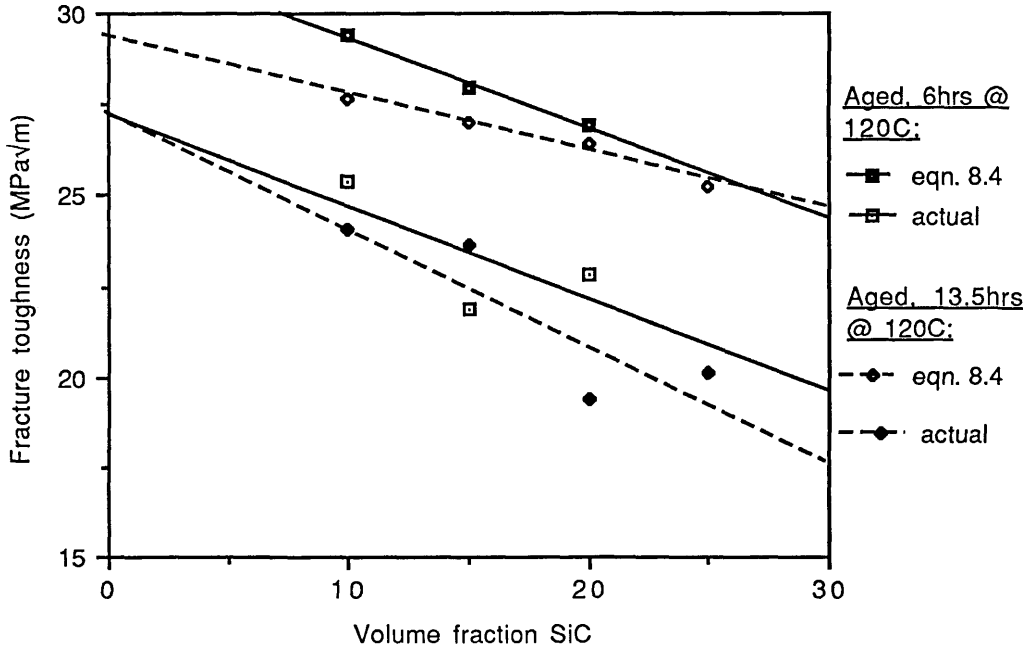

Figure 8.44: Calculated and experimental fracture toughness vs volume fraction of SiC.

the primary feature of the other, and neither is able to account for the influence of a range of particles from precipitate to SiC. Taya and Arsenault[6] quote a relationship which incorporates all the salient properties, but has not been taken beyond the general condition. The fracture toughness is related to both matrix and SiC influences, and is shown below:

$$K_{IC} = \{\sigma_y.\epsilon_f^*.E.f(n)\}^{0.5}.S_p^{0.5} \quad \text{.....8.8}$$

where ϵ_f^* is the strain at the crack tip and $f(n)$ is some function of the work hardening exponent. The equation does, however, circumvent the inclusion of a term for stress concentration at the silicon carbide particles by incorporating the strain at the crack tip. It should also be noted that this equation relates the fracture toughness to the reciprocal of the volume fraction only.

The experimentally determined fracture toughness values conform only loosely to the same trend as the theoretical results, although the fit to the peak aged data has the same gradient as the theoretical data. This is due to the simplicity of the predictive equation and to experimental error. The main failing of equation 8.5 is that it predicts an increase in toughness as yield stress is increased for constant volume fraction of SiC- this was not observed in reality (see figure 8.42).

8.6.3 Fractography of Composites

The fractographs of tensile specimens of composite material are shown in figures 8.45a-d. The general form of the fracture surface was found to be the same for all volume fractions. Matrix dimpling was observed to contain two distinct types, one associated with the SiC particles and the other, with matrix phases or inclusions. Matrix dimpling was observed to be of the type described in section 7.4.3, resembling a flower. In contrast there was little discrepancy between the large dimples and the size of SiC particles (figure 8.45a and b show this). This is indicative of low deformation at the particle/matrix interface. The size of matrix-associated dimple was found to be generally larger in the T4 condition, although this effect was obfuscated by the presence of a greater number of dimples due to the reinforcement in all heat treatment conditions.

Figure 8.45a shows the 10% composite in the T4 condition. A large agglomerate can be observed at the centre of this fractograph, although these were not common in the lower volume fraction composites. Figure 8.45b shows the 25% composite in the T4 condition. There is noticeably less SiC at the fracture surface, although this is difficult to fully assess without examination of the partner surface, as Roebuck suggests[125]. There is little difference in dimple size between high and low volume fraction composite. In the high volume fraction composites in the as extruded condition there was also a large amount of decohesion at the particle boundary. There was also a larger amount of agglomeration, the presence of which may lead to a lowering of the stress to failure. The effect of the heat treatment conditions was difficult to quantify. The increasing obstruction to stress relaxation should manifest as an increased proportion of cracked particles or interface decohesion, but it was difficult to assess

(a) `Tensile: 10% SiC, underaged

(b) Tensile: 25% SiC, underaged

(c) Tensile: 10% SiC, T6

(d) Tensile: 25% SiC, T6

(e) Toughness: 10% SiC, underaged

(f) Toughness: 20% SiC, underaged

(g) Toughness: 15% SiC, T6

(h) Toughness: 15% SiC, 13.5h @ 120°C

Figure 8.45: Fractographs of composite tensile and toughness specimens, extruded at 425°C, 24:1; testing mode as indicated.

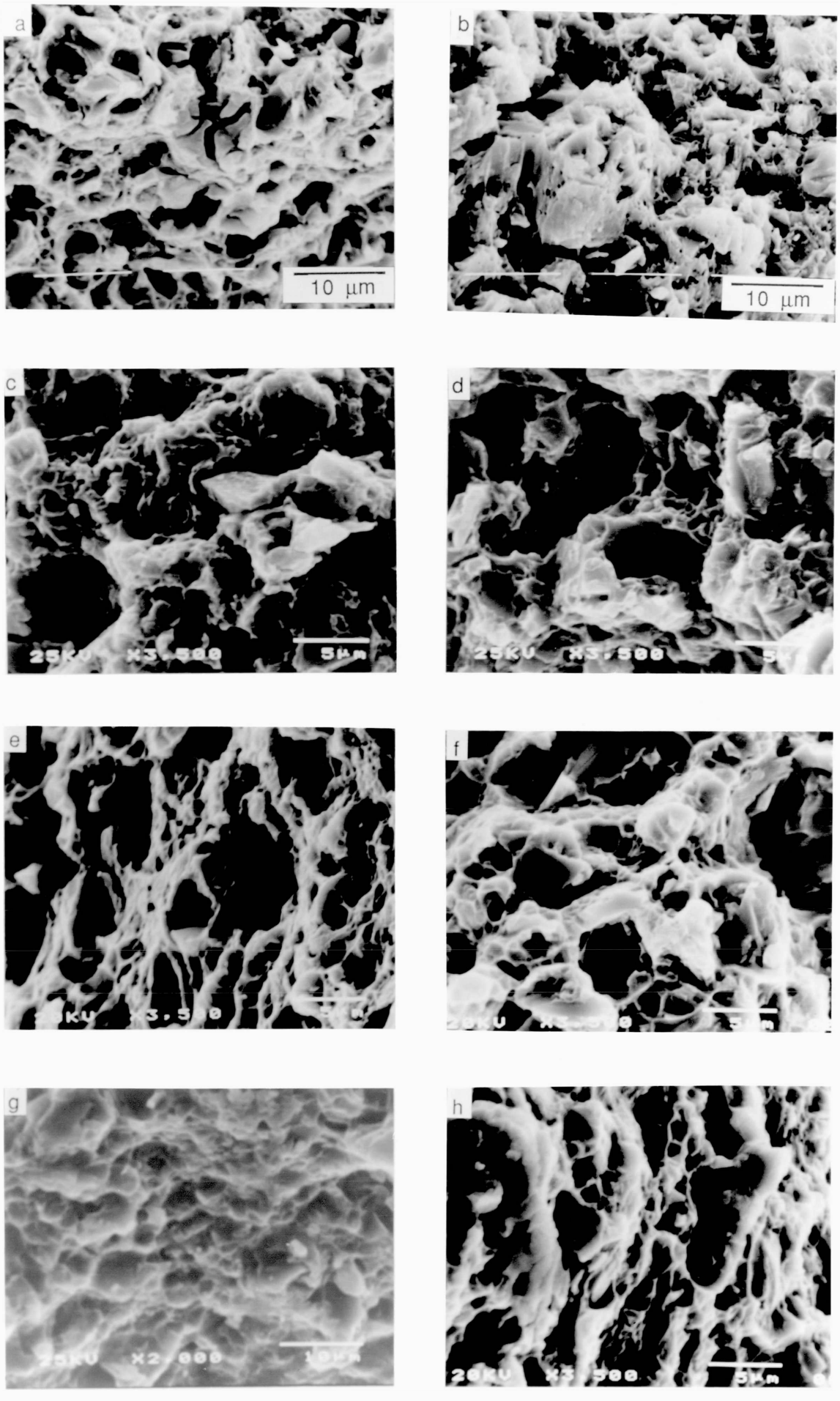
a
10 µm
b
10 µm
c
d
e
f
g
h

the degree of decohesion due to this effect because interface decohesion was also observed in the T4 condition. King[62] notes that decohesion is promoted by a weak interface. The fact that interface decohesion is observed tends to support the theory of build up of un-relaxed stress at the interface. Obviously not all of the SiC particles failed in this way: this is related to particle size and bond strength[63]. Liu and Lewandowski[126] found that particle cracking was evident in underaged 13μm particle composites, whereas in 5μm particle composites using the same 7xxx series type matrix, failure was almost exclusively by interface decohesion. Figure 8.45b also shows some ductile tearing, which seemed to be more prevalent in the composites when compared with the unreinforced material. This can be ascribed to the influence of the silicon carbide on the stress concentration.

Figures 8.45 c and d show 10% and 20% composites in the T6 condition. The underlying matrix-associated dimples are consistent with the decrease in dimple size as heat treatment progresses. There is evidence of decohesion at the particle/matrix boundary in both cases, but there is significantly less SiC at the fracture surface than in the as extruded or T4 conditions (bearing in mind the observations of Roebuck[125]). This is indicative of failure at matrix features such as oxides[62]. At the centre of figure 8.45c decohesion at the surface of one SiC particle can be seen. It might be expected from table 8.9 that the dimple size would be smaller for the 10% composites, but this is not clear from the fractographs, possibly because of the variety of sizes of the particles in the material, or agglomeration.

Throughout the discussion of composite strength the void nucleation has been described as occurring at a single particle. However, reason suggests that an agglomerate will have a greater effect on the build up of dislocations. Thus a further variable is introduced: the effect of agglomeration is to further lower the strain to failure at a local level. The effect of agglomeration is also bound up with, and complicated by, that of porosity. A pore is a pre-existing defect and will have an associated stress concentration which will be shape determined.

Fractographs of failed composite fracture toughness specimens (fig. 8.45 e-h) revealed some difference between under- and overaged material, consistent with observations by other workers[61]. Particle cracking was prevalent in the underaged material (figures 8.45e and f), whereas it was absent from peak aged and overaged material (figures 8.45g and h, respectively): decohesion of the interface seemed to be the dominant mode of failure in the overaged material. this is in agreement with the general trend observed by Liu and Lewandowski[126] for a 7xxx series type alloy (Al-7% Zn-2% Cu-0.14% Zr), although they did not observe cracking in 5μm particles:

this may be a function of alloying and processing[62]. It should be noted that very few cracked particles were observed at the tensile fracture surfaces: this may be due to the less severe stress state accompanying the uniaxially loaded tensile test. However, it should be noted that other workers[126] have observed no difference between three point bend and uniaxial tensile testing. The number of cracked SiC particles at the three point bend fracture surface appeared to increase as SiC volume fraction increased in the underaged condition: this may simply be related to the probability of finding such failure within a larger number of SiC particles at the fracture surface. The failure strain required is much higher for cracked particles than for decohesion of particles[61]. It is probable that microstructural variations due to ageing contribute to the difference between under- and over-aged specimens.

Figure 8.45h (overaged, 15% SiC) shows interface decohesion at a large SiC particle and also some ductile tearing, which occurred occasionally in all specimens. Decohesion of the particle/matrix interface was also observed in the underaged state. A system of matrix dimples was also observed in each case, being derived from the nucleation of voids at silicon carbide and oxide particles, as described in section 7.4.3. Contrary to observations of tensile fracture surfaces, the size of matrix dimple varied little with heat treatment, at around 1-2μm. The variation was less than observed in other tests because all material was heat treated to some degree. The underaged material will have a yield stress high enough to nucleate some voids at larger oxide particles.

8.7 Conclusion to Chapter

The mechanical properties of the alloy CW67 and its composites have been examined in a number of extrusion and heat treatment conditions. These will be summarised with respect to the individual conditions and compositions and also in comparison.

The base alloy was found to have a maximum peak-aged 0.2% proof stress of 572 MPa and U.T.S. of 667 MPa. The fracture toughness of the alloy was found to be a maximum in the underaged condition, with a value from the short rod geometry specimens of approximately 21 MPa$\sqrt{m}$ and 48 MPa$\sqrt{m}$ from the chevron bar geometry. Degassing and hot compaction of the alloy improved the fracture toughness considerably, and also resulted in similar values for all ageing conditions. These fracture toughness values correlate well with K_{IC} figures given by Hildeman et al[110] of 26 MPa$\sqrt{m}$ in the transverse direction (equivalent to short rod geometry) and 47 MPa$\sqrt{m}$ in the longitudinal direction (equivalent to bar geometry). The modulus of the alloy was found to be 73.15 GPa. Fractographs of tensile and toughness specimens

revealed the presence of a dimple structure which is characteristic of failure by microvoid coalescence in ductile materials. The dimple size decreased between solutionising and ageing, which is indicative of failure at smaller matrix particles as the yield stress increases. Tearing was also observed at the fracture surface. Intergranular failure, which might be expected in materials containing precipitate free zones, was not observed in the aged material.

Composite materials showed a slight decrease in peak-aged proof stress and U.T.S. as volume fraction increased; the maximum was found in the 10% SiC composite which exhibited a 0.2% proof stress of 624 MPa and a U.T.S. of 685 MPa. These are a significant improvement on the unreinforced peak properties and are also greater than the composites aged for 13.5 hours. The trend in the tensile properties of these specimens was upward as volume fraction increased up to a maximum at approximately 20% SiC. In this heat treatment condition the 0.2% proof stress is 584 MPa and the U.T.S., 664.8 MPa. This reduction in strength is consistent with the T.E.M. observations of precipitate morphology. The ductility of the composites was substantially lower than that of the unreinforced material. The ductility fell, as volume fraction increased, until a lower limit was reached at which there was no further reduction. This is believed to be related to the size of the supporting ligament of matrix material between the SiC particles. As volume fraction increases, the inter-particle spacing decreases leading to a reduction in ductility. The flattening of the ductility curve is believed to be due to a change in the strain controlling the failure mechanism: up to a certain volume fraction the void formation is growth strain controlled, after which the nucleation strain (which is constant for any given conditions) controls void formation. The physical description of failure is believed to be as follows. As the composite is subjected to increasing load, stresses build up at the particle/matrix interface which must be relaxed by the introduction of further dislocations into the matrix. As dislocations build up, and because of dislocations originally in the material, relaxation of stresses becomes more difficult. Ultimately the stress concentration at the interface is sufficiently high for voids to form and failure to ensue. This mechanism is complicated by the presence of oxides within the matrix and banding or agglomeration of oxide or SiC particles, which impede relaxation. Precipitate phases within the matrix will also have an influence on the failure because of their ability to obstruct dislocation motion, and will contribute to the ductility in proportion to the reciprocal of their effective blocking power. This is reflected in the conventionally determined work hardening exponent, which increases as volume fraction increases. Thus, the trends in variation of strength of CW67 composites in any ageing condition can be explained in terms of volume fraction of reinforcement and matrix heat treatment state. This is shown by comparing the curves

in the T4, T6 and overaged conditions (figures 8.28, 8.29, 8.30). The modulus of the composite material increased as volume fraction increased, although the increase was well below law of mixtures predictions: values ranged from 88.1 GPa at 10% SiC to 111.9 GPa at 25% SiC. These values are close to the range of predictions using the Tsai-Halpin model for short fibres[58]. The specific 0.2% proof stress and U.T.S. values of the CW67/20% SiC composite in the T6 condition were found to be greater than the best specific properties of 8090, 2124[71] and 6061[56,71] containing 20% SIC. The specific modulus of the CW67 composite was found to be similar to the values found for composites of 8090, 2124 and 6061. The absolute strength values are considerably higher than those of other composites.

The fracture toughness of composites was found to be surprisingly high when compared with other results for composites[4] which were generally at around 10-20 MPa$\sqrt{m}$. However, Manoharan and Lewandowski[61] found fracture toughness values for a 7xxx series alloy with 15%, 13μm SiC of 26-28 MPa$\sqrt{m}$ in the underaged condition. It should be noted that all of these comparisons are generalized because of the differences in alloy, SiC particle size and processing methods. In comparison with the values for the unreinforced material quoted above, it was observed that the toughness of the composite can be substantially lower. Fracture toughness was found to be the highest in the underaged condition, with values ranging from 34 MPa$\sqrt{m}$ for the 10% composite to 23 MPa$\sqrt{m}$ for the 25% composite in this heat treatment condition. In the T6 condition the toughness values were found to be 25.41 MPa$\sqrt{m}$ and 22.86 MPa$\sqrt{m}$ for the 10% and 20% composites, respectively. These values are believed to be higher than normally encountered because the material was degassed (an influential operation on the fracture toughness of the unreinforced material) and because the specimens were aligned such that the crack progressing across the extrusion direction instead of along it, as in short rod testing.

Fractographs of both tensile and toughness specimens showed the complexity of the failure of composite materials. Cracking of SiC particles was most evident in the underaged toughness specimens, with interface decohesion becoming more prevalent as ageing time increased. It is thought that cracking of particles was more prevalent in the toughness specimens because of the more severe stress state when compared with the tensile test. Tearing of regions of matrix was observed in many cases. The influence of oxide particles was inferred from a calculation of nucleation stress (table 8.9) at these particles and observed dimple size. The matrix morphology at the fracture surface was a dimple structure comprising dimples of two broad size ranges corresponding to the silicon carbide particles and oxide particles. There was some overlap between these ranges, due to the variety of sizes of the SiC and oxide particles.

Modelling the properties of the composites was expected, and found to be, a complex operation for which no single model was sufficient. This is partly because many models were initially developed for short fibre composites but also because the models did not account for the effect of ageing or the increased dislocation generation found in composite materials. The 'most predictable' property was found to be the modulus: this is because it is the property that is least sensitive to structural variations. These models are thought to be insufficient because of a number of factors:

(i) the SiC particles are not of a unique size: there is a range of sizes from 3μm to 30μm with the majority being in the range 5-8μm;

(ii) oxide particles present in powder materials may contribute to the failure of aged specimens;

(iii) banding and agglomeration of particles will result in a lower failure stress because of the increased effective particle size;

(iv) relaxation of stress build up around particles will become more difficult as volume fraction of particles increases (particle spacing decreases) and matrix precipitate strength increases (relaxation will be further impeded by agglomeration);

(v) although the porosity of the composites is low, as volume fraction increases so does porosity which must exert an influence in reducing the mechanical properties.

9. COMPARISONS AND CONCLUSIONS

9.1 Comparison of Effect of Different Matrix Materials

The different matrix materials, although two are age hardenable and one is not, may be compared and useful information drawn from this comparison. No new data will be presented in this section, however, it has been kept distinct from the conclusions section because of the different nature of the information.

9.1.1 Tensile Properties

It is obvious from the three preceding chapters that the composites have different strengths, which are dependent on the inherent properties of the matrix. The CW67 composites have higher yield and ultimate tensile strengths than composites of 2014, which in turn have higher tensile strengths than composites of C.P. aluminium. Although this is obvious, it is an important point to note. However, within this data it can be seen that the increase in strength over that of the matrix material is greater for the weaker matrix (ie. C.P. aluminium in this investigation). Examining composites with 5μm SiC, the C.P. matrix reinforced with 10% and 20% SiC exhibit increases in yield stress of 50% and 110% respectively in the rolled and fully annealed condition. The increases in the composites of 2014 and CW67 in the T6 condition are 7.5% and 10.7% respectively for 15% reinforcement, although it should be noted for this data that the 2014 was compared with book values[94] for the unreinforced material and the CW67 was compared with unreinforced material that was heat treated for a different time (as the hardness testing indicated). This trend was also observed and noted in the C.P. composites: as heat treatment progressed to full annealing the strength increases in the composites increased (see sections 6.2 and 6.4). The differences between composite and matrix were seen to be only slightly greater, or the same, in the T4 condition for the age hardenable alloys. This information reveals much about the strengthening of composites: the increase in strength is related to the ductility and/or the work hardening capacity of the matrix.

The ductilities of C.P. composites are approximately 25-30% when partially annealed (the only condition in which ductility was measured), values which are within 20% of the unreinforced material, the value for the 10% SIC composite being greater than that of the unreinforced material. In contrast, in the T6 condition, the ductility of the 15% SiC/2014 composite was found to be 50% of the unreinforced value, and that of the 15% SiC/CW67 composite only 45% of the unreinforced alloy (a decrease of 55%). In the T4 condition, the reductions in ductility were not much different: 52.5% for the 2014 composite and 50% for the CW67 composite. For these

composites the work hardening exponent is 0.16 and 0.18, respectively. This data supports the contention that the potential for an increase in strength is greater in the composites of C.P. Al than in those of the age hardenable alloys used in this investigation. It can also be inferred from this data that the differences between matrix and composite in the T4 and T6 conditions of the age hardenable alloys are similar because the reduction in ductility from unreinforced alloy to composite is similar.

Conversely, the modulus of the composite materials (where it was measured) was found to be closer- for the 15% composites of the age hardenable alloys the values were found to be 87.8 GPa and 98.2 GPa for 2014 and CW67, respectively. These are increases of approximately 22% and 34% over the unreinforced material. This similarity may be related to the fact that the modulii of all aluminium alloys is similar, and the introduction of the same reinforcement will have the same effect on that modulus, the only variable likely to dramatically alter the value being the homogeneity and porosity of the mix.

9.1.2 Fracture Toughness

A comparison of fracture toughness values of composites of different matrix materials is difficult because of the different test geometries employed and the absence of data for unreinforced 2014 extruded under the same conditions as material examined in this investigation. A comparison of the data presented in sub-sections 7.4.2 and 8.6.2, suggest that the fracture toughness may be primarily controlled by the amount of reinforcement when comparing the same processing conditions. The toughness of peak heat treated 15% SiC/2014 was found to be 22 MPa$\sqrt{m}$, that of 15% SiC/CW67 to be 24 MPa$\sqrt{m}$. There are, however, other parameters which can not be discussed here; these include reinforcement morphology, size and type. Furthermore, this comparison is filled with factors which may invalidate it, all of which have been noted when comparing results presented in this thesis with those of other workers. These include: the effect of matrix heat treatment structure and oxide content.

9.2 Conclusions

1. The pressure required to extrude composites was found to be greater than pressure required for the unreinforced alloy extruded under the same conditions. However, where the material was canned, the increase in pressure was low.

2. Extrusion pressure was found to increase as volume fraction of reinforcement was increased, but decrease as particle size increased. Both of these observations are consistent with the rationale that extrusion pressure is related to the interparticle spacing.

3. Hot compaction of composites of 2014 resulted in the need for slightly lower extrusion pressures when compared with material which was cold compacted only.

4. Canning of composite material resulted in excellent extrudate surface finish. The surface of non-canned, colloidal graphite lubricated material was poor, with surface cracks extending from between 1/8 to the total length of the extrudate. Material which was lubricated using a leader pad suffered from blistering at the surface, scoring of the lubricant and spiral patterning.

5. Mixing of the R.S.P. and SiC was found to be influential in determining the homogeneity of the product. Mixing conditions were optimised in a 'Turbula T2C' mixer. Under these conditions, the volume fraction measured by the 'linear intercept' method in the transverse plane was found to be in good agreement with the calculated volume fraction added. This indicated good homogeneity. Banding of the SiC was observed in the longitudinal plane.

6. In a comparison of properties resulting from different processing routes it was clear that degassing and hot compaction of the billets led to the best combination of properties. Hot compaction alone was seen to have the greatest influence on tensile properties, whilst degassing and hot compaction together were found to have a large influence on fracture toughness.

7. Matrix material was found to be the primary influence on the absolute values of 0.2% proof stress, tensile strength and ductility. Volume fraction of SiC was found to be the determinant of modulus. It was also postulated that volume fraction of SiC exerted the prime influence on fracture toughness of the composites.

8. The percentage increase in strength of rolled composites of C.P. aluminium and SiC was found to increase as annealing proceeded to completion. The yield stress of fully annealed C.P./SiC composites was found to be able to be modelled, with some success, by the equation:

$$\sigma_{mmc} = \sigma_{Al} + \sigma_o + \gamma.\sigma_{gb} + \sigma_q$$

Deviation of this equation from experimental data was attributed to work hardening.

9. In the fully annealed condition the strength of composites of C.P. Al was found to increase as particle size decreased.

10. As volume fraction increased, for all composites and all particle sizes, the strengths either increased up to a maximum value after which a decrease was observed or increased monotonically within the limits of the volume fractions used in this work. The point at which the maximum occurs was found to be dependent upon:

(i) particle size;
(ii) porosity and agglomeration;
(ii) matrix material;
(iv) matrix heat treatment condition;

and the influence of these parameters on structure, although no formal relationships were found. It can also be inferred that the maximum will depend on the following factors which were not investigated:

(v) quench temperature and rate;
(vi) extrusion temperature;

Composites which did not exhibit a maximum within the bounds of the volume fractions investigated were thought to have a combination of the above listed parameters, (i) to (iv), which led to the maximum occurring at a higher volume fraction than the highest investigated herein.

11. Ductility is thought to be controlled by the strain for void growth up to approximately 15% SiC, after which it is void nucleation strain controlled. The nucleation strain is governed by the heat treatment condition.

12. A number of predictive equations were applied to the proof stress, modulus and fracture toughness of the age hardenable alloy composites. Predictions of yield stress were found to be reasonable although, in general, over-estimates. Prediction of the modulus was more successful, with a good agreement between theory and experiment. The predicted fracture toughness values were generally poor, although a relationship between toughness and square root of volume fraction was found.

In the case of age hardenable alloys, the inability of the equations to produce reasonable results was attributed to the complexity of the strengthening mechanism.

13. Fracture toughness was observed to decrease as ageing progressed for both age hardenable composites, except the 15% SiC/CW67 composite which exhibited a slight rise in toughness after peak ageing which was thought to be due to experimental variance. The decrease in the other composites was thought to be due to the change in matrix precipitate morphology, as is found in unreinforced aluminium alloys. It was inferred from calculations and S.E.M. observations that the oxide particles inherent in powder alloys took part in the fracture process of the materials in their heat treated conditions.

14. The specific 0.2% proof stress and U.T.S. of the CW67/20% SiC composite are superior to the published specific properties of 20% SiC composites of 8090, 6061 and 2124. The specific modulii of these materials are similar.

15. The heat treatment conditions which produced the peak hardness for the unreinforced CW67 were found to be solutionising for 1.5 hours at 475°C, followed by water quenching, and then ageing for 13.5 hours at 120°C. Peak ageing of the CW67 composites required only 6 hours at this temperature.

16. T.E.M. investigation coupled with D.S.C. analysis revealed that ageing of the age hardenable matrix alloys was found to have been accelerated by the presence of the reinforcing particles. This is related to the suppression of peaks in the D.S.C. curves of these alloys and is believed to be due to the higher strain energy of these materials, allowing the surmounting of the activation energy barrier for precipitation, but further work is required in order to validate this.

17. The microstructure of the peak aged CW67 and its composites was found to be a combination of η' and η precipitates with dispersoids of an Al/Fe/Ni phase. Precipitate free zones were observed at the grain boundaries. Peak aged 2014 composite microstructure was primarily θ' phase.

18. Failure in tension was found to be due to particle/matrix interface decohesion in all ageing conditions. Under three point bend loading, the precipitate hardened alloy composites failed by particle cracking in the underaged condition and by interface decohesion in the overaged condition.

9.3 Suggestions for Further Work

During the course of this investigation a number of areas went broadly un-investigated. The most important of these is the extrusion process: only a limited range of temperatures and extrusion ratios was used, the object being primarily to make the extrusion as easy as possible. There is considerable scope to investigate the limits of extrusion of all of the composites used in this investigation. The importance of extrusion texture on the final microstructure was not investigated, but would prove interesting.

Although the mechanisms of composite strengthening have been identified in commercial purity aluminium composites, and an empirical equation applied with some success, the basis of this equation was not studied. Further work, directed at the measurement of grain and sub-grain sizes may reveal the influence of these parameters on the strengthening model and either confirm or deny the use of the correction factor. The strengthening mechanisms in age hardened composites are more complex and less well understood. An '*in situ* straining', T.E.M. investigation into composite material aged for various times would be useful in this case. A more in-depth investigation of matrix structure, such as sub-grain size and quantitative dislocation density measurements, may further aid this investigation. The interface between the silicon carbide and the matrix materials was not examined. An investigation of the influence of matrix factors on strengthening may also be conducted by a controlled variation of the parameters listed in conclusion point 9. The investigation would benefit from the additional use of higher volume fraction composites.

An investigation into the ageing characteristics of high volume fraction composites using differential scanning calorimetry in conjunction with T.E.M. may help to elucidate the ageing process in composites.

There is currently a wide range of differing observation on the failure microstructure of different composites with little explanation as to why and how the different features occur. It was observed in this work that, in general the underaged composites contained more cracked particles than overaged composites, which failed almost exclusively by interface decohesion. There is scope here for an investigation into the effect of particle size, matrix type, matrix heat treatment and test loading on the propensity of the composite to fail by particle cracking or decohesion, or by matrix failure. Such work should include an investigation of longitudinal cross sections of

specimens loaded to failure, but also partially loaded, and an investigation into any relationships between the fracture surface roughness and salient microstructural dimensions, such as SiC and oxide particle size or sub-grain size.

The alloy CW67 is a relatively 'new' alloy in its own right. Limit diagrams for the extrusion of this alloy have yet to be established. The extrusion parameter/structure relationship has only been touched upon in the work on this alloy and should be examined in full, in conjunction with work on the limits of extrusion. The identification of the Al_3Zr phase was by no means conclusive, and thus should be examined in greater detail.

REFERENCES

1. E.A. Feest; Met.s & Mat.s, (1988), **4**,5, 1131.
2. C.A. Stubbington; Met.s & Mat.s, (1988), **4**, 7.
3. D. Charles; Met.s & Mat.s, (1990), **6**, 2, 78.
4. S.V. Nair, J.K. Tien, R.C. Bates; Int. Mets. Reviews, (1985), **30**, 275.
5. R.L. Trumper; Met.s & Mat.s, (1987), **3**, 11, 662.
6. M. Taya, R.J. Arsenault; Metal Matrix Composites- Thermomechanical Behaviour, publ. Pergamon Press, 1989.
7. C.M. Friend, I. Horsfall, C.L. Burrows; Proc.s B.N.F. 7th International Conference, 'The Materials Revolution Through the 90's', vol.2, 3-5th July, 1989, Oxford, England, paper no.28.
8. J.A. Cornie, Y.M. Chiang, D.R. Uhlmann, A. Mortensen, J.M. Collins; Ceramic Bull., (1986), **65**, 293.
9. F.A. Girot, J.M. Quenisset, R. Naslain; Comp. Sci. & Tech., (1987), **30**, 155.
10. T.W. Clyne; p.2.275, Proceedings of the sixth International Conference on Composite Materials, vol.2, Ed.s F.L. Matthews, N.C.R. Buskell, J.M. Hodgkinson, J. Morton, 1987, Elsevier Applied Science.
11. R.L. Trumper, V.D. Scott; ibid, paper no. 27.
12. T.C. Willis; Met.s & Mat.s, (1988), **4**, 8, 485.
13. C. Baker; Proc.s B.N.F. 7th International Conference, 'The Materials Revolution Through the 90's', vol.1, 3-5th July, 1989, Oxford, England, paper no.9.
14. B.P. Krishnan, M.K. Surappa, P.K. Rohatgi; J. Mat. Sci., (1981), **16**, 1209.
15. R. Mehrabian, R.G. Riek, M.C. Flemings; Met. Trans., (1974), **5**, 1899.
16. P.K. Rohatgi, B.C. Pai, S.C. Panda; J. Mat. Sci., (1979), **14**, 2277.
17. Deonath, R.T. Bhat, P.K. Rohatgi; J. Mat. Sci., (1980), **15**, 1241.
18. F.M. Hosking, F. Folgar-Portillo, R. Wunderlin, R. Mehrabian; J. Mat. Sci., (1982), **17**, 477.
19. W. Khal, J. Leupp; Proc.s B.N.F. 7th International Conference, 'The Materials Revolution Through the 90's', vol.1, 3-5th July, 1989, Oxford, England, paper no.8.
20. A. Leatham, A. Ogilvy, P. Chesney, J.V. Wood; Met.s & Mat.s, (1989), **5**, 3, 140.
21. A.R.E. Singer, S. Ozbeck; Powder Met., (1985), **28**, 72.
22. P. Chesney; Met.s & Mat.s, (1990), **6**, 6, 373.
23. A.J. Reeves, W.M. Stobbs, T.W. Clyne; 'MMCs- Property Optimisation and Application', 8-9 Nov., I.o.M., London, 1989.
23. S.R. Nutt, R.W. Carpenter; Mat. Sci. & Eng., (1985), **75**, 169.
24. J.C. Ehrström, W.H. Kool; J. Mat. Sci., (1988), **23**, 3195.
25. D.L. McDanels; Met. Trans., (1985), **16A**, 1105.

26. T.G. Nieh, D.G. Chellman; Scripta Metall., (1984), **18**, 925.
27. C.R. Crowe, R.A. Gray, D.F. Hasson; p.483, Proceedings of the fifth International Conference on Composite Materials, ed. W.C. Harrigan, Jr. et al.
28. Y.L. Liu, N. Hansen, H. Lilholt, C.Y. Barlow; 'MMCs- Property Optimisation and Application', 8-9 Nov., I.o.M., London, 1989.
29. N. Raghunathan, H.B. McShane, T. Sheppard; Proceedings- Advancing with Composites, International Conference on Composite Materials, Milan, May, 1988.
30. R.J. Arsenault, S.B. Wu; Scripta Metall., (1988), 22, 767.
31. J. Sun, I.G. Greenfield; p.2.287, Proceedings of the sixth International Conference on Composite Materials, vol.2, Ed.s F.L. Matthews, N.C.R. Buskell, J.M. Hodgkinson, J. Morton, 1987, Elsevier Applied Science.
32. T.G. Nieh, R.F. Karlak; J. Mat. Sci. Lett.s, (1983), **2**, 119.
33. R.W. Hains, P.L. Morris, P.W. Jeffry; Proc. Int. Symposium on Advanced Struct. Mat.s, Montreal, 1988, 27th Annual Conf. of Metallurgists, vol. 9, Proc.s of Met. Soc. of the CIMM, ed. D.S. Wilkinson, Pergamon.
34. T.F. Bryant, S.T. Derham, A.E.J. Forno, W.S. Miller; 'MMCs- Property Optimisation and Application', 8-9 Nov., I.o.M., London, 1989.
35. Y. Fujita, H. Fukumoto; p.2.340, Proceedings of the sixth International Conference on Composite Materials, vol.2, Ed.s F.L. Matthews, N.C.R. Buskell, J.M. Hodgkinson, J. Morton, 1987, Elsevier Applied Science.
36. A.P. Divecha, S.G. Fishman, S. Karmarkar; J. Met,(1981),**33**, Sept.,12.
37. F.J. Humphreys; 9th Risø International Symposium on Metallurgy & Materials Science: Mechanical and Physical Behaviour of Metallic and Ceramic Composites, 5-9th Sept., 1988.
38. W.S. Miller, F.J. Humphreys; T.M.S.-A.I.M.E. Fall meeting, Oct. 1st-5th, 1989, Indianapolis.
39. R.J. Arsenault, N. Shi; Mat. Sci. & Eng., (1986), **81**, 175.
40. R.J. Arsenault, C.S. Pande; Scripta Metall., (1984), **18**, 1131.
41. Y. Bienvenu, J.C. Flour, Y. Favry, A.R. Bunsell; Proc.s B.N.F. 7th International Conference, 'The Materials Revolution Through the 90's', vol.1, 3-5th July, 1989, Oxford, England, paper no.34.
42. S. Fox, H.M. Flower; M.M.C.'s: Structure and Property Assessment, IoM Conference, November, 1987.
43. Y. Kimura, Y. Mishima, S. Umekawa, T. Suzuki; J. Mat. Sci., (1984), **19**, 3107.
44. T. Erturk, V. Gupta, A.S. Argon, J.A. Cornie; p.2.146, Proceedings of the sixth International Conference on Composite Materials, vol.2, Ed.s F.L. Matthews, N.C.R. Buskell, J.M. Hodgkinson, J. Morton, 1987, Elsevier Applied Science.
45. R.J. Arsenault, R.M. Fisher; Scripta Metall., (1983), **17**, 67.

45. T. Christman, S. Suresh; Acta Metall., (1988), **36**, 1691.
46. T. Christman, S. Suresh; Acta Metall., (1988), **36**, 1691.
47. M. Vogelsang, R.J. Arsenault, R.M. Fisher; Met. Trans. A, (1986), **17A**, 379.
48. B. Derby, J.R. Walker; Scripta Met., (1988), **22**, 592.
49. H.L. Marcus, L. Rabenberg, L.D. Brown, G. Elkabir, Y.M. Ceong; p.2.459, Proceedings of the sixth International Conference on Composite Materials, vol.2, Ed.s F.L. Matthews, N.C.R. Buskell, J.M. Hodgkinson, J. Morton, 1987, Elsevier Applied Science.
50. T.G. Nieh, R.F. Karlak; Scripta Met., (1984), **18**, 25.
51. J.J. Stephens, J.P. Lucas, F.M. Hosking; Scripta Metall., (1988), **22**, 1307.
52. H. Ribes, M. Suéry; Scripta Met., (1989), **23**, 705.
53. J.L. Petty-Galis, R.D. Goolsby; J. Mat. Sci., (1989), **24**, 1439.
54. Hunt, Pitcher, P.J. Gregson; Scripta Met., (1990), **24**, 937.
55. D. Webster; Met. Trans., (1982), **13A**, 1511.
56. D.L. Mc Danels, C.A. Hoffman; N.A.S.A. Technical Paper 2302, July, 1984.
57. M.A. Bayoumi, M. Suery; p.2.481, Proceedings of the sixth International Conference on Composite Materials, vol.2, Ed.s F.L. Matthews, N.C.R. Buskell, J.M. Hodgkinson, J. Morton, 1987, Elsevier Applied Science.
58. Metals Handbook, A.S.M., Ninth edition, vol. 2.
58. V.C. Nardonne, K.M. Prewo; Scripta Metall., (1986), **20**, 43.
59. R.H. Jones, C.A. Lavender, M.T. Smith; Scripta Metall., (1987), **21**, 1565.
60. A.P. Divecha, S.G. Fishman; p.351, Proceedings of I.C.M. 3, vol.3, 1979.
61. M. Manoharan, J.J. Lewandowski; Sripta Metall., (1989), **23**, 301.
62. J.E. King; Met.s & Mat.s, (1989), **5**, 12, 720.
63. Y. Flom, R.J. Arsenault; p.2.189, Proceedings of the sixth International Conference on Composite Materials, vol.2, ed.s F.L. Matthews, N.C.R. Buskell, J.M. Hodgkinson, J. Morton, 1987, Elsevier Applied Science.
64. T.W. Clyne, M.G. Bader, G.R. Cappelman, P.A. Hubert; J.Mat. Sci., (1985), **20**, 85.
65. A. Sato, R. Mehrabian; Met. Trans., (1976), **7B**, 443.
66. J.L. Chermant, M. Coster; J. Mat. Sci., (1979), **14**, 509.
67. S.H. Goods, L.M. Brown; Acta Metall., (1979), **27**, 1.
68. N. Raghunathan, H.B. McShane, C.H.J. Davies, T. Sheppard; J. Mat. Sci., (1990), **25**, to be published.
69. M.Y. Wu, D. Sherby; Scripta Met., (1984), **18**, 773.
69. N.N.Z. Gindy, A.J. Clegg; Proc.s B.N.F. 7th International Conference, 'The Materials Revolution Through the 90's', vol.2, 3-5th July, 1989, Oxford, England, paper no.32.
70. E. Savrun, M. Taya; J. Mat. Sci., (1988), **23**, 1453.

70. H. Lilholt, M. Taya; Proceedings of the sixth International Conference on Composite Materials, vol.2, Ed.s F.L. Matthews, N.C.R. Buskell, J.M. Hodgkinson, J. Morton, 1987, Elsevier Applied Science, p. 234.
71. C.J. Peel, R. Moreton, S.M. Flitcroft; 'MMCs- Property Optimisation and Application', 8-9 Nov., I.o.M., London, 1989.
71. P.G. Partridge, C.M. Ward-Close; Met.s & Mat.s, (1989), **5**, 6, 334.
72. H.L. Cox; Br. J. Appl. Phys, (1952), **3**, 72.
73. D. Hull; An Introduction to Composites, C.U.P., 1981.
74. Engineering Metals Handbook, vol. 1, "Composites", A.S.M. International, 1987.
75. Aluminium Association Handbook "Aluminium Standards and Data", Aluminium Association of America.
76. B.F. Quickley, G.J. Abbaschian, R. Wunderlin, R. Mehrabian; Met. Trans., (1982), **13A**, 93.
76. G.E. Dieter; "Mechanical Metallurgy", McGraw-Hill, 1986.
77. H. Cambell, W.C. Bauer; Chem. Eng., (1966), **73**, Sept., 179.
78. D.F. Hasson, S.M. Hoover, C.R. Crowe; J.Mat. Sci., (1985), **20**, 4147.
78. M.B. Donald, B. Roseman; Brit. Chem. Eng., (1962),**7**: part 1,749; part 2 823; part 3, 922.
79. P.K. Whitman, D.L. Feke; Adv. Cer. Mat.s, (1986), **1**, 366.
80. P.K. Ghosh, P.R. Prasad, S. Ray; Z Metall., (1984), **75**, 934.
81. A. Roosen, H. Hausner; Adv. Cer. Mat.s, (1988), **3**, 131.
82. K. Kendall; Powder Met., (1988), **31**, 28.
83. A. Kelly, R.B. Nicholson; Prog. Mat. Sci., (1963), **10**, 151.
84. "Aluminium- Properties and Physical Metallurgy", ed. J.E. Hatch, A.S.M. 1984.
85. L.F. Mondolfo; Int. Met. Reviews, (1971), **153**, 95.
86. L.F. Mondolfo, N.A. Gjostein, D.W. Levinson; J. Met.s, (1956), **206**, 1378.
87. N. Ryum; Z. Metall., (1975), **66**, 344.
88. P.A. Thackery; J.I.M., (1968), **96**, 228.
89. N. Ryum; Z. Metall., (1975), **66**, 338.
90. M. Raghavan; Met. Trans. A, (1980), **11A**, 993.
91. M. Mahmoud; PhD. Thesis, University of London, 1990.
92. L.M. Barker; Eng. Fract. Mechs., (1977), **9**, 361.
93. W. Shang-Xian; Eng. Fract. Mechs., (1984), **19**, 221.
94. H.B. McShane; PhD. Thesis, Univ. of London, 1978.
95. G.J. Marshall, E.K. Ioannidis, T. Sheppard; Powder Met., (1986), **29**, 1, 57.
96. A.F. Castle, T. Sheppard; Met. Tech., (1976), **3**, 465.
97. L. Ackerman, I. Guillemin, R. Lalauze, C. Pijolat; A.I.M.E. Congress, Toronto, Ontario, 14-17 October, 1985.

98. J. Subramaniyan; PhD Thesis, University of London, 1989.
99. G.K. Tan; PhD Thesis, University of London, 197?.
100. T. Sheppard, M.P. Clode; Proc. 4th Int. Extrusion Tech. Seminar, (1988), vol. 2, 329.
101. J.K. Park, A.J. Ardell; Met. Trans. A, (1984), **15A**, 1531.
101. T. Sheppard; Met. Tech., (1981), **8**, 130.
102. T. Sheppard, S.J. Paterson; Met. Tech., (1982), **9**, 274.
103. N. Hansen; Acta Metall., (1977), **25**, 863.
104. F.J. Humphreys, P.N. Kalu; Acta Metall., (1987), **35**, 2815.
105. J.M. Silcock; J.I.M., (1960-61), **89**, 203.
106. W. Bonfield, P.K. Datta; J. Mat. Sci., (1976), **11**, 1661.
107. M.P. Clode; unpublished research.
108. G.J. Marshall; Proc.s Aluminium Tech. '86. I.o.M., London, 11-13 March,1986.
109. A.S.M. "Metals Handbook", 9th edition, vol. 4.
110. G.J. Hildeman, L.C. Labarre, A. Hafeez, L.M. Angers; private communication.
111. R. Mehrabian; Int. Met.s Reviews, (1982), **27**, 4, 185.
112. F.B. Pickering; "The Basis of Quantitative Metallography", monograph no.1, Inst. of Met. Tech, publ. I.oM..
113. N. Radomsky, O. Kabisch, H. Löffler, J. Lendvai, T. Ungár, G. Honyek; J. Mat. Sci., (1979), **14**, 2906.
114. R. Delasi, P.N. Adler; Met. Trans. A, (1977), **8A**, 1177.
115. P.N. Adler, R. Delasi; Met. Trans. A, (1977), **8A**, 1185.
116. J.D. Embury, R.B. Nicholson; Acta Met., (1965), **13**, 403.
117. I. Kirman; Met. Trans., (1971), **2**, 1761.
118. H.A. Holl; Met. Sci. J., (1976), **1**, 111.
119. E.A. Starke; J. Mets., (1970), Jan., 54.
120. S.E. Naess; Scripta Met., (1969), **3**, 179.
121. C.M. Friend; Proceedings of the sixth International Conference on Composite Materials, vol.2, Ed.s F.L. Matthews, N.C.R. Buskell, J.M. Hodgkinson, J. Morton, 1987, Elsevier Applied Science, p. 402.
122. W.H. Hunt, Jr., O. Richmond, R.D. Young; Proceedings of the sixth International Conference on Composite Materials, vol.2, Ed.s F.L. Matthews, N.C.R. Buskell, J.M. Hodgkinson, J. Morton, 1987, Elsevier Applied Science, p. 209.
123. J.W. Martin; "Micromechanisms in particle hardened alloys", Cambridge Solid State Science Series, C.U.P., 1980.
124. H.Y. Hunsicker; Phil. Trans. of the Royal Society, series A, **282**, no.1307, 359.
125. B. Roebuck; J. Mat. Sci. Lett.s, (1987), **6**, 1138.

126. C. Liu, J.J. Lewandowski; Proc. Int. Symposium on Advanced Struct. Mat.s, Montreal, 1988, 27th Annual Conf. of Metallurgists, vol. 9, Proc.s of Met. Soc. of the CIMM, ed. D.S. Wilkinson, Pergamon.

APPENDICES

Appendix 1: X ray Diffraction Data

The data contained within this appendix is supplementary to the information presented within the text in chapter 8. The plots are not to scale, they merely illustrate the points made with respect to peak broadening and the growth of low angle peaks. Also shown is the peak believed to be due to $Al_9(Fe,Ni)_2$.

A1: As received CW67 powder

Shows two main aluminium peaks: from {111} and {200} reflections.

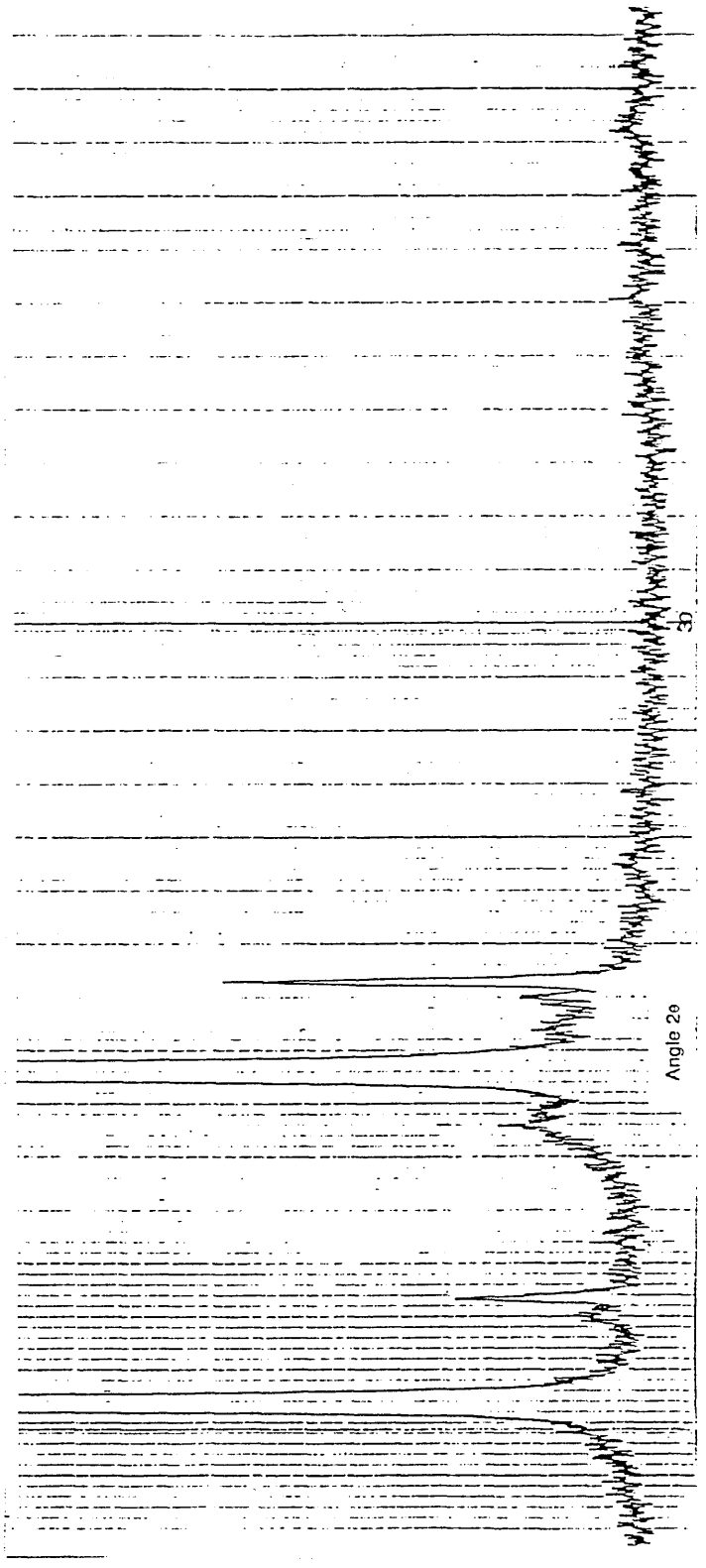

A2: As solutionised CW67 extrudate, extruded at 425°C, 30:1

Shows two main aluminium peaks and also peak believed to be due to $Al_9(Fe,Ni)_2$. Note the broadening of the Al {111} and {200} peaks.

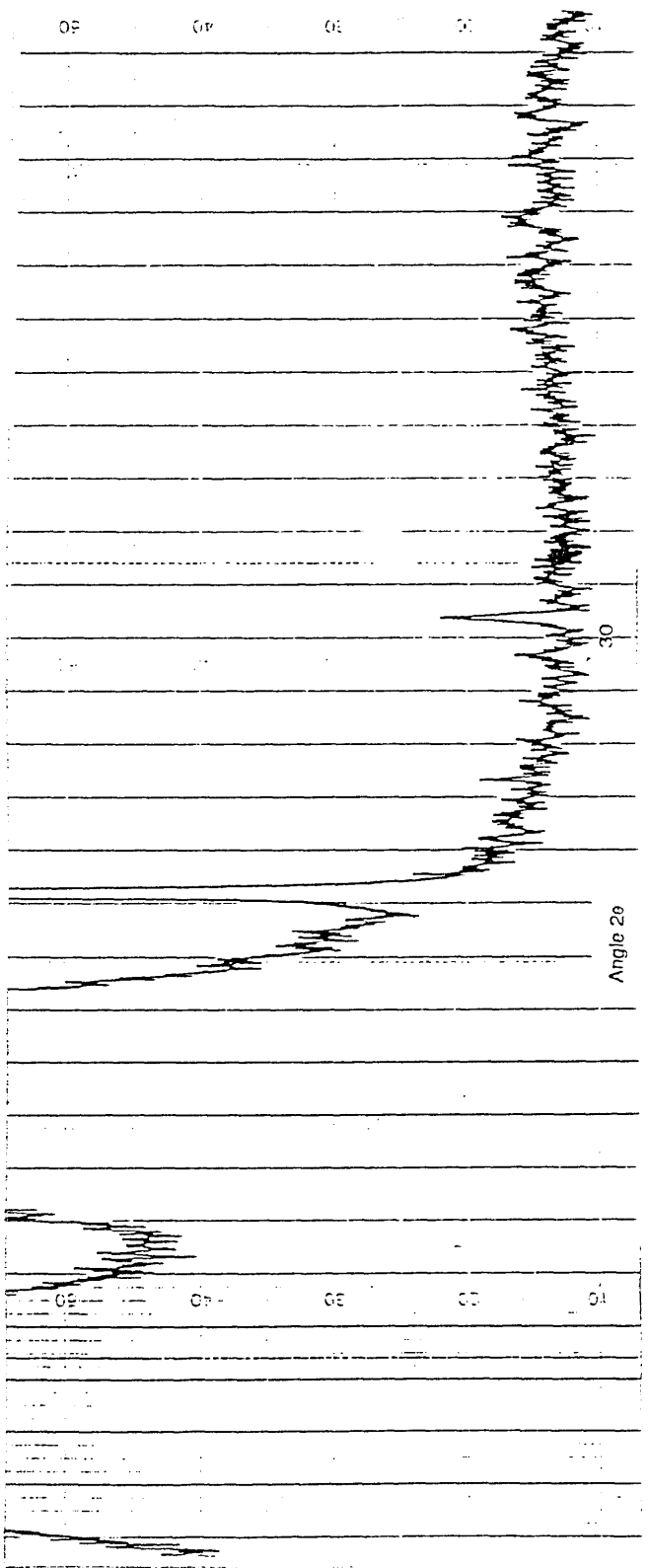

A3: Low angle peak growth- 160°C, 180°C, 200°C.

Shows the growth of the peaks at low angles of diffraction. The series runs sequentially from 160°C to 200°C, the last in the sequence possibly being part of the $MgZn_2$ series of diffraction lines..

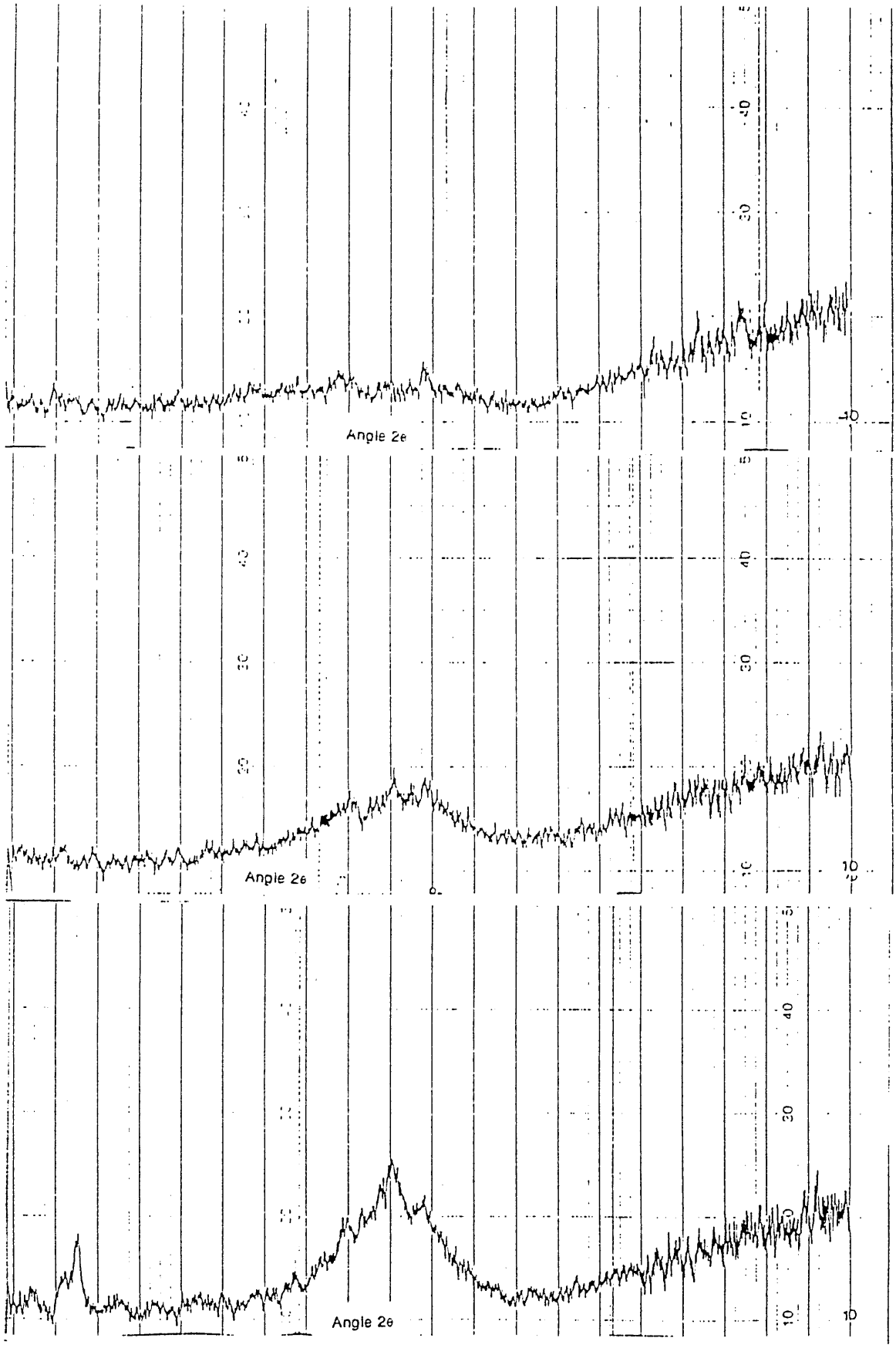

Appendix 2: Standard designation for Aluminium Alloys

A four digit system is used to identify wrought aluminium alloys, as shown below. The first digit indicates the main alloying element, and thus identifies the 'series'. The second digit shows whether any compositional modifications have been made to the alloy- 0 identifies the original alloy. The final two digits identify the alloy within its series: these could indicate other alloying elements within the system or the levels of impurity (in the case of the 1xxx series).

Code	Alloying element
1xxx	'pure' Al
2xxx	copper
3xxx	manganese
4xxx	silicon
5xxx	magnesium
6xxx	Mg & Si
7xxx	zinc
8xxx	lithium

Additional alloy designations exist which rely on different code identification- eg. the 'LM' series of aluminium/magnesium alloys relies on numbers to identify the compositional quantities. Furthermore, experimental alloys are subject to the coding of the individual alloy designers who may operate an 'in-house' code alone. This is the case with MB27 and CW67, which are AlCoA designations for alloys of, broadly, the 2xxx and advanced 7xxx series.